Final Report

AHRI Report No. 8012

DEVELOPING FAN POWER TERMINAL UNIT PERFORMANCE DATA AND MODELS COMPATIBLE WITH ENERGY PLUS

Final Report
January 2014 – November 2016

November 2016

Dennis L. O'Neal, Carl Reid, Douglas Ingram, and Di Lu
BAYLOR UNIVERSITY
Waco, TX 76798

John A. Bryant, Saurabh Gupta, Basel Kanaan, and Stephen Bryant
TEXAS A&M UNIVERSITY
College Station, TX 77843

Peng Yin
UNIVERSITY OF LOUISIANA, LAFAYETTE
Lafayette, LA 70503

Prepared for

AIR-CONDITIONING, HEATING AND REFRIGERATION INSTITUTE
2111 Wilson Boulevard, Suite 500, Arlington, Virginia 22201-3001

DISCLAIMER

This report was prepared as an account of work sponsored by the Air-Conditioning, Heating, and Refrigeration Institute (AHRI). Neither AHRI, its research program financial supporters, or any agency thereof, nor any of their employees, contractors, subcontractors or employees thereof - makes any warranty, expressed or implied; assumes any legal liability or responsibility for the accuracy, completeness, any third party's use of, or the results of such use of any information, apparatus, product, or process disclosed in this report; or represents that its use would not infringe privately owned rights. Reference herein to any specific commercial product, process, or service by trade name, trademark, manufacturer, or otherwise, does not necessarily constitute nor imply its endorsement, recommendation, or favoring by AHRI, its sponsors, or any agency thereof or their contractors or subcontractors. The views and opinions of authors expressed herein do not necessarily state or reflect those of AHRI, its program sponsors, or any agency thereof.

Executive Summary

This report summarizes the findings from AHRI Project 8012, whose purpose was to develop new models of fan powered terminal units (FPTUs) for use in building simulation programs that utilize mass and energy balance methodologies. The models can be used to provide better estimates of the energy performance of FPTUs. The work was completed by a team of researchers from Baylor University, Texas A&M University, and the University of Louisiana at Lafayette.

The work was divided into six tasks:

1. Develop a broad range of fan/motor efficiency data for use in EnergyPlus,
2. Develop laboratory and field in situ measurements of FPTUs,
3. Characterize leakage for use in parallel FPTU models,
4. Develop models for alternative configurations/operations of series and parallel units,
5. Compare FPTU models with those in prior work and EnergyPlus, and
6. Communicate with EnergyPlus developers to help ensure model data are incorporated into EnergyPlus

A summary of results from each task is summarized below:

Task 1 – Develop a broad range of fan/motor efficiency data for use in EnergyPlus

Data on the performance of FPTU fan/motor combinations that had permanent split capacitor motors (PSCs) controlled with silicon controlled rectifiers (SCRs) and had electronically commutated motors (ECMs) were evaluated in Chapters 2 and 3. Relationships were developed between fan/motor efficiency and fan total pressure as well as fan motor power and fan airflow. Three manufacturers provided detailed PSC/SCR experimental data on 12 fan/motor combinations employed in commercially available FPTUs. The fan motors ranged in size from 1/8 hp (93 W) to 1 hp (746 W). The maximum fan airflows ranged from 690 to 4524 ft^3/min (0.33 to 2.14 m^3/s). The performance data included SCR voltage, discharge static pressure, airflow, volts, amps, volt-amps, power factor, power, motor speed, motor size, and power divided by airflow. Data were also provided on fan discharge area and motor size. A linear relationship between fan/motor total efficiency and fan total pressure was inferred for the units evaluated. By use of the definition of fan efficiency, it was also shown that the relationship between fan motor power and fan airflow should also be linear. The correlations developed

should be in a form that can be readily used in energy simulation programs to better estimate the performance of fan powered terminal units.

Four manufacturers provided detailed performance data on 36 ECM fan/motor combinations applied in commercially available series and parallel fan powered terminal units. The fan motors ranged in size from 0.33 to 1 hp (249 to 746 W). Data were provided for fan static discharge pressures ranging from 0.1 to 0.75 in w.g. (25 to 187 Pa). The performance data were analyzed to develop a generalized performance model that would be suitable for use in building energy simulation programs. The model developed had two components to it. First, the data for static discharge pressures ranging from 0.1 to 0.5 in w.g. (25 to 125 Pa) were used to develop a correlation between the full load power and the maximum airflow of the fan/motor combinations. These data were fit with a simple linear regression model. Second, part load power and airflow data were evaluated over a wide range of controller settings for each fan/motor combinations. The data were normalized to airflow and power corresponding to the maximum controller setting for each static pressure. It was found that the normalized data for those fan motors whose full maximum power operations were less than 80% of the rating of the motor were problematic and were not used in the part load evaluation. The normalized power and air flow were fit with a third degree polynomial. The resulting full load power correlation along with the part-load correlation could be used together in a building simulation program to estimate the part load energy use of fan/motor combinations used in fan powered terminal units that utilize electronically commutated motors.

Mathematical models were developed for estimating the performance of ECM fan powered terminal units in both constant and variable airflow applications. The required inputs for the constant airflow model included only the design airflow for the space and the capacity factor. The capacity factor was a measure of the maximum capacity of the ECM FPTU relative to the design airflow in a zone. Estimates of the power and energy use of the fan powered terminal unit could be made. For the variable airflow model, the operating airflow rate was required in addition to the design airflow and capacity factor. The model for fixed airflow operations was used to analyze the impact of using fan powered terminal units with electronically commutated motors in applications where the airflow capacity of the unit was larger than the design airflow for the zone but the FPTU was operated at the design airflow. The analysis showed that a reduction in power (and energy use) of approximately 30% for a unit whose capacity was 25%

larger than the design airflow but was operated at the design airflow. A more general model was also developed for fan powered terminal units in variable airflow applications. This general model could be programmed into a building simulation programs to estimate power and energy savings of fan power terminal units used in variable airflow applications.

Task 2 – Develop laboratory and field in situ measurements of FPTUs

Differential in situ laboratory and field measurements on FPTUs is summarized in Chapter 4. Static pressure laboratory measurements were made on a series FPTU for airflow rates ranging from a low of 500 to a maximum of 1,300 ft^3/min (0.236 to 0.613 m^3/s). This FPTU was an older unit with a PSC motor and SCR control. Downstream static pressures were held at 0.25 in. w.g. (62.3 Pa) using an 8 inch (20.3 cm) VAV series fan powered terminal unit. The differential static pressure rise for this fan ranged from a low of 0.128 to a maximum of 0.246 in. w.g. (31.9 to 61.3 Pa). From these data, a linear relationship between total airflow and series fan differential static pressure could be inferred. The results show that though the static pressure rise across the fan was low, it was tied quite well to total airflow.

Data from one manufacturer's 8 and 12 inch (20.3 and 30.5 cm) series ECM FPTUs were also evaluated in a laboratory and compared to the in-situ data from the PSC unit. Results were comparable and the units also showed a linear relationship for flow versus differential pressure rise. The 8 inch (20.3 cm) ECM unit had a differential pressure increase in the range of 0.24 to 0.28 in. w.g. (60 – 70 Pa). While the 12 inch (305 mm) had a pressure rise range of 0.24 – 0.37 in. w.g. (60 – 92 Pa). These data supported the base hypothesis that fan differential pressure rise was much less than commonly assumed.

A simple set of simulations were run with EnergyPlus to investigate the impact on annual HVAC energy use of using fan pressure rise inputs and fan/motor efficiencies that varied from those measured in this study to those found either as default inputs in EnergyPlus or found as recommended in various literature and user groups. It was found that at a fan pressure rise of less than 0.5 in. w.g. (124 Pa), a wide range in fan/motor efficiencies would result in an annual HVAC system energy difference of less than 5%. However, FPTU fan energy could be up to 80% less and energy for supplemental heat was also substantially different depending on these input values.

Additional data were gathered in a limited field study on the main campus of Texas A&M University. Several series and two parallel FPTUs were instrumented for short-term temperature

and pressure data. The results showed a consistent fan pressure rise of between 0.20 and 0.30 in. w.g. (60 – 75 Pa) for series FPTU. These FPTU all had PSC motors with SCR control. These results added more support to the need to use of a correct fan pressure rises in an energy simulation program. In addition to the pressure rise, temperatures were recorded in the plenum near the FPTU and at the induction port to evaluate whether leakage was occurring in the parallel FPTUs.

Of the two parallel FPTUs, only one showed leakage. The first parallel FPTU served an auditorium and during the monitoring period was operating at minimum primary airflow. The unit had occasional short periods of heating during this same period. No leakage was noted at the induction port through either infrared thermography or temperature measurements. The second FPTU served a lobby/entrance area of an office building. The consistent 60° (15.5°F) temperature at the induction port showed that the parallel FPTU was leaking primary air past the backflow damper out of the induction port and into the plenum. Leakage for this FPTU was also qualitatively determined through infrared thermography. The images clearly showed that cold air was leaking at the seams and backdraft damper of the unit.. The data clearly showed that some parallel units do leak.

Task 3 – Characterize leakage for use in parallel FPTU models

Air leakage data from six parallel fan powered terminal units that utilized electronically commutated motors were evaluated in Chapter 5. The original data were from an earlier investigation by Edmondson et al (2011). Units with both 8 in. (20.3 cm) and 12 in. (30.5 cm) primary inlets from three manufacturers were evaluated. The analysis included the impact of downstream static pressure, upstream static pressure, and primary airflow on the leakage from the units. Data for downstream static pressures ranged from approximately 0.1 in. w.g. to 0.5 in. w.g. (25 Pa to 125 Pa) and for upstream static pressures ranged from approximately 0.4 in. w.g. to 2.0 in. w.g. (100Pa to 498 Pa). Because the original data included some primary airflows outside the expected range of operation of the 8 in. (20.3 cm) and 12 in. (30.5 cm) fan powered terminal units, the data set was reduced to include only data in the expected primary airflow operating ranges of these sized units. All the original leakage data were collected with the fan powered terminal unit fan off and with only primary air flowing through the unit. No attempt was made to quantify how much leakage was from differing sources of leakage, such as the seams, penetrations, or backdraft damper.

Leakage was found to be primarily dependent on downstream static pressure. Leakage airflow showed little variation with either upstream static pressure or primary airflow when the downstream static pressure was held constant. Three leakage classifications were identified: low, medium, and high, based on the measured data. Correlations that describe the leakage as a function of downstream static pressure for each classification were developed. Calculations for a system with downstream static pressures varying with the square of primary airflow were performed and results presented. These leakage correlations can be used in building simulation models that utilize mass and energy balance approaches to modeling fan powered terminal units.

Task 4 - Develop models for alternative configurations/operations of series and parallel units,

A traditional mass and energy balance component approach was used to characterize the performance of both fixed (Chapter 6) and variable airflow (Chapter 7) series and parallel fan powered terminal units for applications in building simulation programs. The approach included developing relevant energy and mass balance equations for the components in a fan powered terminal unit – heating coil, fan/motor combination, and mixer. Fan motors that included permanent split capacitor motors controlled by silicon controlled rectifiers or electronically commutated motors were included in the model development. Chapters 6 and 7 demonstrated how to incorporate the fan/motor performance models into the system models in both fixed and variable airflow FPTUs. For the parallel FPTU models, two locations of the heating coil were considered. One location, designated as the traditional configuration, was at the discharge of the unit. The second location, designated as the alternative configuration, was at the secondary air inlet. Leakage was included in the parallel FPTU models.

Task 5 - Compare FPTU models developed here with prior work and EnergyPlus

The results of both the series and parallel mass and energy balance models were compared in Chapter 8 to a "black box" model developed by Davis (2010). The annual energy use from both approaches compared favorably. Comparisons were made for a small, five zone office building in five cities: Houston, Phoenix, Chicago, New York, and San Francisco. Davis (2010) reported results from these locations in his original analysis. Simulations were run for both PSC/SCR and ECM FPTUs. The heating and cooling loads in the building were generated by Davis (2007 and 2010) using the original DOE-2 building simulation program and were used as input into the EES model developed here. Davis (2010) normalized the loads in his simulations so all zones had the same design load. These normalized loads were used for the comparisons.

The two modeling approaches agreed to within 4% in annual energy use for all FPTUs (parallel and series) except for one case in San Francisco for the PSC/SCR series FPTU where the differences were 6%. For that case, the main contributor to the differences in energy use was the chiller energy use, not the FPTU fan or coil. While the two approaches used different ways to model the FPTU, the small differences in total energy use point to the fact that both the mass and energy balance and black box approaches can be used to simulate FPTUs.

Energy comparisons were also made with EnergyPlus in Chapter 9 where a single story, five zone office building was modeled in five different U.S. cities using EnergyPlus. The EnergyPlus model provided the zone peak load and hourly zone loads throughout a year. The models developed in Chapters 6 and 7 were incorporated into Engineering Equation Solver (EES). With the same input parameters, the system annual energy consumption was estimated by both the EES and EnergyPlus models, which included the energy consumption of the primary cooling coil, preheat coil, primary supply fan, terminal unit fan, and supplemental heating coil. Multiple runs were performed by using EnergyPlus and EES with various combinations of motor types (PSC and ECM), terminal unit types (series and parallel), and ECM capacity factor (0, 25%, and 50% larger than design airflow). The energy consumption of the FPTUs with PSC motors was selected as the baseline scenario, and the energy use of other cases were compared against this baseline and presented as the percentage increase or decrease relative to the baseline. The comparisons between the EnergyPlus and EES models only included fixed airflow FPTUs because EnergyPlus cannot model variable airflow FPTUs.

The EES model was then used to estimate the annual energy consequences of different FPTU performance options. In the comparison of series FPTUs, the annual energy consumption resulted from various combinations of airflow control (fixed and variable) and ECM capacity factor (0, 25%, and 50% larger than the design airflow) were compared with the baseline scenario (FPTU with PSC and fixed airflow operation) and presented in terms of percentage energy changes. In a similar way, comparisons of parallel units were conducted by using the results from combinations of airflow control (fixed and variable) and leakage level (0, 5%, and 10%) with the baseline scenario (FPTU with PSC and fixed airflow operation). Comparisons were also made between series and parallel FPTUs to investigate whether parallel units always yielded energy savings relative to series units. Additionally, the effect of moving the location of the heating coil in a parallel unit was evaluated.

Task 6 - Communicate with EnergyPlus developers to help ensure model data are incorporated into EnergyPlus

From the analysis conducted in this study, six specific improvements or changes needed in EnergyPlus were identified. These changes were identified in Chapter 7 and included: 1. PSC fan motors with SCR control, 2. ECM fan motors for fixed and variable airflow applications, 3.Realistic fan pressure differentials and fan/motor efficiencies, 4. Leakage in parallel FPTUs, 5. Alternative heating coil location in parallel FPTUs, and 6. Mixing of secondary air to ensure no condensation on registers or cold drafts. The Department of Energy (DOE) has a process for suggesting changes that include smaller issues that would be considered bug fixes to major issues which would be larger new features for EnergyPlus. In our estimate, Items 1 and 3 should fall under the smaller issues/bug fixes while Items 2, 5, and 6 would be larger new features. Item 4 (leakage in parallel FPTUs) might fall somewhere between being a minor or major implementation in EnergyPlus. Smaller issues/bug fixes can be submitted to a website (identified in Chapter 7). However, getting larger changes into EnergyPlus would require either submission to the DOE website for EnergyPlus and getting enough user support for DOE to include it in their update plan or separately contracting with an entity that has the expertise to program the changes into the appropriate EnergyPlus modules and submitting the final product to DOE.

ACKNOWLEGEMENTS

We wish to thank all the members of the Air Control and Distribution Devices Committee for their input and advice during the course of this project. In particular, the recommendations from Gus Faris (Nailor Industries) and Dan Int-Hout (Kreuger Air Systems Components) were invaluable in understanding the operations of fan powered terminal units in the field. In addition, we would like to acknowledge Jerry Sipes (Price Industries), who passed away before the completion of this project. He provided assistance in the early phases of this project when we trying to characterize the operations of electronically commutated motors. We would also like to thank Cheryl Tucker of Baylor University for her tireless efforts in helping put this report together.

NOMENCLATURE

$a_1 \ldots a_4$	Regression coefficients in part load power fraction
A	Cross-sectional area
$A_1 \ldots A_2$	Regression constants in leakage equation
AHRI	Air Conditioning, Heating, and Refrigeration Institute
AHU	Air handler unit
AMCA	Air Movement and Control Association
ASHRAE	American Society of Heating, Refrigeration, and Air Conditioning Engineers
CAV	Constant Air Volume
$C_{1 \ldots} C_3$	Regression constants in air leakage equation
COP	Coeffecient of performance
c_p	Specific heat
"Black Box" approach	"Black Box" fixed airflow FPTU model (Davis)
DOE	Department of Energy
E+	EnergyPlus
ECM	Electronically commutated motor
EES	Engineering Equation Solver
EIA	Energy Information Administration
f_{air}	Fraction of fan waste heat that enters airstream
f_{flow}	Part load airflow fraction (dimensionless)
f_{flow_do}	Part load airflow fraction for an ECM FPTU operating at the design airflow
f_{flowd}	Part load airflow fraction for an ECM FPTU whose maximum airflow just meets the design airflow
f_{flowo}	Part load airflow fraction for an ECM FPTU whose maximum airflow is larger than the design airflow
f_{leak}	Fraction leakage
f_{leakc}	Fraction leakage in cooling operations
f_{leakh}	Fraction leakage in heating operations
f_{pl}	Part load power fraction
FPTU	Fan Powered Terminal Unit
FPTU Coil	Total amount of supplemental heating energy added to the airstream by the heating coils over the entire year
FPTY Fan	Total energy used by 5 FPTU fans over the entire year
h	Enthalpy
h_{leak}	Euthalpy of leakage air
h_{out}	Enthalpy at FPTU outlet
h_{pri}	Enthalpy of primary air
h_{sec}	Enthalpy of secondary air
HVAC	Heating, ventilation, and air conditioning
m_{design}	Design air flow rate
m_{leak}	Leakage airflow
m_{min}	Minimum ventilation airflow for the zone
m_{pri}	Primary airflow

m_{sec}	Secondary airflow
m_{tot}	Total airflow of FPTU
MEB	Mass and energy balance
P_{dwn}	Downstream static pressure
$P_{dwn@design}$	Downstream static pressure at design airflow
P_{iav}	Inlet air velocity pressure
PIU	Powered induction unit
PLAF	Part load airflow fraction
PLPF	Part load power fraction
Pow_{dxo}	Fan motor power for an ECM FPTU operating at the design airflow
Pow_{fan}	Fan motor power at a given airflow
Pow_{fan_design}	Fan/motor power at the fan's maximum design airflow
Pow_{max}	Fan motor power at the maximum ECM setting
Pow_{rat}	Ratio of the power of an ECM FPTU operating at the design airflow to the power of a FPTU operating at maximum ECM setting to meet the design airflow
Pow_{sav}	Fractional savings in power of an ECM FPTU operating at the design airflow compared to a unit operating at its maximum ECM setting to meet the desisgn airflow
$Power_{fan}$	Ideal power consumed by FPTU fan, hp (W)
Primary Chiller	Estimated annual amount of energy required at the primary chiller plant to provide the primary cooling coil with chilled water
Primary Fan	Amount of energy used by the primary fan over the entire year
PSC	Permanent split capacitor
P_{up}	Upstream static pressure
P_v	Velocity pressure
q	Airflow delivered by the fan
q_{coil}	Energy input to the heating coil
$q_{Cramlet}$	Airflow for S8C FPTU in Cramlet's study
$q_{current}$	Airflow for S8C FPTU in current study
q_o	Airflow capacity of the fan above the design airflow
q_{z_design}	Design sensible load of the zone
q_{zl}	Latent load of the zone
q_{zs}	Hourly sensible load in the zone
Q	Airflow
Q_d	Fan airflow at the design load for the zone
Q_{fan}	Fan volumetric flow rate
Q_{fan_design}	Design airflow for the fan at its maximum design rating
Q_{flow}	Volumetric airflow
$Q_{induced}$	Airflow induced by terminal unit fan
$Q_{leakage}$	Airflow leaking from the FPTU
Q_{max}	Fan airflow at the maximum ECM setting
Q_o	Maximum fan airflow capacity for the a unit whose capacity exceeds the design airflow requirement of the zone
Q_{out}	Airflow downstream of the FPTU
$Q_{primary}$	Primary airflow

$Q_{primary@design}$	Primary airflow at design conditions
$QPow_{dxo}$	Fan motor power for the oversized unit at the design airflow
Q_{tot}	Volumetric flow rate of the air through fan
Q_{supply}	Volumetric supply airflow
Q_{zs}	Sensible heating or cooling load in the zone
RH	Relative Humidity
SCR	Silicon Controlled Rectifier
T	Temperature
T_{coil}	Heating coil outlet temperature
$T_{Cramlet}$	Air temperature in study by Cramlet
$T_{current}$	Air temperature in current study
$T_{f,out}$	Series fan outlet temperature
T_{mix}	Mixed air temperature
T_{oa}	Temperature of outside air
T_{out}	Outlet temperature from FPTU
T_{pri}	Primary air temperature
T_{sec}	Secondary air temperature
$T_{sec,out}$	Primary secondary outlet air temperature from fan for alternate parallel configuration
T_z	Zone air temperature
TPE	Total Plant Energy
TPE_{Davis}	Total Plant Energy by Davis model
TPE_{MEB}	Total Plant Energy by MEB model
Unit Type	A series or parallel FPTU
V	Average airflow velocity through test section
VAC	AC Voltage
VAV	Variable Air Volume
VSD	Variable Speed Drive
x_o	Capacity factor (dimensionless)
ΔP_{fan}	Air pressure rise across the fan
ΔP_{rise}	Differential total pressure rise across fan, in. w.g. (Pa)
ΔP_{tot}	Fan total pressure in w.g. (Pa)
ΔT	Temperature differential between zone and secondary air
ΔT_{fan}	Temperature increase of the air across the fan
α	Constant for FPTU outlet temperatures versus load
α_ρ	Regression coeffecient for fan power versus airflow
α_η	Regression coeffecient for SCR efficiency versus total pressure
β	Constant for FPTU outlet temperature versus load
η_{fan}	Fan total efficiency
η_{fm}	Fan/Motor total efficiency
η_{mot}	Fan motor efficiency
η_{tot}	Fan total efficiency
ρ_{air}	Density of the air
Υ	Constant for airflow versus sensible load
δ	Constant for airflow versus sensible load

TABLE OF CONTENTS

CHAPTER 1

INTRODUCTION

Variable air volume (VAV) systems are designed to vary the amount of conditioned air delivered to a zone to maintain space comfort. Conditioned air from an air handler unit (AHU) is delivered by the central primary (supply) fan through the duct system to VAV terminal units. These terminal units provide air to each zone. Terminal units with fans are called fan-powered terminal units (FPTUs). FPTUs mix secondary with primary air, provide additional pressurization to the air, and supplemental heat (when needed) to the air before the air is delivered to the zone the FPTU is serving. They also make it possible to reduce the central supply fan operating pressure and reduce the air distribution system's energy consumption (ASHRAE 2012).

FPTUs come in two configurations: series and parallel. When the fan in the FPTU is in series with the primary supply fan, the configuration is called a "series" FPTU. In a series FPTU, all primary and secondary (induced) air passes through the FPTU blower, which operates continuously during the normal operating hours of the HVAC system. In a parallel FPTU, the fan operates intermittently. It is located in the secondary airstream and operates in "parallel" with the primary airstream. It is used to induce air into the FPTU during heating and deadband operations.

1.1. Background

Manufacturers utilize permanent split capacitor (PSC) motors and electronically commutated motors (ECM) to drive the fans in FPTUs. While the speed of both PSC motors and ECMs can be varied, PSC motors are applied in situations where the airflow provided by the FPTU fan is fixed. A silicon controlled rectifier (SCR) is used to control the speed of a PSC motor. For FPTU applications, the airflow for a SCR controlled PSC motor is set by a technician in the field and typically not changed after installation or commissioning. The speed of ECMs is varied with the use of a DC voltage controller. ECMs in series FPTUs can be used to either run the fan at a fixed airflow or their speed can be varied so the airflow from the FPTU matches the required load in the zone. For a fixed airflow application, the field technician sets the ECM controller to supply the design airflow during installation and/or commissioning of the FPTU similar to what is done with a PSC fan motor controlled by a SCR. For a variable airflow application, the ECM

can be tied into a building automation system and the airflow varied to provide the desired amount of airflow to just meet the thermal load requirement of the zone.

The fan motors in FPTUs are matched with FPTU fans and come as an integrated assembly. While the fan motors in FPTUs are small, typically one hp (746 W) or less, there may be many of these in a building, so their contribution to the total energy use may be significant.

EnergyPlus (2013) is a widely used building simulation program that can be used to estimate the annual energy usage of a wide range of buildings and the systems in the building. Both series and parallel FPTUs can be modeled. The EnergyPlus *Engineering Reference* (EnergyPlus 2013) discusses the calculation procedures used to model FPTUs. Within EnergyPlus, a FPTU is called a powered induction unit (PIU). Rather than using their PIU terminology, the more generic FPTU term is used in this study.

EnergyPlus uses a simple component approach to simulate the performance of FPTUs. It makes the assumption that both series and parallel FPTUs can be modeled as a combination of three major components: a mixer, a constant volume fan, and a heating coil. Figures 1.1 shows the placement of the components used to model a series FPTUs in EnergyPlus.

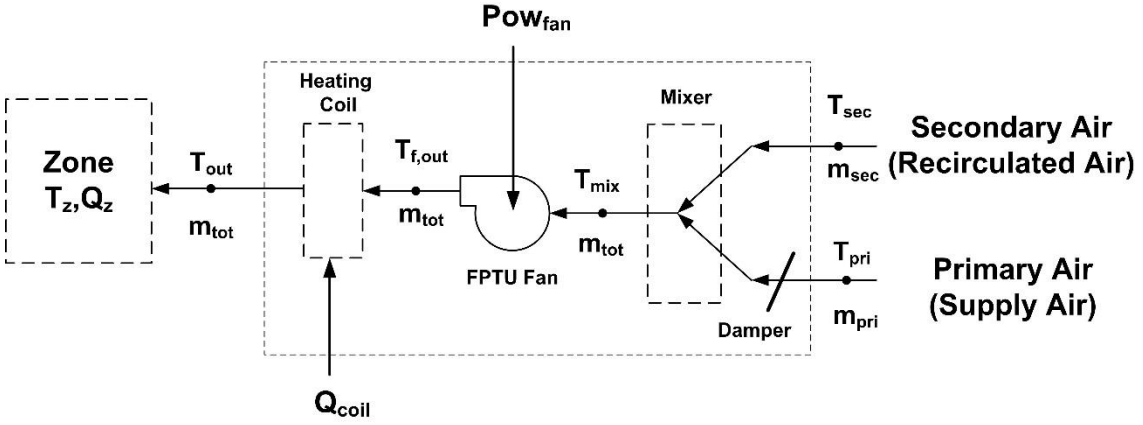

Figure 1.1: Components and energy and mass flows in the simulation of a series fan powered terminal unit in EnergyPlus

EnergyPlus assumes that there is no pressure interaction between the components in a FPTU. Each component has a submodel which is connected via mass and energy balances to the other components. Once the zone loads are determined, then the mass and energy balances can be used to determine the energy use and airflow requirements of the FPTU. While the damper is not explicitly modeled in EnergyPlus, the program does use an energy and mass balance calculation to estimate the distribution of airflows between the primary and secondary air

streams. This calculation mimics the main function of the damper (i.e., control the amount of airflow).

Before a simulation is started for a series FPTU, the user can specify a number of design flow rates (maximum total airflow rate, maximum primary air flow rate, and minimum primary airflow fraction) or these values can also be autosized by the program. The user is required to input the fan properties shown in Table 1.1. The fan calculation submodel assumes a constant speed fan for both series and parallel FPTU fans. Even though the fan motor controller can vary the speed of the FPTU fan, the controller voltage is typically set during installation of the unit or commissioning of the building to meet airflow requirements in the zone and stays at that value unless manually adjusted later. The assumption that the fan is at a constant speed is only true if the pressure differential across the fan remains constant. If the pressure differential varies, then the controller will adjust fan speed in an attempt to keep the fan airflow constant.

Table 1.1. - Fan Characteristics Used for Series FPTUs in EnergyPlus

EnergyPlus Fan Input Characteristics
Design air pressure rise across the fan, ΔP fan
Design volumetric flow rate, m_{design}
Fan total efficiency, η_{fan}
Fan motor efficiency, η_{mot}
Fraction of fan waste heat that enters airstream, f_{air}

The user inputs the fan total efficiency (η_{tot}) and the fan motor efficiency (η_{mot}) separately as well as a "design air pressure rise across the fan", ΔP. It is assumed that the pressure rise is the total pressure rise across the fan. The static pressure rise could be used, but the definition of the fan efficiency would require use of fan static efficiency rather than fan total efficiency. Typically, pressure differentials should be substantially less than 1 in w.g. (250 Pa) for fans in FPTUs. The static pressures downstream of the FPTU are typically set less than 0.5 in w.g.(125 Pa). The FPTU test procedure (AHRI 2011) requires downstream static pressures of 0.25 in w.g.(62 Pa). The fan efficiency is assumed to be associated with the total pressure across the fan rather than the static pressure, but the documentation is not clear. The individual fan and motor efficiencies are rarely provided separately by the FPTU manufacturers. For the small fans

and fan motors used in FPTUs, the fan and motor are usually tested as a unit rather than individually.

EnergyPlus has a default fan efficiency of 70%, which is a value more appropriate for a central air handler, but not for the smaller fan/motor combinations used in FPTUs. O'Neal, et al (2014) recently published efficiency data for a SCR controlled FPTU fan/motor combination where the SCR controlled motor used 400 W at the 277 VAC rating point. The total efficiency of this fan/motor combination varied from 5 to 20% for fan static pressures ranging from 0.2 to 0.6 in. w.g. (50 to 149 Pa). While these data were for just one FPTU fan/motor combination, it illustrated that the fan/motor efficiencies for these smaller fans were less than the default fan efficiency used in EnergyPlus. Better performance data for FPTUs are needed for use in building simulation programs to help building professionals better evaluate the energy use in buildings that utilize FPTUs.

1.2. Purpose

This report summarizes the work performed under Project 8012 that was funded by the Air Conditioning, Heating, and Refrigeration Institute (AHRI) and involved numerous manufacturers throughout the course of the project. The primary purpose of this project was to develop models of fan powered terminal units that could be used in building simulation models that utilize a mass and energy balance approach, such as EnergyPlus. The models developed included both series and parallel terminal units, SCR/PSC and ECM motor technologies, fixed and variable airflow FPTUs, leakage in parallel units, and FPTU control strategies not currently employed in EnergyPlus.

Following this introductory chapter, there are nine more chapters in this report. The initial focus of the project was collecting data and developing models of different types of fan/motor combinations used in FPTUs. Chapter 2 summarizes the data and development of the model used to characterize the performance of PSC fan motors controlled by SCRs. Chapter 3 focuses on the development of two models used to characterize the fan/motor performance fans controlled by ECMs. One of the models can be used for fixed airflow cases and the second model for variable airflow cases. Chapter 5 summarizes measurements made on FPTUs in the laboratory and the field. Items of interest included pressure differential across the FPTU fan, downstream static pressure, and qualitative data on leakage of parallel FPTUs. The fixed airflow series and parallel FPTU models are developed in Chapter 6 while the variable airflow models

are developed in Chapter 7. Comparison between the fixed airflow models and he FPTU model developed by Davis (2010) are presented in Chapter 8. Chapter 9 summarizes the comparisons between the FPTU fixed airflow models in EnergyPlus and those developed here. In addition, estimates of the savings of using variable airflow FPTUs are presented in this chapter. Chapter 10 presents conclusions and recommendations.

CHAPTER 2
SCR FAN/MOTOR PERFORMANCE MODELS

Both permanent split capacitor (PSC) motors and electronically commutated motors (ECMs) are used to drive the fans in FPTUs. The speed of a PSC motor can be controlled by a silicon controlled rectifier (SCR). ECM's speed can be varied with the use of a controller that provides a DC voltage to the motor. In traditional applications, the field technician sets the speed of the motor to supply the design airflow into the zone served by the FPTU. Once the speed of the fan is set during installation and/or commissioning of the FPTU, the controlled setting of the motor typically does not change. With ECMs, the motor can either be set at a fixed setting or can be integrated into a building automation system so the speed of the motor (and fan) can be varied to meet the load within the zone served by the FPTU.

Unlike large central air handling units, the fan motors in FPTUs are matched with FPTU fans and come as a working pair. The fan motors in FPTUs are small - typically one hp (746 W) or less. It is not unusual in large commercial buildings to have dozens or even hundreds of FPTUs installed, depending on the size of the building. Such large numbers of FPTU fan/motors in a building means that the sum of the FPTUs can make a significant contribution to the energy use of a commercial building.

The purpose of this chapter was to evaluate performance data and develop models for a wide size range of SCR controlled PSC fan/motor combinations used in FPTUs. The models generated in this chapter should allow an energy modeler to more accurately estimate the annual performance of FPTUs in building energy simulation programs.

2.1. Data Collection

Three FPTU manufacturers provided data to this study. The manufacturers are identified as manufacturers A, B, and C in the tables and figures below. The data covered a wide range in fan motor sizes from 1/8 hp (93 W) to 1 hp (746 W). Table 2.1 shows the fan motor sizes provided by each manufacturer. Overall, there were 12 fan/motor combinations evaluated that should cover much of the range of FPTUs' fans and motors expected to be used in the field. Manufactures apply these fan/motor combinations in a range of cabinet sizes and cabinet styles (underfloor or overhead) and "low" and "standard" profile cabinet styles. Each cabinet design potentially produces different flow conditions entering the FPTU fan which could generate differing air system effects that impact the overall performance of the fan.

Data were collected on fan/motor combinations by manufacturers in their own laboratories and provided to the authors through a representative of the Air Conditioning Heating and Refrigeration Institute (AHRI) so that the identity of the manufacturer remained anonymous. All FPTUs were designed for 277 volt applications. Manufactures were asked to provide both descriptive (see Table 2.2) and performance data (see Table 2.3) on the fan/motor combinations. Table 2.4 summarizes the range in SCR voltage settings and discharge static pressures in the data sets provided by each manufacturer. The SCR voltage settings ranged from a low of 110 V in one of manufacturer B's units to a high of 277 V in all of manufacturer A's units. The discharge static pressures were set at anywhere from 0 in w.g. (0 Pa) upto 0.75 in w.g. (187 Pa).

Table 2.1 – FPTU Fan/Motor Data Provided by the Manufacturers

Fan Motor Size hp (W)	Manufacturer A	Manufacturer B	Manufacturer C
1/8 (93)		X	
1/6 (125)	X		
1/4 (187)	X		
1/3(248)	X	XX*	
1/2 (373)	X	XX*	XX
3/4 (560)			
1 (746)		X	
2 x 3/4 (560)			

*Multiple "Xs" in an entry indicate the manufacturer provided more than one unit at that size.

Table 2.2 – Descriptive Data for FPTU and Fan/Motor Combinations

Item
Fan Model Number
Series or Parallel FPTU Application
Primary Inlet Diameter
Design range of airflow of FPTU
Recommended operating pressures
Maximum recommended airflow
Minimum recommended airflow
Fan manufacturer
Motor manufacturer
Motor Size
Fan discharge dimensions

Table 2.3 – Detailed Measured Performance Data on each FPTU Fan/Motor Combination

Item	Units
SCR voltage	volts*
discharge static pressure	in w.g. (Pa)
airflow	ft^3/min (m^3/s)
current	amps
volt-amps	volt-amps
power factor	-
power	W
motor speed	rpm
power/airflow	W/(ft^3/min) W/(m^3/s)

Table 2.4 – SCR and Discharge Static Pressure Ranges Provided by each Manufacturer

Quantity	Range of Values		
	Manufacturer A	**Manufacturer B**	**Manufacturer C**
SCR Voltage	140 to 277 V	110 to 276 V	Low to High*
Discharge Static Pressure	0 to 0.62 in w.g. (0 to 154 Pa)	0.1 to 0.75 in w.g. (25 to 187 Pa)	0.1 to 0.6 in w.g. (25 to 149 Pa)

*Manufacturer C provided low, mid low, mid high, and high for the SCR voltage settings.

An identification procedure was developed for reporting each fan/motor combination. Because all of the fan motors in this paper were SCR controlled, all designations start with "SCR". Fan motor sizes ranged from 1/8 to 1 hp (93 to 746 W). The fan motor size in horsepower was converted to its decimal equivalent (1/2 = 0.50) and multiplied by 1000. For example, a 1/2 hp (373 W) fan's decimal equivalent is 0.500. Multiplying by 1000 gives a value of 500. Three manufacturers (A, B, and C) provided data. Combining the SCR designation, motor size, and manufacturer provided the identifier used in this paper. A 1/2 hp (373 W) fan/motor from manufacturer A is identified as SCR-500A. If a manufacturer had more than one fan/motor combination of the same size, such as manufacturer B had for 1/2 hp (373 W), then one fan/motor was identified as SCR-500B1 and the second as SCR-500B2.

2.2. Data Analysis

Each manufacturer provided their data in spreadsheets. With the discharge area of the fans provided, it was possible to calculate the exit air velocity from the discharge area and measured airflow. With the exit velocity known, the velocity pressure was calculated and added to the measured static pressure differential across the fan to obtain a fan total pressure. The fan/motor total efficiency, η_{fm}, was calculated using fan total pressure, mass flow of the air, and fan power.

$$\eta_{fm} = \frac{Q_{flow} * \Delta P_{tot}}{Pow_{fan}} \quad (2.1)$$

Where,

ΔP_{tot} = fan total pressure – in w.g. (Pa)

Pow_{fan} = power of the fan motor – W

Q_{flow} = fan volumetric airflow – ft^3/min (m^3/s)

Figures 2.1 and 2.2 show sample data for the fan/motor total efficiency versus fan total pressure for the 1/4 hp (187 W) and 1/2 hp (373 W) fan/motor combinations from manufacturers A and B, respectively. The fan/motor efficiency showed a direct dependence on the fan total pressure.

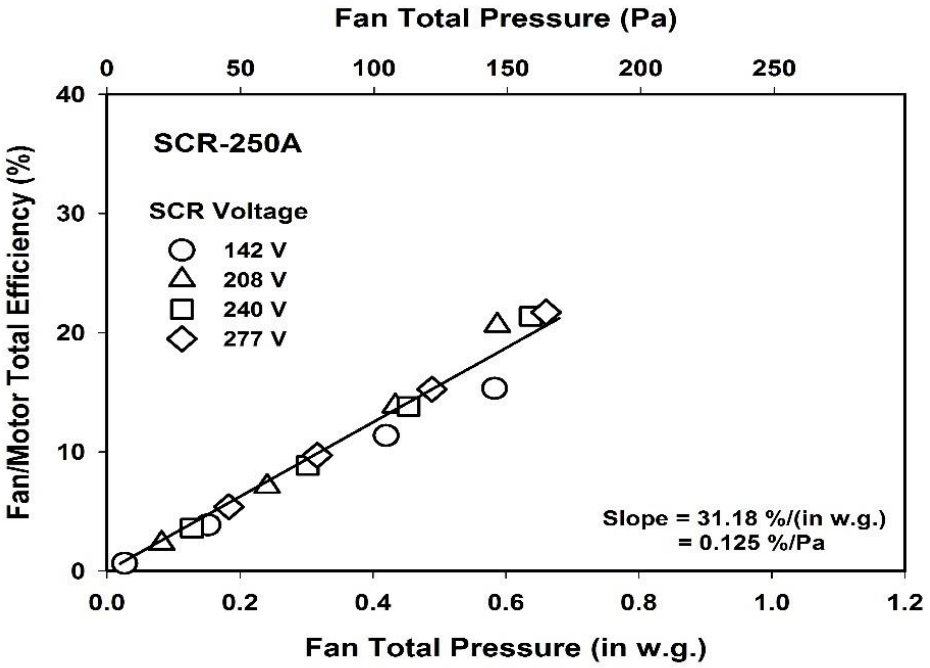

Figure 2.1: Fan/Motor Performance Data for SCR-250A

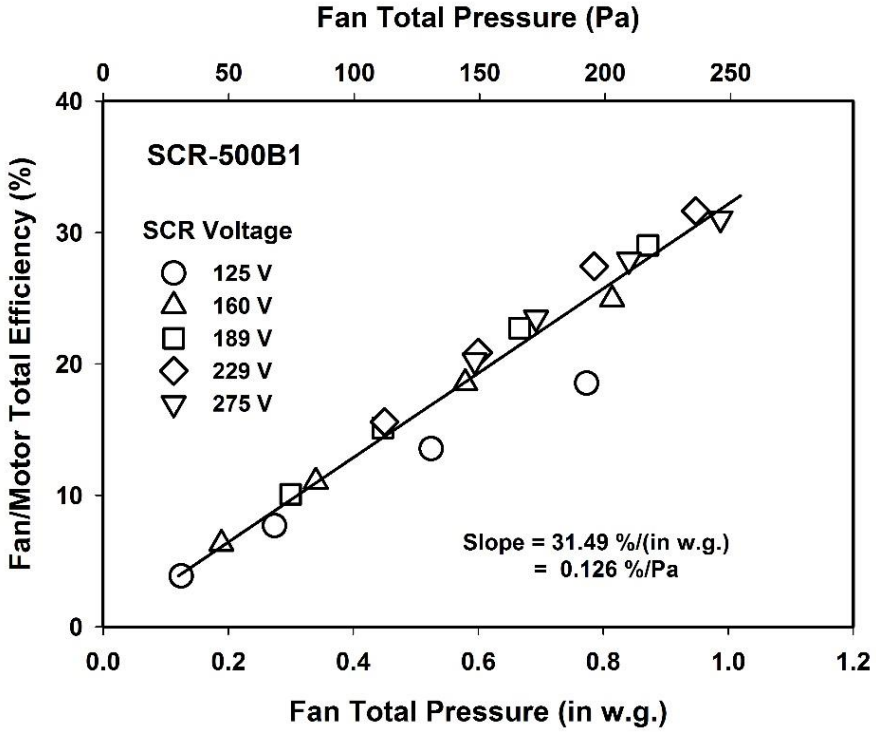

Figure 2.2: Fan/Motor Performance daSCR-500B1.

Four observations can be made from the data in Figures 2.1 and 2.2. First, there was an almost linear relationship between fan/motor efficiency and fan total pressure. The r-squared values for the regressions in Figures 2.1 and 2.2 were 0.99 for both SCR fan/motor combinations. In building simulation programs such as EnergyPlus, the fan efficiency and fan total pressure are treated as independent variables. Figures 2.1 and 2.2 showed that they should not be treated independently for SCR controlled PSC motors applied to FPTUs. If the total pressure was specified, then the fan/motor efficiency was also known within the uncertainty of the correlation. A second observation was that both Figures 2.1 and 2.2 showed that there was not a single efficiency for a particular fan/motor combination. The fan/motor efficiency depended on the total fan pressure. If there were variations in total fan pressure during the operation of a FPTU over the course of a day, week, or year, then the efficiency would also vary. Unfortunately, there were little data on the operating total pressures across the fan within a FPTU for operating conditions found in the field. A third observation from these figures was that the fan/motor efficiencies of small SCR fan/motor combinations were relatively low. For the SCR-250A, the fan/motor efficiencies ranged from low single digits up to 22% while for SCR-500B, they ranged from about 5% to 32%. A fourth observation from these plots was the relatively low total pressures these fans can produce. For the SCR-250A, the maximum total pressure was 0.66 in w.g. (164 Pa), while for SCR-500B, it was 0.99 in w.g. (247 Pa). The discharge static pressures that the two fans in Figure 2.1 and 2.2 operated at varied from 0 in w.g. (0 Pa) up to 0.75 in w.g. (187 Pa). These total pressures were a fraction of the total pressures expected to be produced by a large central air handler in a commercial building.

Because the fan/motor total efficiency data appeared to be nearly linear with respect to total pressure, the data were fit with a simple line that went through the origin. This meant that the total efficiency and total pressure were related by a simple constant, α_η:

$$\eta_{fm} = \alpha_\eta * \Delta P_{tot} \tag{2.2}$$

α_η has units of %/(in w.g.) in the IP system and %/Pa in the SI system of units. The fan/motor total efficiency in Equation 2.2 was substituted back into Equation 2.1 and rearranged to solve for the fan power. The result showed that the fan airflow, Q_{flow}, and fan motor power should also be linearly related since α_η is a constant:

$$Pow_{fan} = \frac{Q_{flow}}{\alpha_\eta} \tag{2.3}$$

If the airflow is in ft^3/min (m^3/s) and the power is in W, then the constant, α_η, would need to be multiplied by the proper unit conversions to get the units in Equation 2.3 to come out correctly. Equation 2.3 can be rewritten with a new constant, α_p, which includes the unit conversions:

$$Pow_{fan} = \alpha_p * Q_{flow} \tag{2.4}$$

Equation 2.4 was a surprising result. It was completely unexpected that the fan power would be simply related to the airflow by a constant. However, Equation 2.4 was derived directly from the definition of fan efficiency and the experimental data that showed the linear relationship between fan/motor total efficiency and fan total pressure. Figures 2.3 and 2.4 showed the power and airflow plots for the same two fan/motor combinations in Figures 2.1 and 2.2, respectively.

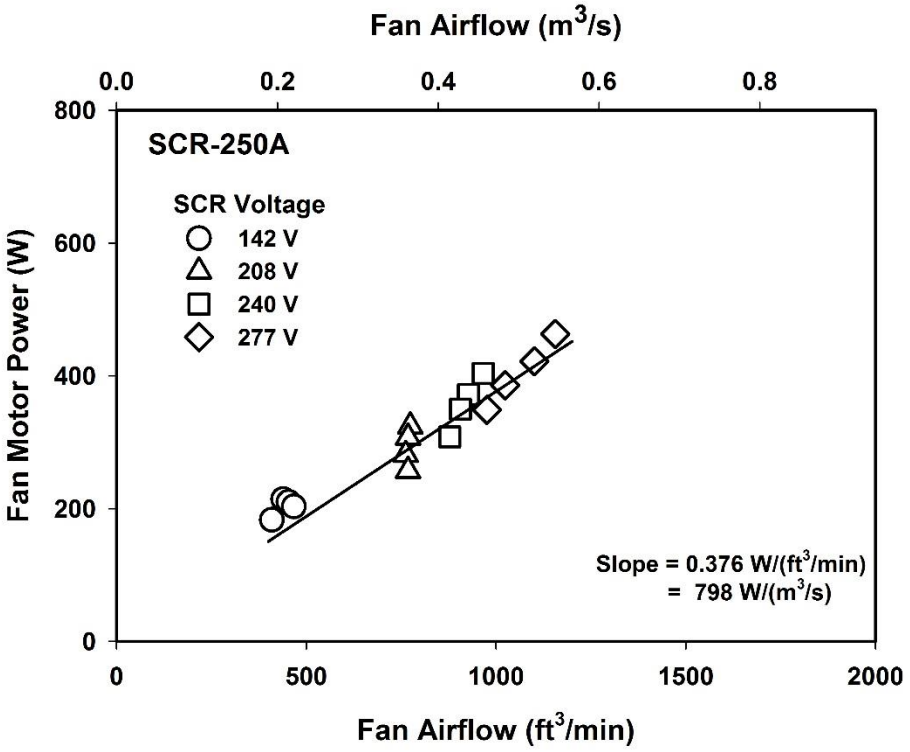

Figure 2.3: Fan Motor Power Versus Fan Airflow for SCR-250A

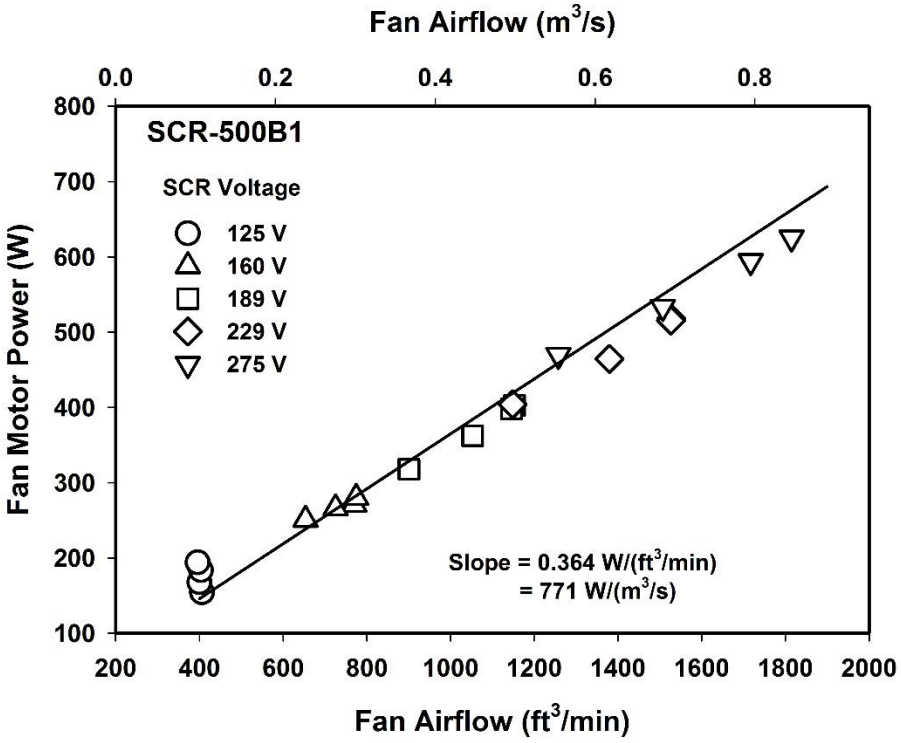

Figure 2.4: Fan Motor Power Versus Fan Airflow for SCR-500B1.

While there was scatter in the data, the plots showed the same general linear trends that would be predicted from Equation 2.4. Some of the scatter in Figure 2.3 occured at specific SCR voltages. For example, at 208 volts, the airflow varied over a very narrow range of 762 to 774 ft^3/min (0.36 to 0.37 m^3/s) while the power varied from a low of 257 to 324 W. This resulted in some horizontal compression of data in the plots around a narrow range of flows for some of the units.

The general linear trend in the plots was powerful, because it implied, when modeling SCR controlled PSC motors in FPTUs in building simulation programs, the efficiency and pressures did not need to be known or specified explicitly for the FPTU. Instead, for the modeler, if the airflow was known, then the power consumed by the fan motor could be estimated from relationships similar to what was found in Figures 2.3 and 2.4. The constant, α_p, is a familiar term in that it is the power divided by airflow. In IP units, it is W/(ft^3/min) and in SI units, it is W/(m^3/s). Essentially, Equation 2.4 implied that for modeling purposes, the power divided by airflow can be treated as a constant for SCR controlled PSC motors. While there was scatter around the average slope (α_p), it would appear a constant can be used for relating the power and airflow of SCR controlled PSC fan/motor combinations in building simulation programs. If

building simulation programs do not have this simple option of modeling SCR controlled fan motors, then they should be modified. This relationship provided realistic performance information based on experimental data. Manufacturers typically have data on power/airflow for their specific units. Such data combined with the model in Equation 2.4 could provide the energy modeler with the capability to quickly estimate the power used by specific FPTUs that had SCR controlled fan motors. With the absense of specific data, then the more generic numbers developed below could be used.

As mentioned above, the constant, α_p, had units of W/(ft^3/min) in IP units. α_p was related numerically to α_η by the following in the IP system:

$$\alpha_p = \frac{11.75}{\alpha_\eta} \tag{2.5}$$

For SI units, α_p had units of W/(m^3/s) and α_η had units of %/(Pa), then α_p was related numerically to α_η by the following:

$$\alpha_p = \frac{100}{\alpha_\eta} \tag{2.6}$$

For both fan/motor combinations, the data for the lower SCR voltages showed a lower efficiency compared to the rest of the data at higher total pressures. This drop-off showed up more in data from manufacturer B than either A or C. In previous work done on SCR fan/motor combinations by Furr et al (2007), they found it was difficult to get the SCRs consistently to operate below about 160 V. In communicating with engineers with two manufacturers who provided data to this study, they indicated that the efficiency decreased at the lower voltages (and speeds) for a SCR controlled PSC motor. They also indicated they did not like to see the speed of the motor operate below about 600 rpm. Furr et al (2007) measured the speed of three SCR controlled fan motors. One of the motors was 1/4 hp (187 W). It operated below 600 rpm when SCR voltages were below 190 V. Based on the data from Furr et al (2007) and communications with engineers from the companies providing the data, it was decided to exclude all performance data below 160 volts from the analysis presented below.

Figures 2.1 through 2.4 showed the results for two fan/motor combinations from two different manufacturers. A very relevant question was: "Do the linear relationships shown in those figures hold for other fan/motor combinations?" To answer that question, data from all of the fan/motor combinations for each manufacturer were plotted to see if the linear relationship still held within the units provided by each manufacturer. Figures 2.5 and 2.6 showed the

fan/motor total efficiencies plotted against total pressure for all of the fans provided by manufacturers A and B. Because manufacturer C only provided data on two fan/motor combinations and both had the same motor size, their data were only included in the final two plots later in this chapter. While there was scatter in the data from both manufacturers, it was surprising how well the efficiency/pressure data fell along roughly the same slopes for the two manufacturers. The r-squared for the data in Figure 2.5 was 0.979 while that for the data in Figure 2.6 was 0.994. As implied above, if the efficiency versus total pressure relationship was linear, then the fan motor power versus airflow was also linear. Figures 2.7 and 2.8 again showed that fan motor power can be correlated linearly with fan airflow.

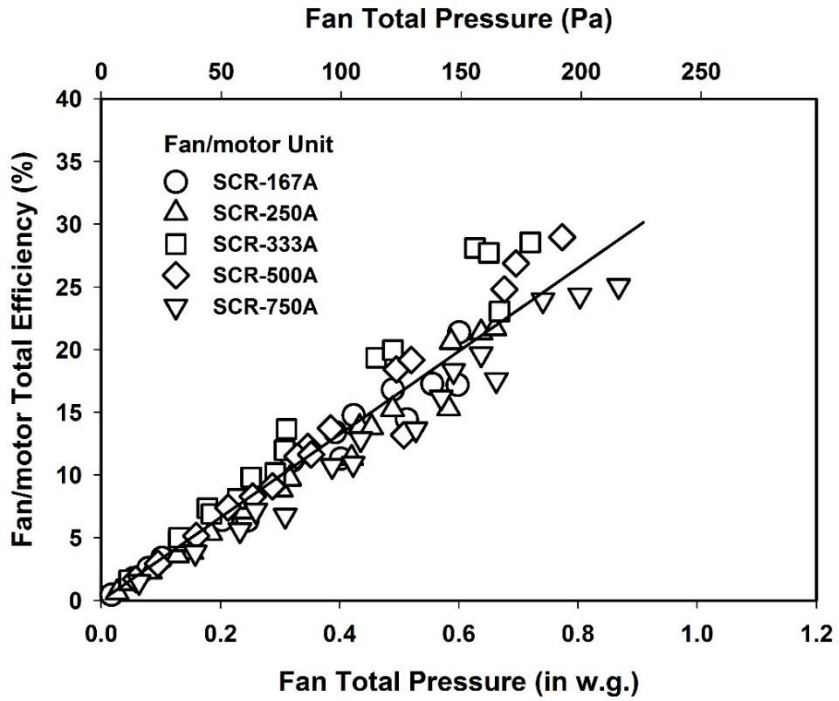

Figure 2.5: Fan/Motor Total Efficiency Versus Fan Total Pressure for all Fan/Motors from Manufacturer A

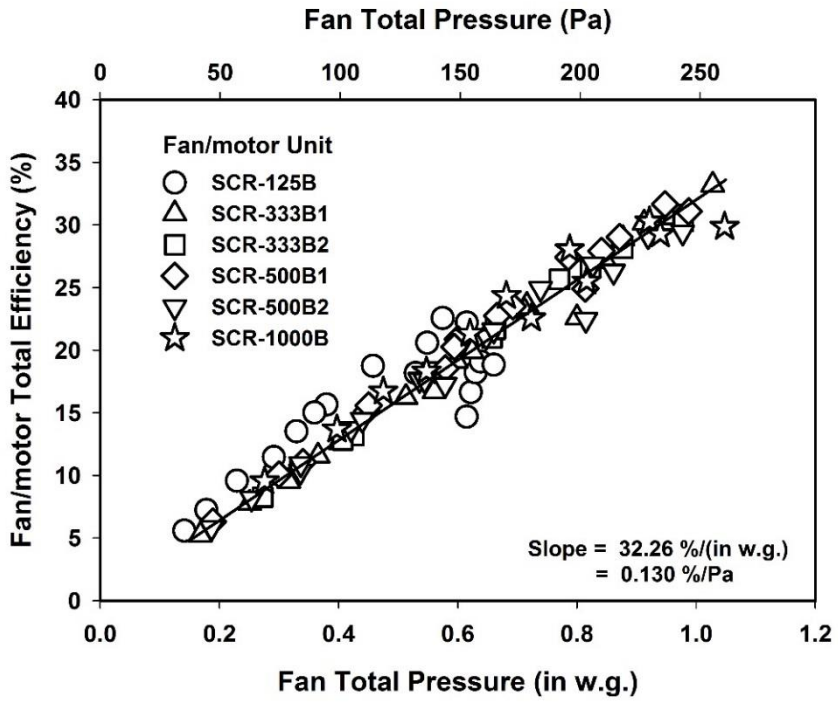

Figure 2.6: Fan/Motor Total Efficiency Versus Fan Total Pressure for all Fan/Motors from Manufacturer B

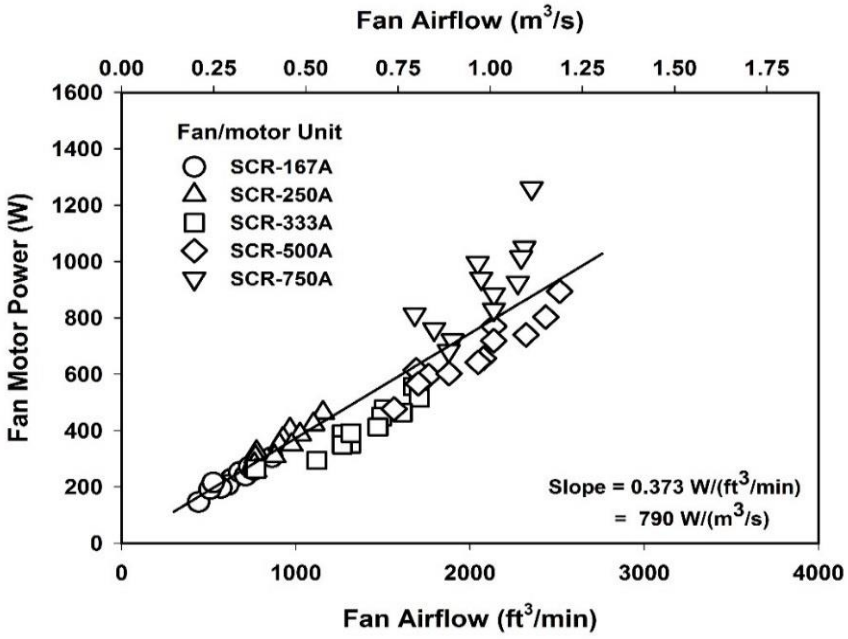

Figure 2.7: Fan Motor Power Versus Fan Airflow for all Fan/Motors from Manufacturer A

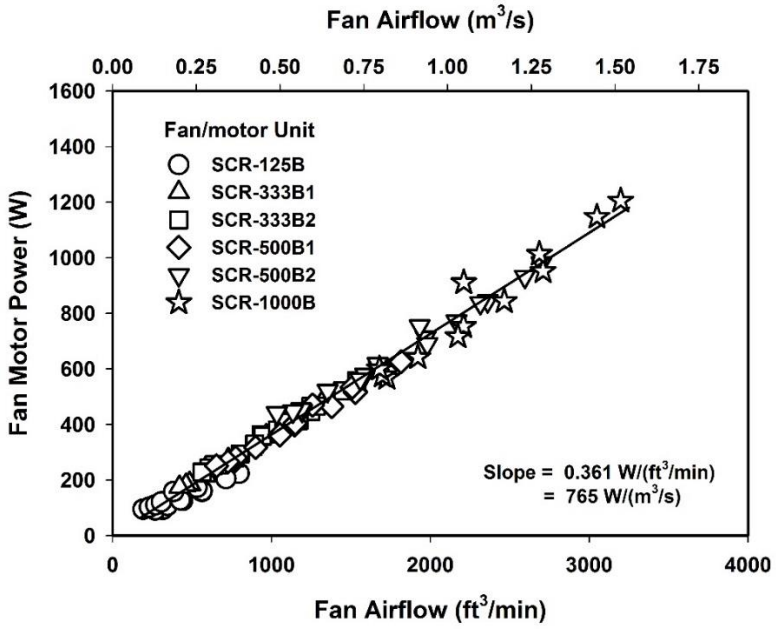

Figure 2.8: Fan Motor Power Versus Fan Airflow for all Fan/Motors from Manufacturer B

The data from manufacturer A showed more scatter than that from manufacturer B. The r-squared for manufacturer's A data was lower (0.971 vs 0.997) when compared to manufacturer's B data. However, given the wide range in fan motor sizes, from 1/8 hp (92 W) to 1 hp (746 W), both the efficiency/total pressure data and the power/airflow data showed high correlation.

In modeling energy use in buildings, the modeler often may not be interested in a specific manufacturer's line of FPTUs, but is looking for more generic relationships for the performance of the fan/motors in the FPTUs. To get to a more generic or averaged values of the fan/motor efficiency and power, the data from all manufacturers were combined into the same plots. Figure 2.9 shows the fan/motor efficiencies plotted versus fan total pressure for the three manufacturers.

As with the individual manufacturer's data, there continued to be a strong correlation between fan/motor efficiency and fan total pressure. The line fit to the data in Figure 2.9 had a r-squared of 0.983. The fan motor power versus fan airflow for all manufacturers is shown in Figure 2.10 and also shows an excellent correlation with a r-squared of 0.978.

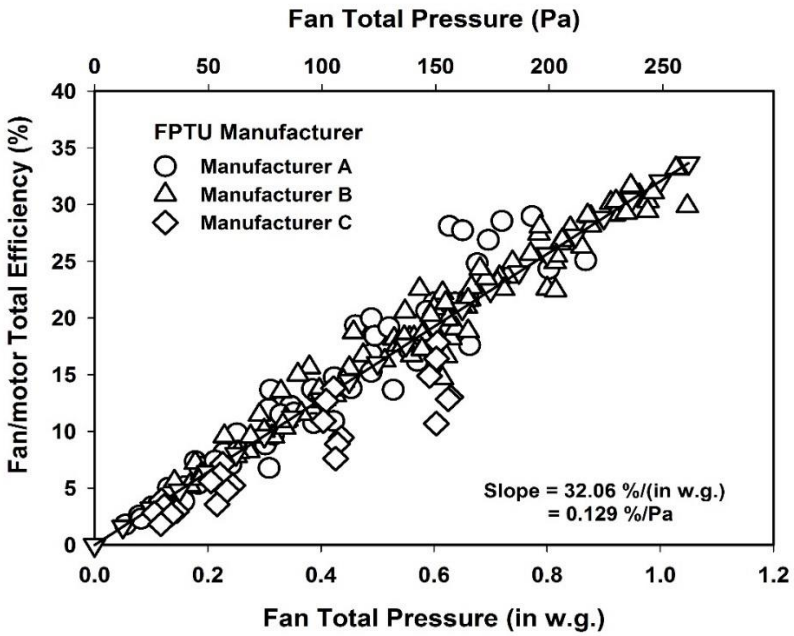

Figure 2.9: Fan/Motor Total Efficiency Versus Fan Total Pressure for all Fan/Motors from all Manufacturers

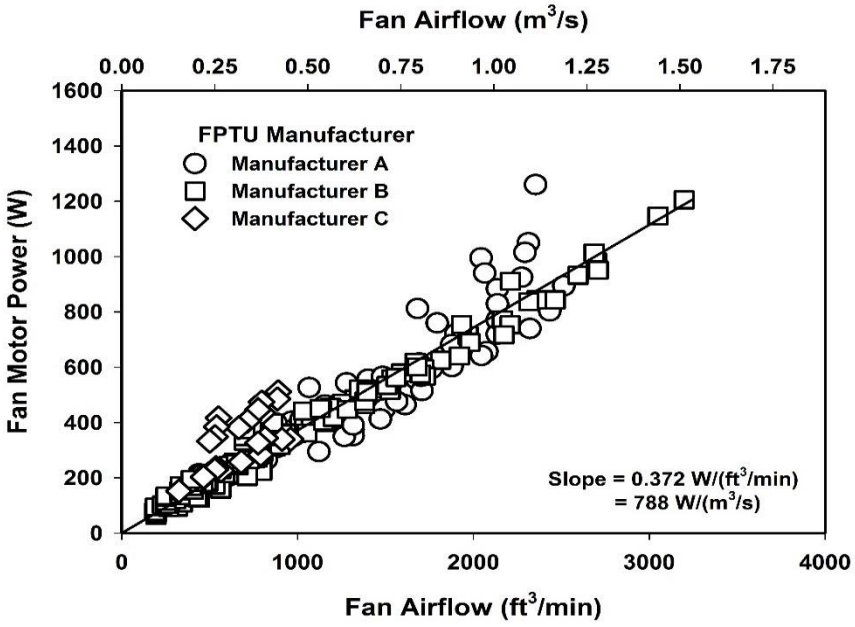

Figure 2.10: Fan Motor Power Versus Fan Airflow for all Fan/Motor Manufacturers

Even with the high r-squared values, there was still significant scatter in the data. For example, in Figure 2.9, the fan/motor efficiency varied from as low as 10.5% to as high as 28% for a fan total pressure of 0.6 in w.g. (149 Pa). Likewise, in Figure 2.10, the fan motor power varied from about 750 W to over 1200 W for an airflow of about 2300 ft^3/min (1.09 m^3/s). The slopes for

both figures represented the average relationships between the two variables in each plot. For building modelers attempting to simulate a generic SCR controlled FPTU, the values of the slopes in either Figures 2.9 or 2.10 should provide average input performance characteristics for the fan/motor. To model a specific manufacturer's FPTU, the above methodology could be used along with the appropriate power/airflow values for the fan/motor used in the FPTU.

2.3. Summary

This chapter sought to fill a gap in performance data and models for SCR controlled fan/motors used in fan powered terminal units. Three manufacturers provided detailed experimental data on 12 fan/motor combinations employed in commercially available fan powered terminal units. The fan motors ranged in size from 1/8 hp (93 W) to 1 hp(746 W). The fan maximum airflows ranged from 690 to 4524 ft^3/min (0.33 to 2.14 m^3/s).

The models developed from the data were simple linear relationships between fan/motor efficiency and fan total pressure and between fan motor power and fan airflow. These relationships should provide a user of building energy simulation programs with the input and models needed to provide reliable estimates of the hourly and annual performance of SCR controlled fan motors used in FPTUs. There was still significant scatter in the data to use these relationships to model a particular manufacturer's specific FPTU. However, for the modeler desiring to model a generic FPTU, the fan/motor relationships should provide the modeler with data that would provide estimates near the average of the SCR controlled fan/motor combinations that are currently in use in FPTUs.

CHAPTER 3
ECM FAN/MOTOR PERFORMANCE MODELS

Electronically commutated motors (ECMs) are increasingly being used as the motors of choice to drive the fans in (FPTUs). As a consequence, it is important that accurate and simple-to-use models be developed for ECM FPTUs that can be implemented in building simulation programs. One approach to modeling FPTUs was to break the FPTU into its components (fan, motor, mixer, and heating coil) and utilize energy and mass balances of each components (EnergyPlus 2013). The user inputs on the fan include efficiency and pressure drop across the fan. The fan motor efficiency was input separately from the fan efficiency. However, manufacturers test the FPTU fan/motor combinations together rather than separately. Thus, efficiency should be specified for the fan/motor combination not the individual components in these models. The user of building simulation programs requiring input of fan efficiency and total pressure was left to estimate these values and hope those estimates were reasonable. It would be useful to have an alternative approach to modeling ECM FPTUs that didn't require knowledge of fan efficiency and total pressure. Ideally, the alternative modeling approach would utilize data that manufacturers were already providing in their engineering data sheets and would provide a reasonably accurate way to model ECM FPTUs.

Another aspect of the performance of series ECM FPTUs related to their additional capacity relative to the design cooling or heating loads (and airflows) in the zone the FPTU serves. There are two ways in which an engineer is encouraged (or required) to install a FPTU with capacity larger than the airflow at the design load. The first is found in ASHRAE 90.1(2010), section G3.1.2.2, where for simulating the baseline annual energy use in a building, equipment capacities are required to be oversized by 15% for cooling and 25% for heating. For the modeler, if the FPTU is run at this additional capacity value, it could mean that the energy used by a fixed airflow series FPTU in the building simulation model could be higher than that for a series FPTU that is just sized to the design load. For a fixed airflow application, an ECM FPTU set at the design airflow would use less fan energy than if that same ECM FPTU were set at the 15% to 25% oversized airflow requirement. If the ECM was operating in a variable airflow mode where it tracked the load, then the potential for savings was even larger than for a fixed airflow application. What would be useful to the modeler is a way to estimate the savings of a larger

capacity ECM FPTU that operated at a lower speed to meet loads in the zone – whether it were a fixed or variable airflow FPTU.

Another factor encouraging the installation of larger series FPTUs is the desire to reduce the noise produced in the air distribution system. Some manufacturers in their engineering and application guides encourage "upsizing" (or oversizing) series FPTUs fan relative to the design airflow and then operating the FPTU at a reduced airflow to meet the design airflow requirements (Nailor 2014, Trane 2014). While the motivation (noise reduction) is different from the ASHRAE 90.1 (2010) requirements, the outcome is the same - the installed FPTU has an airflow capacity that is larger than the design airflow requirement for the zone. If this unit was then operated at a lower airflow than its full rated capacity, it would have the potential for reduced power and energy use, whether the ECM FPTU was operated in fixed or variable airflow modes. The application procedures for FPTUs related to noise reduction led to a similar need to be able to estimate the performance of ECM FPTUs when they have more capacity than the design airflow, but operate at or below the design airflow. Having a definitive procedure for estimating the power and energy savings from operating a larger ECM FPTU unit at lower airflows would provide a modeler with a way to more realistically model ECM FPTUs.

The purpose of this chapter was to develop simplified models of ECM fan/motor units used in FPTUs that allowed the user to easily model the ECM FPTU when its maximum capacity was either just sized to or was larger than the design airflow requirement for the zone. The models were based on data from four manufacturers of ECM FPTUs. It was the intent that these ECM models can be incorporated into building energy simulation models to provide more accurate estimates of the annual energy use of ECM FPTUs.

3.1. Background

Recent studies by Cramlet (2008), Edmondson, et al (2011a and 2011b) and Yin and O'Neal (2014a and 2014b) have done much to characterize the steady state and part load performance of FPTUs utilizing ECMs. Cramlet (2008) developed a set of equations for characterizing the performance of a single ECM FPTU. Edmondson et al (2011a and 2011b) conducted detailed measurements and developed performance models of ECM controlled FPTUs from three manufacturers. The experimental studies of Cramlet (2008) and Edmondson, et al (2011a and 2011b) treated the FPTU as a system. Semi-empirical relationships were developed from the experimental data that could be used to estimate the electrical, pressure, and airflow performance

of FPTUs. As demonstrated by Davis et al (2012), the models developed from the prior experimental work allowed a modeler to use the sets of equations to simulate the hourly performance of a particular FPTU in a building if the static pressures inside the duct system were known. Some building energy simulation programs utilized a much simpler model of FPTUs that relied on energy and mass balances of the FPTU to estimate performance. Utilizing the data from Cramlet (2008) and Edmondson et al (2011a and 2011b) would require a different approach to modeling air-side systems than was commonly found in some building simulation programs.

Recently, Yin and O'Neal (2014a and 2014b) measured the performance of the individual components (fan/motor combination, the damper, and cabinet) of ECM controlled FPTUs. Their strategy was to determine if the individual component models could be combined together to predict overall system performance. The system performance predicted with this approach was compared to the measured system performance of the FPTU collected by Edmondson, et al (2011a). There was general agreement in the trends and it demonstrated that a component approach could be used if the performance of the fan/motor/controller, damper, and housing were known. Some of the differences in performance between the component and measured system performance focused on the airflow effects on the fan performance within the FPTU. Specifically, Yin and O'Neal (2014b) found that when the fan/motor combination was tested outside the FPTU, it was not possible to reproduce the changes in performance caused by fan system effects that occurred because of the constrained space within the housing of the FPTU.

3.2. Simplified Fan Models

Because ECM fan motors in FPTUs can be used in a constant or variable airflow mode, any model of ECM fan motors needs to be able to capture both types of applications. The public domain building simulation program, EnergyPlus, modeled both series and parallel FPTUs (EnergyPlus 2013). It treated the fan in FPTUs as operating at constant airflow. The user was required to input the fan properties shown in Table 3.1. EnergyPlus calculated the power of the fan motor shown in Equation 3.1 based on the variables defined in Table 3.1.

$$Pow_{fan} = \frac{Q_{flow}\,\Delta P_{tot}}{\eta_{fan}\eta_{mot}} \tag{3.1}$$

Manufacturers typically provide FPTU data in their literature for engineers to correctly apply FPTUs in the field. These data were typically at a FPTU system level and not at the level of the components that make up a FPTU. Thus, some of the data needed in Equation 3.1 were not

available to the energy modeler. One example was the fan/motor assembly. The fan/motor in a FPTU was a matched assembly and tested as a unit. If manufacturers were to publish efficiency data, it would be a combined fan/motor efficiency, not the individual efficiencies of the fan and motor. Another example was the design air pressure rise across the fan. Fans in a FPTU (whether a series or parallel unit) are installed inside the FPTU. Determining the pressure rise across the fan would require installation of a pressure tap in the FPTU housing to measure the static pressure inside the FPTU housing. The pressure rise across fans inside a FPTU was not measured even though this information was an input required by EnergyPlus. Some limited pressure differential measurements across FPTU are presented in Chapter 4.

Table 3.1. - Fan Characteristics Used for Series FPTUs in EnergyPlus

Design air pressure rise across the fan, ΔP_{fan}
Design volumetric flow rate, Q_{flow}
Fan total efficiency, η_{fan}
Fan motor efficiency, η_{mot}
Fraction of fan waste heat that enters airstream, f_{air}

If the ECM in the FPTU was programmed to follow the load in the zone, then the fan would be operating as a variable speed fan. EnergyPlus (2013) had an option for modeling variable speed fans, though not directly in a FPTU (or powered induction unit as they're called in EnergyPlus) because the FPTU was assumed to operate at a fixed airflow. For a variable speed fan, the power required by the fan, Pow_{fan}, at a particular airflow was determined by:

$$Pow_{fan} = f_{pl} * \frac{Q_{fan\_design}\Delta P_{fan}}{\eta_{fan}\eta_{mot}} \quad (3.2)$$

Where:

f_{pl} = part load power fraction of fan/motor unit operating a specific airflow

Q_{fan_design} = design airflow for the fan – ft^3/min (m^3/s)

Because building simulation programs often separate the fan and motor performance in their input, Equation 3.2 was usually written solely in terms of the power requirement of the fan. To calculate the power to the fan motor would require dividing the fan power by the fan motor efficiency.

The fan part load power fraction (PLPF), f_{pl}, was defined as the power of the fan at a given airflow divided by the power at design airflow:

$$f_{pl} = \frac{Pow_{fan}}{Pow_{fan\_design}} \tag{3.3}$$

The fan part load power fraction was modeled as a fourth degree polynomial (EnergyPlus 2013):

$$f_{pl} = c_1 + c_2 f_{flow} + c_3 f_{flow}^2 + c_4 f_{flow}^3 + c_5 f_{flow}^4 \tag{3.4}$$

The part load airflow fraction (PLAF), f_{flow}, in the above equation was defined as the airflow produced by the fan at a given speed to the design airflow produced by the fan:

$$f_{flow} = \frac{Q_{fan}}{Q_{fan\_design}} \tag{3.5}$$

Applying this equation required detailed flow and power information from a manufacturer for the particular fan. Specifically, to fit a fourth degree polynomial, a minimum of five data points were needed over the range of flow and power of the fan. Some of the manufacturers who provided data for this study only tested at three or four part load settings for the ECM controller. Thus, for the ECM controlled fans used in FPTUs, there may be limited data available at part-load conditions, which may make it difficult to get a fit for the fourth degree polynomial in Equation 3.4. A second issue with the fourth degree polynomial fit was that it is a higher degree polynomial than what was normally expected for a relationship between fan power and airflow. With the fan affinity laws, one would generally expect the fan power to vary with the cube of the airflow because the airflow is proportional to the speed of the fan at a given pressure differential across the fan:

$$f_{pl} = \frac{Pow_{fan}}{Pow_{fan\_design}} \alpha \left(\frac{Q_{fan}}{Q_{fan\_design}}\right)^3 \tag{3.6}$$

A third degree polynomial approach to modeling variable speed fans was used in other building simulations programs (Knebel 1983 and BLAST 1986) to estimate f_{pl}:

$$f_{pl} = a_1 + a_2 f_{flow} + a_3 f_{flow}^2 + a_4 f_{flow}^3 \tag{3.7}$$

Where $a_1..a_4$ are constants and are given in Table 3.2. This variable speed fan model was also in the ASHRAE toolkit of models put together by Brandemuehl (1993). The original figure from which the third degree polynomial model used by Knebel (1983) and others was given by Janisse (1969). In a 1986 paper, Spittler et al (1986) made the following comments about Janisse's figure:

> "The performance data used for comparison were given by Janisse (1969) The origin of these curves is undocumented....However, a comprehensive on-line literature search revealed no documented data on the effect of different methods of modulation on fan performance."

While it was probable that there were original data used to develop the part load performance model of variable speed fans by Janisse (1969), it was never documented. This left the user of the model in Equation 3.7 and Table 3.2 on questionable grounds when trying to defend energy calculations for variable speed fans in building simulation programs that utilized this model. The lack of substantive data indicated there was a need for data that could be used to justify a better part load performance model of variable speed fans.

Table 3.2 – Values of Constants in Equation 3.7 (Knebel 1983 and BLAST 1986)

Constant	Value
a_1	0.00153
a_2	0.005208
a_3	1.1086
a_4	-0.11636

Knebel (1983) appeared to be the first author to provide the coefficients in Table 3.2 in the open literature. As a consequence, the model in Equation 3.7 and Table 3.2 was called the Knebel (1983) model in this paper.

Both the third and fourth degree polynomial fits were used to estimate the normalized part load performance of only the fan in building simulation programs. As has been mentioned previously, for FPTU applications, the fan performance cannot be separated from the motor because they were a matched assembly. While the forms of the above equations could be used for ECM FPTUs fan/motor assemblies, the part load power fraction, f_{pl}, in Equations 3.4 and 3.7 would have to be redefined to include the combined fan and motor. If the fan motor efficiency varied with speed, then the shape of the polynomial describing part load performance may vary from a part load performance curve that was developed for just the fan alone.

The models represented in either Equations 3.4 or 3.7 described the fraction of airflow and power based off a given design condition. For a model to be complete, the user must know the full load design airflow and power requirements of the fan/motor assembly. With the full load

design performance, the part load performance could be estimated with the part load models developed from Equations 3.4 or 3.7.

3.3. Data Collection

Four FPTU manufacturers provided data on their units for this study. The manufacturers were identified as Manufacturers A, B, C, and D in the tables and figures below. The data covered a range in nominal fan motor sizes from 0.33 hp (249 W) to 1 hp (746 W) and included data from both series and parallel terminal units. Table 3.3 shows the fan motor sizes provided by each manufacturer. Overall, data were provided on 36 fan/motor combinations. Six of the combinations were from parallel and thirty were from series terminal units. Data were also provided on two dual fan/motor assemblies that had 0.33 hp (249 W) and 0.75 hp (560W) motors. Manufacturer A provided data on 24 of the 36 units in Table 3.3. The units should cover much of the range of fans and motors expected to be found in FPTUs used in the field. Manufacturers applied these fan/motor combinations in a wide range of cabinet sizes and cabinet styles (underfloor or overhead) and cabinet profiles ("low" and "standard"). Each cabinet design potentially produced different flow conditions entering the FPTU fan which could generate differing air system effects that impacted the overall performance of the fan.

Data were collected on fan/motor combinations by manufacturers in their own laboratories and provided to the authors through a representative of the Air Conditioning Heating and Refrigeration Institute (AHRI) so that the identity of the manufacturer remained anonymous. Manufactures were asked to provide both descriptive (see Table 3.4) and performance data (see Table 3.5) on the fan/motor combinations. In Table 3.5, the settings on the controllers were specified in DC voltages (typically from 0 to 10 V) or from 0 to 100%.

Table 3.3 - ECM FPTU Fan/Motor Data Provided by Manufacturers

Nominal Fan/Motor Size –hp(W)	Manufacturer A	Manufacturer B	Manufacturer C	Manufacturer D
0.33 (249)	XXXXXXXXX XXX*	X		XXX*
2 x 0.33 (249)	XX*			
0.50 (373)	XXX*	X	X	
0.75 (560)	XXXXX*			X
2 x 0.75 (560)	XX*			X
1.0 (746)		XX		XX

*Multiple "Xs" indicate the manufacturer provided more than one unit's data at that size.

Table 3.4 – Descriptive Data for FPTU and Fan/Motor Combinations

Item
Fan Model Number
Series or Parallel FPTU Application
Primary Inlet Diameter
Design range of airflow of FPTU
Recommended operating pressures
Maximum recommended airflow
Minimum recommended airflow
Fan manufacturer
Motor manufacturer
Motor Size
Fan discharge dimensions

Table 3.5 – Detailed Measured Performance Data on Each FPTU Fan/Motor Combination

Item	Units
ECM Setting	voltage or value
discharge static pressure	in w.g. (Pa)
airflow	ft^3/min (m^3/s)
current	Amps
volt-amps	volt-amps
power factor	-
power	W
motor speed	rpm
power/airflow	$W/(ft^3/min)$ $W/(m^3/s)$

An identification procedure was developed for reporting each fan/motor combination. Because all of the fan motors in this paper were ECMs, all designations start with "ECM". This designation distinguished these units from the SCR units evaluated in the previous chapter. The rated fan motor size, in horsepower, was converted to its decimal equivalent and multiplied by 1000. For example, the identification of a 0.5 hp (373 W) unit would be 0.500 multiplied by 1000 to give a value of 500. The four manufacturers were each given a letter designation of either A, B, C, or D. A 0.5 hp (373 W) fan/motor from manufacturer A was identified as ECM-500A. If a manufacturer had more than one fan/motor combination of the same size, such as manufacturer B had for 0.5 hp (373 W), then the first fan/motor was identified as ECM-1000B1 and the second as ECM-1000B2. For cases where there were dual fan/motors in a FPTU, the unit was identified with a 2x before the unit size. For example, the first 0.75 hp (560 W) from manufacturer A would be designated as ECM-2x750A1.

3.4. Data Analysis

Each manufacturer provided their data in spreadsheets. With the discharge area of the fans provided, it was possible to calculate the exit air velocity from the discharge area and measured airflow. With the exit air velocity known, the velocity pressure was calculated and added to the measured static pressure differential across the fan to obtain a fan total pressure. The fan/motor total efficiency, η_{fm}, was calculated using fan total pressure, mass flow of the air, and fan power.

$$\eta_{fm} = \frac{Q_{flow} * \Delta P_{tot}}{Pow_{fan}} \tag{3.8}$$

Where:

ΔP_{tot} = fan total pressure – in w.g. (Pa)

Pow_{fan} = power of the fan motor – W

Q_{fan} = fan volumetric airflow – ft^3/min (m^3/s)

Figure 3.1 showed sample data for the fan/motor total efficiency versus fan total pressure for the one hp (746 W) fan/motor combination from manufacturers B. The fan/motor total efficiency showed an increase as the fan total pressure was increased. As the ECM setting was increased, the fan and motor rotated faster and the data showed a consistent decrease in efficiency. This figure illustrated the difficulty in attempting to use a single efficiency to describe the efficiency of the ECM fan/motor combination. The efficiency increased with fan total pressure, but ECM setting (i.e., airflow) also had a large influence. For example, at a total pressure of 0.3 in w.g. (75 Pa), the fan/motor efficiencies ranged from about 11% at an ECM setting of 100 to 28% at the lowest setting of one. These wide ranges in efficiency were also found at both higher and lower fan total pressures. Manufacturers typically don't provide in their product literature the detailed data on efficiencies found in Figure 3.1. Even if they did, the energy modeler would be left with a large range of efficiencies from which to choose. Unless the modeler knew the ECM setting and total pressure for the FPTU, they would only be guessing at a value that might correspond with the actual performance of the FPTU fan/motor. If the ECM in the FPTU were programmed to follow the load in the zone, the ECM would be varying the airflow (and ECM setting) in response to changes in the loads in the zone. Figure 3.1 would also imply that a single efficiency should not be used to model the FPTU in a variable airflow application.

The fan/motor behavior in Figure 3.1 showed that the efficiency increased with pressure and decreased with increased ECM setting. Many of the fan/motor combinations that were 0.5 hp (373 W) and above had plots similar to Figure 3.1. If there were deviations from Figure 3.1, it was generally in the data at the lowest ECM power setting, which was at 2V or 20% of full scale.

Figure 3.2 showed the plot of ECM-750A3. While there were differing slopes to the lines for each ECM setting, the trend of lower efficiencies at higher ECM settings was consistent with ECM-1000B in Figure 3.1.

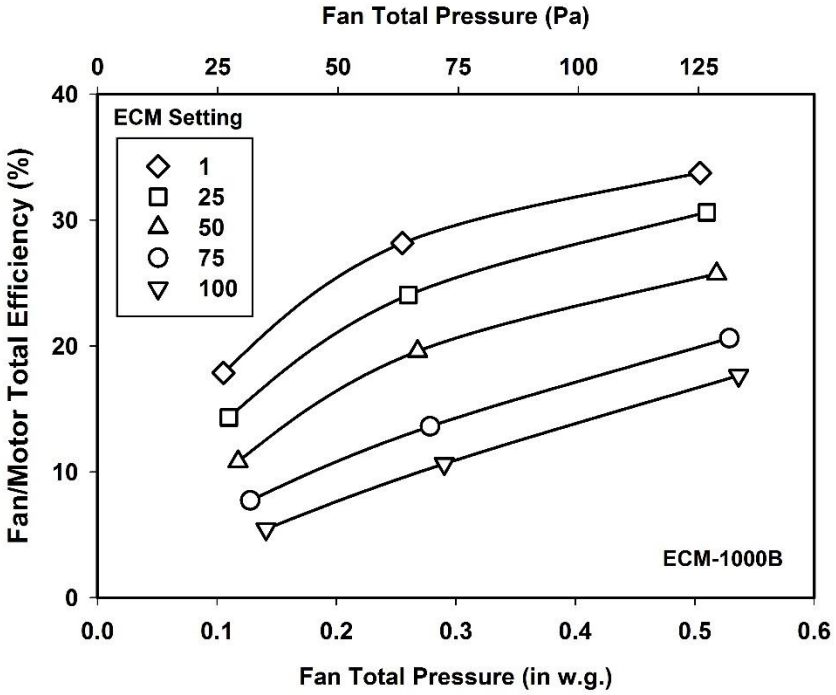

Figure 3.1: Sample Data for Total Efficiency Versus Fan Total Pressure for ECM-1000B, which had a Nominal Sized 1 hp (746 W) motor

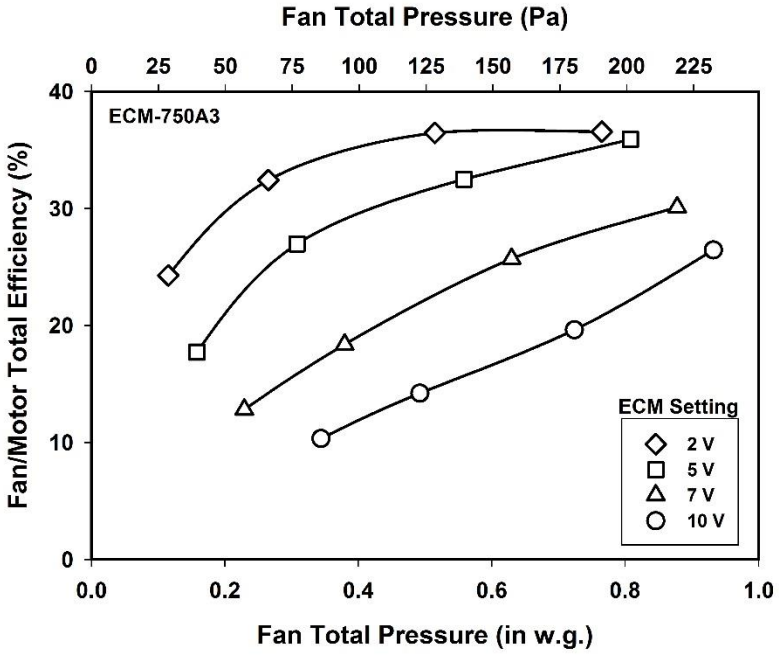

Figure 3.2: Sample Data for Total Efficiency Versus Fan Total Pressure for ECM-750A3, which had a Nominal Sized 0.75 hp (560 W) Motor

A substantial number of the 0.33 hp (249 W) fan/motor combinations showed a large variance from the more predictable behavior shown in Figure 3.1. Figure 3.3 shows a sample efficiency plot for ECM-333A3. In this case, the lowest efficiencies occurred at the lowest ECM setting (2 V). The efficiency peaked at the 7 V setting, and then decreased at the highest ECM setting (10 V). The efficiency at the 10 V setting initially started near the efficiency of the 2 V setting at the lowest total pressure. It then increased as the total pressure increased, crossing the 5 V efficiency at about 0.4 in w.g. (100 Pa) and finally intersecting the line for the 7 V setting at nearly 0.8 in w.g. (200 Pa). While the efficiencies generally increased with increasing total pressure, the increase in efficiency with increasing total pressure at 10 V was much larger than at the other settings.

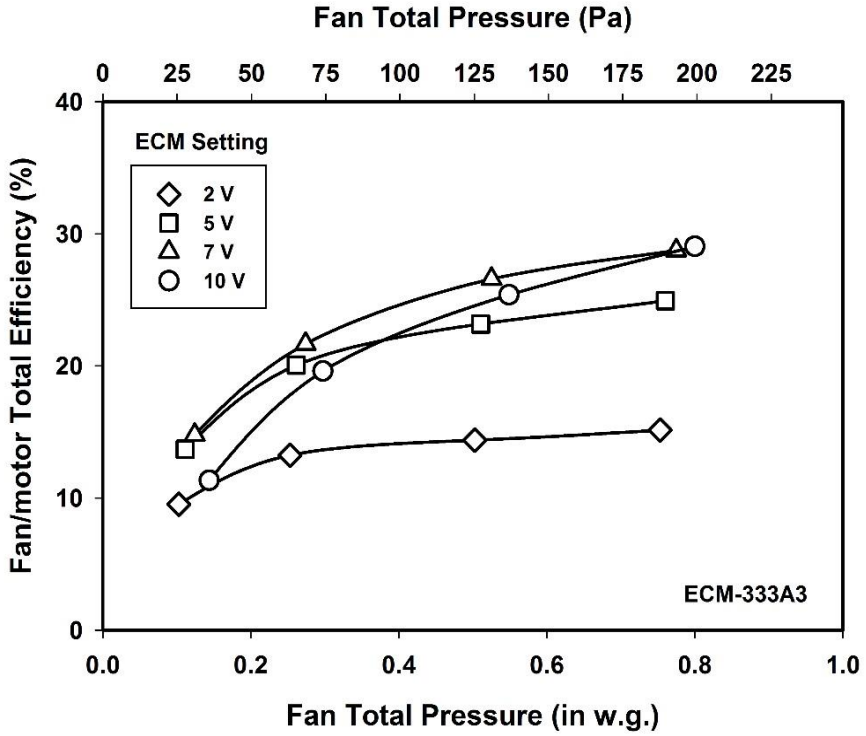

Figure 3.3: Sample Data for Total Efficiency Versus Fan Total Pressure for ECM-333A3, which had a Nominal 0.33 hp (249 W) Motor

Building a model that accounted for efficiency as a function of ECM settings and total pressure could potentially be done for individual units such as ECM-1000B and ECM-750A3. However, the behavior of ECM-333A3 and some of the other 0.33 hp (249 W) units were so different, that it would not be possible to develop a generalized model relating fan/motor efficiency to fan total pressure and power setting for all the ECM units evaluated. As discussed

later in this section, some of the unusual behavior may be the result of the relative size of the motor to the maximum power required for the airflow application. Even with the more predictable performance behavior of the larger sized ECMs like those in Figures 3.1 and 3.2, the wide variation in fan/motor efficiencies would make it difficult for a building modeler to choose a single value of efficiency for input into a building simulation program. These considerations led to the conclusion that an alternative approach should be evaluated. Specifically, it was decided to consider whether the simpler third or fourth degree polynomial models for part load performance such as those used by Knebel (1983) or EnergyPlus (2003) could be used.

Manufacturers collected data for discharge static pressures ranging from 0.1 to 0.75 in w.g. (25 to 187 Pa). Table 3.6 showed the discharge static pressures that each manufacturer used in their data collection. Three manufacturers (A, C, and D) took data at four settings while one (B) took data at three settings. All manufacturers reported data for 0.10 in w.g. (25 Pa) discharge static pressure. Three manufacturers (A, B, and C) reported data at 0.5 in w.g. (125 Pa). The top discharge static pressures ranged from 0.5 to 0.75 in w.g. (125 to 187 Pa).

Table 3.6 – ECM FPTU Fan/Motor Discharge Static Pressure Tests Conducted by each Manufacturer

Discharge	Discharge Static Pressure – in w.g. (Pa)			
Pressure Setting	Manufacturer A	Manufacturer B	Manufacturer C	Manufacturer D
Lowest	0.10 (25)	0.10 (25)	0.10 (25)	0.10 (25)
Mid-Low	0.25 (63)	0.25 (63)	0.20 (50)	0.30 (75)
Mid-High	0.50 (125)	n.a.	0.40 (100)	0.50 (125)
Highest	0.75 (187)	0.50 (125)	0.60 (150)	0.70 (174)

Figure 3.4 showed sample data from ECM-1000B of the measured fan/motor power versus fan airflow for a range of ECM settings and discharge static pressures. The relationship between fan/motor power and fan airflow was non-linear for a given discharge static pressure. As the discharge static pressure was increased, the power increased. The general shape of these curves shown in Figure 3.4 was similar to those of the other units evaluated. In some instances, the differences between the curves over the range in static pressures was small and in some cases, there was overlap in the power versus flow curves at different discharge static pressures. However, all showed the same non-linear trend for power versus airflow along a specific static pressure line. The shape of the curves in Figure 3.4 should be similar if the data were

normalized to the airflow and power at the maximum ECM setting for a given discharge static pressure. The data should also lend itself to a polynomial fit.

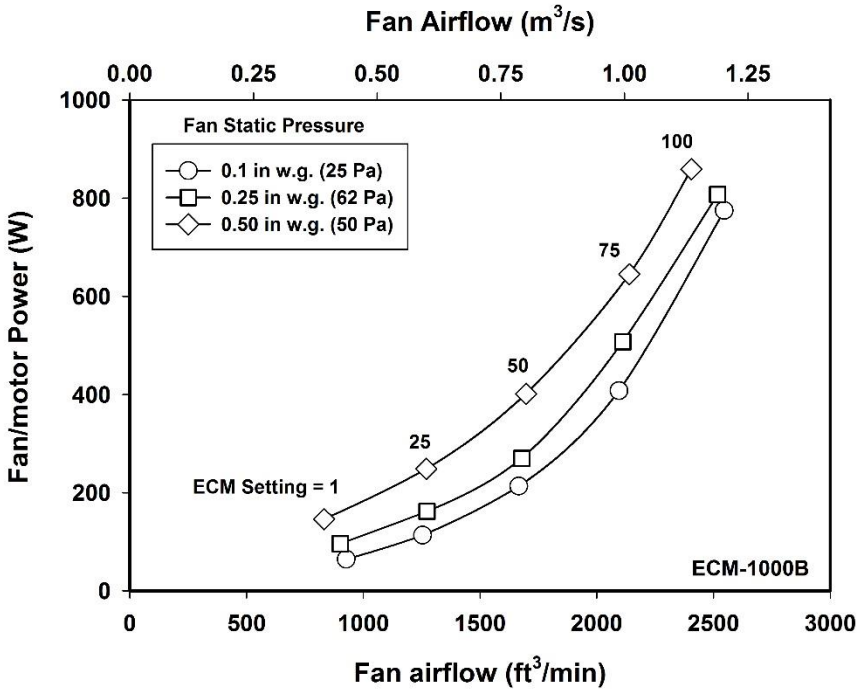

Figure 3.4: Fan/Motor Power Versus Fan Airflow as a Function of ECM Setting and Discharge Static Pressure

In the prior experimental studies of FPTUs by Edmondson et al (2011a and 2011b), significant data were taken at 0.25 in w.g. (63 Pa) static pressure because FPTUs are rated at this discharge pressure (AHRI 2011 and ASHRAE 2006). It was decided to focus on the data collected for discharge static pressures ranging from 0.1 to 0.5 in w.g. (25 to 125 Pa) for the part load airflow and power analysis. This discharge pressure range bracketed the 0.25 in w.g. (63 Pa) in the FPTU test procedure and should cover a wide range of FPTU applications in buildings.

3.5. Modeling Part Load Performance

Figure 3.5 showed the part load power fraction, f_{pl}, versus the part load airflow fraction, f_{flow}, at a discharge static pressure of 0.5 in w.g. (125 Pa) for the 0.33 hp (249 W) fan/motor combinations provided by the manufacturers. Fan/motor combinations ECM-333A9 and ECM-333A10 were omitted from the plot because they did not have enough data to plot the part load power fraction.

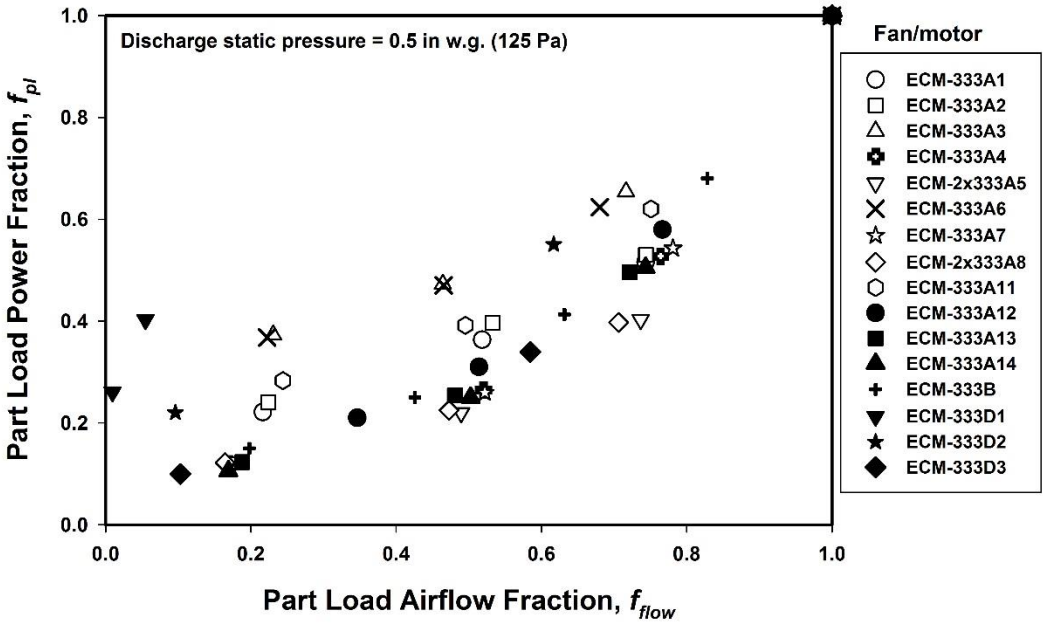

Figure 3.5: Fan Part Load Power Fraction Versus Part Load Airflow Fraction at 0.5 in w.g. (125 Pa) for the 0.33 hp (249 W) Fan/Motor Combinations

The definitions of the f_{pl} and f_{flow} were modified in Equations 3.9 and 3.10 so the denominator was redefined to mean the power and airflow of the fan/motor at the maximum ECM setting rather than the design power and airflow:

$$f_{pl} = \frac{Pow_{fan}}{Pow_{max}} \tag{3.9}$$

$$f_{flow} = \frac{Q_{flow}}{Q_{max}} \tag{3.10}$$

Where:

Pow_{max} = fan motor power at the maximum ECM setting at a specified discharge pressure

Q_{max} = fan airflow at the maximum ECM setting at a specified discharge pressure

For most of the ECM controllers, the maximum setting was 10V or 100%. Figure 3.5 showed there was a large spread in the data, which was also typical of the plots at other discharge static pressures. A closer look at the data indicated a possible explanation for some of the scatter shown in Figure 3.5. Table 3.7 listed the nominal motor size, the maximum fan power draw, the power ratio, and maximum airflow for each of the 0.33 hp (249 W) fan/motor combinations at 0.5 in w.g. (125 Pa). The power ratio was the maximum fan motor power at 0.5

in w.g. (125 Pa) used by the ECM fan motor at the maximum ECM setting divided by the nominal motor size. Each of the fan motors was nominally rated at 249 W. Comparing the fan/motor combinations in Table 3.7 with the data in Figure 3.5, a trend emerged. Those ECMs with a power ratio less than 0.8 tended to have the poorer part load performance (i.e., higher part load power fraction for a given part load airflow fraction). Without detailed design characteristics and performance data on each of the individual fans and motors, it would be difficult to pinpoint the exact reasons why the part load performance was so different for those with power ratios below 0.8. One possible factor may have to do with the power used by the ECM controller. This controller probably used a fixed amount of power even at low settings and this power, while perhaps "in the noise" at high ECM settings, may be significant at the lower settings. For example, ECM-333D1 at its lowest ECM setting (2 V) used only 28.9 W at 0.5 in w.g. (125 Pa). If the controller only used 10 W, then one-third of the power at the low setting would be due to the controller. Another factor may be the performance of the motors at very low loads. The 28.9 W for ECM-333D1 was less than 12% of the nominal power rating of the motor. The authors were not aware of any study showing the part load efficiency of ECM motors. If there was any efficiency drop in the motor at extremely low loadings, then it would potentially create a smaller overall power savings at the lower settings than those fan/motor combinations with higher power ratios. In either case, neither the amount of controller power or ECM motor efficiency were separately measured or provided in the data we evaluated. It may be worthwhile in a future study to obtain and analyze more detailed information on the units that could shed some insights into the differences in part load performance for these units with the low power ratios.

Even though those units with power ratios less than 0.8 did not achieve as large a drop in part load power fraction, their full load power performance was typically better than the units with power ratios above 0.8. Those units with power ratios below 0.8 had an average full load power to airflow ratio of 0.29 W/ft^3/min (615 W/m^3/s) compared to 0.38 W/ft^3/min (805 W/m^3/s) for the units with a power ratio above 0.8.

Table 3.7 – Maximum FPTU Power Application, Power Ratio, and Airflow for the 0.33 hp (249 W) Units Operating at 0.5 in w.g. (125 Pa) Discharge Static Pressure

Fan/Motor	Nominal Motor Size (W)	Maximum FPTU Application (W)	Power Ratio	Max Airflow ft^3/min (m^3/s)
ECM-333A1	249	190	0.765	480 (0.23)
ECM-333A2	249	179	0.721	477 (0.23)
ECM-333A3	249	110	0.443	433 (0.20)
ECM-333A4	249	360	1.449	884 (0.42)
ECM-2x333A5	2x249	720	1.448	1732 (0.82)
ECM-333A6	249	117	0.471	454 (0.21)
ECM-333A7	249	370	1.489	861 (0.41)
ECM-2x333A8	2x249	730	1.468	1816 (0.86)
ECM-333A9	249	210	0.843	459 (0.22)
ECM-333A10	249	440	1.767	915 (0.43)
ECM-333A11	249	166	0.668	625 (0.30)
ECM-333A12	249	300	1.208	882 (0.42)
ECM-333A13	249	260	1.047	519 (0.24)
ECM-333A14	249	380	1.530	907 (0.43)
ECM-333B1	249	349	1.405	1140 (0.54)
ECM-333D1	249	111	0.447	452 (0.21)
ECM-333D2	249	195	0.785	755 (0.36)
ECM-333D3	249	497	2.001	1427 (0.67)

Seven of the 0.33 hp (249 W) fan/motor combinations had power ratios less than 0.8. These were separated from the rest of the fan/motor combinations along with two of the larger units. None of these were used for the analysis below. After removal of the units with the low power ratios from the population of the 0.33 hp (249) units in Figure 3.5, the remaining units were plotted in Figure 3.6 for static discharge pressures ranging from 0.1 to 0.5 in w.g. (25 to 125 Pa). While there was some scatter in the data, the data tended to group together along a non-linear curve that could be fit with the third degree polynomial shown in Equation 3.7 except that the definitions in Equations 3.9 and 3.10 would be substituted for the PLPF, f_{pl}, and the PLAF, f_{flow}.

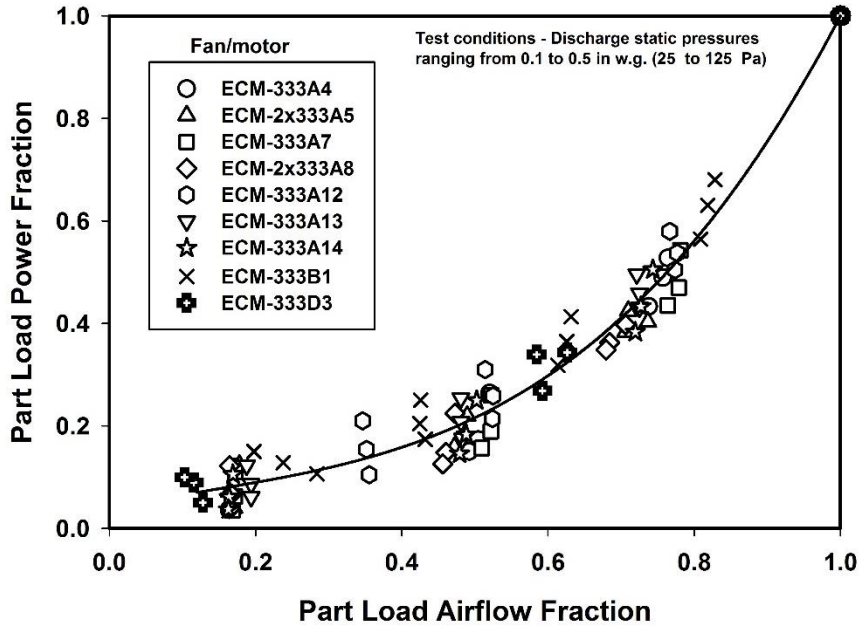

Figure 3.6: Fan Part Load Power Fraction Versus Part Load Airflow Fraction at Discharge Pressures Ranging from 0.1 to 0.5 in w.g. (50 to 125 Pa) for the 0.33 hp (249 W) Fan/Motor Combinations

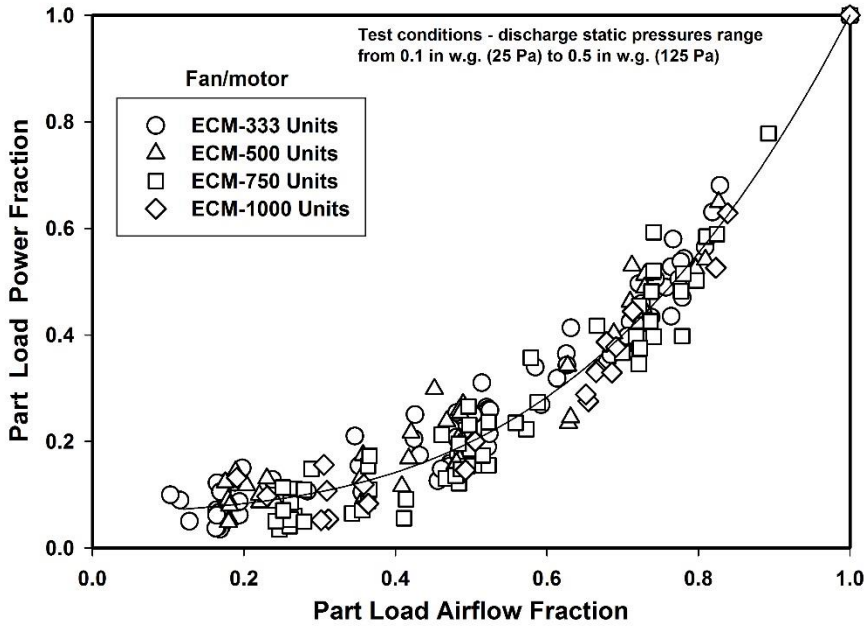

Figure 3.7: Fan Part Load Power Fraction Versus Part Load Airflow Fraction at Discharge Pressures Ranging from 0.1 to 0.5 in w.g. (25 to 125 Pa) for the Range of Fan/Motor Combinations in this Study

The PLPF versus PLAF data for the ECM-500, 750, and 1000 were added to the ECM-333 units and all were plotted together in Figure 3.7. Besides the units with low power ratios, there were four fan/motor combinations (ECM-333A9, ECM-333A10, ECM-750A5, and ECM-750A6) with only partial data sets available that were also not used in the analysis below. All four of these were from parallel terminal units. A regression analysis was performed and the data fit to the third degree polynomial of Equation 3.7. The regression coefficients were shown in Table 3.8. The r-squared was 0.981, which indicated an excellent fit for the third degree polynomial. Because the lowest data for PLAF only went down to about 0.10, the regression should be used with caution below this value. The PLPF for the third degree polynomial leveled off to a value of PLPF of 0.062 for values of PLAF below 0.1. The non-zero value of PLPF at low values of PLAF may be due to the presence of the controller that requires a small amount of power even when the controller is operating at low values.

Table 3.8 – Values of Coefficients in Equation 3.7 for the Best Fit Curve to the Data in Figure 3.7

Coefficients	Value
a_1	0.061715
a_2	0.093022
a_3	-0.11627
a_4	0.961538

Because EnergyPlus uses a fourth degree polynomial fit to characterize part load performance of fans, a fourth degree polynomial was also fit to the same data. The coefficients for a fourth degree polynomial are provided in Table 3.9.

Table 3.9 – Values of Coefficients in Equation 3.4 for Fourth Degree Polynomial Fit Curve for the Data in Figure 3.7

Coefficient	Value
c_1	0.116008
c_2	-0.46192
c_3	1.679005
c_4	-1.31496
c_5	0.982138

The third and fourth degree polynomials were plotted in Figure 3.8 along with the Knebel (1983) model and the curve for the traditional fan law relating fan airflow and power. Both the polynomial fits generally fell nearly on top of each other. The only exception was at values of the PLAF below 0.17 where the PLPF estimated by the fourth degree polynomial fit increased with decreasing values of PLAF. At a zero PLAF, the fourth degree polynomial had a PLPF of 0.116. While the fourth degree polynomial fit the data closely for most of the range of data, the third degree polynomial did not have the upward trend in the values of PLPF at low PLAFs. For these data, there was no advantage to using the more complicated fourth degree polynomial fit. The Knebel (1983) model estimated higher PLPFs for all PLAFs down to about 0.3, then it predicted lower values of PLPFs down to zero PLAF. At a PLAF of 0.6, the third degree polynomial fit estimated a PLPF of 0.28 while the Knebel (1983) model estimated a PLPF of 0.39, which was nearly 40% more power fraction for the same airflow fraction. When modeling an ECM fan/motor on a FPTU that was operating between 30% and 100% of design airflow, the current third degree polynomial fit estimated significant less energy use than would the Knebel(1983) model. The curve for the fan law estimated lower power load fractions than all the other curves. The fan laws apply to the power input to the fan only and not the power input to the motor driving the fan. The fan motor introduced additional losses in efficiency not present in just the fan alone. Thus, it should not be surprising that the fan law curve estimated a more optimistic reduction in power fraction than did the regression for the fan/motor combinations.

One potential problem with the fourth degree polynomial was encountered when analyzing some of the fan data from Manufacturer A. Data from six units operating at 0.50 in w.g. (125 Pa) were initially plotted at ECM settings of 2, 5, 7, and 10 V, with 10 V being full scale.

The surprising result of the best fit was shown in Figure 3.9. Having only a small amount of data with most of it “clumped” near the same PLAFs didn’t provide a wide enough scatter in data to allow a fourth degree polynomial to provide a curve with a physically realistic shape. Rather than having a fit where the fractional power continually decreased with decreasing fractional flow, the curve began to assume a very shallow slope at a PLAF of about 0.4, and then dropped quickly as the PLAF decreased below 0.2. The curve went negative at a PLAF of 0.07. Clearly, negative values of the fractional power would be unacceptable. This figure illustrated one danger in using a fourth degree polynomial with limited part load data.

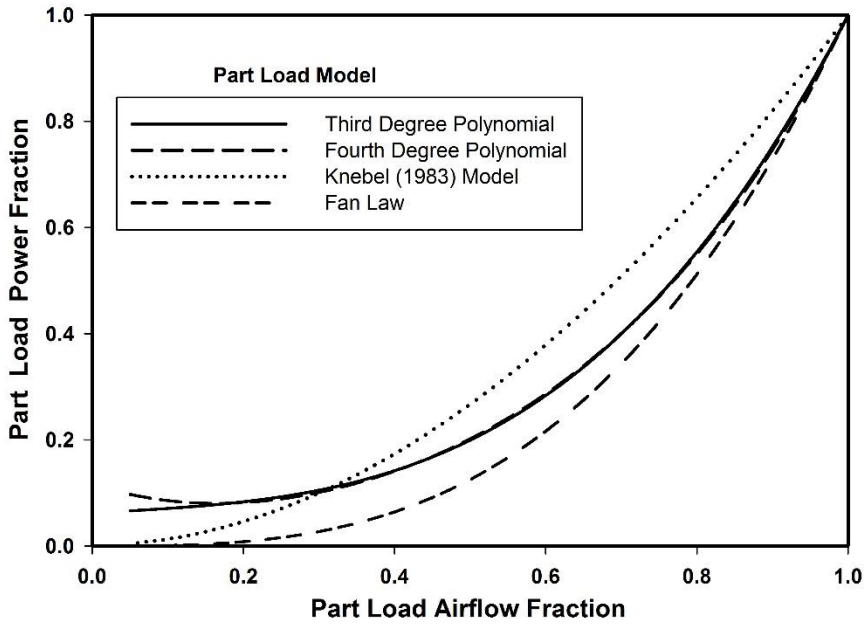

Figure 3.8: Plots of the Third and Fourth Degree Polynomial Fits of the Data Shown in Figure 3.7 along with the Knebel (1983) Model and the Fan Power Law

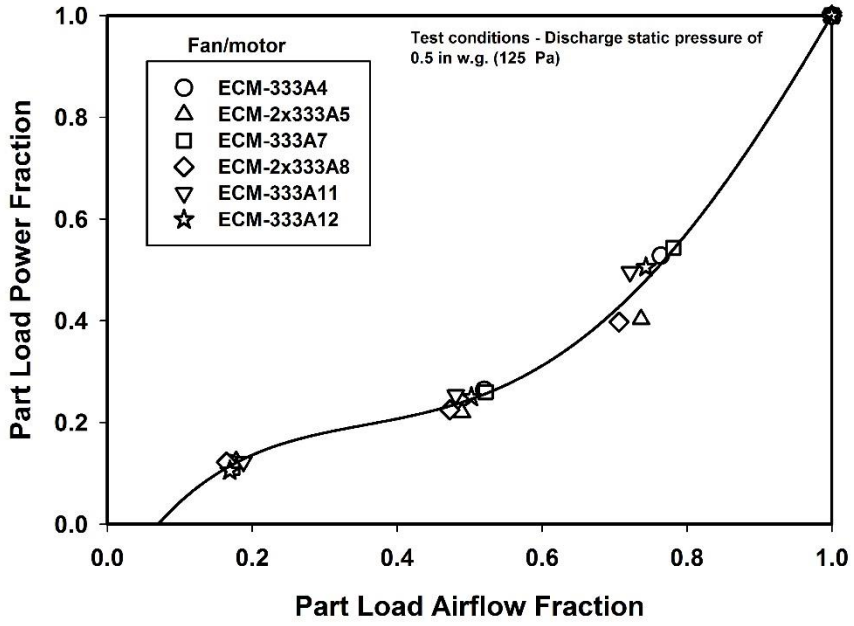

Figure 3.9: Plot of the Fourth Degree Polynomial Fit of the Data Shown for Six Units from Manufacturer A

3.6. Power and Airflow at Maximum ECM Setting

The PLPF versus PLAF curve shown in Figure 3.7 was generated with the power and airflows normalized to their respective values at the maximum settings of the ECMs. To calculate the power and airflow at part load conditions in a building simulation model, the values of power and airflow at the maximum ECM settings need to be known.

The airflow and power data at the maximum ECM settings for the units used in Figure 3.7 were plotted and shown in Figure 3.10. There was significant scatter in the data, particularly near an airflow of 1500 ft^3/min (0.71 m^3/s) for two units. One was a 0.5 hp (373 W) unit and the other was a 0.75 hp (560 W) unit. All of the data were fit with a linear regression that went through the origin. The relationship between the power of the fan and the fan airflow at maximum ECM is given by:

$$Pow_{max}(Q_{max}) = C_1 * Q_{max} \quad (3.11)$$

Where,

C_1 = 0.380 W/(ft^3/min) or 805 W/(m^3/s).

A second degree polynomial was also fit to the data, but only provided a marginally improved r-squared over a linear model. It was decided to use the simpler linear model.

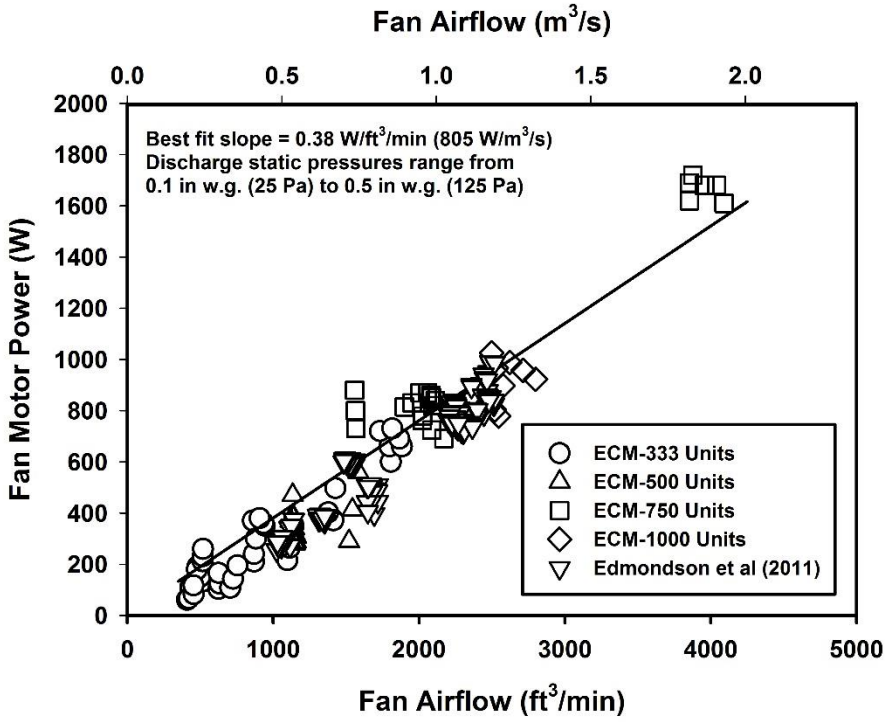

Figure 3.10: Fan Motor Power and Fan Airflow at the Maximum ECM Setting for the Fan/Motor Units in the O'Neal et al (2016) and Edmondson et al (2011)

The slope of the line in Figure 3.10 was surprisingly close to the 0.372 W/ft^3/min (788W/m^3/s) slope for the SCR units in Chapter 2 from the same group of manufacturers. This result would suggest that at full load, there was not a significant difference in performance, as measured by W/ft^3/min (W/m^3/s), between the SCR and ECM fan/motor units evaluated in this study. However, as discussed below, there was a large reduction in W/ft^3/min (W/m^3/s) of the ECM controlled units if they were run at part load rather than at the maximum ECM setting. This performance improvement was not reflected in the linear regression shown in Figure 3.10. The improvement in part load performance is discussed below.

With the power and airflow at the maximum ECM settings (Figure 3.10) and the part load performance curve (Figure 3.7), it was now possible to calculate the power requirement for a given airflow at part load conditions. The part load performance curve of Figure 3.7 and Equation 3.7 were integrated into the plot (See Figure 3.10) of the power and airflow performance at the maximum ECM settings. This integration resulted in a set of part load curves that dropped down from the line representing the power and airflow at the maximum ECM setting (See Figure 3.11).

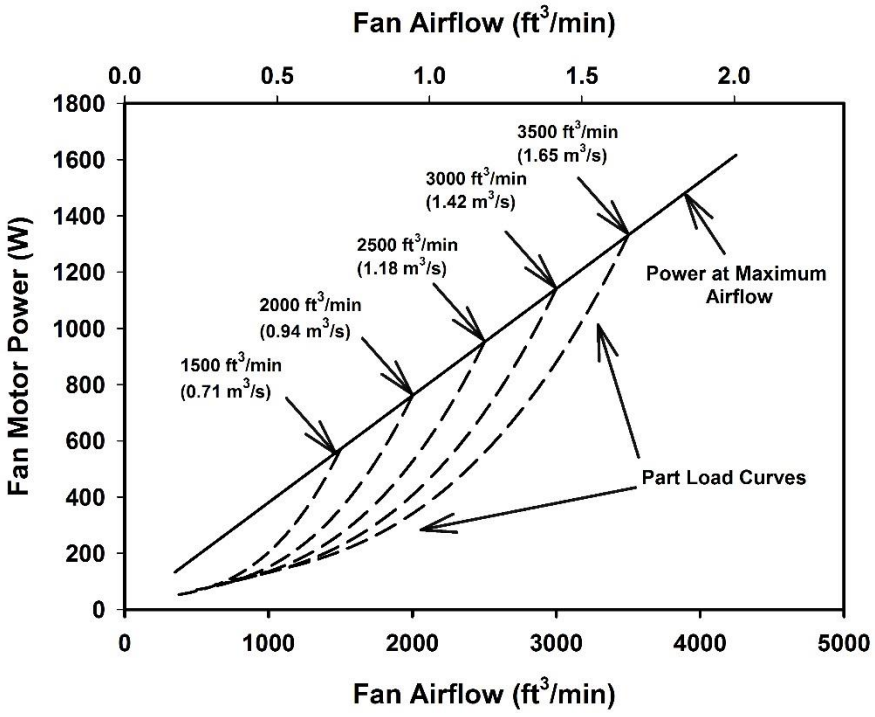

Figure 3.11: Relationship between the Part Load Curves to the Airflow and Power Curve at Maximum ECM Setting

The part load curves illustrated in Figure 3.11 started at 1500, 2000, 2500, 3000, and 3500 ft^3/min (0.71, 0.94, 1.18, 1.42, and 1.66 m^3/s). These were created by multiplying the third degree polynomial of Equation 3.7 (having the coefficients of Table 3.8) with the values of power at the maximum ECM settings for the respective airflows calculated from Equation 3.11. For example, at 2000 ft^3/min (0.94 m^3/s), the power at maximum ECM setting was 760 W. For the curve that dropped down from 2000 ft^3/min (0.94 m^3/s), the PLAF at a partial airflow value was calculated, then used to determine the PLPF. The PLPF was then multiplied by the full load power (760 W) to determine the power the fan motor would use at the lower airflows. This process was repeated over a range of partial airflows to estimate reduction in power as the airflow decreased. The results for the PLPFs are shown in Table 3.10 for a unit having 2000 ft^3/min (0.94 m^3/s) airflow at the maximum ECM setting. This table also demonstrates how rapidly the power/airflow drops under part load operation. At the maximum ECM setting, where the PLAR and PLPR are both one, the fan/motor unit had an estimated 0.38 W/ft^3/min (805 W/m^3/s) while at a PLAR of 0.5, it had improved to 0.15 W/ft^3/min (322 W/m^3/s). The combination of the part load curve (Equation 3.7) and the power/airflow at the maximum ECM setting (Equation 3.11) give the modeler the tools necessary to estimate the part load power for a given airflow.

Table 3.10 – Sample Value of Part Load Airflows and Power for Unit with a Maximum Airflow of 2000 ft^3/min (0.94 m^3/s) and Power of 760 W

Airflow ft^3/min (m^3/s)	PLAF	PLPF	Power (W)	Power/Airflow W/ft^3/min (W/m^3/s)
2000 (0.94)	1.00	1.00	760	0.38 (805)
1900 (0.90)	0.95	0.870	661	0.35 (737)
1800 (0.85)	0.90	0.752	572	0.32 (673)
1700 (0.80)	0.85	0.647	492	0.29 (613)
1600 (0.76)	0.80	0.554	421	0.26 (558)
1500 (0.71)	0.75	0.472	358	0.24 (506)
1400 (0.66)	0.70	0.400	303	0.22 (459)
1300 (0.61)	0.65	0.337	256	0.20 (417)
1200 (0.56)	0.60	0.283	215	0.18 (380)
1100 (0.52)	0.55	0.238	181	0.16 (349)
1000 (0.47)	0.50	0.199	152	0.15 (322)
900 (0.43)	0.45	0.168	127	0.14 (299)
800 (0.38)	0.40	0.142	108	0.14 (286)

3.7. Application of ECM FPTUs with Fixed Airflow Setting

A traditional approach to applying ECM FPTUs is to set the airflow of the ECM to a fixed value to satisfy the design load in the space. For this type of application, a modeler might be tempted to use the relationship in Equation 3.11 with the design airflow to calculate the required power. However, the data plotted in Figure 3.11 would suggested that if a modeler used such a simple approach, their estimate of the power (and energy use) for the ECM FPTU would be larger than might be obtained if a slightly larger airflow capacity ECM FPTU were installed. The curves that dropped down from the higher airflow capacity units usually provided lower power than those with airflow at the maximum ECM setting just matching the design airflow.

To illustrate the potential benefit of utilizing the part load performance of a higher capacity ECM unit, consider the following example. Assume that a space called for 2000 ft^3/min (0.94 m^3/s) of air to satisfy the design load and a FPTU with an ECM fan/motor was specified that can produce 2000 ft^3/min (0.94 m^3/s) at the maximum ECM setting. Using Equation 3.11, the expected power used by the ECM fan would be calculated to be 760 W. This value of power was shown in Figure 3.12 where the 2000 ft^3/min (0.94 m^3/s) airflow intersected the line for fan power at the maximum ECM setting.

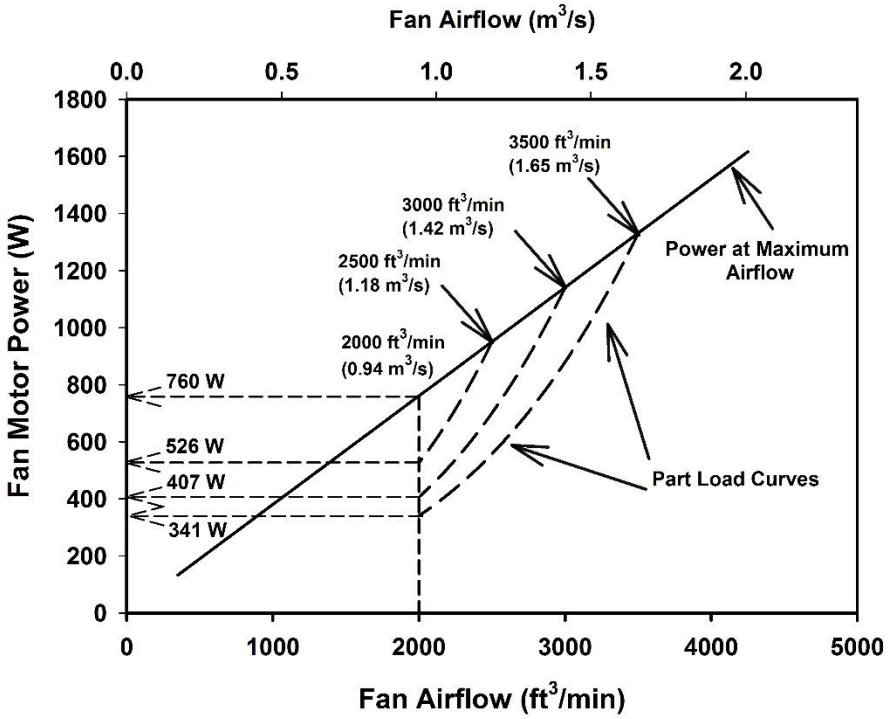

Figure 3.12: Illustration of how Larger ECM Fan/Motor Units can be used to Reduce Power at 2000 ft^3/min (0.94 m^3/s)

If a slightly larger FPTU was chosen which had a capacity of 2500 ft^3/min (1.18 m^3/s) at its maximum ECM setting, but was set at a lower airflow so that it produced the required 2000 ft^3/min (0.94 m^3/s), then its PLAF would be 2000/2500 = 0.8. Using Equation 3.7 and the coefficients in Table 3.8, the PLPF would be 0.554 for a PLAF of 0.8. The power at the maximum ECM setting for the 2500 ft^3/min (1.18 m^3/s) unit was 950 W from Equation 3.11. The expected power at 2000 ft^3/min (0.94 m^3/s) would be the full load power (950 W) multiplied by the PLPF (0.554), which would be 526 W (See Figure 3.12). This power usage represented a savings of 30.8% over the unit that was sized to just meet the thermal load requirements of the zone at the maximum ECM setting. Figure 3.12 illustrates the savings for several other units with capacities larger than the design airflow. If a unit with a maximum capacity of 3000 ft^3/min (1.42 m^3/s) were chosen and only run at the required 2000 ft^3/min (0.94 m^3/s) airflow, then the models developed from the data would suggest that the power usage would drop to 407 W. If the application were in a series FPTU where the fan was on continuously, then the lower power usage could represent a significant annual savings in energy use. Whether an engineer should take advantage of the larger FPTU would depend on variables such as the incremental cost of the larger FPTUs, noise requirements, and size of the cabinet. Because FPTUs are installed in plenum and underfloor areas, there may not be enough physical space to install a larger unit that has a higher airflow capacity than what is required to meet the design airflow. These considerations go beyond the scope of this paper, but are important considerations in the application of a FPTU.

The sample problem above illustrated that an energy modeler should have some leeway in sizing a FTPU for the particular application. It was not clear from the documentation of some building simulation programs that the modeler was provided much guidance on selection of the FPTU to best fit the application. The sample problem showed that the choice of sizing of the FPTU relative to the design load can potentially have a profound impact on the estimated energy use of FPTU in a particular application. With the data and correlations available above, it should be possible to determine a strategy to provide an optimum sized FPTU for a particular application.

The discussion relative to Figure 3.12 was based on the combination of the power and airflow at the maximum ECM setting and the third degree polynomial part load curve. One could legitimately ask how realistic were the reductions in power and power/airflow shown in

Figure 3.12. To try to answer that question, a simple test from the data supplied by the manufacturers was evaluated. Unit ECM-333A11 had an airflow and power at a maximum ECM setting of 517 ft^3/min (0.24 m^3/s) and 231 W, respectively, at 0.25 in w.g. static pressure. If the design requirement for a space were 517 ft^3/min (0.24 m^3/s), then this unit would just match the load at its maximum ECM setting. We then considered three other units that had higher airflow rates at their maximum ECM settings: ECM- 333A4, ECM-500A2, and ECM-750A1. The airflow at maximum ECM setting for all four are listed in Table 3.11.

Table 3.11 – Four ECM Units with their Capacity and Power Ratings at the Maximum ECM Setting at 0.25 in w.g. (62 Pa) Static Pressure

Unit	Capacity – ft^3/min (m^3/s)	Power (W)
ECM-333A11	517 (0.24)	231
ECM-333A4	892 (0.42)	370
ECM-500A2	1144 (0.54)	710
ECM-750A1	2086 (0.85)	850

If the three alternative units were used to provide the design airflow then each would be set at 517 ft^3/min (0.24 m^3/s). The power consumption at that airflow could be calculated for each of the units based on the data provided by the manufacturers for those units. Table 3.12 shows the PLAF, the power, and the power/airflow for the base unit (ECM-333A11) and the three alternative ECM units. The trend in Table 3.12 with decreasing power and power/airflow with increasing capacity was consistent with that shown in Figure 3.12. Table 3.12 suggests that considerable savings in power can be achieved by using an ECM FPTU that has a maximum airflow larger than the design airflow, but operated at a reduced speed to meet the design airflow requirements. The table did not say whether some of the larger units would be practical due to economics or physical constraints, but the table supported the trends shown in Figure 3.12.

Table 3.12 – PLAF, Power, and Power/Airflow for Four ECM Units Operating at 517 ft^3/min (0.24 m^3/s)

Unit	PLAF	Power (W)	Power/Airflow – W/ft^3/min (W/m^3/s)
ECM-333A11	1.00	231	0.449 (951)
ECM-333A4	0.58	89	0.172 (364)
ECM-500A2	0.45	66	0.128 (271)
ECM-750A1	0.25	50	0.096 (203)

3.8. Modeling FPTU Performance

There are two applications of ECM FPTUs. In the first, the ECM FPTU is installed, the airflow is set at a specific value, and the unit attempts to maintain a fixed airflow whenever the FPTU fan motor is on. For the second application, the ECM controller is integrated into the building energy management control systems so the airflow of the FPTU can be varied to meet the load in the zone as the load changes. The mathematical models needed to fully integrate ECM fan/motors into building simulation models are discussed below for both the fixed and variable airflow cases.

3.8.1 Fixed Airflow Case For a building energy simulation program to estimate the power and energy used by an ECM FPTU, it is necessary to develop mathematical relationships between power, airflow, and sizing. Figure 3.13 shows the line relating the power to the airflow at maximum ECM setting along with the part load curves for several ECM units of different capacities.

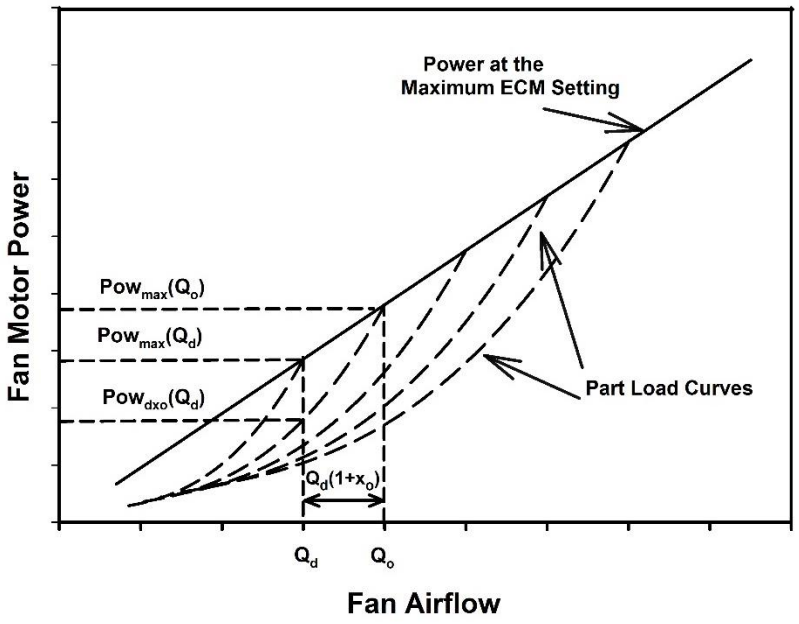

Figure 3.13: Representation of the Power used by Different Sized Units at the Design Airflow (Q_d) and a Unit having an Airflow of Q_o Larger than the Design Airflow at its Maximum ECM Setting

If the airflow needed to satisfy the design load of the space is assumed to be Q_d, then at that design airflow, an ECM FPTU could be selected whose airflow at its maximum ECM setting would just match the design airflow. In that case, the power demand for the unit, given as

Pow_{max} (Q_d) in Figure 3.13, would be on the straight line that related the power and airflow at the maximum ECM setting. The calculation of the power for this unit would be accomplished by utilizing Equation 3.11 and substituting Q_d for Q_{max} in that equation.

$$Pow_{max}(Q_d) = C_1 * Q_d \tag{3.12}$$

While a unit could be selected whose airflow at its maximum ECM setting just matched the design airflow, it can be observed in Figure 3.13 that a unit with a larger capacity should use less power than that from the unit that was just sized to meet the design load at its maximum ECM setting. If this unit was considered and its airflow capacity was some arbitrary amount q_o above the capacity of the design load, then the maximum capacity, Q_o, of this unit would be given by:

$$Q_o = Q_d + q_o \tag{3.13}$$

A new variable, x_o, can be defined as the "capacity factor." It captures the fraction of airflow capacity of the FPTU that is above the design load. It is related to q_o by the following:

$$q_o = x_o Q_d \tag{3.14}$$

Equation 3.14 can be substituted into Equation 3.13 and simplified to obtain:

$$Q_o = Q_d + x_o Q_d = Q_d(1 + x_o) \tag{3.15}$$

Equation 3.15 shows that capacity of the FPTU can be written in terms of the capacity factor, x_o, and the design airflow capacity.

Assuming the FPTU of capacity Q_o was run at its maximum ECM setting, then its power, $Pow_{max}(Q_o)$, could be calculated from Equation 3.11 if the airflow for the unit, Q_o, was substituted for Q_{max}:

$$Pow_{max}(Q_o) = C_1 * Q_o \tag{3.16}$$

In Figure 3.13, the power of the FPTU operating at the design airflow is given by $Pow_{dxo}(Q_d)$. This operating point can be calculated from the product of the part load power fraction of the FPTU at the design airflow, $f_{pl}(f_{flow\_do})$ and power at the maximum ECM setting for that unit:

$$Pow_{dxo}(Q_d) = f_{pl}(f_{flow\_do}) * Pow_{max}(Q_o) \tag{3.17}$$

In the above equation, f_{flow_do} is the part load airflow fraction for the FPTU operating at the design airflow which is lower than the maximum airflow of the FPTU. The part load power fraction would be given by:

$$f_{pl}(f_{flow\_do}) = a_1 + a_2 * f_{flow\_do} + a_3 * {f_{flow\_do}}^2 + a_4 * {f_{flow\_do}}^3 \tag{3.18}$$

The part load airflow fraction, f_{flow_do} would be:

$$f_{flow\_do} = \frac{Q_d}{Q_o} \tag{3.19}$$

The constants $a_1..a_4$ in Equation 3.19 were given in Table 3.8. For the continued mathematical derivation of the model, it would be more convenient to utilize the ratio of Q_d/Q_o rather than f_{flow_do}. Equation 3.18 can then be rewritten as:

$$f_{pl}(f_{flow\_do}) = a_1 + a_2 * \left(\frac{Q_d}{Q_o}\right) + a_3 * \left(\frac{Q_d}{Q_o}\right)^2 + a_4 * \left(\frac{Q_d}{Q_o}\right)^3 \tag{3.20}$$

Equation 3.15 relates Q_d, Q_o, and the capacity factor, x_o. The equation for the part load power fraction can be rewritten as:

$$f_{pl}(f_{flow\_do}) = a_1 + a_2 * \left(\frac{Q_d}{Q_d(1+x_o)}\right) + a_3 * \left(\frac{Q_d}{Q_d(1+x_o)}\right)^2 + a_4 * \left(\frac{Q_d}{Q_d(1+x_o)}\right)^3 \tag{3.21}$$

Simplifying the above yields:

$$f_{pl}(f_{flow\_do}) = a_1 + a_2 * \left(\frac{1}{1+x_o}\right) + a_3 * \left(\frac{1}{1+x_o}\right)^2 + a_4 * \left(\frac{1}{1+x_o}\right)^3 \tag{3.22}$$

Equation 3.22 is an important result because the capacities, Q_d and Q_o, disappeared with the simplification and the only variable remaining on the right hand side of the equation was the capacity factor (x_o) of the unit which expressed the fractional airflow capacity the FPTU had above the design airflow. Therefore, the part load power fraction for an ECM FPTU with larger airflow capacity than the design airflow only depended on the capacity factor and not the specific capacity of the unit. It wouldn't matter for the calculation of the part load power fraction, $f_{pl}(f_{flow\_do})$, if the design airflow was 500 ft^3/min (0.24 m^3/s) or 2500 ft^3/min (1.18 m^3/s). As long as the capacity factor (x_o) was known, then the part load power fraction could be calculated for an ECM unit whose speed was "dialed back" to operate at the design load using Equation 3.22.

Figure 3.14 shows a graphical representation of Equation 3.22 for the capacity factor ranging from 0 to 2. A value of 1.0 for the capacity factor represented installing a unit with twice the airflow capacity of the design airflow. The dashed lines in Figure 3.14 showed the decreasing marginal benefit for increasing the capacity factor. At a 0.25 capacity factor, which corresponded to a FPTU with a maximum airflow 25% larger than the design airflow, the part load power fraction dropped by 44.6% to a value of 0.554. Increasing the capacity factor by another 0.25 to a value of 0.50 reduced the part load power fraction to 0.375 or a reduction of 35.5% over the case for a capacity factor of 0.25.

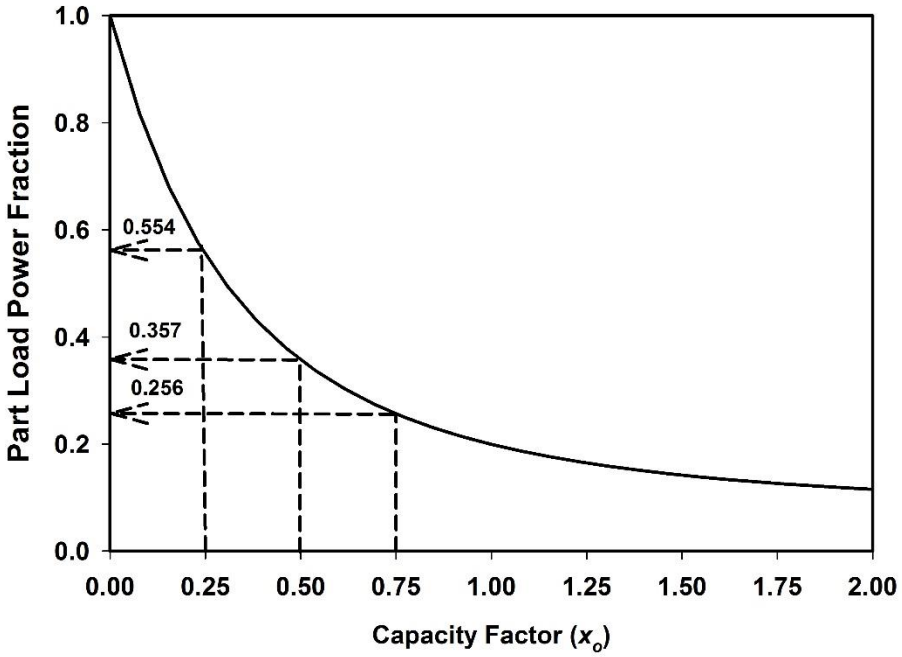

Figure 3.14: Part Load Power Fraction as a Function of ECM Fan/Motor Capacity Factor

While the behavior of the part load power fraction was important in the calculation of power, it was not the only variable that must be considered. As shown in Equation 3.17, the calculation of the power used by the ECM fan/motor unit required both the part load power fraction and the power used by the fan motor at the maximum ECM setting for the unit, $Pow_{max}(Q_o)$. In Figure 3.10, the power of the ECM unit was linearly related to the airflow capacity at their maximum ECM settings. The part load power fraction, $f_{pl}(f_{flow\_do})$, the first term on the right hand side of Equation 3.17, was shown to be dependent on only the capacity factor (x_o) of the ECM unit. The second term on the right hand side of Equation 3.17 was the power at the maximum ECM setting for the unit, $Pow_{max}(Q_o)$. It can be divided by power at the maximum ECM setting for a unit that just satisfied the design capacity, $Pow_{max}(Q_d)$ to obtain:

$$\frac{Pow_{max}(Q_o)}{Pow_{max}(Q_d)} = \frac{C_1 * Q_o}{C_1 * Q_d} = \frac{Q_o}{Q_d} = \frac{Q_d(1+x_o)}{Q_d} = (1 + x_o) \tag{3.23}$$

As shown in the above equation, it was possible to simplify this ratio to show that it was only dependent on the capacity factor, x_o. Equation 3.23 can also be rearranged to solve for the power used by the FPTU at its maximum ECM setting:

$$Pow_{max}(Q_o) = Pow_{max}(Q_d) * (1 + x_o) \quad (3.24)$$

Referring back to Equation 3.17, both the power at the maximum ECM setting for the FPTU and the part load power fraction for the unit operating at the design airflow must be known to be able to calculate the power of the FPTU operating at the design airflow, $Pow_{dxo}(Q_d)$. Equation 3.24 can be substituted into Equation 3.17 to get the following:

$$Pow_{dxo}(Q_d) = f_{pl}(f_{flow\_do}) * Pow_{max}(Q_d) * (1 + x_o) \quad (3.25)$$

In Equation 3.25, the power for the fan operating at the maximum ECM for the design airflow, $Pow_{max}(Q_d)$ can be calculated from Equation 3.12 and substituted into Equation 3.25 which results in:

$$Pow_{dxo}(Q_d) = f_{pl}(f_{flow\_do}) * C_1 * Q_d * (1 + x_o) \quad (3.26)$$

Looking at Equation 3.26, the only variables an energy modeler would need to estimate the power of an ECM unit with a maximum capacity larger than the design airflow but operating at the design airflow would be the design airflow, Q_d, and the capacity factor, x_o. The power/airflow slope, C_1, was given in Equation 3.11. The coefficients, $a_1 \ldots a_4$ were given in Table 3.8 for calculating the part load power fraction. There was no requirement in Equation 3.26 for specifying motor efficiencies, fan efficiencies, fan pressure differentials, etc. as is currently required by some building energy simulation models. The above result was based on fits of a large number of currently produced ECM units from four manufacturers. A modeler could use a different value of C_1 if manufacturer's data were available. For example, should future units be shown to be more efficient than those used here, then C_1 should decrease, which would be reflected in a drop in power requirements for a given design airflow and capacity factor. Likewise, should more data be analyzed that provide a different part load curve, then the coefficients a_1 through a_4 could be recalculated and modified to calculate a new part load power fraction.

Figure 3.15 shows a plot of the power calculated using Equation 3.26 for design airflows ranging from 500 to 2500 ft^3/min (0.24 to 1.18 m^3/s) and for the capacity factor ranging from 0 to 2. In all cases, the maximum power is at zero capacity factor and then rapidly drops with increasing capacity factor then begins to level off at about 1.5 or a ECM FPTU maximum airflow that would be 150% larger than the design airflow.

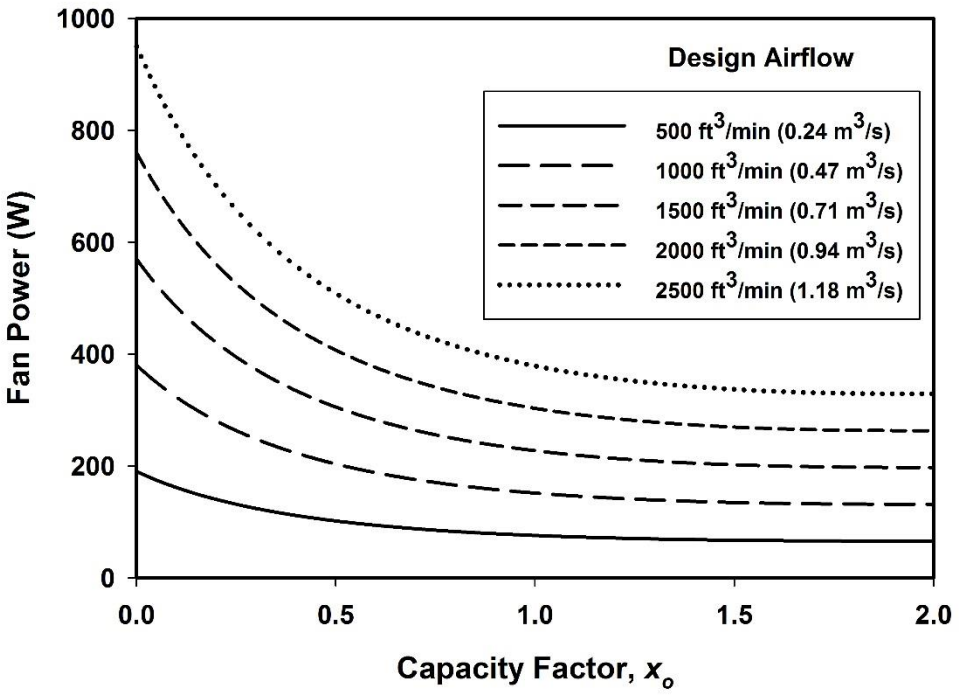

Figure 3.15: Fan Power Variation with Capacity Factor and Design Airflow

Equation 3.26 can be used to calculate the power used by either a parallel or series ECM FPTU. However, it may be useful to pose the question, "Is there a mathematical limit to how large a FPTU should be installed so that there is no longer an increasing benefit in reduced power when operating at a given design airflow?" As was shown in Equation 3.26, the power used by a unit was the product of the part load power fraction (a cubic equation) that decreased with increased capacity factor and a second term on the right hand side of Equation 3.26 which was a linear term that increased with capacity factor. With one term increasing and the other decreasing, it would be possible that multiplying the two together could produce a minimum value for power. Thus, there may be an increase in the size of the ECM FPTU where the power no longer decreased.

To investigate this possibility, it would be useful to normalize the power, $Pow_{dxo}(Q_d)$, used by any FPTU whose speed was lowered to meet the design airflow to the maximum power, $Pow_{max}(Q_d)$, that would be used by the power used by a FPTU operating a maximum airflow to just meet the same design airflow. Both sides of Equation 3.26 can be divided by $Pow_{max}(Q_d)$ to normalize the power for the units to $Pow_{max}(Q_d)$.

$$\frac{Pow_{dxo}(Q_d)}{Pow_{max}(Q_d)} = \frac{f_{pl}(f_{flow\_do}) * C_1 * Q_d * (1+x_o)}{Pow_{max}(Q_d)} \quad (3.27)$$

Because $Pow_{max}(Q_d)$ is equal to $C_1 * Q_d$, this can be substituted into right hand side of Equation 3.27 to produce:

$$Pow_{Rat} = \frac{Pow_{dxo}(Q_d)}{Pow_{max}(Q_d)} = f_{pl}(f_{flow\_do}) * (1 + x_o) \quad (3.28)$$

For convenience, the ratio of the power of the larger unit operating at the design airflow divided by the power of the unit sized to just meet the design airflow was defined with the symbol Pow_{Rat}. On the right hand side of Equation 3.27, the part load power ratio was only dependent on x_o. The second term on the right hand side only contained x_o as a variable, so the power ratio was only dependent on the capacity factor, x_o, and not the actual capacity of the unit.

A plot of Equation 3.28 is shown in Figure 3.16. The power ratio ranged from 1.0 for a unit just sized to meet the design airflow (x_o=0) to a low of about 0.35 for a unit with a capacity factor of 2.0, which would correspond to a unit with a maximum airflow capacity three times larger than the design airflow. Above a capacity factor of two, the power ratio began to increase indicating the units should never be sized larger than a capacity factor of two.

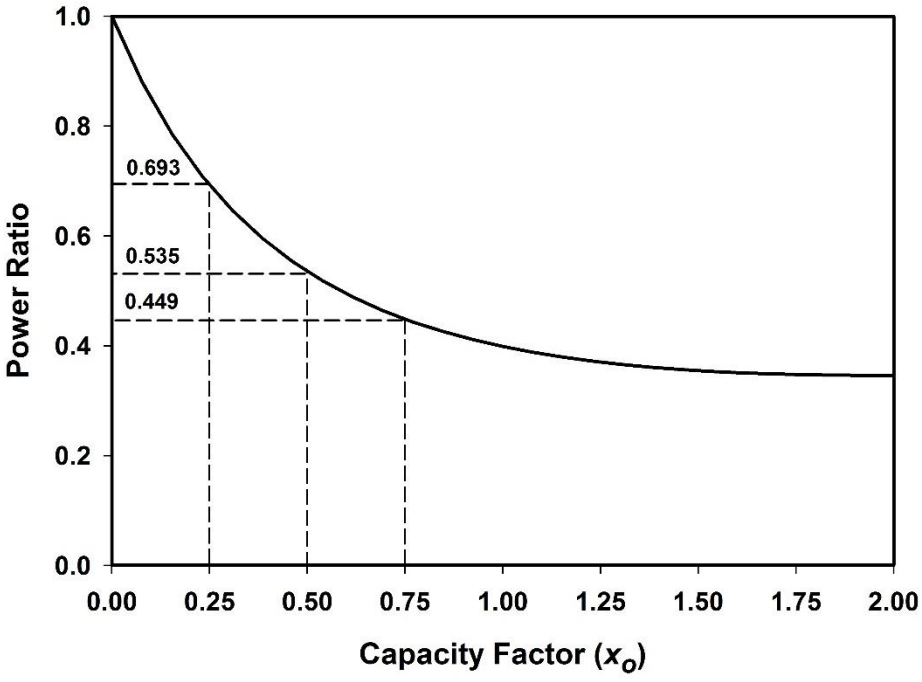

Figure 3.16: Power Ratio as a Function of Capacity Factor

Another way of presenting the data in Figure 3.16 was to calculate the fractional power savings that would result from operating the larger FPTU at the design airflow. The fractional power savings can be calculated from Equation 3.24 by subtracting the power ratio from one:

$$Pow_{sav} = 1 - Pow_{Rat} \tag{3.29}$$

Table 3.14 shows the percentage power savings as a function of the capacity factor when a larger capacity ECM FPTU was operated at the design airflow. The calculations show that a unit with a capacity factor of 25% and operated at the design airflow should produce a power savings of about 30% over a unit that was just matched in size to the design airflow. These numbers showed that the recommendations of manufacturers to "upsize" or oversize FPTUs and then reduce the operating airflow to the design airflow to reduce noise can also provide a significant energy savings for ECM FPTUs. Table 3.14 shows that there was essentially little power savings benefit for applying a unit that had a capacity factor more than 1.0, which would correspond to a unit with 100% more airflow capacity than needed at the design airflow. Implementing the equations that provided the curves for Figure 3.14 and data in Table 3.14 in a building simulation program would allow an energy modeler to choose an infinite range of sizes of FPTUs along the continuous curve of Figure 3.16. In contrast, the applications engineer operating in the field would be faced with a discrete number of ECM FPTUs with capacities larger than the design airflow because manufacturers only offer a limited number of FPTUs in their product offerings. However, an applications engineer should be able to use either Figure 3.16 or Table 3.14 to get a quick estimate of the savings from applying a larger ECM FPTU and operating it in a fixed airflow mode at the design airflow.

Table 3.14 – Calculated Percentage Power Savings for an ECM FPTU over a Range of Capacity Factors using Equation 3.29.

Capacity Factor	Percentage Power Savings
0.05	8.1%
0.10	15.0%
0.15	21.0%
0.20	26.2%
0.25	30.1%
0.30	34.7%
0.35	38.2%
0.40	41.3%
0.45	44.0%
0.50	46.5%
1.00	60.1%
1.50	64.5%
2.00	65.4%

3.8.2 Varying Airflow to Meet the Load An ECM FPTU can be integrated into a building automation system so that the ECM can vary the airflow to match the load requirements in the zone. There were two scenarios that were considered. The first was when the ECM FPTU was sized to just meet the design airflow requirement for the space. The second case was when the maximum airflow capacity of the FPTU was larger than the design airflow requirement for the zone. Each was discussed below.

Figure 3.17 presents an ECM unit that is sized to just meet the design airflow (Q_d) requirements of the space.

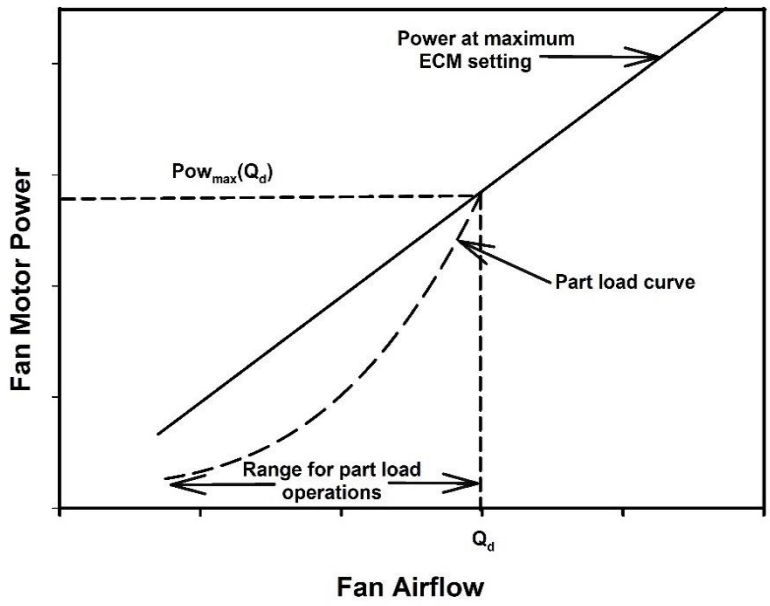

Figure 3.17: Part Load Power for an ECM Unit Sized to Just Meet the Design Load

The ECM can operate over its complete design range as shown in the curved dotted line (marked "part load curve") below the solid line representing the power at the maximum ECM setting. The unit would operate along the dashed line in response to changes in load in the space.

The part load curve in Figure 3.17 at a given airflow, Q_{flow}, was the power used by the ECM fan/motor, $Pow_{fan}(Q_{flow})$. This power was given in a general form in Equation 3.11. For use here, the design airflow, Q_d , was substituted for Q_{max}, and the part load airflow fraction was given the symbol, f_{flowd} rather than f_{flow} because the reference for the part load airflow fraction was the design airflow. These changes are shown below:

$$Pow_{fan}(Q_{flow}) = f_{pl}(f_{flowd}) * Pow_{max}(Q_d) \tag{3.29}$$

For Equation 3.29, the part load power fraction, $f_{pl}(f_{flowd})$ and part load airflow fraction were given by:

$$f_{pl}(f_{flowd}) = a_1 + a_2 * (f_{flowd}) + a_3 * (f_{flowd})^2 + a_4 * (f_{flowd})^3 \tag{3.30}$$

and

$$f_{flowd} = \frac{Q_{flow}}{Q_d} \tag{3.31}$$

The constants, $a_1 \ldots a_4$ were the same as those listed in Table 3.13. The ratio of Q_{flow} divided by Q_d was the part load airflow fraction for an ECM unit whose capacity at its maximum ECM

setting would just equal the design airflow for the zone served by the ECM FPTU. The part load power ratio would be 1.0 when the airflow was at the design airflow rate and would decrease for lower values of the airflow.

The second term on the right hand side of Equation 3.29 was the power for the fan motor operating at the maximum ECM setting to just satisfy the design airflow. For a unit operating at its maximum ECM setting, the power was related to the airflow by a constant, C_1, as shown in Equation 3.11. Thus, Equation 3.29 can be rewritten in terms of this constant and the design airflow.

$$Pow_{fan}(Q_{flow}) = f_{pl}(f_{flowd}) * C_1 * Q_d \quad (3.32)$$

If the FPTU was sized to just meeting the design airflow when the ECM was at its maximum setting, then Equation 3.32 can be used to calculate the power at any airflow that was less than the design value. It should be straightforward to implement Equation 3.32 into a building energy simulation program. The design load would either be specified by the user or calculated by the program. At any given airflow requirement, the part load airflow fraction, Q_{flow}/Q_d, the part load power fraction, and the power would be calculated.

The example above was for the simple case where the ECM FPTU was sized to just meet the design airflow requirements. As discussed in the previous section for the fixed airflow case, there was the potential for significant power and energy savings if the maximum capacity of the ECM FPTU was larger than the design airflow requirements. For the case where the ECM would be at a fixed airflow, the analysis showed that calculating the power only required knowledge of the capacity factor and the design airflow. Figure 3.18 showed the power versus airflow for two ECM units. One was sized to the design load, Q_d, and the other had a capacity of Q_o at its maximum ECM setting. These plots were made from utilizing Equations 3.7 and 3.11. The part load curve for the larger unit started at a higher power requirement at its maximum ECM setting than did the unit that was just matched to the design airflow. However, the power of the larger unit rapidly dropped as the airflow requirements decreased. When its airflow capacity crossed the design airflow, Q_d, the larger unit had a lower power requirement than the unit sized to match the design airflow. As the airflow was further decreased, the larger unit continued to have a lower power requirement until the part load curves for the unit matched to the design load and the larger unit eventually crossed at very low airflows. The plot in Figure

3.18 would indicate that the unit with larger airflow capacity should provide over a unit matched to the design load for varying airflows below the design airflow.

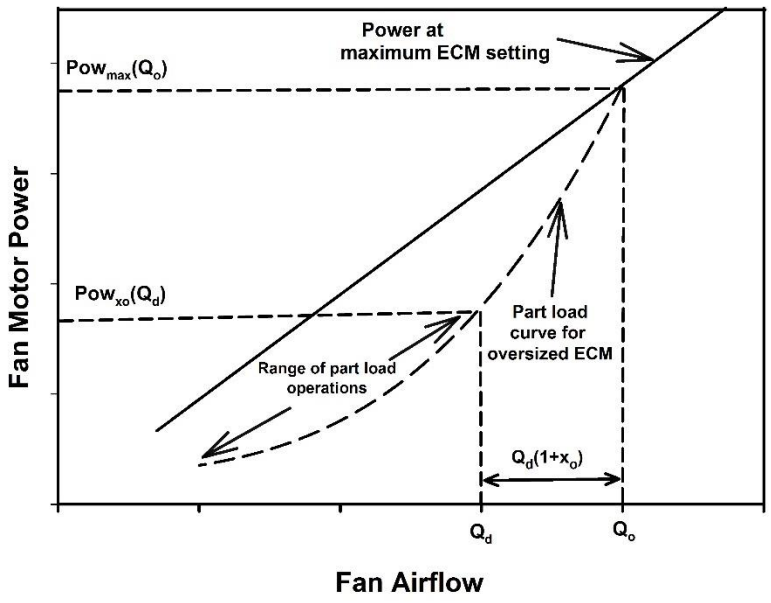

Figure 3.18: Power of an ECM Unit with a Maximum Airflow Capacity (Q_o) whose Speed is Reduced to Meet the Design Load (Q_d) and the Range of Part Load Operations where Speed is Varied to Meet the Airflow Requirements of the Space

Developing a mathematical model to describe the part load performance for an ECM unit with maximum capacity above the design airflow followed a similar strategy to what was used for the unit matched to the design airflow. The general equation for power used by the ECM fan motor along the part load curve for the larger unit was the same as for Equation 3.29 except the maximum airflow was not at the design airflow but at the airflow, Q_o, of the FPTU operating at its maximum ECM setting. Likewise the part load airflow and power fractions were referenced to Q_o rather than Q_d. With these changes, we now have:

$$Pow_{fan}(Q_{flow}) = f_{pl}(f_{flowo}) * Pow_{max}(Q_o) \quad (3.33)$$

$$f_{pl}(f_{flowo}) = a_1 + a_2 * (f_{flowo}) + a_3 * (f_{flowo})^2 + a_4 * (f_{flowo})^3 \quad (3.34)$$

$$f_{flowo} = \frac{Q_{flow}}{Q_o} \quad (3.35)$$

Equations 3.33 through 3.35 also had the restriction that the airflow, Q_{flow}, must be less than the design airflow, Q_d. In Figure 3.18, $Q_{flow} < Q_d$ was represented by the airflow that was labeled "Range for part load operations". If the design load represented the maximum airflow

the zone should need, then all part load operations would be below that airflow. Figure 3.18 showed that the FPTU with larger capacity than the design airflow unit used a "truncated" portion of the part load curve because the airflow would never go above Q_d. In contrast, the ECM unit in Figure 3.18 that was sized to match the design airflow would utilize the full range of its part load curve. Even though the ECM unit that matched the design airflow utilized its full part load curve, it still used more power over most of the range than the larger unit that had a maximum capacity larger than the design airflow.

Equation 3.24 related the fan power for the maximum ECM setting for the larger unit to the unit that just matched the design load. Equation 3.33 can be rewritten with the relationship from Equation 3.24 to obtain:

$$Pow_{fan}(Q_{flow}) = f_{pl}(f_{flowo}) * Pow_{max}(Q_d) * (1 + x_o) \quad (3.36)$$

The only term left in Equation 3.36 that still directly had the larger unit's capacity embedded in it was the part load power fraction, $f_{pl}(f_{flowo})$. The relationship for Q_o in Equation 3.15 could be substituted into the expression for the part load airflow fraction (Equation 3.35) and substituted into the part load power fraction (Equation 3.34) to get:

$$f_{pl}(f_{flowo}) = a_1 + a_2 * \left(\frac{Q_{flow}}{Q_d(1+x_o)}\right) + a_3 * \left(\frac{Q_{flow}}{Q_d(1+x_o)}\right)^2 + a_4 * \left(\frac{Q_{flow}}{Q_d(1+x_o)}\right)^3 \quad (3.37)$$

Once an ECM FPTU unit was selected by a modeler for a simulation, the capacity factor, x_o, would be known. Equation 3.37 could be simplified by incorporating the $(1+x_o)$ terms into the constants and redefining the constants in the following way:

$$a_2' = \frac{a_2}{(1+x_o)} \qquad a_3' = \frac{a_3}{(1+x_o)^2} \qquad a_4' = \frac{a_4}{(1+x_o)^3} \quad (3.38)$$

The constant a_1 through a_4 are the same as those in Table 8. Substituting the new constants into Equation 3.37 gave the following:

$$f_{pl}(f_{flowo}) = a_1 + a_2' * \left(\frac{Q_{flow}}{Q_d}\right) + a_3' * \left(\frac{Q_{flow}}{Q_d}\right)^2 + a_4' * \left(\frac{Q_{flow}}{Q_d}\right)^3 \quad (3.39)$$

The ratio, Q_{flow}/Q_d in Equation 3.39 was already defined as the part load airflow fraction, f_{flowd}, in Equation 3.35. This substitution can be made into Equation 3.39 to obtain:

$$f_{pl}(f_{flowo}) = a_1 + a_2' * (f_{flowd}) + a_3' * (f_{flowd})^2 + a_4' * (f_{flowd})^3 \quad (3.40)$$

The redefined constants in Equations 3.40 would vary depending on the capacity factor of the FPTU and would need to be calculated for each application of an ECM FPTU in a model. The

above expression in Equation 3.40 for the part load power fraction for the FPTU can be compared to the one in Equation 3.30 for the case where the unit just matched the design airflow. The two expressions were very similar except for the definition of the constants. However, if a unit was just sized to match the design load, then the capacity factor would be zero. In that case, x_o would equal zero and the term, $1 + x_o$, would be equal to one and each of the redefined constants would drop back down to the original values:

$$a_2' = a_2 \qquad a_3' = a_3 \qquad a_4' = a_4 \tag{3.41}$$

The part load power fraction calculated from Equation 3.40 for the case where x_o=0 would equal to the part load power fraction of Equation 3.30. Thus, Equation 3.40 could be viewed as the "general" case and could be applied to both situations where the ECM unit's airflow capacity was larger than the design airflow but whose fan speed was reduced so the unit's airflow just matched the design airflow.

In Equation 3.36, there was also a term for the fan power at the maximum ECM setting for the unit that just matched the design load. By utilizing Equation 3.16, this power term can be written in terms of the design airflow and the constant C_1.

$$Pow_{fan}(Q_{flow}) = f_{pl}(f_{flowo}) * C_1 * Q_d * (1 + x_o) \tag{3.42}$$

The fan power at a given airflow, Q_{flow}, can easily be calculated because all of the terms on the right hand side only depended on Q_{flow}, Q_d, and x_o. There was no requirement for fan or motor efficiencies or pressure differentials across the fan. Equation 3.42 could be implemented into a building simulation program to estimate the power used by an ECM fan as the airflow was varied to meet the thermal load in the space and should apply to both heating and cooling applications.

3.9. Summary

This chapter presented an analysis of a wide range of ECM fan/motor combinations provided by four FPTU manufacturers. While the data showed scatter which could be expected to occur because each manufacturer used different fans and motor combinations as well as their own design strategies for each unit. Even with the scatter, it was possible to develop a third degree polynomial fit to the part load data in the general format used by prior building energy simulation models. Unlike models in prior building energy simulation programs that focused solely on the fan, the part load model developed here included the fan/motor assembly. While

the data showed the same general shape as the third degree polynomial of Knebel (1983), the drop in power was much steeper for higher part load airflows. Unlike the Knebel (1983) model that went to zero PLPF at zero PLAF, the model for the ECM fan/motor units leveled off near 0.062 for PLAF values less 0.1. The non-zero value of PLPF may correspond to a small amount of power required by the controller in the ECM even where there is little or no airflow.

The analysis of the data also provided estimates of the power/airflow relationship for ECM fan/motors operating at their maximum ECM setting. An energy modeler should be able to directly use this relationship along with the third degree polynomial regression to estimate the hourly performance of ECM fan/motors in FPTUs.

The part load methodology provided simple models that can be used to estimate the performance of ECM FPTUs either sized to just meet the design airflow requirements for the zone or have capacities larger than the design airflow requirement but whose speed is lowered to meet the design airflow. The models can be used in applications where the airflow is fixed or varied to meet the load requirements in the space. The models relied on data that can be readily obtained from manufacturers of ECM FPTUs in contrast to current models that require the user to input fan and motor efficiency and fan pressure differential (EnergyPlus 2013).

The model developed here for fixed airflow applications needed only the design airflow and capacity factor to estimate the power used by the ECM unit. The capacity factor was a measure of the maximum airflow capacity of the FPTU relative to the design airflow requirement of the zone. The model was used to analyze the potential savings of FPTUs whose maximum capacities were larger than the design airflow requirement but operated at the design airflow. Based on the analysis, applying a unit that was 0.25 capacity factor produced over a 30% power reduction compared to a unit that was just sized to match the design airflow. The 0.25 capacity factor would correspond to a unit with a maximum capacity that was 25% larger than the design airflow. There appeared to be little benefit in power reduction for a unit that had a capacity factor larger than 1.0. The analysis produced a continuous curve for the power savings for FPTUs with capacities larger than the design airflow but operating at the design airflow. In reality, units offered by manufacturers are in discrete sizes, so an engineer may be able to choose only a select number of units whose capacities are larger than the design airflow. The discrete options will limit the potential savings with these larger units. While costs were not included in the analysis, the choice of a larger unit will depend on whether the savings it provides offset its

additional costs. There may also be other factors that constrain the application of a larger unit. For example, a larger unit may require choosing a larger cabinet size, which may not fit the specific application. Another factor is how low a speed an ECM can be run. Most of the data provided by the manufacturers typically covered a range that went from 15 to 20% of the maximum setting on the controller. If the ECM FPTU is too large relative to the design airflow, it may be required to operate below the data collected by the manufacturer. Manufacturers typically have their reasons for not operating below these lower limits and an engineer needs to verify that the ECM can operate below these limits with the manufacturer.

For a variable airflow application, the actual airflow required for a specific load in the space would be the only additional input needed beyond the capacity factor and design airflow for the space. This model should be straightforward to incorporate into a building simulation program because the hourly thermal and airflow requirements are calculated in the program.

Both the fixed and variable airflow models capture the power used by the fan/motor combination. Assuming all the fan power is expended in the airstream, a reduction in fan power with an ECM fan/motor unit would reduce the calculated cooling energy because less heat energy would be added to the airstream in an FPTU. However, the opposite would occur with heating. The exact annual benefits in cooling or penalty in heating would need to be calculated with a building simulation program and is discussed in Chapter 9.

CHAPTER 4
IN SITU LABORATORY AND FIELD MEASUREMENTS

The purpose of this chapter was to report on the laboratory and field measurements of in situ fan differential pressure for fan/motor combinations in series FPTUs and field measurements to better characterize performance of both series and parallel FPTUs. A range of primary airflow and induced airflow was used to characterize the differential pressure performance of this fan. Results show that a correlation can be developed for fan differential that was linear with total airflow as the dependent variable. The velocity differential pressure for these same flow ranges was also calculated and show similar promising correlations. Models suggested for pressure rise for series FPTU should allow an energy modeler to more accurately estimate the annual performance of FPTUs in building energy simulation programs.

The main campus of Texas A&M University was chosen as the site for the field observations and measurements. The Energy and Utility staff at Texas A&M helped identify candidate buildings/FPTUs and assisted with installation of monitoring hardware and programming of the campus building management system (BMS) to provide coincident FPTU performance data. The efforts started with qualitative assessment of several FPTUs across campus. The FPTU chosen were of similar size and age to be consistent across measurements. The second effort consisted of direct measurements of performance data for several series and parallel FPTU. Some of these data were used to make qualitative judgements concerning parallel FPTU leakage.

4.1. Background – Need for Measurements

In EnergyPlus (2013), the user is required to provide inputs for fan total efficiency (η_{tot}), fan motor efficiency (η_{mot}), and a "design air pressure rise across the fan", ΔP. It is assumed that the pressure rise is the total pressure rise across the fan and this is because the definition of fan efficiency normally uses total pressure. Fan static pressure could be used because there is usually not a significant difference in the static and total pressures for the small diameter fans typically used in FPTUs. But it was not clearly stated in the EnergyPlus documentation which differential pressure rise was appropriate. As discussed in earlier chapters, individual fan and motor efficiencies were rarely provided separately by the FPTU manufacturers. For the small diameter fans and fan motors used in FPTUs, the fan and motor are usually tested as a unit rather than individually.

Regardless of definition used, the small fan/motor sets used in FPTUs should generate either static or total differential pressure rises substantially less than 1.0 in w.g. (250 Pa) as shown in Chapters 2 and 3. Static pressures downstream of the FPTU are usually less than 0.5 in w.g. (125 Pa) with 0.25 in w.g. (62.5 Pa) being a very common engineering design point. Because the differential pressure rise was one of the fundamental fan inputs to EnergyPlus (2013), fan performance data are needed for these units. Accepting "default" or using inappropriate values for the fan inputs can potentially have a major impact on the energy estimate of the simulation models using FPTUs, especially series types, in VAV systems. Modeling of FPTU VAV systems using correlations based upon actual fan pressure rise data should result in better energy use models and allow building professionals to make better system application decisions.

4.2 Laboratory Experimental Description

An experimental apparatus was constructed to allow measurement of the static differential pressure rise across a FPTU fan. It was constructed from equipment used from previous research projects (Peng and O'Neal, 2013 and Furr et al 2008). The basic apparatus used in the laboratory experiments is shown schematically in Figure 4.1. The system consisted of a fan (primary air), straight duct section, 8 inch (20.3 cm) inlet diameter series FPTU, straight duct section, and a suction (assist) fan. The series FPTU was a unit that had been used in a previous research project (Furr et al., 2008) and in that study had been assigned the designation of SCR-S8C. This designation indicated that the motor was a PSC type, controlled by an SCR, with an 8 inch (200 mm) primary inlet diameter and supplied by manufacturer "C".

The two fans and FPTU were connected to each other with rectangular, uninsulated sheet-metal ductwork. The length of this duct (Figure 4.1) followed specifications outlined in ANSI/ASHRAE Standard-130 (2006). The upstream duct was a 16 in. (40.6 cm) x 15 in. (381 mm) rectangular duct and the downstream rectangular duct was 8 in. (20.3 cm) x 9 in. (23.0 cm). All of the fans had 277V, single phase motors. The series S8C FPTU was supplied with a 0.5 hp (373 W) motor and opposing blade dampers at its inlet. Pictures of the setup are shown in Figures 4.2 and 4.3.

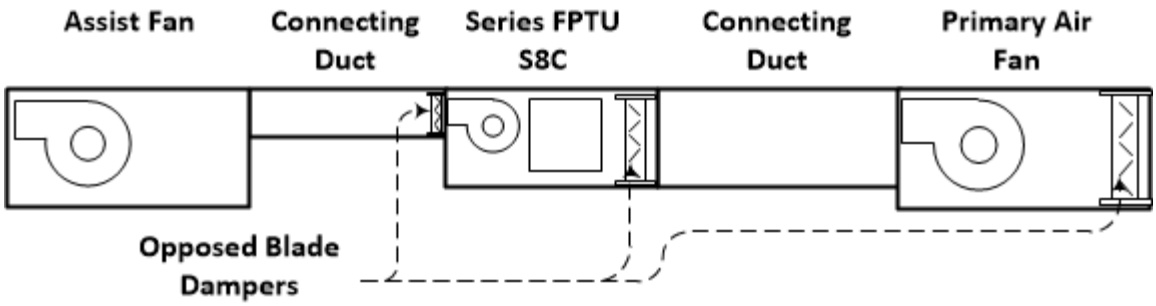

Figure 4.1: Schematic of Test Apparatus used to Measure FPTU Differential Pressure Rise

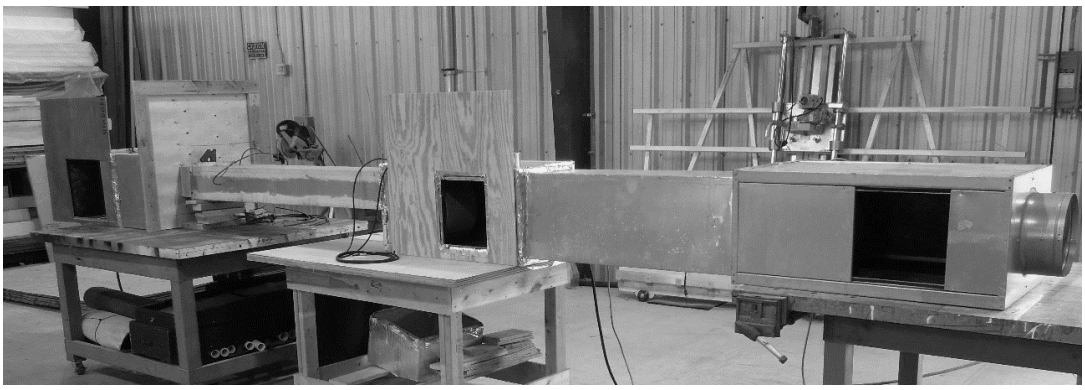

Figure 4.2: Side View of Experimental Apparatus, Right to Left: Primary Fan, Duct Section, S8C FPTU, Duct Section, Assist Fan

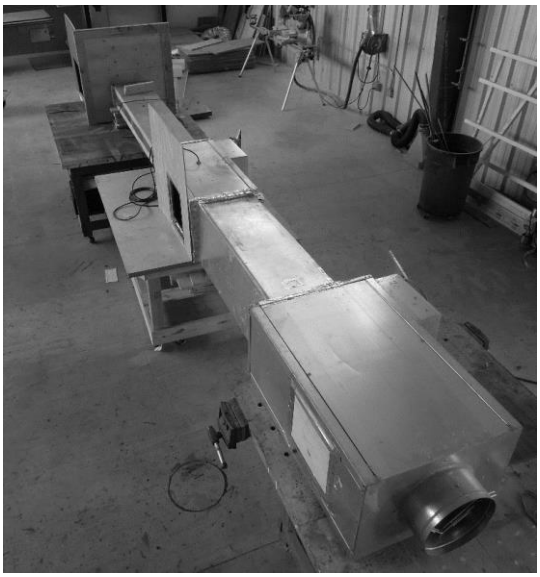

Figure 4.3: Overhead View of Experimental Apparatus, Bottom to Top: Primary Fan, Duct Section, S8C FPTU, Duct Section, Assist Fan

4.2.1. Testing Sequence Tests were run under as wide a range of airflows and voltages as supported by the S8C FPTU. The units were each turned on in a sequence of primary fan, S8C FPTU fan, then assist fan. The primary fan was set to maximum airflow through its controller. The SCR controller on the S8C was started at a minimal setting with the assist fan then modulated to maintain the desired static pressure in the discharge duct immediately downstream of the S8C FPTU. Discharge static pressure was set at 0.25 in. w.g. (62.3 Pa) because this value is set forth for FPTU testing under the ANSI/AHRI Standard 880 (AHRI, 2011).

As the system came to steady state, the discharge static pressure would be adjusted to 0.25 in. w.g. (62.3 Pa) through adjustment of the assist fan or the opposed blade damper in the discharge duct. Once the desired set point had settled to an acceptable level, the static differential pressure across the FPTU fan would be measured. Static pressure probes with a magnetic base were used for these measurements. Velocity pressure was measured in the discharge duct and primary air duct. These velocity pressure measurements allowed for calculation of the total airflow from the FPTU, total airflow supplied to the FPTU. The difference between these was the airflow induced through the FPTU induction port. Once a data set was completed, the flows would be reset for the FPTU primary fan and the discharge static pressure subsequently set back to 0.25 in w.g. (62.3 Pa) and the process repeated for the next data set. Table 4.1 shows the primary data collected and applicable ranges.

Instrumentation used for data collection included micromanometers to measure duct static, velocity pressure, and static differential pressure across the FPTU fan. A flowhood was used to measure total and induction port airflow. S8C FPTU fan power was measured with an industrial power quality meter. Differential pressure measurements were taken continuously for one minute and averaged for each data point.

Table 4.1 - S8C FPTU Test Points

Independent Variable		Range of Values
Fan Power		220 – 400 Watts
Primary Airflow		0 – 1,400 ft^3/min (0 – 0.66 m^3/s)
Induced Airflow		0 – 850 ft^3/min (0 – 0.40 m^3/s)

4.2.2 Laboratory Experimental Results Static pressure probe placement was an important part of this study. Two positions were evaluated at the discharge of the FPTU fan. Multiple positions were evaluated upstream of the FPTU fan. Because of the chaotic nature of the flow field entering through the FPTU and into the FPTU fan, it was felt that there might be significant issues with measurement stability or other measurement issues. The centerline of the FPTU fan (transverse to the FPTU cabinet) was chosen as a datum and static pressure tap holes were placed along the centerline of the longitudinal axis of the FPTU cabinet at four inches (100 mm) on center towards the inlet port of the FPTU. Figure 4.4 shows a photo of this arrangement. Testing revealed that what was referred to as position +2,-3 provided the most stable and consistent measurements of differential static pressure rise across the S8C FPTU fan. All subsequent testing was completed for static differential pressure rise using these measuring positions.

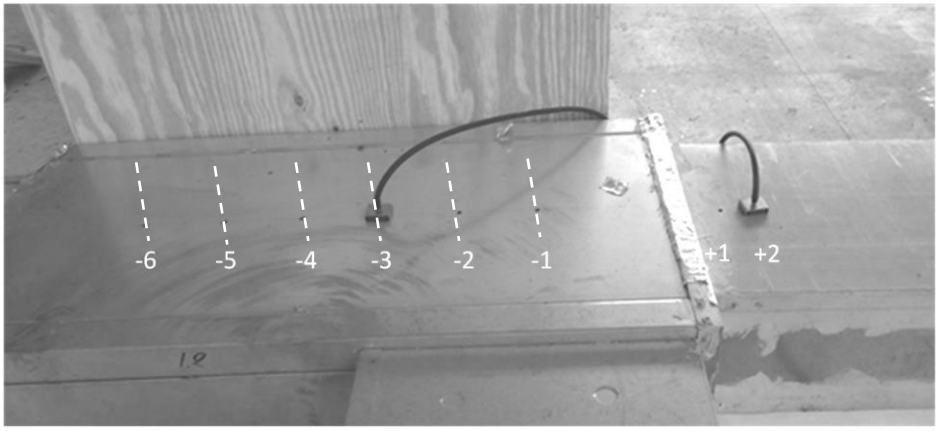

Figure 4.4: View of Static Pressure Tap Locations in the S8C FPTU Cabinet (left) and Discharge Static Pressure Points (right)

Power data for the S8C FPTU was taken as a function of airflow in a previous research project (Cramlet, 2008). Data from this study was compared to the data taken in that project to ensure reliable measurement techniques and that the fan was still performing consistently. These data are shown in Figure 4.5. The original data from the Cramlet study were taken under slightly different ambient conditions. To insure a proper comparison, data from that study were adjusted for air temperature as shown in the Equation 4.1.

$$q_{current} = q_{Cramlet} \left(\frac{273.1 + T_{current}}{273.1 + T_{Cramlet}}\right) \quad (4.1)$$

Where,

$q_{current}$ = airflow for S8C FPTU in current study, ft^3/min (m^3/s)

$q_{Cramlet}$ = airflow for S8C FPTU in Cramlet (2008) study, ft^3/min (m^3/s)

$T_{current}$ = air temperature at FPTU inlet for current study, °C

$T_{Cramlet}$ = air temperature at FPTU inlet for Cramlet (2008) study, °C

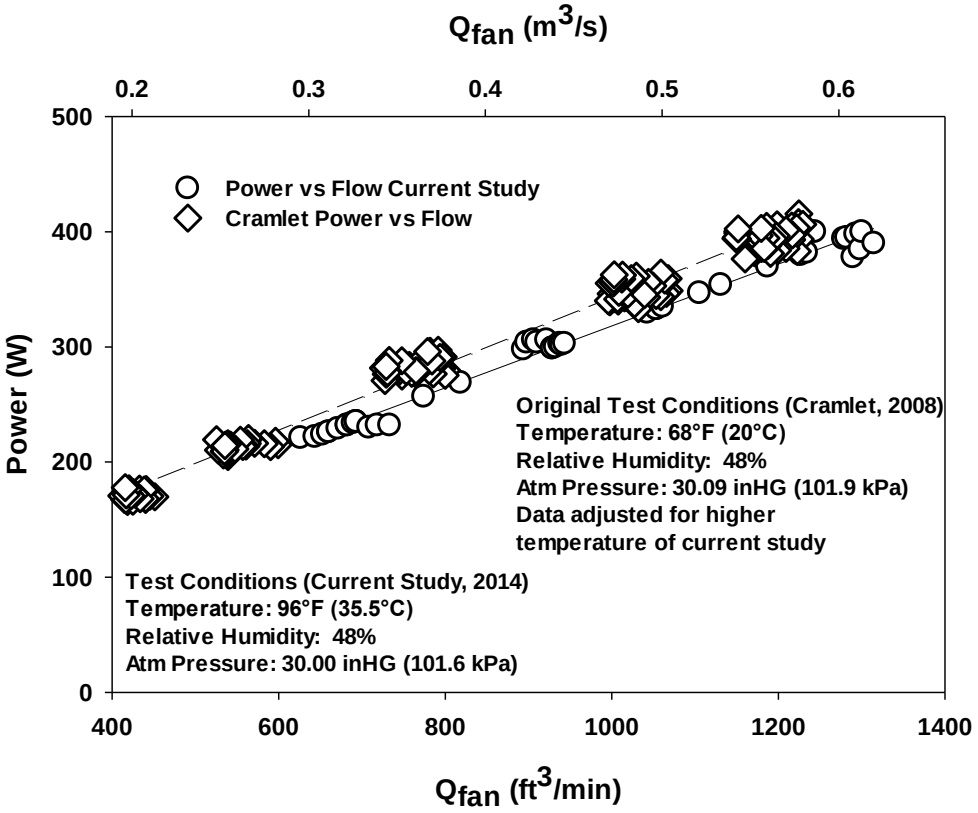

Figure 4.5: Airflow Performance Versus Power for S8C Compared to Cramlet (2008)

After the adjustment for temperature (air density), the data for both studies agree within 2% and have almost the same slope. This demonstrated that the power/flow measurements were reliable and consistent with those taken in work done several years ago on this S8C FPTU and that the measurement technique for this study could replicate that earlier data.

Figure 4.6 shows a nearly linear relationship between total airflow through the FPTU and static differential pressure rise across the FPTU fan. The data ranged from about 0.10 – 0.25 in. w.g. (24.9 – 62.3 Pa) over the airflow range of 600 – 1300 ft^3/min (0.283 – 0.613 m^3/s).

The relationship between airflow and velocity pressure was also investigated. It was not possible to measure velocity pressure directly because of the extreme non-uniform airflow through the FPTU. The average velocity through the FPTU was determined from Equation 4.2,

$$q = \bar{V}A \tag{4.2}$$

Where,

q = airflow in ft^3/min (m^3/s)

$\bar{V}$ = average airflow velocity through test section in ft/s (m/s)

A = cross-sectional area for airflow – ft^2 (m^2)

For the apparatus shown in Figure 4.2, the cross-sectional area was measured and found to be 1.67 ft^2 (0.155 m^2) for the FPTU and 0.72 ft^2 (0.067 m^2) in the discharge duct immediately following the FPTU. Airflow was measured for each test run from data taken with a pitot tube reading at the inlet to the FPTU and in the discharge duct downstream from the FPTU. Once the average velocity was obtained from Equation 4.2, then the velocity pressure, P_v, could be found as shown in Equation 4.3 (4.3a for SI units),

$$P_v = \left(\frac{\bar{V}}{1096.2}\right)^2 \rho_{air} \tag{4.3}$$

$$P_v = \frac{\rho air \bar{V}^2}{2} \tag{4.3a}$$

Where,

ρ_{air} = density of air at test conditions – lb/ft^3 (kg/m^3)

Figure 4.7 shows the resulting data for the flow range tested with the S8C FPTU. As with static pressure rise and total airflow, this Figure 4.7 shows that there was a generally linear trend that allowed one to predict static pressure rise with velocity pressure in this FPTU.

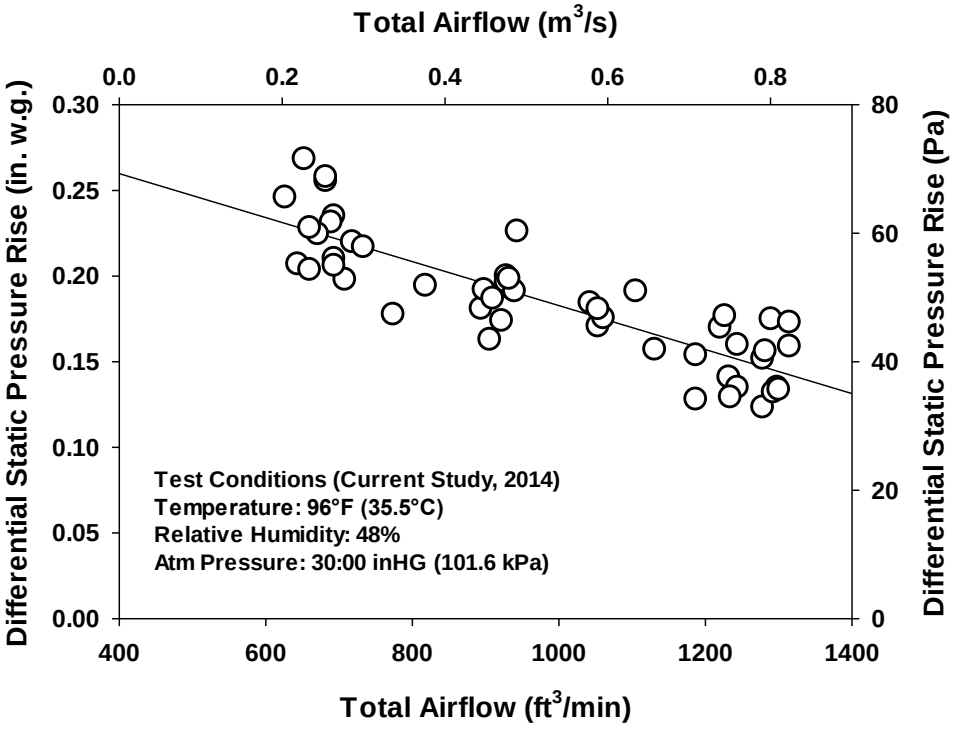

Figure 4.6: Differential Pressure Rise for S8C FPTU Fan as a Function of Total Airflow

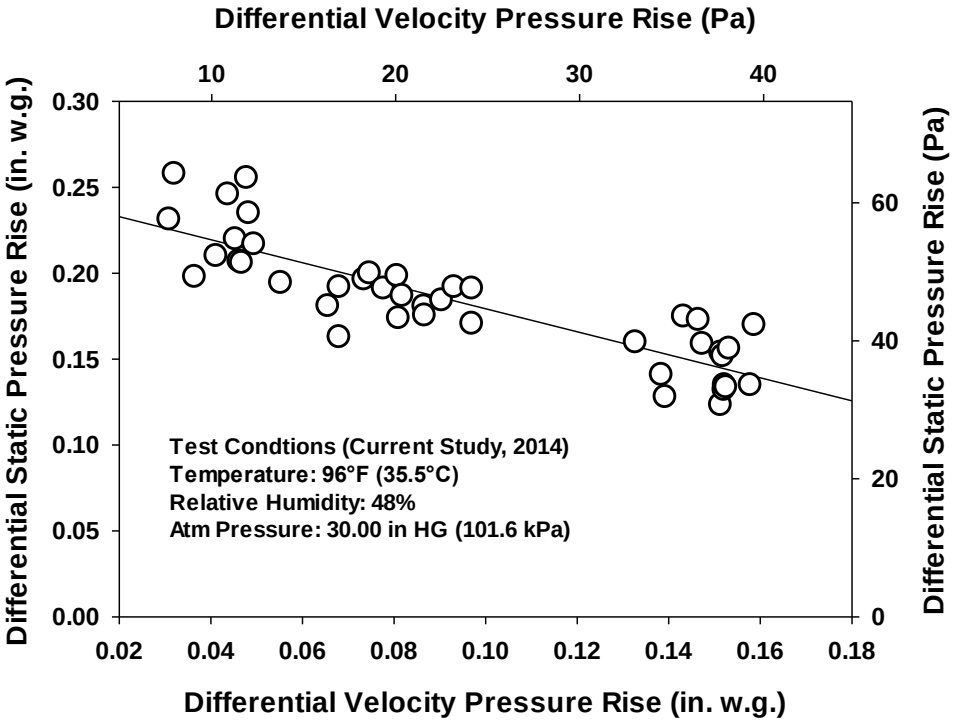

Figure 4.7: Differential Static Fan Pressure Rise for S8C FPTU versus Differential Velocity Pressure

4.2.3 Discussion of Laboratory Test Results The power versus flow comparisons for this study and the work done by Cramlet showed very good agreement. The values were within 2% when the Cramlet data were adjusted for the high temperature conditions of this study. Most gratifying were that measurements taken in this study could replicate data taken in a much more sophisticated laboratory setting. This laboratory measurement of fan differential pressure should help provide EnergyPlus users with a more realistic values of fan differential pressure. To our knowledge, there were no known sources of such data available to those using EnergyPlus to model VAV systems using series or parallel FPTUs. In fact, an online reference for EnergyPlus suggested a pressure rise of 1.5 in. w.g. (373 Pa) as a common value when modeling constant volume fans (DesignBuilder, 2014). Another online forum for EnergyPlus modelers had suggested a value as high as 3.0 in. w.g. (747 Pa) for fan pressure rise (EnergyPlus Support, 2014). From Figure 4.7 it is obvious that the in-situ measured static differential was much less than either of these values. Values for the range of airflow for the S8C FPTU of 0.25 – 0.10 in. w.g. (62.3 – 25.0 Pa) for the range of 1300 – 500 ft^3/min (0.613 – 0.236 m^3/s) were easily an order of magnitude less than what would be expected at the primary AHU fan of a typical HVAC system. The error on FPTU fan power, Pow_{fan}, when over-estimating the fan total pressure rise as described above was quite clear as shown in Equation 4.4 (4.4a for SI units),

$$Pow_{fan} = \frac{\Delta P_{tot} Q_{fan}}{6356} \tag{4.4}$$

$$Pow_{fan} = \Delta P_{tot} Q_{fan} \tag{4.4a}$$

Where,

Pow_{fan} = Ideal power consumed by FPTU fan, hp (W)

ΔP_{tot} = differential total pressure rise across fan, in. w.g. (Pa)

Q_{fan} = airflow delivered by the fan, ft^3/min (m^3/s)

The static and total differential pressure rises were similar in magnitude for the small diameter fans typically found in FPTUs. The intent with showing Equation 4.4 was to highlight the problem with using differential pressure values that were as much as an order of magnitude too high. The results shown in Figure 4.7 seemed to indicate that the static differential pressure rise for a series FPTU could be determined with a simple linear relationship with total FPTU airflow. Similarly, if differential velocity pressure for an FPTU was known, Figure 4.8 indicated that a linear relationship again would predict the static differential pressure rise for a series

FPTU. With additional data for a wider range of series and FPTU models and from different manufacturers, it appeared that solid linear relationships would be able to be developed for wider use in modeling programs such as EnergyPlus.

4.3 Manufacturer's Measurements

Results from the initial testing presented above provided results on fan differential pressure rise from a single series FPTU and a single manufacturer. More units needed to be evaluated to be able to provide support for more generalized results. Initially, the intent was to work with two manufacturer's laboratory facilities, located in Houston and Dallas, to test units from their respective company's inventory.

Meetings were held with the engineering laboratory directors in the spring (Houston) and summer (Dallas) to discuss arrangements for conducting testing on series FPTU and fan pressure rise using their respective laboratories. The discussions at both laboratories revealed impediments to timely scheduling or access to these facilities for additional testing. The Houston laboratory director suggested that since they were doing product testing "anyway", that it should be a simple matter to add the instrumentation needed to acquire FPTU fan differential pressure while doing their in-house tests. We provided guidance on the suggested methodology for conducting tests at the Houston laboratory. Another laboratory in Canada was added to the above locations. The following section presents results from this effort.

4.3.1 Manufacturer's Results Figure 4.8 shows results from the three sets of test data that have been collected for series FPTUs. All units have similar slope though an offset is clearly displayed between the data tested in the Houston laboratory and the S8C 8 inch (20.3 cm) unit evaluated earlier in this chapter. Though both 8 inch (20.3 cm) inlet type series FPTU, the Houston units were powered using ECM controlled motors while the S8C (Bryant) unit used an older SCR controlled permanent split capacitor (PSC) motor type unit. Additionally, the Houston unit was almost 15 years newer than the S8C. These design differences could easily account for the difference in the data for these units.

The most important attribute of these data were that the differential pressure rise values were consistently much lower than those commonly found in the literature. For the general case, it would be convenient to be able to predict fan differential pressure rise as a function of series FPTU inlet diameter and primary air flow rate (ft^3/min or m^3/s). A multiple linear regression was performed using the data for 8 and 12 inch (20.3 and 30.5cm) series FPTUs tested in the

Houston laboratory. The result is shown in IP units (ft^3/min) in Equation 4.5 and SI units (m^3/s) in equation 4.5a. These regressions had an R^2 of 0.98.

$$Fan\ Pressure\ Rise = Inlet\ Size \times (0.021) - PrimaryAirflow \times (6.1 \times 10^{-5}) + 0.144 \quad (4.5)$$

$$Fan\ Pressure\ Rise = Inlet\ Size \times (0.209) - PrimaryAirflow \times (32.44) + 35.95 \quad (4.5a)$$

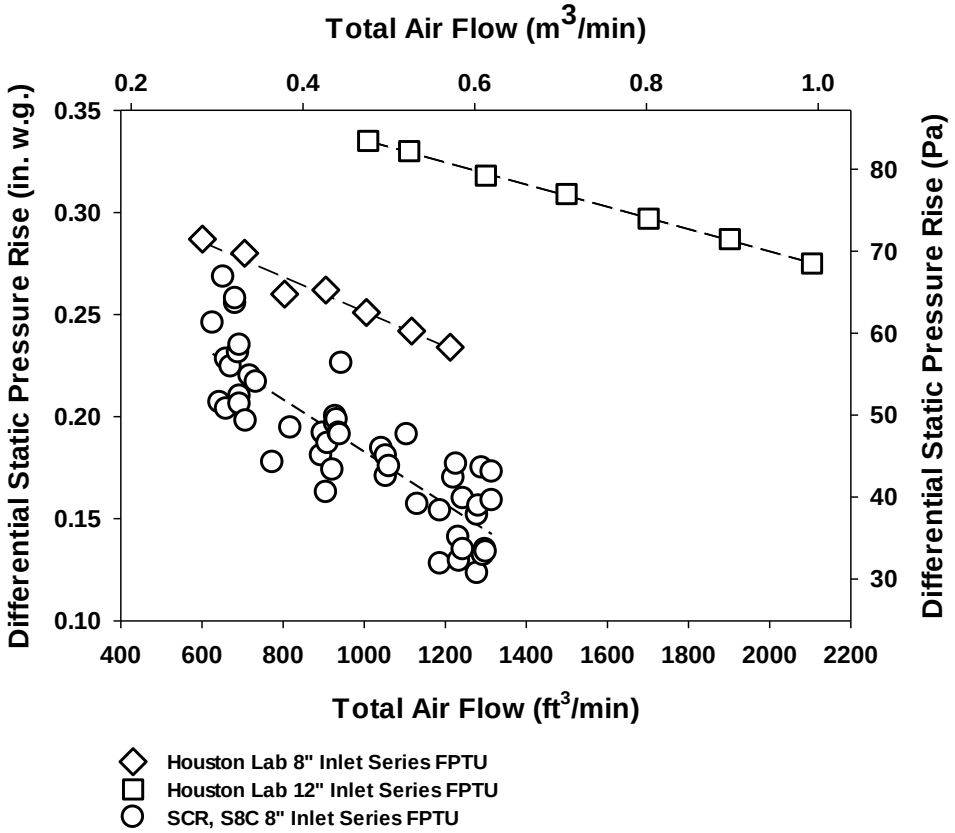

Figure 4.8: Houston Laboratory Fan Differential Pressure Rise Testing Results for 8 and 12 Inch (20.3 and 30.5 cm) Inlet Series FPTU with ECM versus S8C results.

The results for this regression are shown in Figure 4.9. Because the manufacturer's units tested in the Houston laboratory and those of evaluated by Bryant (2014) used different fan/motors and had other internal design differences, a separate linear regression was performed on the experimental data presented earlier in this chapter. This regression result is shown in Figure 4.10. The result is shown using standard units (ft^3/min) in Equation 4.6 and SI units (m^3/s) in equation 4.6a. These regressions had an R^2 of 0.76.

$$Fan\ Pressure\ Rise = Primary\ Air\ Flow\ \times (-1.3 \times 10^{-4}) + 0.311 \quad (4.6)$$

$$Fan\ Pressure\ Rise = Primary\ Air\ Flow\ \times (-67.76) + 77.52 \quad (4.6a)$$

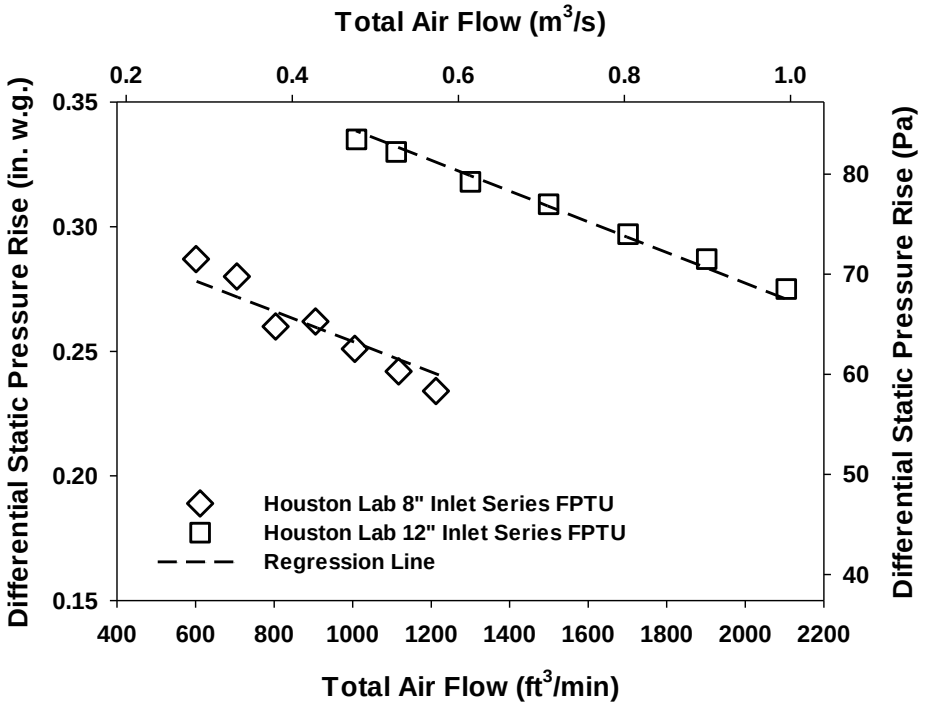

Figure 4.9: Multiple Linear Regression for 8 and 12 Inch (20.3 and 30.5 cm) Series FPTU with ECM Fan/Motor Combination

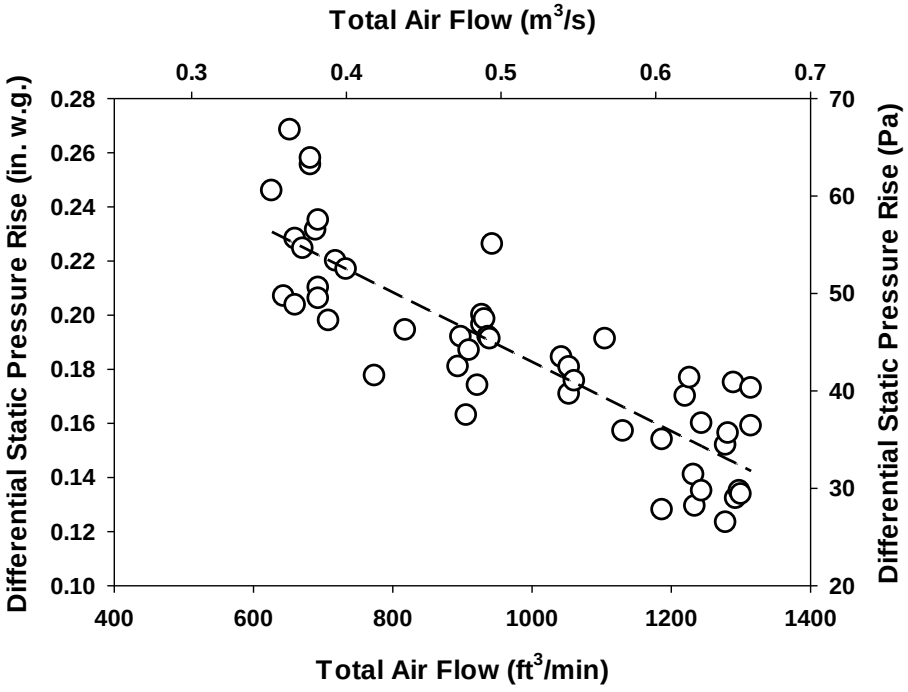

Figure 4.10: Linear Regression for 8 Inch (20.3 cm) Series FPTU with SCR and PSC Fan/Motor Combination

4.4 Effect of Fan/Motor Efficiency on Series FPTU Energy Use

One major issue with EnergyPlus has been the required inputs when modeling FPTUs. One of the motivations of this portion of the project was to measure the expected fan pressure rise and determine exactly *which* pressure rise is the correct input? EnergyPlus documentation has not been clear on this input. A search of fan literature would show that the proper (technical) input for pressure rise should be the fan *total* pressure rise. This would be especially true when using larger air handler type fan simulations. However, for small fan/motor combinations such as those used in series FPTUs, it is often assumed that fan static and fan total pressures are of approximately equal magnitude. Data from the initial experiment tests of the 8 inch (20.3 cm) series FPTU earlier in this chapter were used to test this hypothesis. The result is shown in Figure 4.11.

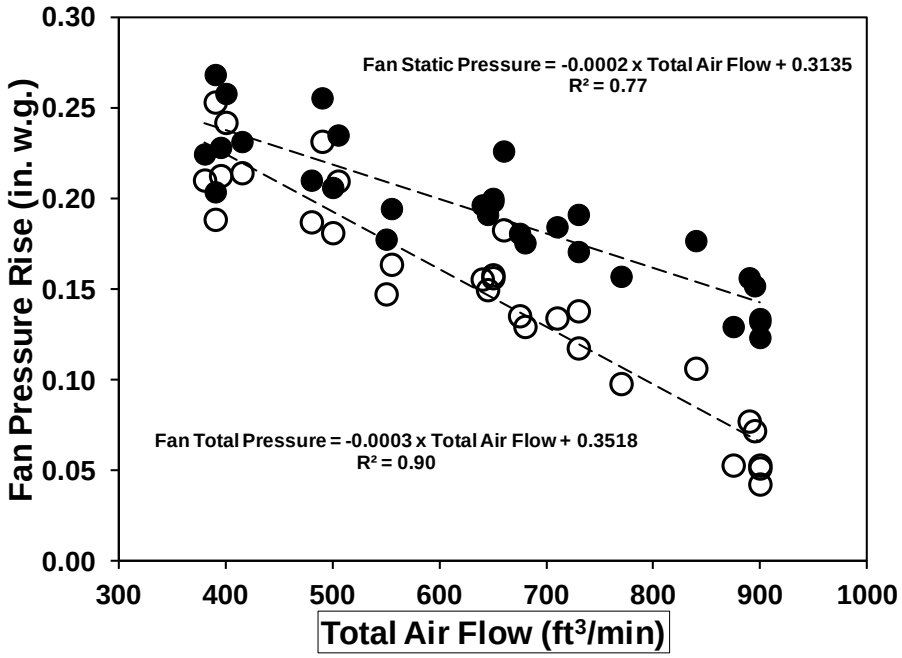

Figure 4.11: Fan Total Versus Fan Static Pressure Rise as a Function of Total Airflow for an 8 inch (20.3 cm) Series FPTU with SCR and PSC Fan/Motor Combination

Though fan total pressure did diverge from fan static pressure as flow increased, the magnitudes of the two measurements for this series FPTU were remarkable equal over the range of airflows. This was especially true when the total airflow through the FPTU was mid-range or lower. These results support the assumption of use of fan static measurements in lieu of fan total

pressure. As an aside, fan static pressure measurements are much easier to obtain than are total pressure measurements. This was especially true of in-situ field measurements.

To complete the required inputs for an EnergyPlus FPTU model, one must also have the fan/motor efficiency for the FPTU. Anecdotal and some published on-line references indicated use of efficiency values as high as 80% or at least not much lower than 70%. It seemed clear that EnergyPlus was using fan law relationships to calculate energy use of the FPTU fans and this was the same model used for larger air handling fans as well within EnergyPlus. In Chapter 2, data for a number of different sized series FPTUs from several manufacturers were used to develop a relationship between fan/motor efficiency and fan total pressure. This mathematical relationship is shown below:

$$\eta_{fm} = \alpha_n \times \Delta P_{tot} \qquad 4.7$$

The constant, α_n, was a regression coefficient from the fit of the fan/motor efficiency and fan total pressure rise. It was described in Chapter 2.

Figure 4.12 is repeated from Chapter 2 and shows the fan/motor efficiency over a range of total pressure from 0.0 to 0.7 in. w.g. (0 to 174 Pa) for series FPTUs. The efficiency of these fan/motor combinations ranges from 0 to about 22% for the range of fan total pressures. For the range of fan pressure rises that have been measured under this study for series FPTUs, 0.2 to 0.35 in. w.g. (50 to 82 Pa), the corresponding range of fan/motor efficiencies would be about 5 to 15% These values were considerably less than those often found recommended in training literature or in on-line modeling forums. The next question to ask would be what are the impacts of using such values in an EnergyPlus simulation?

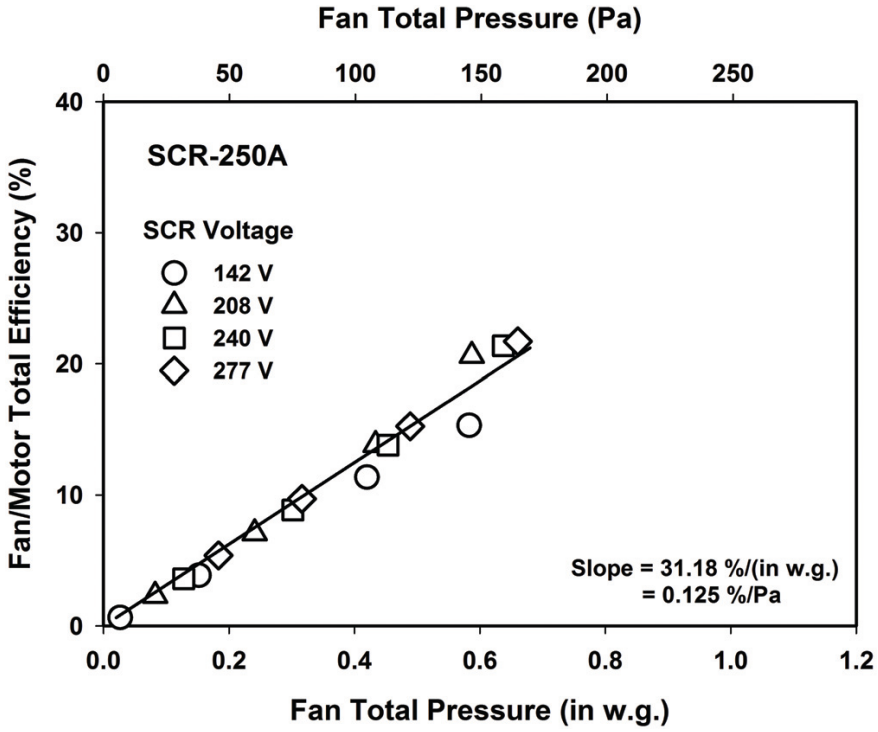

Figure 4.12: Fan/Motor Efficiency Versus Fan Total Pressure Rise for Series FPTUs with SCR and PSC Fan/Motor Combinations.

4.4.1 EnergyPlus Model using Fan Pressure Rise and Fan/Motor Efficiency Data A simulation was generated using the five zone model (described in Chapter 9) and using FPTU fan pressure data from the laboratory measurements and fan/motor efficiency data from Chapter 2 and other values found in various sources. Those values from other sources would be fan/motor efficiency of 70% or greater and fan pressure rises of 1.5 to 3.5 in. w.g. (374 to 872 Pa). Figure 4.13 shows the impact on total fan energy (primary AHU + FPTU fans) for a five zone simulation with a Houston location. As one would expect, total fan energy increased for a given efficiency and increasing fan total pressure.

Default values of 70% efficiency and fan total pressure of 2 in. w.g. (498 Pa) or greater had estimated annual energy uses of 15,000 kWh or greater. All values converged at around 10,000 kWh which could be considered the "base" energy value for this simulation. The takeaway from this figure was that the person considering input values for a given series FPTU model in EnergyPlus (assuming SCR control) should choose a fan total pressure of around 0.5 in. w.g. (125 Pa) or less. Efficiency had a smaller effect when this level of fan pressure was used.

However, it was also clear that a poor choice of a combination of fan pressure and efficiency of say, 2.0 in. w.g. (498 Pa) and 30%, resulted in FPTU fan energy that was approximately three times greater than the "correct" values for these inputs.

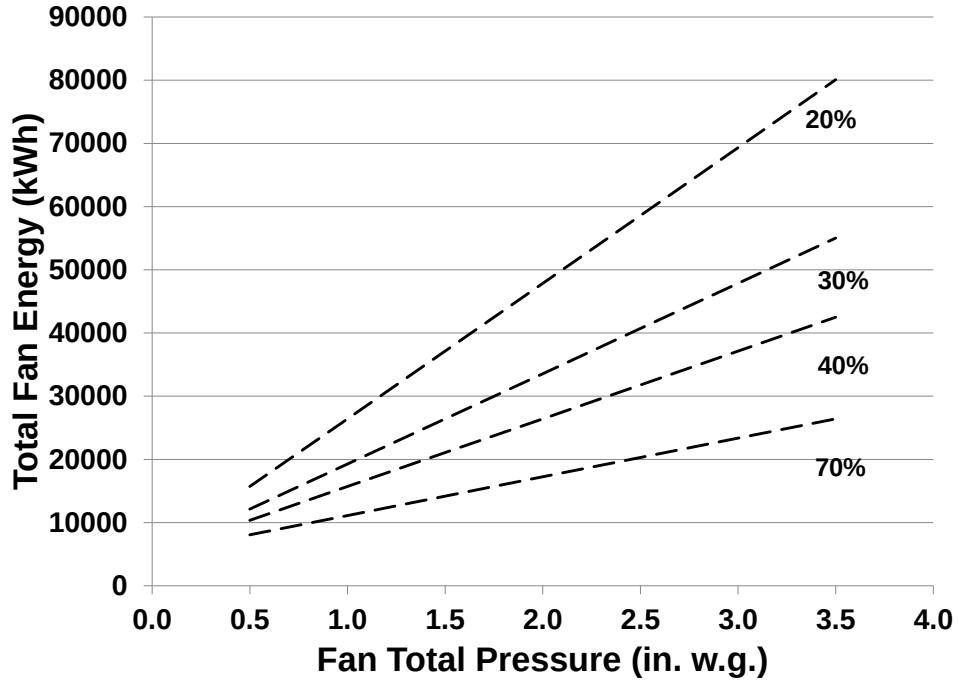

Figure 4.13: Total Yearly Fan Energy Versus Fan Total Pressure as a Function of FPTU Fan/Motor Efficiency for Five Zone EnergyPlus Model in Houston

Next, the impact of these inputs on heating energy were investigated. The base EnergyPlus model for the five zone building assumes that the supplemental heating energy is supplied by a natural gas fired boiler (hot water). The results for the Houston case are shown in Figure 4.14. As with fan energy, "correct" inputs of less than 0.5 in. w.g. (125 Pa), and 10% efficiency show natural gas energy consumption of about 65,000 kWh. However, a default value of 3.0 in. w.g. (747 Pa) and 70% fan efficiency results in annual heating energy use of about 58,000 kWh. This was a difference of 11%. Choosing a large fan differential pressure rise forces the program to calculate a coincident large temperature rise (large motor power required) and that, in turn, reduces the impact on natural gas needed to meet supplemental heating needs.

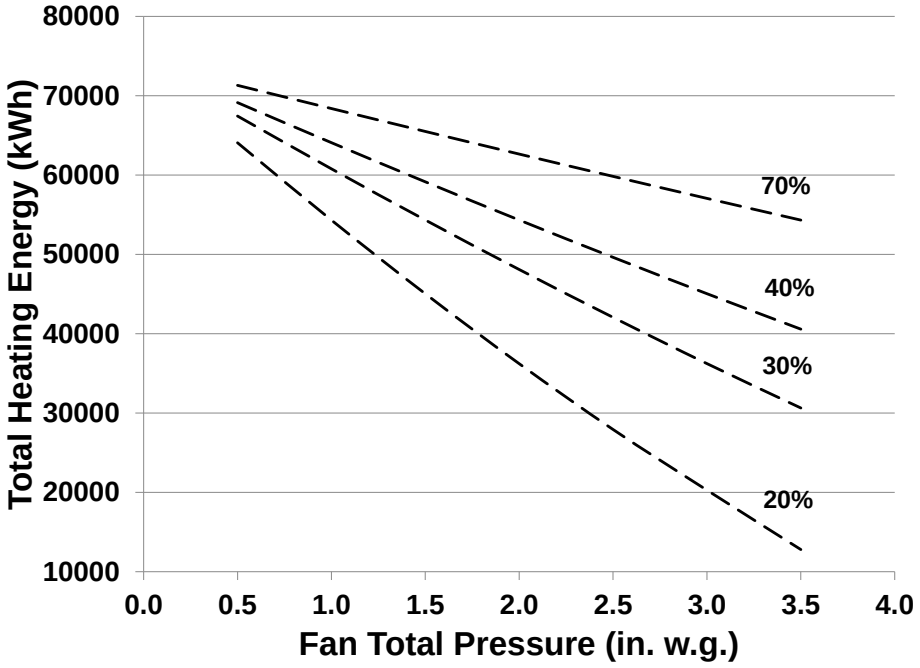

Figure 4.14: Annual Heating Energy Versus Fan Total Pressure as a Function of FPTU Fan/Motor Efficiency for Five Zone EnergyPlus Model in Houston

The modeling showed that as long as the input was 0.5 in. w.g. (125 Pa) or less, one could be off in the efficiency and the impact on the heating energy consumption would be minimal. However, the low fan total pressure and corresponding low efficiency (say, 10%) would be the most appropriate values to use in EnergyPlus.

When all HVAC energy was considered, choosing an inappropriate figure for fan total pressure and fan/motor efficiency did not yield significant differences with EnergyPlus. Figure 4.15 displayed total HVAC energy data for the Houston model versus fan total pressure and fan/motor efficiency.

Using the "correct" values of 0.5 in. w.g.(125 Pa) and 10% efficiency yielded total HVAC energy use of about 168,000 kWh. While accepting defaults of 3 in. w.g. (747 Pa) and 70% efficiency showed energy use of about 170,000 kWh. This was only a difference of about 2%. The trend in this graph was similar to the previous energy use graphs. As long as the model inputs for fan total pressure were kept at reasonable values of 0.5 in. w.g. (747 Pa) or less, the EnergyPlus model for series FPTU should yield reasonable results for total HVAC energy use.

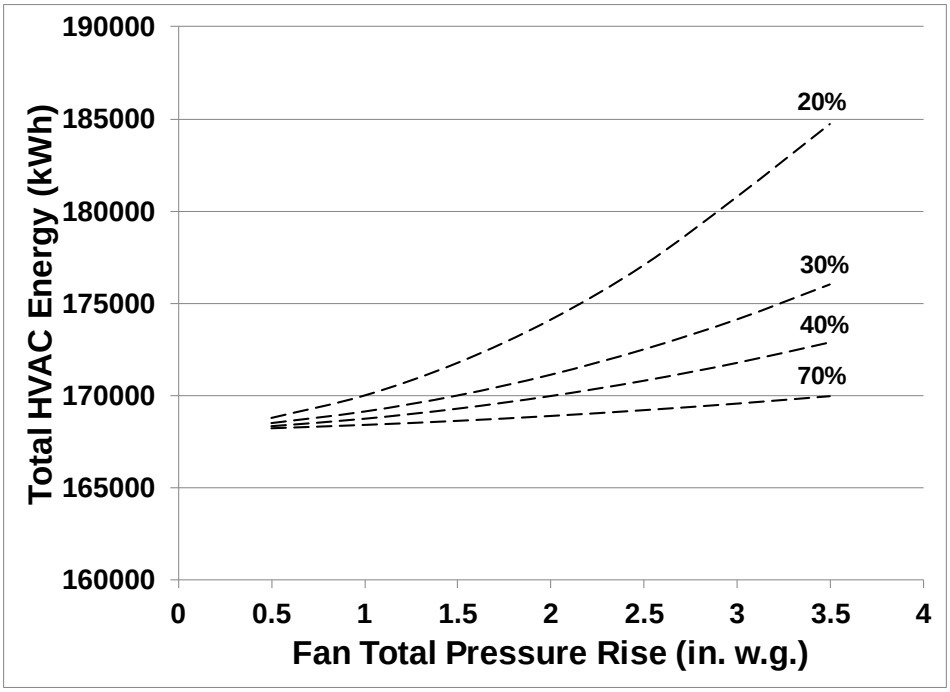

Figure 4.15: Total Yearly HVAC Energy Versus Fan Total Pressure as a Function of FPTU Fan/Motor Efficiency for Five Zone EnergyPlus Model in Houston

4.5 In-Situ Field Measurements of Series and Parallel FPTU

Based on input from AHRI, the scope of the project was expanded to include in-situ performance measurements of series and parallel FPTUs in the field. The main campus of Texas A&M University was chosen as the site for these observations and measurements. The Energy and Utility staff at Texas A&M were most helpful in this endeavor and not only helped identify candidate buildings/FPTUs, but assisted with installation of monitoring hardware and programming of the campus BMS to provide coincident FPTU performance data. The efforts started with a qualitative assessment of several FPTUs across campus. The FPTU chosen were of similar size and age to be consistent across measurements. The second effort consisted of direct measurements of performance data for several series and parallel FPTU. Again, some of these data were used to make qualitative judgements concerning parallel FPTU leakage.

4.5.1 Qualitative Study of Field FPTUs A first qualitative set of observations was done on some series and parallel FPTU located in two of the older buildings on the A&M campus. An infrared camera was used for the thermal imaging. The intent of these in-situ observations was to develop qualitative support for the laboratory and anecdotal observations of leakage in parallel FPTU. The following images were from both parallel and series FPTUs. The first set were for

parallel FPTUs in a student services building on the A&M campus. These units were about seven years old and were part of a retrofit in this building. The ceiling plenum space was very tight in this installation. In all of the following images, the temperature in the upper left was the "bull's eye" center of image temperature. The temperature displayed in the lower left of the thermal image was the lowest temperature in that image and the lower right is the highest temperature in the image.

Figure 4.16 is a set of images showing the filter at the induction port of a parallel FPTU. The companion IR image clearly showed that the filter media temperature was about 60°F (15.6°C) and this was a clear indication of "backflow" or leakage of primary air out through the induction port of the parallel FPTU. The surrounding temperatures in that image were representative of the plenum temperature of about 78°F (25.6°C). Again, this qualitative result supported the assertion that parallel FPTUs can leak.

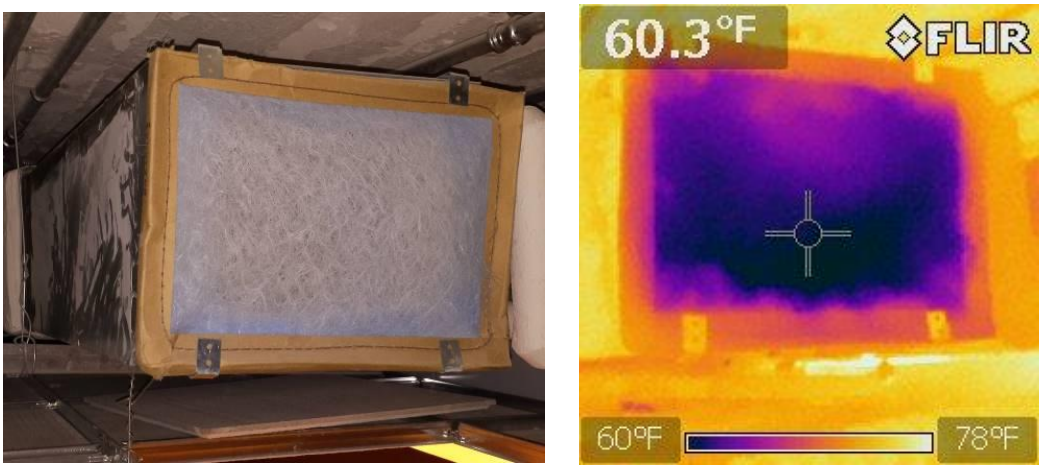

Figure 4.16: Induction Port of a Parallel FPTU at Full Primary Airflow

Figure 4.17 shows another parallel FPTU in the same plenum area as the unit shown in Figure 4.16. Though not as prominent as the previous image, the leakage from the induction port was present in this unit as well.

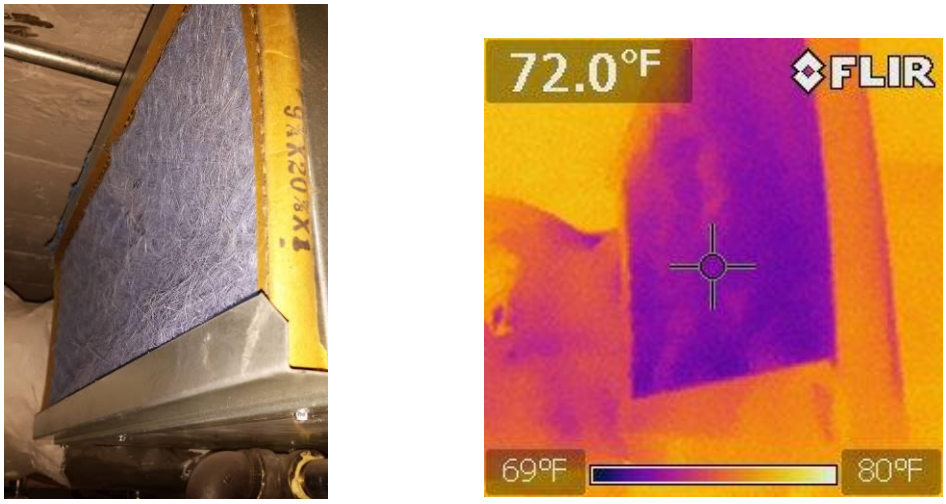

Figure 4.17: Induction Port of a Parallel FPTU at Full Primary Airflow

Figure 4.18 shows the service access panel for the parallel FPTU of Figure 4.17. Evidence of the leak was shown by the horizontal, deep purple line in the center of the image. This temperature was the same as the leaking induction port for this unit.

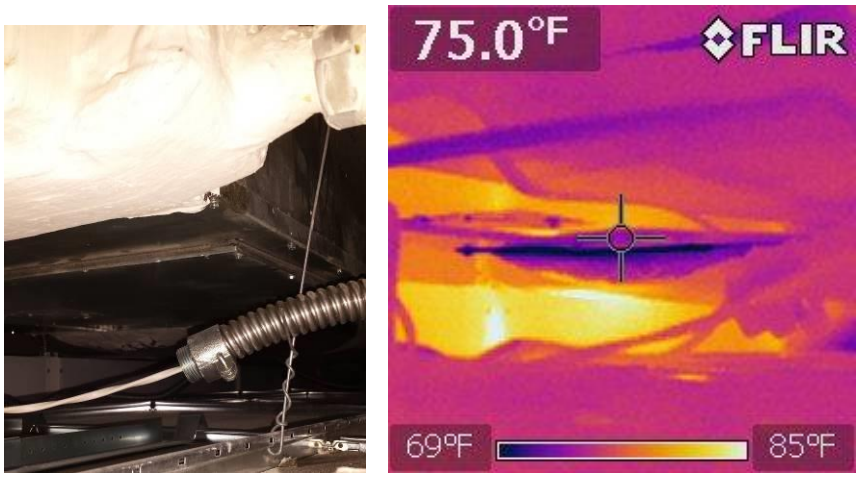

Figure 4.18: Access Panel Seam Leakage in a Parallel FPTU at Full Primary Airflow

Figure 4.19 shows similar leakage at the service panel seam of the FPTU of Figure 4.16. The panel was at the "lower left" of the image. The large area of cold temperature in the center of this image was caused by a poor insulation connection to the sheet metal collar of the parallel FPTU. Cold primary air was in direct contact with the insulation in this area of the FPTU.

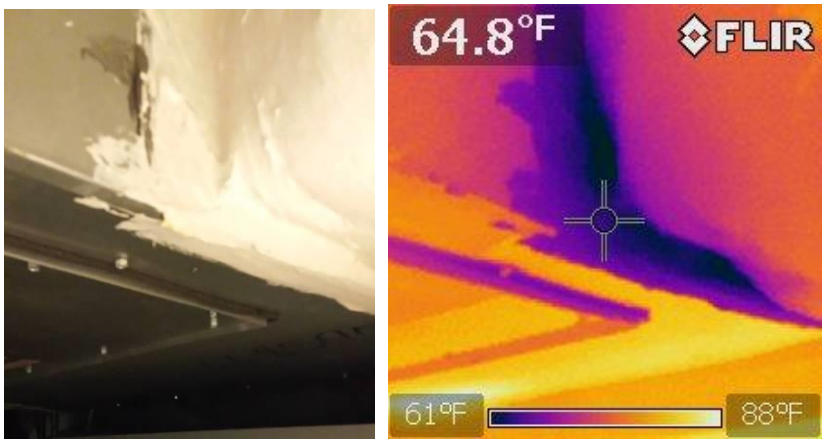

Figure 4.19: Access Panel Seam Leakage in a Parallel FPTU at Full Primary Airflow

Figures 4.20 and 4.21 show a series FPTU with leakage from the sheet metal seams in the unit. The BMS operator had fully opened the inlet damper to the unit allowing full cooling airflow through the unit. With the primary air supply pressure available, this series FPTU was actually flowing more air than at design conditions. This situation resulted in an over-pressure for the series FPTU and that caused leakage similar to what parallel FPTUs experienced.

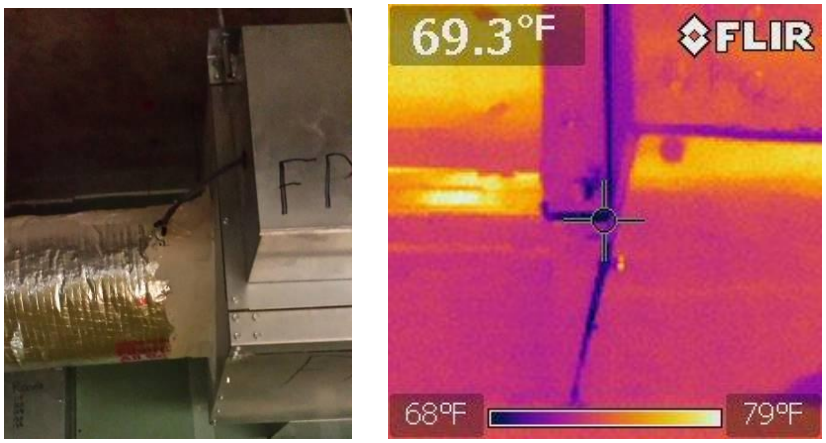

Figure 4.20: Construction Seam Leakage for a Series FPTU in Over-Pressure Operation

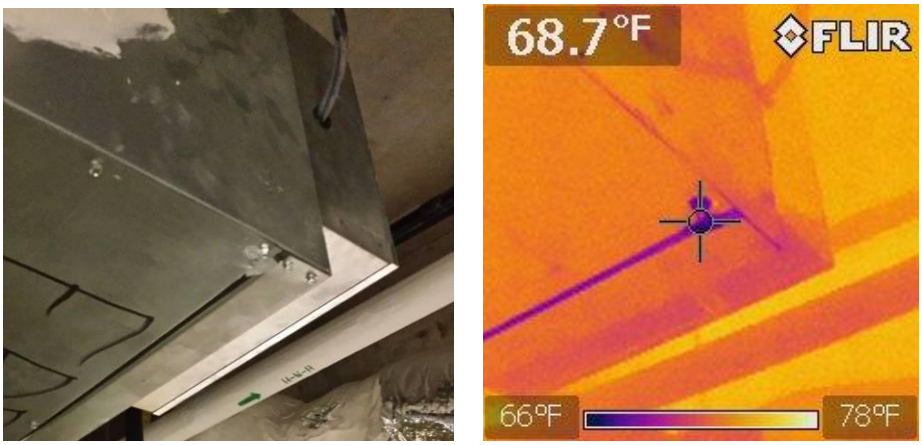

Figure 4.21: Construction Seam Leakage for a Series FPTU in Over-Pressure Operation

The series FPTU in this building was about four years old. The A&M campus BMS manager said that it was not uncommon to find series boxes leaking (outward) because of poor test and air balancing at commissioning. This was evident in these boxes at full cooling flowrates.

4.5.2 In-Situ Field Performance Measurements Seven FPTUs were identified as candidates for installation of instrumentation to measure FPTU performance. The primary difficulty in collecting these data was access. The FPTUs had to be physically accessible and in a space where minimal or no disturbance of a classroom or office space could be allowed. The seven FPTUs were chosen with these criteria in mind. Data were collected that could be used to compliment, or contradict, the laboratory fan pressure rise results that were collected in this study. Typical instrumentation installations were completed in an hour or so and data points were recorded on 15 minute intervals. A portable data logger was used to record the data points in Table 4.2, and as noted, the Texas A&M BMS was used for additional point monitoring.

Table 4.2: - Data Logging Points for In-Situ Measurements on the Main Campus of Texas A&M University

Point No.	Description (BMS denotes point monitored through A&M Building Management System)
1	Two Plenum temperature sensors (platinum RTD) near the FPTU. One general, and one near the FPTU induction port
2	Static pressure (Onset Pressure transducer) downstream of the FPTU
3	Static pressure (Onset Pressure transducer) at the entrance to the FPTU
4	Fan static pressure rise (Solomat Zephyr II+) for the series FPTU
5	Primary air supply temperature entering FPTU - BMS
6	Secondary air supply temperature delivered from FPTU to zone - BMS
7	Primary air duct static pressure - BMS
8	FPTU Primary air damper position - BMS
9	FPTU air volume delivered to zone - BMS

The FPTU pressure readings were spot checked with a hand-held micro-manometer to verify readings. Fan static pressure was found to be a constant and was only measured during the initial installation of the logging equipment.

Figure 4.22 shows results from the first logging installation. This series FPTU was installed in an agriculture building on the Texas A&M University campus. This location was a classroom space on the first floor of the building with windows facing northwest, approximately 1,400 ft^2 (130 m^2) in area, and served by two series FPTUs. The data showed essentially constant static pressure values during the monitoring period. Upstream static pressures averaged 0.92 in. w.g. (229 Pa), fan static pressure rise averaged 0.23 in. w.g. (57 Pa), and downstream static pressure averaged 0.09 in. w.g. (22 Pa).

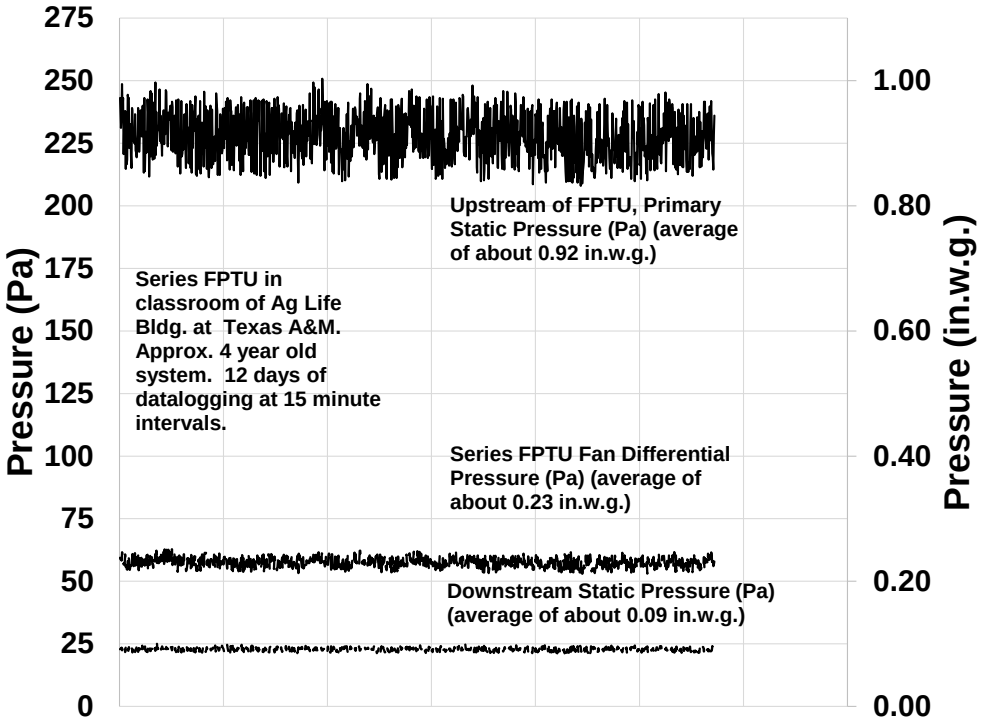

Figure 4.22: Pressure Monitoring Results for Series FPTU at an Agriculture Building at Texas A&M University

From the same FPTU, Figure 4.23 shows temperature data for the same time period for the induction port and plenum area. As would be expected for a series FPTU (under slightly negative pressure relative to the plenum area), the temperatures tracked each other so closely that the two data stream lines were virtually the same. If the FPTU were leaking, it would manifest itself through lower than average plenum temperatures near the induction port of the FPTU. The data showed that this unit was not leaking at the induction port.

In total, seven FPTUs were instrumented with data collected shown in Table 4.2. These included four series FPTUs and three parallel FPTUs. As the other instrumentation was being installed, fan static pressure rise was measured with a hand-held micro-manometer. In all series FPTUs measured this way, the fan static pressure rise was found to range from 0.20 to 0.25 in. w.g. (50 to 75 Pa). Upon installation, the instrumentation was allowed to remain in place for one to two weeks of FPTU operation logging.

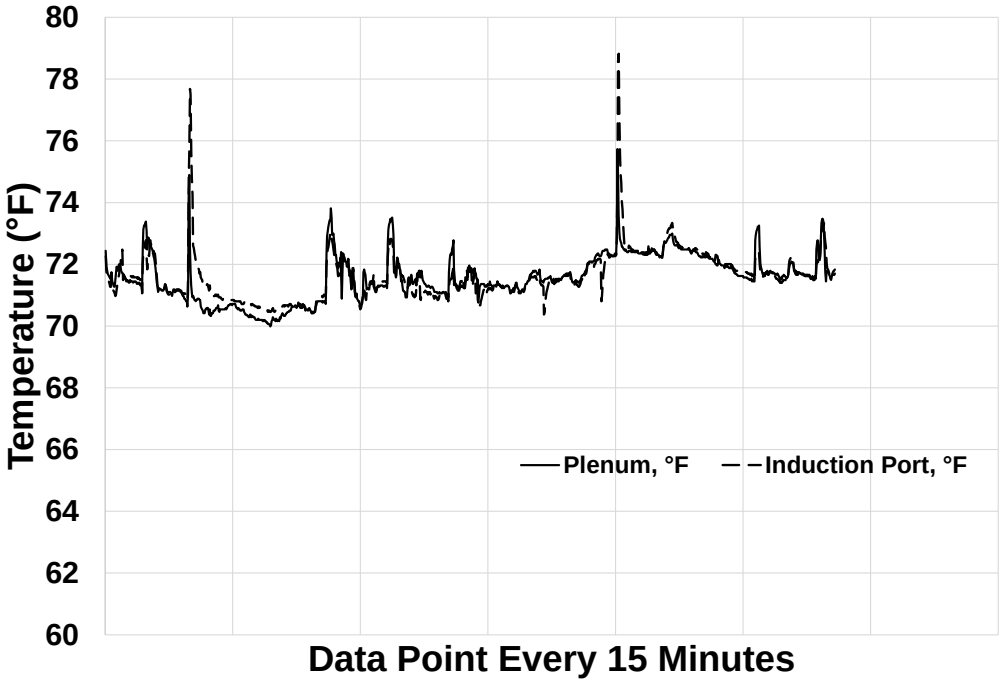

Figure 4.23: Plenum and Induction Port Temperature Monitoring Results for Series FPTU at an Agriculture Building at Texas A&M University

Figure 4.24 shows the plenum and induction port temperatures for a parallel FPTU serving the entrance lobby area of a research building on the A&M campus. In contrast to Figure 4.23, the induction and plenum area temperatures did not track together which provided evidence that this parallel FPTU was leaking. This particular unit exhibited behavior similar to the qualitative IR images seen earlier in this chapter. The leakage through the induction port was quite evident as the induction port temperatures was mostly around 62°F (16.7 °C). The more general plenum temperature was found to be around 72°F (22.2°C) for this same period. With Primary air being supplied to this unit of around 60°F (15.6°C), it was clear that this unit was leaking air into the plenum space. Leakage was further supported by noting that there were three "excursions" in the data. One of these was at 125°F (51.7°C) and two that reached 90°F (32.2°C). These excursions were events where the supplemental hot water heating coil valve was energized to provide heating for the zone being served. Some of the heated air leaked out through the induction port. This data showed that even in heating mode, when the parallel fan should also be on, the unit *still* leaked out of the induction port.

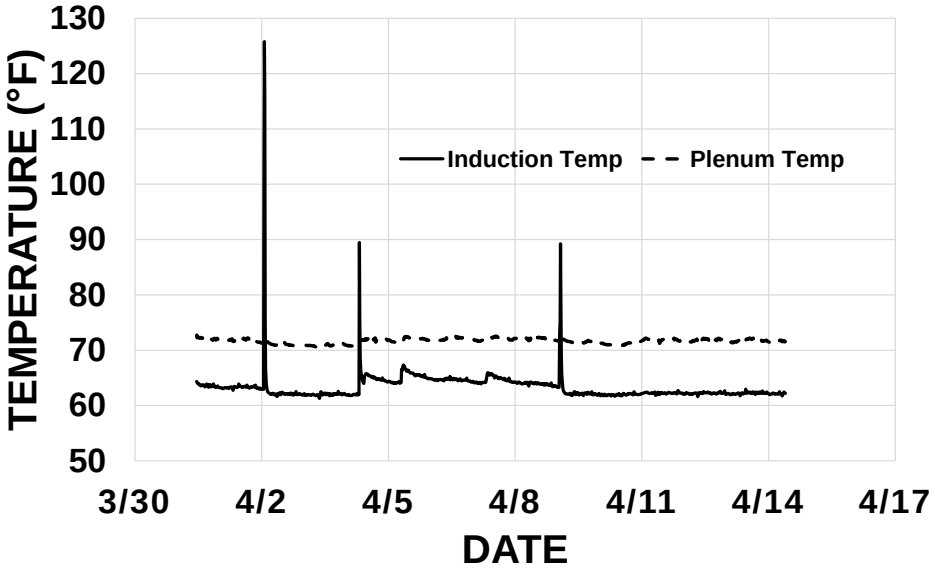

Figure 4.24: Plenum and Induction Port Temperature Monitoring Results for a Parallel FPTU at a Research Building at Texas A&M University

Figure 4.25 shows the induction port of the parallel FPTU reference in Figure 4.24. As with the earlier images, this pair was a digital and infrared image. The IR image shows that the induction port temperature was about 61°F (16.1°C) and the objects in the plenum are closer to 72°F (22.2°C). This difference in temperature of 11°F (6.1°C) was caused by the leakage of cold primary air leaking from the induction port. This port was shown in the photo with the filter in place and the RTD temperature sensor near that intake.

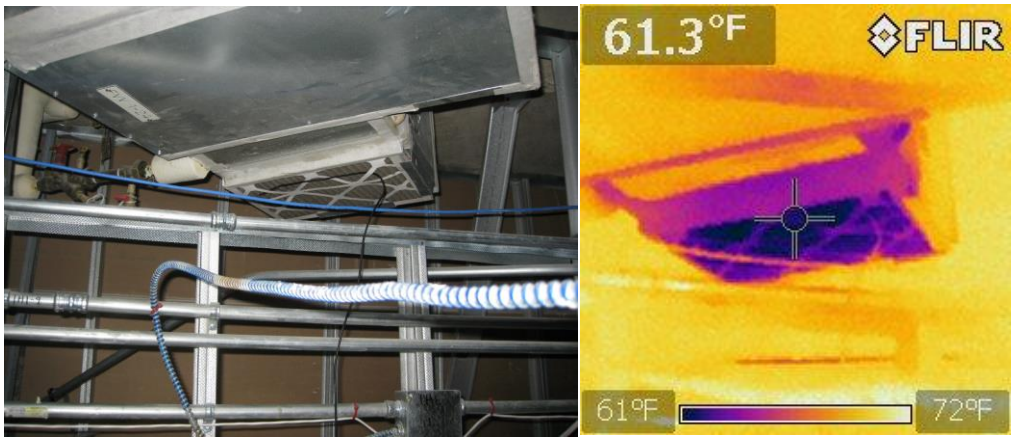

Figure 4.25: Plenum and Induction Port Temperature Images for Parallel FPTU at a Research Building at Texas A&M University

Figure 4.26 shows this same parallel FPTU and a bottom service panel that had been (previously) taped. Part of the tape was shown as starting to come off the unit, revealing the seam. The low temperature in the image is shown at the seams of this panel and at the junction of the primary air ductwork with the sheet metal collar of the FPTU. Where the tape has come loose, it clearly showed leakage at the service panel in the (cold) region of the pictures.

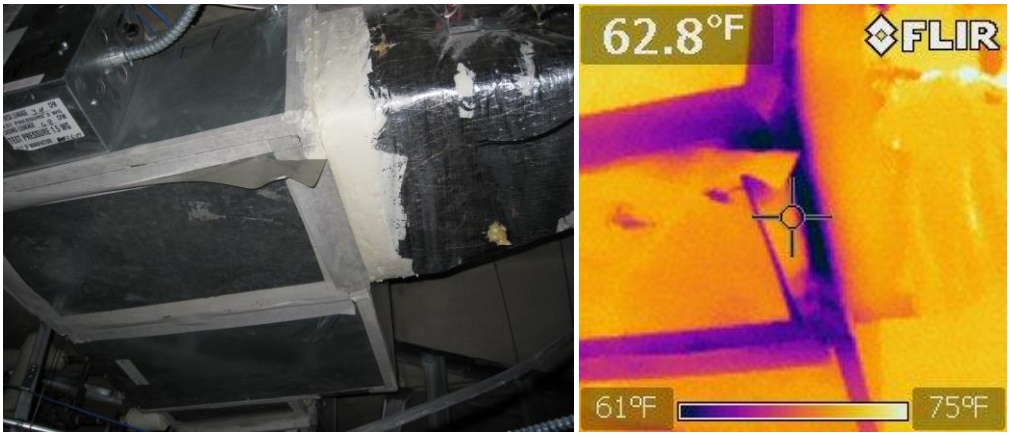

Figure 4.26: Taped Service Panel at the Bottom of a Parallel FPTU at a Research Building at Texas A&M University

4.6. Summary

The data on in-situ static fan differential pressure rise showed that the pressure rise was as much as an order of magnitude lower than some sources have recommended. The data brought into question any past modeling efforts that might have been commissioned with such values for series or parallel FPTUs. The range for static differential pressure rise was measured to be in the range of 0.10 to 0.35 in. w.g. (25 to 87 Pa) for the range of 500 to 1300 ft^3/min (0.24 to 0.61 m^3/s) for an 8 inch (203 mm) inlet series FPTU supplied with a PSC motor and SCR controller.

The models developed from the data indicated a simple linear relationship between total airflow and fan differential static pressure. These models should provide a user of building energy simulation programs with the input and models needed to provide reliable estimates of the hourly and annual performance of SCR controlled fan motors used in FPTUs. The scatter in the data would make it difficult to use these relationships to model a particular manufacturer's FPTU. However, for the modeler desiring to model a generic VAV FPTU, the data presented here were a significant improvement over anecdotal information available from internet sources.

Data from one manufacturer's 8 and 12 inch (20.3 and 30.5 cm) series FPTUs were also used for comparison to the in-situ data. These units used an ECM fan/motor combination as opposed to the PSC/SCR used in the in-situ test. However, results were comparable and the linear relationship for flow vs. differential pressure rise also held. The 8 inch (20.3 cm) ECM unit had a differential pressure increase in the range of 0.24 to 0.28 in. w.g. (60 to 70 Pa) while the 12 inch (30.5 cm) had a pressure rise range of 0.24 to 0.37 in. w.g. (60 to 92 Pa). These data support the hypothesis that fan differential pressure rise was smaller than commonly assumed.

EnergyPlus requires fan pressure rise and fan/motor efficiency when modeling a FPTU. These data are typically not provided by manufacturers for fan/motors found in FPTUs. Work done in Chapter 2 showed that PSC motors with SCR control had fan/motor efficiencies that ranged from 5 to 15% for fan pressure rises from 0.2 to 0.4 in. w.g. (50 to 100 Pa). The "ideal" input for a FPTU in EnergyPlus would be a fan pressure rise less than 0.4 in. w.g. (100 Pa) and an efficiency less than 15%. These inputs are considerably lower than commonly assumed, or default, values found in training materials and in on-line forums. An EnergyPlus model using a range of fan pressure rise inputs and fan/motor efficiencies confirmed, for the current version of EnergyPlus, that use of a "generic" pressure rise of less than 0.5 in. w.g. (124 Pa) and almost any efficiency would result in an annual HVAC system energy difference of less than 5%. However, FPTU fan energy could be up to 80% less and energy for supplemental heat was also substantially different depending on these input values.

Additional data were gathered in a limited field study on the main campus of Texas A&M University. Several series and two parallel FPTUs were instrumented for short-term temperature and pressure data. The results showed a consistent fan pressure rise of between 0.20 and 0.30 in. w.g. (60 – 75 Pa) for series FPTU. These FPTU all had PSC motors with SCR control. These results added more support to the need to use of a correct fan pressure rises in an energy simulation program. In addition to the pressure rise, temperatures were recorded in the plenum near the FPTU and at the induction port to evaluate whether leakage was occurring in the parallel FPTUs.

Of the two parallel FPTUs, only one showed leakage. The first parallel FPTU served an auditorium and during the monitoring period was operating at minimum primary airflow. The unit had occasional short periods of heating during this same period. No leakage was noted at the induction port through either infrared thermography or temperature measurements. The

second FPTU served a lobby/entrance area of an office building. The consistent 60° (15.5°F) temperature at the induction port showed that the parallel FPTU was leaking primary air past the backflow damper out of the induction port and into the plenum. Leakage for this FPTU was also qualitatively determined through infrared thermography. The images clearly showed that cold air was leaking at the seams and backdraft damper of the unit.. The data showed that leakage can be found in parallel units in the field.

CHAPTER 5

AIR LEAKAGE IN PARALLEL FPTUS

When a parallel FPTU is operating, the cabinet of the FPTU is pressurized slightly higher than the air surrounding the FPTU in the plenum space. Any openings in the cabinet creates paths for air to flow from inside the cabinet of the FPTU to the plenum space. A backdraft damper is used in parallel FPTUs to prevent primary air from leaking back towards the fan and into the plenum space when the FPTU fan is off (Figure 5.1). In cooling operations, all of the air provided to the FPTU is conditioned air from the primary cooling coil upstream of the FPTU. Any conditioned air that leaks from the FPTU into the return plenum never reaches the space serviced by the parallel FPTU. Leakage from parallel FPTUs requires additional conditioned air be supplied to the FPTU from the primary airstream. The primary fan must supply more air to the FPTU and the primary cooling coil must also cool and dehumidify this additional air. Davis et al (2012a) concluded that parallel FPTUs with leakage required more energy use than those without leakage. The modelling by Davis et al (2012a) was based on measurements of leakage taken by Furr et al (2008) and Edmondson et al (2011).

Because of its impact on energy use, leakage should be included in building simulations programs that model parallel FPTUs. While current building simulation programs, such as EnergyPlus (2013), do provide for modeling of leakage in the ducts, it does not provide a way to directly account for leakage in a parallel FPTU.

The only leakage data for parallel FPTUs found in the literature were those collected by Furr et al (2008) and Edmondson et al (2011). The data from Furr et al (2008) focused on parallel FPTUs PSC/SCR motors. The data from Edmondson et al (2011) focused on FPTUs with electronically commutated motors.

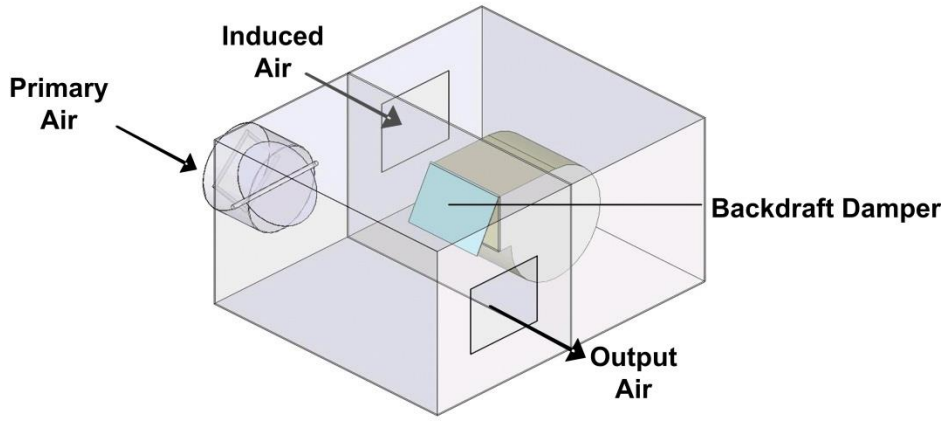

Figure 5.1: Basic Parallel Fan Powered Terminal Units

The purpose of this chapter was to re-examine the original leakage data collected by Edmondson et al (2011) on parallel FPTUs with ECMs driving the FPTU fans and develop a way to characterize leakage from parallel FPTUs that would be compatible with the mass and energy balance approach used in building simulation programs such as EnergyPlus (2013). Many FPTUs today utilize ECM technology and some codes (CEC 2013) and standards (ASHRAE 2013) now require the use of ECMs for the size motors typically found in FPTUs. The analysis in this chapter has also been summarized in a paper published in the open literature (O'Neal and Edmondson 2016).

5.1. Background

Furr et al (2008) conducted extensive airflow, power, pressure, and measurements on series parallel FPTUs that had SCR controlled fan motors. Six parallel units were evaluated from three manufacturers (designated manufacturer A, B, and C). Three of the units had primary air inlets of 8 in. (20.3 cm) and three had inlets of 12 in. (30.5 cm). From the measurements, semi-empircial models were developed for the airflow and power of the FPTU. Furr et al (2008) provided the first documented published data on leakage in parallel FPTUs. They found that all of the parallel units had some amount of leakage. However, there was no consistent pattern of leakage with respect to the size or manufacturer of the units. One of the 8 in. (20.3 cm) units had the highest amount of leakage and another 8 in. (20.3 cm) had the smallest amount of

leakage. While Manufacturer A had the highest leakage among the 8 in. (20.3 cm) units, Manufacturer C had the highest leakage among the 12 in. (30.5 cm) units.

Furr et al (2008) developed a simple linear regression model of the leakage airflow that was a function of downstream static pressure, P_{dwn} , and the inlet air velocity sensor pressure, P_{iav}. The model took the form:

$$Q_{leakage} = C_1 + C_2 \cdot P_{dwn} + C_3 \cdot P_{iav} \tag{5.1}$$

C_1, C_2, and C_3 were constants developed from regression fits of the experimental data. This simple model provided reasonable fits (r-squared values greater than 0.85) to the six units evaluated.

In a follow-up study, Edmondson et al (2011) performed simliar measurements of airflow, power, pressure on series and parallel FPTUs that had ECMs. As with Furr et al (2008), the units were provided by the same three manufacturers (A, B, and C) and included units with 8 in. (20.3 cm) and 12 in. (30.5 cm) primary air inlets. One manufacturer (C), provided two versions of their parallel FPTU, each with a different ECM to drive the fan. Edmondson et al (2011) also developed semi-empirical models of the airflow and power of the FPTUs similar to those developed by Furr et al (2008). Edmondson et al (2011) also found that all of the ECM parallel FPTUs leaked and utilized the same form for the leakage airflow (Equation 5.1) as Furr et al (2008).

Equation 5.1 could potentially be used in a FPTU simulation model where both the downstream static pressure and the inlet air velocity sensor pressure were known. However, building simulation programs that utilize a mass and energy balance approach to model FPTUs, such as EnergyPlus (2013), could not directly utilize Equation 5.1 because the downstream static pressure and inlet air velocity sensor pressure are typically not included as variables in the simulations. If the data from Edmondson et al (2011) is to be useful in building simulation models, an alterative way of modeling leakage is required.

The impact of leakage on the annual energy performance of parallel FPTUs was modeled by Davis et al (2012a). They developed a five zone building model that was used to estimate the annual energy use of a VAV system in a small office building that had five FPTUs controlling the airflow into each zone. The building simulation model incorporated the FPTU models of the parallel and series fan powered terminal units developed by Furr et al (2008) and Edmondson et al (2011). The building energy model included upstream and downstream static pressures to

capture the model variables provided by the semi-empirical FPTU models. For leakage, Davis et al (2012a) did not utilize the model of Equation 5.1 to predict leakage of parallel units. Instead, they used a simple percentage leakage of the total primary airflow rate. They examined 5%, 10%, and 20% leakage rates in parallel units. Their results for a small office buiding in Houston are shown in Table 5.1 (Davis eta al 2012a and 2012b).

Table 5.1 – Simulation Results from Davis et al (2012a and 2012b) for ECM Series and Parallel FPTUs

System	Leakage	FPTU Fan Energy (MWh)	FPTU Heating Coil (MWh)	Primary Fan Energy (MWh)	Cooling Plant Energy (MWh)	Total Plant Energy (MWh)
ECM Series	---	11	89	3	58	161
ECM Parallel	0%	3	93	3	56	156
ECM Parallel	5%	3	96	4	58	161
ECM Parallel	10%	3	99	4	59	165
ECM Parallel	20%	5	105	5	61	175

The building simulation model demonstrated the negative impact of leakage in parallel FPTUs on the annual energy use in the five zone office building (Davis et al 2012a and 2012b). For example, 5% leakage increased the total plant energy use of the heating, ventilating, and air conditioning (HVAC) system from 156 to 161 MWh compared to the ECM parallel FTPU that had no leakage (Table 5.1). Their analysis also showed that a parallel unit with 10% leakage had a higher plant energy use than did an ECM series unit. The results indicated that enough leakage in parallel FPTUs could negate the potential energy savings that are typically attributable to parallel FPTUs when compared to series FPTUs (Kolderup et al, 2003).

A simple percentage model would be easy to implement in a parallel FPTU model. It assumes that the total amount of leakage (in ft^3/min or m^3/s) from the cabinet of a FPTU increases as the amount of primary airflow increases. Data from both Furr (2008) and Edmondson (2011) both showed a relatively constant amount of leakage with respect to primary

airflow when the downstream static pressure was held constant. The fraction leakage, f_{leak}, can be expressed as:

$$f_{leak} = \frac{Q_{leakage}}{Q_{primary}} \tag{5.2}$$

Where,

$Q_{primary}$ = primary airflow – ft^3/min (m^3/s)

If the leakage airflow ($Q_{leakage}$) was independent of the primary airflow (i.e, constant) in Equation 5.2, then at smaller primary airflows, the fraction (or percentage) leakage would be higher and it would decrease with increasing amounts of primary airflow because the denominator of Equations 5.2 would increase. The correlations that both Furr (2008) and Edmondson(2011) developed from their data showed a strong dependence on the downstream pressure, P_{dwn}.

The dependence on primary airflow, as indicated by the inlet air velocity pressure (P_{iav}) was small and mixed. In some cases, the leakage showed a small increase with P_{iav} and in other cases, it showed a small decrease. There were no clearly discernable trends in their data.

While a simple percentage leakage model is attractive, the original data should be re-examined to determine if that approach can be used as a satisfactory way to model leakage that adequately captures the trends found by both Furr et al (2008) and Edmondson et al (2011).

5.2. Original Experimental Measurements and Data

Edmondson et al (2011) collected data on the leakage of parallel FPTUs by utilizing two airflow chambers: one upstream and one downstream of the parallel FPTU (See Figure 5.2). A detailed description of the experimental setup and procedures for measurements with the airflow chambers was provided by Edmondson et al (2011).

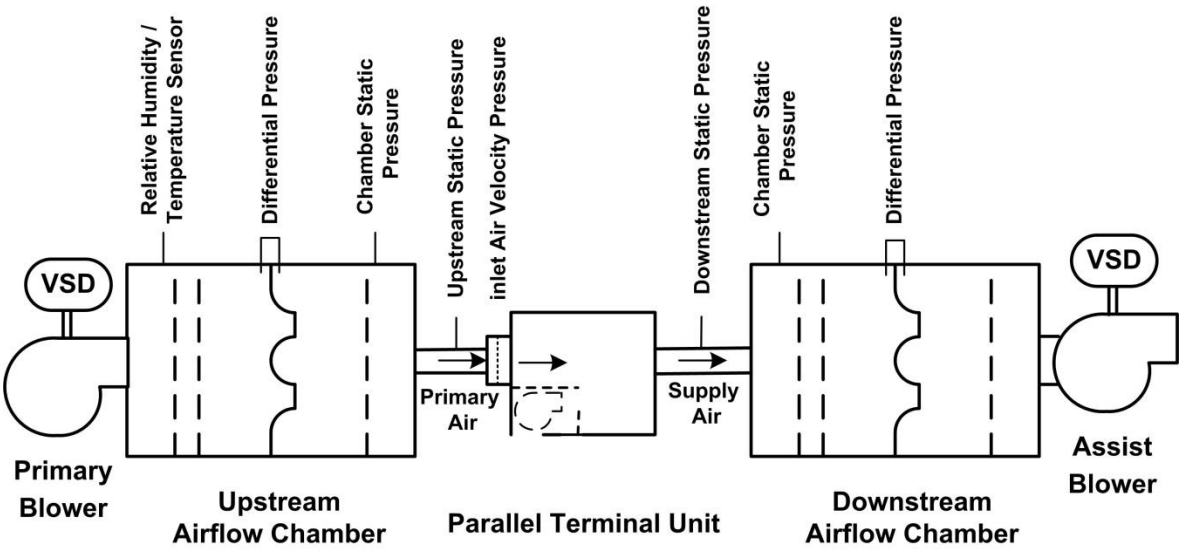

Figure 5.2: Experimental Setup for the Leakage Tests Conducted by the Furr et al (2008) and Edmondson (2011)

A brief overview is provided here. All duct fittings leading into and out of the FPTU and the airflow chambers were sealed with masking tape to help eliminate leakage contributions by the ducts. The primary damper in the FPTU could be set to a specified position during a test. Both of the airflow chambers had assist blowers whose speed could be adjusted to independently adjust the static pressures at the primary inlet and discharge to the FPTU to the desired values for each test. With independent control of the upstream and downstream static pressures, controlled tests could be run by keeping the downstream static pressure constant and varying the upstream static pressure or vice versa. The assist blowers had enough airflow capacity to provide as much as 3000 ft^3/min (1.42 m^3/s) through the FPTU, which was approximately twice the rated airflow of the largest FPTU evaluated. Pressure differential measurements across the nozzle banks in each airflow chamber were made to determine the airflow through each chamber. The difference in the airflow measurements upstream and downstream of the FPTU provided the estimated leakage of the FPTU. For all tests, the FPTU fan was turned off and the backdraft damper would have been in its closed position. With the fan off, these tests would help simulate normal cooling operations for a parallel FPTU. Because the backdraft damper was located inside the FPTU and not viewed during the tests, no attempt was made to verify visually how well the damper was successful in sealing during the tests.

Edmondson et al (2011) identified three primary sources of leakage in parallel FPTUs: (1) sheet metal seams, (2) backdraft damper, and (3) penetrations through the exterior of the cabinet

of the FPTU. Because the measurements were made on the FPTU as a whole, it was not possible to determine the exact contribution from each source of leakage for each FPTU evaluated. Some visualization tests were also conducted by attaching small paper streamers at the seams of one of the more "leaky" units. Figure 5.3 shows the difference in the streamers under 0.2 in w.g. (50 Pa) and 0.5 in w.g. (125 Pa) downstream static pressure.

(a) 0.2 in w.g. (50 Pa) downstream static

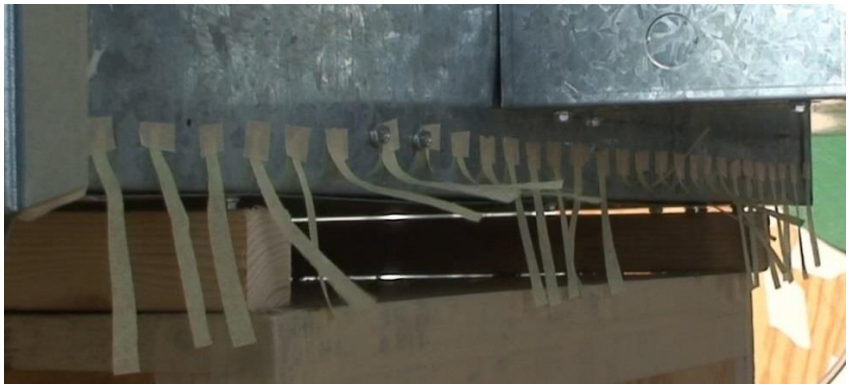

(b) 0.5 in w.g. (125 Pa) downstream static

(c)

Figure 5.3: Visualization of Leakage along the Seam of a Parallel FPTU at Downstream Static Pressures of (a) 0.2 in w.g. (50 Pa) and (b) 0.5 in w.g. (125 Pa)

At 0.5 in w.g. (125 Pa) downstream static pressure, more of the streamers (circled in the pictures) were moved by the leaking air at the bottom seam in the unit. Some of the streamers were horizontal or nearly horizontal because of the air leaking from the seams near those streamers.

All the leakage measurements were made with the FPTU fan off. While the fan is normally off during cooling operations in the field, the fan is on during heating operations. Any portion of the leakage attributable to the backdraft damper would not be relevant when the FPTU

fan is on because the backdraft damper would be open to allow air to flow into the unit from the plenum. The other sources of leakage, such as penetrations and seams would still apply. Thus, the leakage data from Edmondson et al (2011) may over predict leakage for times when the FPTU fan is on and should be used with caution for that mode of FPTU operation.

The leakage was measured by subtracting the airflow measured by the downstream airflow chamber from the airflow measured by the upstream airflow chamber. Both airflow chambers utilized a bank of nozzles and different combinations of nozzles within the airflow chambers were used as the airflow through the FPTU was either increased or decreased. Each change in nozzle banks potentially introduced more uncertainty in the measurements.

The two airflow chambers were connected in series by a short duct without the FPTU to determine potential measurement differences in airflow between the two chambers. The results of these measurements are shown in Table 5.2. For the size FPTUs used, the maximum nominal airflows should be about 700 ft^3/min (0.33 m^3/s) and 1550 ft^3/min (0.73 m^3/s), respectively, for FPTUs with a 8 in. (20.3 cm) and 12 in. (30.5 cm) primary air inlet diameters.

As seen in Table 5.2, there was a systematic bias in the measurements, with the downstream airflow chamber always reading slightly less than the upstream airflow chamber. On average, the downstream airflow chamber measured 10.6 ft^3/min (0.005 m^3/s) lower in airflow than the upstream chamber over the range of airflows. While the differences in airflow rates were small, these differences should be used to correct the leakage measurements made by Edmondson et al (2011) because the differences were all in the same direction (i.e., the airflow of the upstream airflow chamber was always larger than the downstream airflow chamber). A simple linearly regression was fit to the data in Table 5.2. The regression was used to estimate the amount of airflow to subtract from the leakage measurements based on the measurements of the upstream airflow. The data presented in this report were all corrected based on the regression fit to the airflow chamber difference data in Figure 5.1.

Table 5.2 – Differences in Measured Airflows between the Upstream and Downstream Airflow Chambers when Connected in Series (Edmondson et al 2011)

Test Point	Upstream Airflow ft^3/min (m^3/s)	Downstream Airflow ft^3/min (m^3/s)	Difference ft^3/min (m^3/s)
1	214.3 (0.101)	211.8 (0.100)	-2.5(0.001)
2	520.5 (0.246)	511.8 (0.242)	-8.7 (0.004)
3	852.5 (0.402)	841.5 (0.397)	-11.0 (0.005)
4	1193 (0.563)	1178.2 (0.556)	-14.8 (0.007)
5	1532.9(0.723)	1516.9 (0.716)	-16.0 (0.008)

Edmondson et al (2011) also conducted chamber comparison tests up to airflows of 3000 ft^3/min (1.42 m^3/s). Between approximately 1600 ft^3/min (0.71 m^3/s) and 3000 ft^3/min (1.42 m^3/s), the difference in measured airflows between the upstream and downstream airflow chambers leveled out at approximately 17 ft^3/min (0.008 m^3/s). These data were outside the range of the maximum airflows for size of the FPTUs evaluated and were not used in this report.

The FPTUs evaluated by Edmondson et al (2011) were given designations to identify the type of motor controller (ECM), series (S) or parallel (P), size (8 or 12), and manufacturer (A, B, or C). All of the fan motors in the FPTUs were ECMs. Thus, all the units started with an "ECM" designation. Because the only units of interest were parallel units, all of the units identified in this report had a "P" designation. An 8 in. (20.3 cm) unit from manufacturer A had the designation "ECM-P8A." A 12 in. (30.5 cm) unit from manufacturer C had the designation "ECM-P12C." Edmondson et al (2011) also evaluated two fan motors for each of the FPTUs that Manufacturer C provided. In their study, these were designated with a M1 and M2 identifier. For this report, only data from those FPTUs utilizing the fan motor M2 were used and the M2 designation was dropped when identifying units from Manufacturer C.

Table 5.3 through 5.5 showed the range in downstream static pressures, upstream static pressures, and primary (upstream) airflows that were used to evaluate the leakage of parallel FPTUs in this report. The ranges shown in these tables are a smaller subset of all the data that were collected by Edmondson et al, 2011. There were slight variations in the ranges for each tests because of the inability of the operator to hit a precise value of the pressure or airflow for a particular test. The downstream static pressures ranged from a low of approximately 0.1 in w.g. (25 Pa) to a high of approximately 0.5 in. w.g. (125 Pa). This range in downstream static pressures bracketed the test condition, 0.25 in w.g. (62 Pa) used in the test procedure for FPTUs

(AHRI 2011). The upstream static pressures were varied from as low as 0.4 in w.g. (100 Pa) up to slightly above 2.0 in w.g. (498 Pa).

The booster fans in the airflow chambers were capable of producing airflows far beyond the maximum rated capacities of the individual FPTUs. For example, the 12 in. (30.5 cm) FPTUs were subjected to primary airflows of approximately 3000 ft^3/min (1.42 m^3/s) during the leakage tests. Only data that were at airflows of approximately 800 ft^3/min (0.38 m^3/s) or less were used for the 8 in. (20.3 cm) FPTUs and 1600 ft^3/min (0.76 m^3/s) or less were used for the 12 in. (30.5 cm) FPTUs in the analysis below:

Table 5.3 – Range in Downstream Static Pressure for the Leakage Tests on the ECM FPTUs Evaluated by Edmondson et al (2011)

	Upstream Static Pressure – in w.g. (Pa)	
FPTU	**Minimum**	**Maximum**
ECM-P8A	0.09 (22)	0.51 (127)
ECM-P8B	0.09 (22)	0.55 (137)
ECM-P8C	0.10 (25)	0.50 (125)
ECM-P12A	0.10 (25)	0.52 (130)
ECM-P12B	0.10 (25)	0.49 (122)
ECM-P12C	0.09 (22)	0.50 (125)

Table 5.4 – Range in Upstream Static Pressure for the Leakage Tests on the ECM FPTUs Evaluated by Edmondson et al (2011)

	Upstream Static Pressure – in w.g. (Pa)	
FPTU	**Minimum**	**Maximum**
ECM-P8A	0.47 (117)	2.01 (501)
ECM-P8B	0.39 (97)	2.09 (521)
ECM-P8C	0.47 (117)	2.03 (506)
ECM-P12A	0.48 (120)	1.96 (488)
ECM-P12B	0.45 (112)	2.06 (513)
ECM-P12C	0.50 (125)	2.00 (498)

Table 5.5 – Range in Primary Airflow for the Leakage Tests on the ECM FPTUs Evaluated by Edmondson et al (2011)

FPTU	Primary Airflow – ft^3/min (m^3/s)	
	Minimum	Maximum
ECM-P8A	226 (0.107)	760 (0.359)
ECM-P8B	229 (0.108)	805 (0.380)
ECM-P8C	184 (0.087)	805 (0.380)
ECM-P12A	356 (0.168)	1600 (0.755)
ECM-P12B	530 (0.250)	1422 (0.6711)
ECM-P12C	292 (0.138)	1526 (0.720)

5.3. Leakage Data Analysis

Figures 5.4 and 5.5 showed the leakage for the 8 in. (20.3 cm) and 12 in. (30.5 cm) FPTUs, respectively. The data showed a linear relationship between leakage and downstream static pressures for the FPTUs.

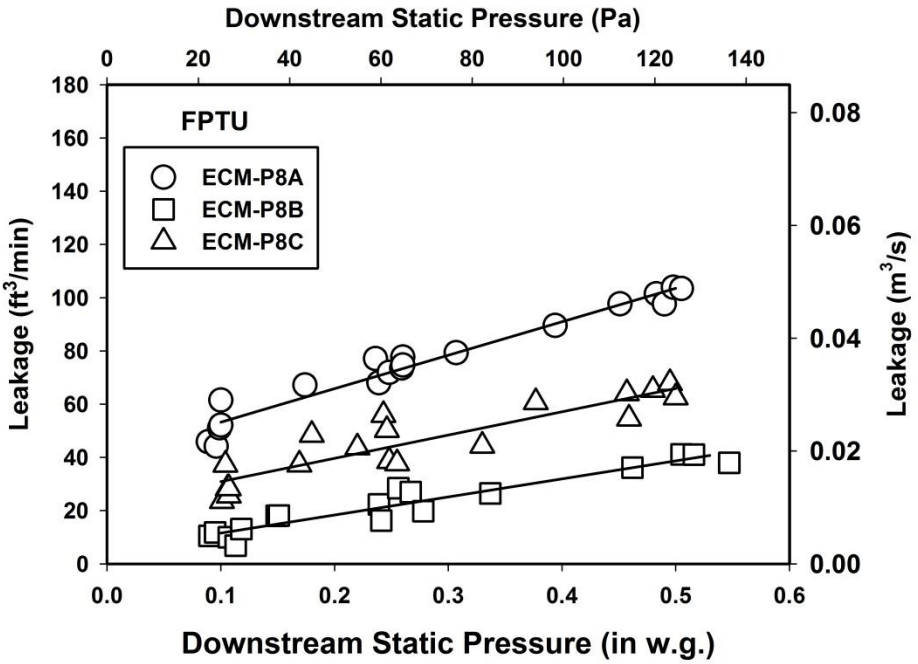

Figure 5.4: Leakage as a Function of Downstream Pressure for the 8 in. (20.3 cm) ECM FPTUs

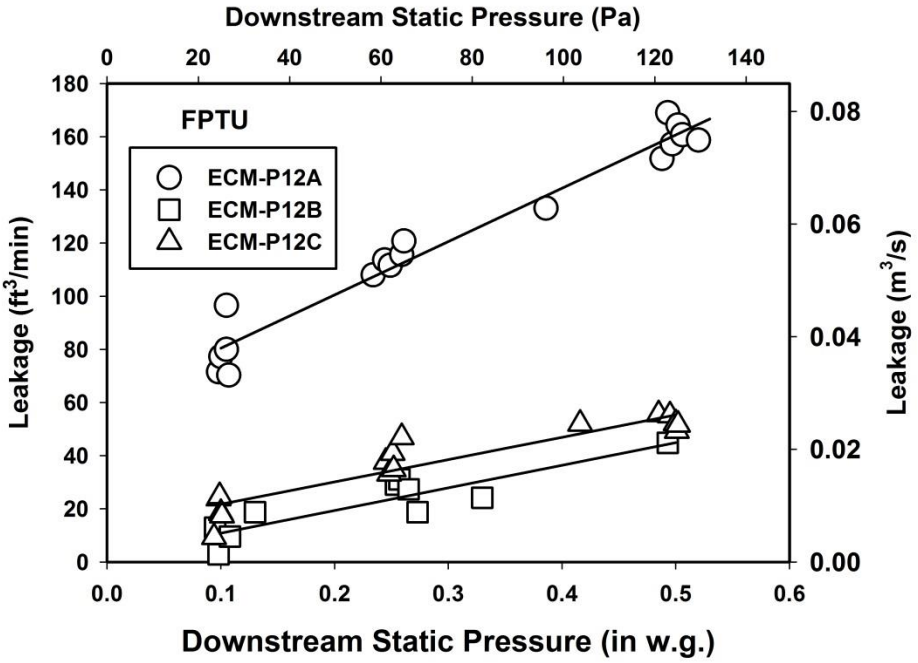

Figure 5.5: Leakage as a Function of Downstream Static Pressure for the 12 in. (30.5 cm) FPTUs

With ducts, the leakage usually varies with the downstream static to the Nth power, where N is assumed to be 0.65 (ASHRAE 2012). The linear relationship of leakage with downstream static pressure was consistent with the fits of the data by Edmondson et al (2011) and with the fits reported by Furr et al (2008) for the SCR units they evaluated. It was not clear why the relationship between leakage and downstream static pressure for FPTUs was linear compared to the non-linear relationship found in ducts. FPTUs do have a moveable component (backdraft damper) in the leakage flow path. It was possible that the opening area between the cabinet and the backdraft damper changed with increases in static pressure which would have allowed more flow than expected. However, the backdraft damper was not observed during the tests.

All of the leakage data were fit with a simple linear regression in the form shown in Equation 5.3.

$$Q_{leakage} = C_1 + C_2 * P_{dwn} \quad (5.3)$$

The regression coefficients were shown in Table 5.6 along with the r-squared values. As seen from the r-squared values in Table 5.6 and the plots in Figures 5.4 and 5.5, downstream static pressures had a major influence on leakage from all of the parallel FPTUs evaluated. The r-squared values for the fits (0.80 to 0.96) were not as high as those reported by Edmondson et al

(2011) who had a range of values from 0.83 to 0.97. Their data included primary airflows up to 3000 ft^3/min (1.42 m^3/s) which provided a larger dataset for the regression. In addition, they included an extra regression variable (primary air velocity pressure, P_{iav}). The additional data and regression variable would be expected to improve the regression over what is reported in Table 5.6. As mentioned previously, the inlet air velocity pressure was not a useful variable in a building simulation program because it would not be known by the modeler. While the downstream static pressure was not a variable in models utilizing a mass and energy balance approach, it could potentially be included in approaches that utilize static pressures. Equation 5.3 and Table 5.6 provided the data necessary for a modeler to evaluate leakage at a range of downstream pressures if desired.

Table 5.6 – Coefficients and R^2 Values of the FPTU Leakage Model in Equation 5.3 for Each of the Parallel FPTUs Evaluated by Edmondson et al (2011)

FPTU	C_1 ft^3/min (m^3/s)	C_2 ft^3/(min*in w.g.) (m^3/(s*Pa))	R^2
ECM-P8A	40.64 (1.92e-2)	125.8(2.38 e-04)	0.96
ECM-P8B	4.79 (0.23 e-2)	67.8 (1.28e-04)	0.91
ECM-P8C	22.15 (1.04e-2)	87.4 (1.66e-04)	0.81
ECM-P12A	60.43 (2.85e-2)	200.5(3.79e-04)	0.96
ECM-P12B	2.32 (0.11e-2)	85.1 (1.62e-04)	0.80
ECM-P12C	13.3 (0.63e-2)	84.0 (1.59e-04)	0.86

The plots in both Figures 5.4 and 5.5 also showed that there was a wide range in leakage for both sized units. In the 8 in. (20.3 cm) units, ECM-P8A had the largest amount of leakage, varying from a low of about 50 ft^3/min (0.02 m^3/s) at 0.1 in w.g.(25 Pa) up to over 100 ft^3/min (0.05 m^3/s) at about 0.5 in w.g.(125 Pa). In contrast, ECM-P8B had only about 10 ft^3/min (0.005 m^3/s) leakage at 0.1 in w.g. (25 Pa) and 40 ft^3/min (0.019 m^3/s) leakage at 0.5 in w.g. (125 Pa). Thus, ECM-P8B had less leakage at the highest downstream static pressure (0.5 in w.g. (125 Pa)) than did ECM-P8A at the lowest downstream static pressure (0.1 in w.g. (25 Pa)). For the 12 in. (30.5 cm) units, ECM-P12A had the largest amount of leakage and varied from as much as eight times the amount of leakage of ECM-P12B at the lowest downstream static pressure to about four times at the highest downstream static pressure.

The test procedures (ASHRAE 2006 and AHRI 2011) for FPTUs specified a downstream static pressure of 0.25 in w.g. (62 Pa) for rating FPTUs. Most of the FPTU airflow and power performance data collected by Furr et al (2008) and Edmondson et al (2011) were also at the 0.25 in w.g. (62 Pa) downstream static pressure to match the test procedure. It was also our understanding from informal conversations with engineers from the three FPTU manufacturers who provided the units for this study that many units in the field are set at or near this static pressure for the design airflow conditions and that downstream static pressures can be expected to decrease as the primary airflow decreases for off-design conditions. Given this downstream static pressure was a common rating point for all FPTUs and a value expected to be common in the field, we listed the average and standard deviation of the leakages for the six units at this pressure in Table 5.7. We believe it was coincidental that Manufacturer A's FPTUs had the highest leakage and Manufacturer B's had the lowest leakages for each of the two size FPTUs. The SCR FPTU leakage data presented by Furr et al (2008) did not show the same consistency of leakage by manufacturer that was found in the data collected by Edmondson et al (2011).

Table 5.7 – Average and Standard Deviation of Leakage for Each FPTU at a Downstream Static Pressure of 0.25 in w.g. (62 Pa)

FPTU	Average Leakage ft^3/min (m^3/s)	Standard Deviation ft^3/min (m^3/s)
ECM-P8A	74.6 (0.035)	3.3(0.002)
ECM-P8B	23.4 (0.011)	4.3 (0.002)
ECM-P8C	45.1(0.021)	6.4(0.003)
ECM-P12A	117.2 (0.055)	8.3 (0.004)
ECM-P12B	26.1(0.012)	4.3 (0.002)
ECM-P12C	38.7 (0.018)	4.9 (0.002)

The variations in air leakage with upstream static pressure are shown in Figures 5.6 and 5.7 for the 8 in. (20.3 cm) and 12 in. (30.5 cm) FPTUs. For all units, the downstream static pressures were held at 0.25 in w.g. (62 Pa).

The upstream static pressures varied from approximately 0.5 in w.g. (125 Pa) to 2.0 in w.g. (498 Pa). The solid lines in both figures represented the average leakage for each unit at a downstream pressure of 0.25 in w.g. (62 Pa) - see Table 5.7.

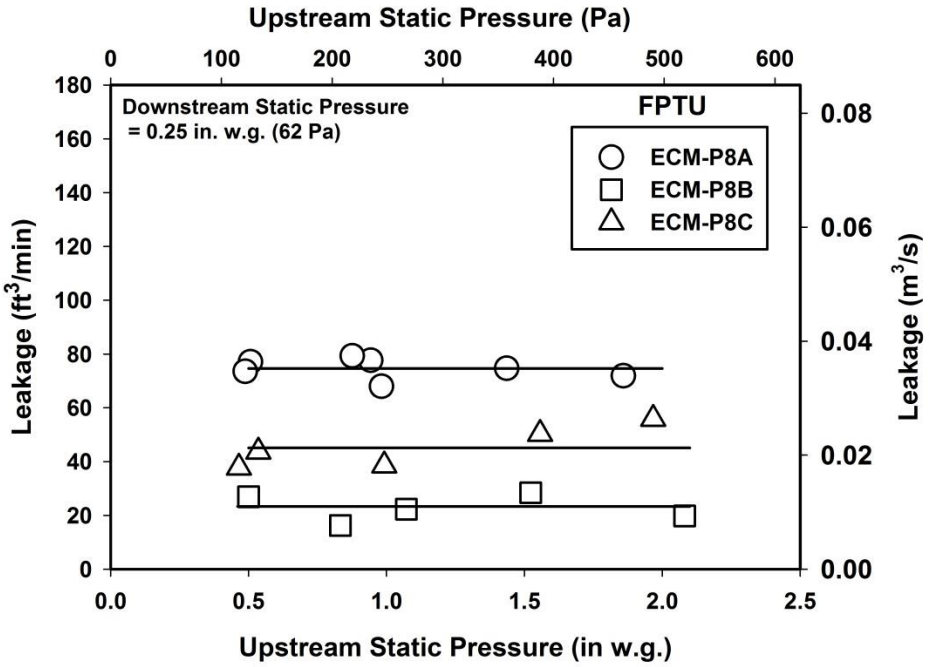

Figure 5.6: Leakage as a Function of Upstream Static Pressure for the 8 in. (20.3 cm) FPTUs and Downstream Static Pressure of 0.25 in. w.g. (62 Pa)

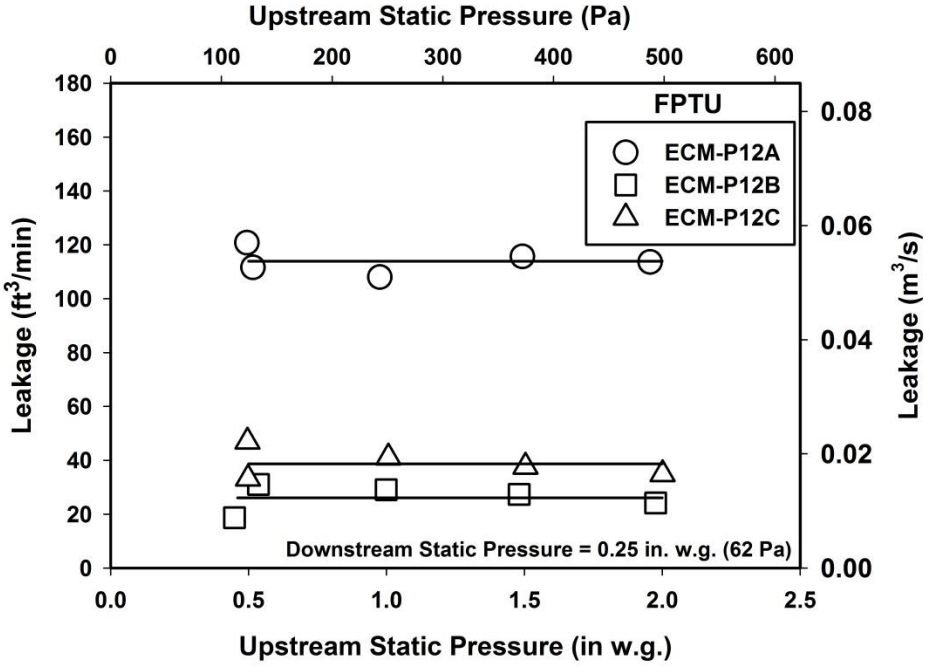

Figure 5.7: Leakage as a Function of Upstream Static Pressure for the 12 in. (30.5 cm) FPTUs and Downstream Static Pressure of 0.25 in w.g. (62 Pa)

There appeared to be no consistent trends of air leakage with respect to the upstream static pressure. Some units showed a slight upward trend and some showed a slight downward trend. For modeling purposes, because there were no consistent trends, leakage in the units can be treated as independent of upstream static pressure.

Primary airflow was varied to determine if it affected the leakage from the parallel units. Figures 5.8 and 5.9 show how leakage varied with the primary airflow for the 8 in. (20.3 cm) and the 12 in. (30.5 cm) units, respectively.

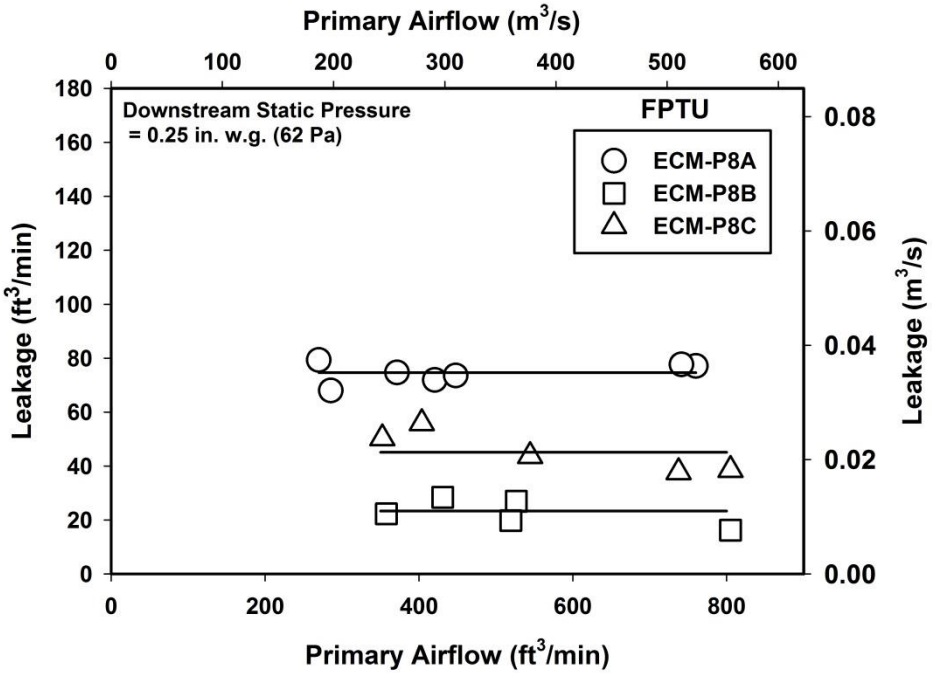

Figure 5.8: Leakage as a Function of Primary Airflow for the 8 inch FPTUs at a Downstream Static Pressure of 0.25 in w.g.(62 Pa)

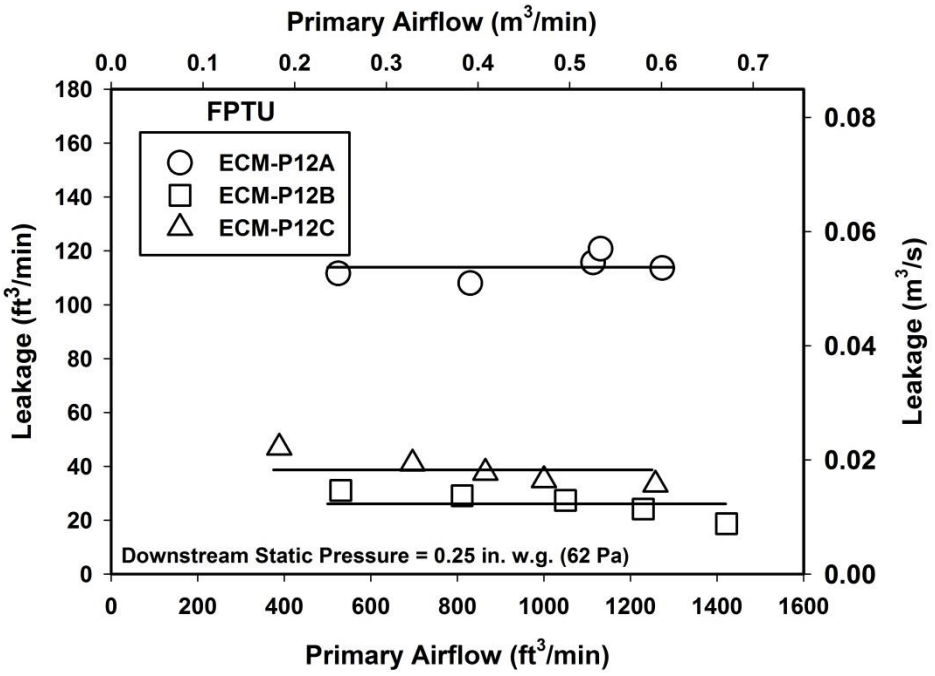

Figure 5.9: Leakage as a Function of Airflow for the 12 inch FPTUs at a Downstream Static Pressure of 0.25 in w.g. (62 Pa)

As with the previous plots, the lines in both plots were the average leakage (see Table 5.7) measured at a constant downstream static pressure of 0.25 in w.g. (62 Pa). These two figures showed that increases in air velocities inside the FPTU, as represented by the increase in primary airflow, did not affect the leakage from the FPTU. One might expect that increases in primary air should create higher air velocities and turbulence inside the FPTU cabinet. Air at higher velocities, directly impinging on a seam or penetration in the housing of the FPTU might be expected to increase the leakage. However, the leakage from the units showed no consistent trends with respect to primary airflow. ECM-P8A and ECM-P12A both showed either a flat or slightly increasing leakage with primary airflow. All of the others showed a slight decrease. These trends with airflow were consistent with the variations in value of the coefficient (see Equation 5.1) for inlet velocity pressure that Edmondson et al (2011) calculated. They found that the coefficient was positive for some units and negative for other units. The trends shown in Figures 5.8 and 5.9 show that if the downstream static was held constant, primary airflow did not directly affect leakage for their tests. The data did not show that leakage can be treated independent of primary airflow. In a typical field application, the downstream static pressure would be expected to decrease as the primary airflow decreased. This decrease in static pressure,

driven by the decrease in primary airflow, would impact the leakage as shown in Figures 5.4 and 5.5.

Looking at the leakages in Table 5.7, it was decided to arrange the individual FPTUs into three groupings: low, medium, and high (Table 5.8). The average amount of leakage for each classification is shown in Table 5.9 for a downstream static pressures of 0.10 in w.g. (25 Pa), 0.25 in w.g. (62 Pa), and 0.50 in w.g.(125 Pa). A plot of the low, medium and high leakages are shown in Figure 5.10.

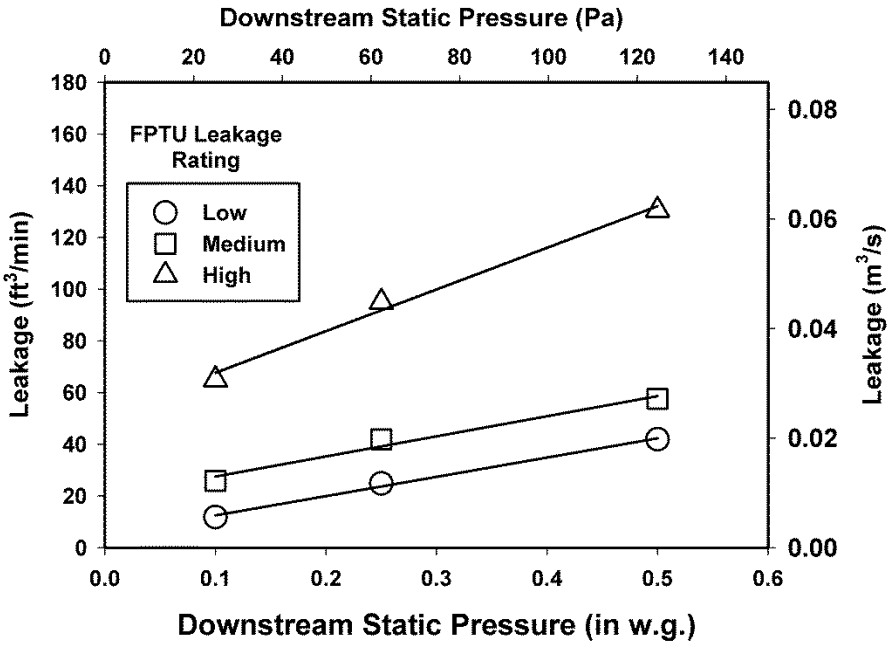

Figure 5.10: Leakage Versus Downstream Static Pressure for the Three Leakage Classifications

The three leakages were fit with a straight line of the form shown below:

$$Q_{leakage} = A_1 + A_2 * P_{dwn} \quad (5.4)$$

Where A_1 and A_2 were regression coefficients. The plots of the leakage with a linear fit are consistent with the original data on each FPTU which had linear fits (see Equation 5.3 and Table 5.6). Table 5.10 provides the regression fits for the three leakage classifications.

For a user attempting to model a parallel FPTU with leakage, it would be possible to use the leakages shown in Table 5.9 and the regressions in Table 5.10 to provide an estimate of the range of impact of leakage on the energy use of FPTUs and the HVAC system. The values in Tables 5.9 and 5.10 were based on both 8 in. (20.3 cm) and 12 in. (30.5 cm) primary diameter inlet

FPTUs and should be usable for these size FPTUs in a simulation model. While these values can be used for larger or smaller FPTUs, there were no data to show that larger or smaller FTPUs would have similar ranges in leakages. In addition, because the original range of the data included downstream static pressures between 0.1 and 0.5 in w.g. (25 to 125 Pa), the regressions should be used with caution when attempting to estimate leakages outside this range of static pressures.

Table 5.8 – Leakage classification of the six parallel FPTUs.

Leakage Classification		
Low	Medium	High
ECM-P8B	ECM-P8C	ECM-P8A
ECM-P12B	ECM-P12C	ECM-P12A

Table 5.9 – Average Leakage Airflow at Three Downstream Static Pressures and the Three Leakage Classifications

Leakage Classification	Average Leakage - ft^3/min (m^3/s)		
	@ 0.1 in w.g. (25 Pa)	@0.25 in w.g. (62 Pa)	@0.50 in w.g. (125 Pa)
Low	11.8 (0.006)	24.8 (0.012)	41.9 (0.020)
Medium	25.8 (0.012)	41.9 (0.020)	57.6 (0.027)
High	65.0 (0.031)	95.9 (0.045)	130.6 (0.062)

Table 5.10 – Coefficients and R^2 Values for the Three FPTU Leakage Classifications

Leakage Classification	A_1 ft^3/min (m^3/s)	A_2 $ft^3/(min*in\ w.g.)$ ($m^3/(s*Pa)$)	R^2
Low	5.02 (0.24e-2)	74.6(1.41e-04)	0.99
Medium	19.70 (0.93e-2)	77.8 (1.47e-04)	0.98
High	51.45 (2.43e-2)	161.3 (3.06e-04)	0.99

It was possible to illustrate how the data in Table 5.9 and the regressions in Table 5.10 can be used in a simulation program. One possible option would be to relate the change in downstream static pressure to the change in primary airflow as shown below:

$$P_{dwn} = P_{dwn@design}\left(\frac{Q_{primary}}{Q_{primary@design}}\right)^2 \quad (5.5)$$

The primary airflow at design ($Q_{primary@design}$) would be the primary airflow of the FPTU at the design conditions for the zone. That airflow corresponded to the downstream static pressure ($P_{dwn@design}$) at the design conditions. Equation 5.5 assumed the static pressure downstream of the FPTU varied with the square of the primary airflow. Thus, as the primary airflow decreased by a factor of two, the amount of downstream static decreased by a factor of four. This assumption would only hold true when the FPTU fan was off which occurred in the cooling mode of a parallel FPTU. Once the FPTU fan was engaged, the downstream static pressure would depend on a combination of the FPTU fan and the upstream air handler.

Figures 5.11 and 5 12 showed a sample set of estimates of the percentage leakages for an 8 inch (20.3 cm) parallel FPTU which had a design airflow of 800 ft^3/min (0.38 m^3/s) and downstream static pressures of 0.25 and 0.50 in w.g. (62 and 125 Pa), respectively, occurring at the design (maximum) airflow.

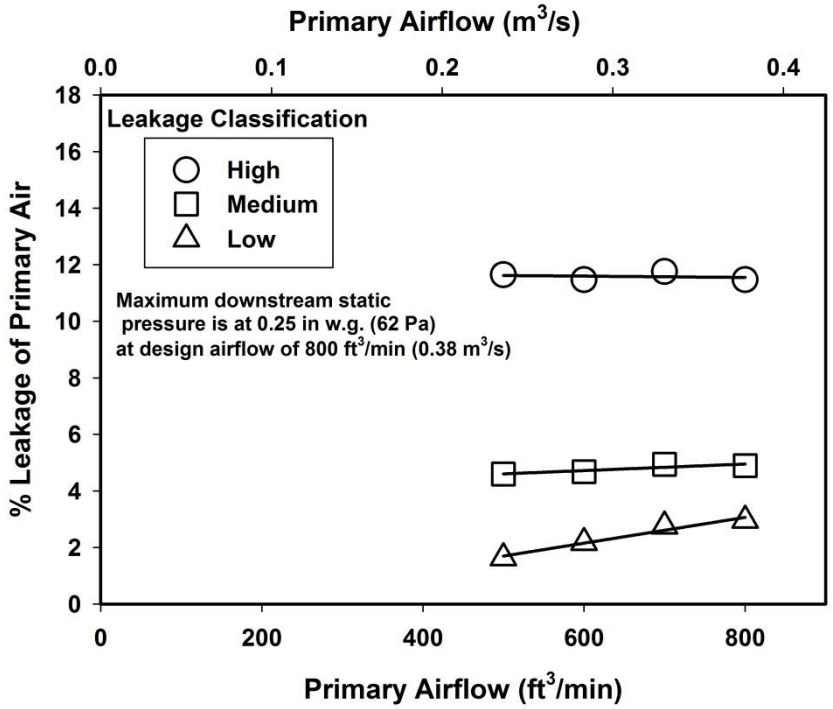

Figure 5.11: Percentage Leakage Versus Primary Airflow when the Downstream Static Pressure is Set at 0.25 in w.g. (62 Pa) for a Design Airflow of 800 ft^3/min (0.38 m^3/s)

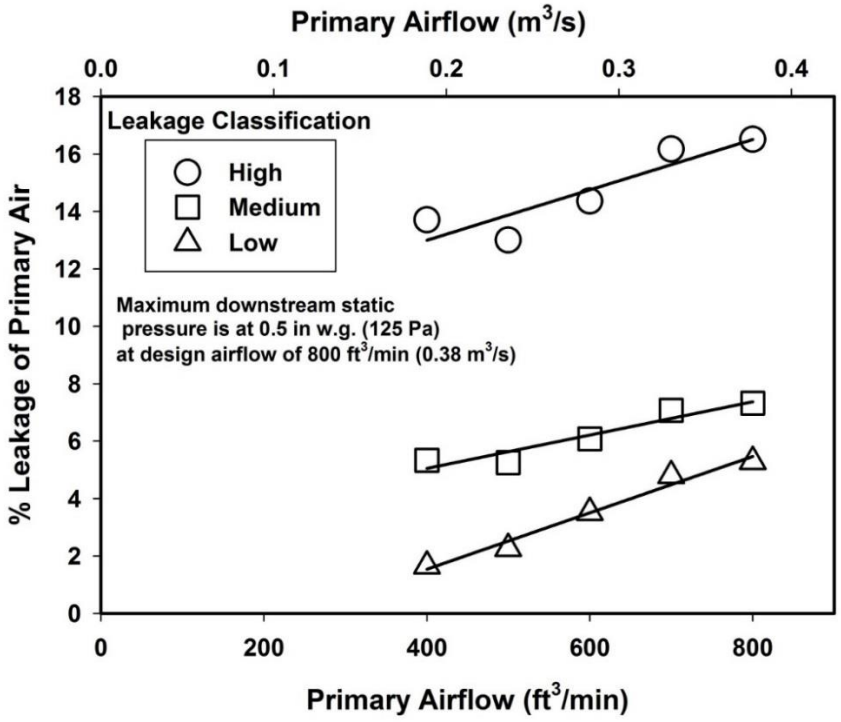

Figure 5.12: Percentage Leakage Versus Primary Airflow when the Downstream Static Pressure is Set at 0.50 in w.g. (125 Pa) for a Design Airflow of 800 ft^3/min (0.38 m^3/s)

As the airflow decreased in the FPTU, the downstream static pressure was reduced using Equation 5.5. This downstream static pressure was then substituted into Equation 5.4 to yield a leakage airflow rate. This rate was then divided by the primary airflow to obtain the percentage leakage. For the FPTU operating at a downstream static pressure of 0.25 in w.g. (62 Pa) for a design airflow of 800 ft^3/min (0.38 m^3/s), the percentage leakage was nearly constant for the high leakage case. It showed a decrease with decreasing primary airflow for the medium and low leakage cases. At the higher static pressure at design, 0.5 in w.g. (125 Pa), the percentage leakages for all three of the classifications (low, medium, and high) decreased as the primary airflow decreased from the design of 800 ft^3/min (0.38 m^3/s). If one wanted to use a constant percentage leakage to characterize the leakages from a parallel FPTU, then for three cases in Figure 5.11, those values would be 2.4%, 4.8%, and 11.6%, respectively for the low, medium, and high leakages. With the higher downstream design static pressure, those values would be 3.5%, 6.2%, and 14.8%, respectively for the low, medium, and high leakage classifications. FPTUs with a 12 in. (30.5 cm) primary inlet should have higher design airflows than the 8 in.

(20.3 cm) units in Figure 5.11 and 5.12. Thus, it could be expected that the percentage leakages for the larger FPTUs should be less than the values shown in these figures.

5.4. Summary

Parallel FPTU leakage data and models that had been published previously by both Furr et al (2008) and Edmondson et al (2011) were evaluated. The focus of the analysis was the ECM FPTU air leakage data of Edmondson et al (2011). Downstream static pressure was the major variable driving leakage in parallel FPTUs. Should a modeler need to include downstream static pressure as a variable for estimating air leakage, the regressions provided in Table 5.6 can be used to simulate different FPTUs.

The data showed that air leakage was independent of both upstream static pressure and primary airflow when the downstream static pressure was held constant. Because a downstream static pressure of 0.25 in w.g. (62 Pa) was a common rating point for FPTUs (ASHRAE 2006 and ARI 2011), average air leakage data for each FPTU were determined at this downstream pressure. The leakage data from each of the FPTUs were used to group the FPTUs into three classifications with respect to leakage: low, medium, and high. The average leakage rates for the FPTUs at 0.1 in w.g. (25 Pa), 0.25 in w.g. (62 Pa), and 0.5 in w.g. (125 Pa) were used to develop a simple correlation for leakage as a function of downstream static pressure. To illustrate how these correlations could be used to estimate percentage leakage, the downstream static pressure was related to the square of the primary airflow for an 8 in. (20.3 cm) FPTU that had a design airflow of 800 ft^3/min (0.38 m^3/s). For a design downstream static pressure of 0.25 in w.g. (62 Pa), the average percentage leakages ranged from 2.4% for the low leakage FPTU to 11.6% for the high leakage FPTU. While there was a decreasing percentage leakage with decreasing primary airflow for five of the six cases, it would appear that a user of a building simulation program could use a constant percentage leakage to characterize leakage from a FPTU when the FPTU fan is off.

The leakage measurements analyzed for this study were with the FPTU fan off. Edmondson et al (2011) had identified three possible sources of air leakage in FPTUs: seams, penetrations, and the backdraft damper. The leakage estimates should be applicable for a FPTU that operates a large majority of its time in cooling mode when the FPTU fan is off. However, if the FPTU operates a significant amount of time in heating mode, then the air leakage estimates from this study may overstate the actual leakage because there would be no leakage through the backdraft

damper. Thus, this leakage data and correlations should be used with caution for that mode of FPTU operation.

Davis et al (2012a) used a simple percentage leakage model to show that leakage can have a large impact on the estimated energy performance of parallel FPTUs. His high leakage case assumed leakages as high as 20%. Based on the percentage leakages in Figures 11 and 12, it would appear that a value of 12 to 15% should be used for the upper limit for percentage leakages in parallel FTPUs rather than 20%.

While building energy simulation programs, such as EnergyPlus (2013), allowed inclusion of leakage of ducts, it needs to allow for leakage in parallel FPTUs if a simulation is going to capture the expected field performance of these systems. Without leakage in parallel FPTU models, building simulation programs will continue to provide an optimistic estimate of the energy use of parallel FPTUs. The low, medium and high values of leakages should be used when estimating the range in leakages of FPTUs in building simulation programs.

The leakage curves in Figures 5.11 through 5.12 assumed a simple relationship between downstream static pressure and primary airflow. The authors are not aware of any data that has been published on the variation of downstream static pressure with primary airflow for the two sizes of FPTUs used in this study. We recommend that data be collected that could be used to better characterize downstream static pressure as a function of primary airflow for a range in size of parallel FPTUs. The data collected from the study could be used with the Equation 5.4 to develop a refined model for estimating leakage in parallel FPTUs.

CHAPTER 6

FIXED AIRFLOW SERIES AND PARALLEL FPTU PERFORMANCE MODELS

The purpose of this chapter was to show the derivation and operation of the basic mass and energy models for fixed airflow series and parallel FPTUs. The models combined the PSC/SCR and ECM performance data developed in Chapters 2 and 3 to provide a comprehensive FTPU model that could be integrated into building simulation programs such as EnergyPlus (2013). The analysis presented in this chapter has also been summarized in three papers published in the open literature: O'Neal et al (2015a and 2015b) and O'Neal (2015).

6.1. Series FPTU

The mass and energy balance approach (MEB) has been used to model components in the HVAC system of a building (Knebel 1983). The MEB approach treats each sub-system, such as a FPTU, in a HVAC system as a set of equations to describe the mass and energy flows into and out of each sub-system. A series FPTU can then be decomposed into its major components: mixer, fan/motor, and heating coil. Figure 6.1 shows a control volume around the whole FPTU.

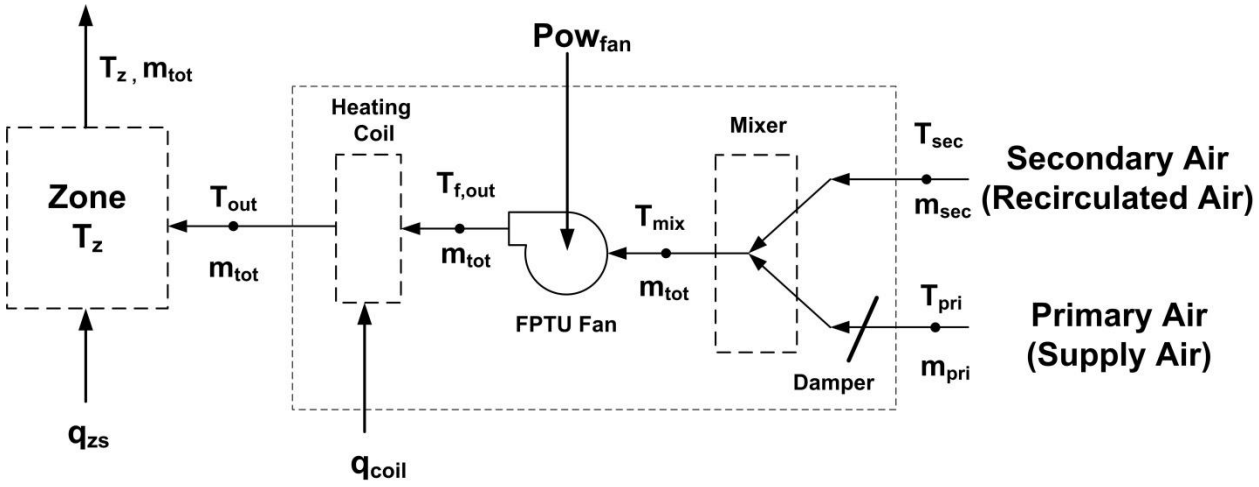

Figure 6.1: Mass and Energy Flows into and out of a Series FPTU

With the MEB approach, an analysis can be performed on each component to estimate overall airflows into and out of the FPTU as well as the energy used by the FPTU fan/motor for each time step of a simulation. Each FPTU component can be treated with a smaller control volume with mass and energy inputs and outputs.

Looking at the overall control volume around the series FPTU, energy is input to the FPTU via electrical energy to the fan, heat energy to the heating coil, and energy associated with the

primary and secondary airstreams. The only mass and energy leaving the series FPTU is with the airstream at the discharge of the FPTU. The series FPTU consists of three major components: mixer, fan, and heating coil. A mass and energy balance needs to be performed on each of the components and the conditioned zone to estimate temperatures and airflows to determine the performance of the FPTU. The approach outlined below incorporates empirical models for the FPTU fan/motor to calculate the fan power.

Before starting an analysis, it is important to outline some basic assumptions we used in developing the MEB model. First, the system in Figure 6.1 was assumed to operate at quasi-steady state during each time step. During a particular time-step, the temperature and airflows remained constant and were averaged over the time step. Given that the typical time step was an hour, this type of analysis cannot capture rapid transients occurring in a control system at smaller time steps. We also assumed that the thermo-physical properties are constant. This allowed the specific heat and density of the air to be treated as constants. Given the small temperature differences in the airstreams, constant specific heats and density should introduce small errors (less than a 1%) in the analysis. Third, the energy input to the fan motor was assumed to be completely converted into the heat energy in the airstream. This assumption was discussed in more detail later in the paper. Fourth, the FPTU must always operate with a minimum amount of primary air to ensure enough fresh air is introduced into the zone. Thus, even when the zone called for heating or a very low amount of cooling, there would always be a minimum amount of primary air provided to the FPTU.

The mass and energy balances for a general control volume at steady state are given by Equations 6.1 and 6.2, respectively:

$$\left\{ \begin{matrix} Airflow \\ Out\ of\ FPTU \end{matrix} \right\} = \left\{ \begin{matrix} Airflow \\ Into\ FPTU \end{matrix} \right\} \tag{6.1}$$

$$\left\{ \begin{matrix} Energy \\ Out\ of\ FPTU \end{matrix} \right\} = \left\{ \begin{matrix} Energy \\ Into\ FPTU \end{matrix} \right\} \tag{6.2}$$

For the FPTU control volume shown in Figure 6.1, the mass flow into the control volume included the primary, m_{pri}, and secondary, m_{sec} airstreams. The only mass out of the control

volume was the total airflow, m_{tot}. Application of the mass balance in Equation 6.1 to the control volume yielded the mass balance shown in Equation 6.3.

$$m_{tot} = m_{pri} + m_{sec} \tag{6.3}$$

The value of m_{pri} *is* often an unknown that must be estimated using the analysis discussed below. The only exceptions are when the series FPTU is operating under minimum or maximum primary flow conditions.

The energy transfer into the control volume included the energy carried by the two airstreams, the energy input in the heating coil, q_{coil}, and the energy input to the fan, Pow_{fan}. The energy into and out of the control volume can be substituted into Equation 6.2 to obtain the general energy balance for the control volume given in Equation 6.4.

$$m_{tot}h_{out} = q_{coil} + Pow_{fan} + m_{pri}h_{pri} + m_{sec}h_{sec} \tag{6.4}$$

Equations 6.3 and 6.4 provided the foundation for the analysis of a series FPTU. The unknowns in these equations varied depending on the mode of operation (heating, cooling, or dead-band) of the FPTU. Solving for the unknowns required applying mass and energy balances to each of the components in the FPTU. The process typically started from the left at the FPTU discharge to the zone and moved to the right to the primary and secondary air inlets.

For the case of a fixed airflow with either a PSC/SCR or ECM fan/motor, the total airflow, m_{tot}, in the above equations was a fixed value. With constant air properties, Equation 6.4 can be rewritten in terms of temperatures and specific heats.

$$m_{tot}\, c_p T_{out} = q_{coil} + Pow_{fan} + m_{pri}\, c_p T_{pri} + m_{sec}\, c_p T_{sec} \tag{6.5}$$

Proceeding with the analysis required decomposing the FPTU into its components and performing mass and energy balances on each component as described below.

6.1.1 Zone Analysis Figure 6.2 showed the mass and energy flows into and out of the conditioned zone.

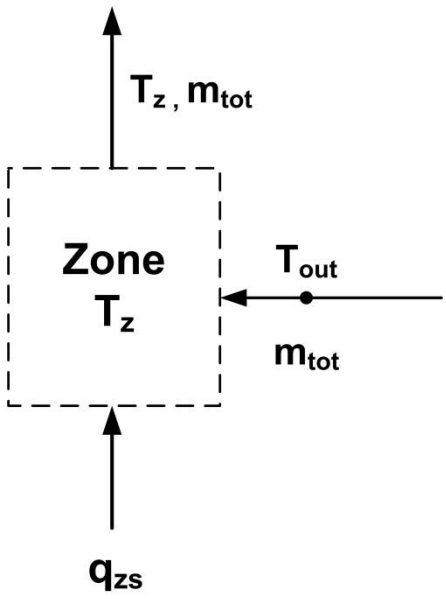

Figure 6.2: Energy and Mass Flows into and out of the Zone Control Volume

Energy is carried into and out of the zone via the total airflow, m_{tot}. The load in the zone due to people, equipment, solar gain, infiltration, etc. was represented by q_{zs}.

The value of the FPTU discharge temperature, $T_{out,}$ must be calculated. This was done with an energy and mass balance on the zone in Figure 6.2. During heating operations, T_{out} was not allowed to drift above 90°F (32.2°C). The rationale for this assumption was provided in the heating coil analysis below. During cooling operations, this value cannot drop below the sum of the primary air temperature plus temperature increase due to the FPTU fan. An energy balance was performed on the zone to yield Equation 6.6, which was used to determine the discharge temperature of the air at the outlet of the FPTU unless the heating coil is engaged. The assumption for constant properties was used throughout the system.

$$q_{zs} = m_{tot} c_p (T_z - T_{out}) \tag{6.6}$$

The way that Equation 6.6 was used in an analysis depended on whether the system was in heating or cooling mode. For example, for a fixed airflow application, m_{tot} is known. In addition, the zone load q_{zs}, specific heat c_p, and zone set-point temperature T_z are also known. For cooling applications, Equation 6.6 can be rewritten and solved for the discharge outlet temperature, T_{out}, for the FPTU:

$$T_{out} = \frac{q_{zs}}{m_{tot} c_p} + T_z \tag{6.7}$$

For heating calculations, T_{out} was calculated from Equation 6.7 but has an upper limit of typically15°F (8.3°C) above the zone set-point temperature or a fixed value of 90°F(32.2°C) to help reduce temperature stratification in the zone (Hydeman and Eubanks, 2014; Faris and Int-Hout, 2014). Procedures were provided later in this chapter for the calculation of T_{out} for heating and cooling applications.

6.1.2 Heating Coil Analysis Figure 6.3 shows the mass and energy flows into and out of the heating coil.

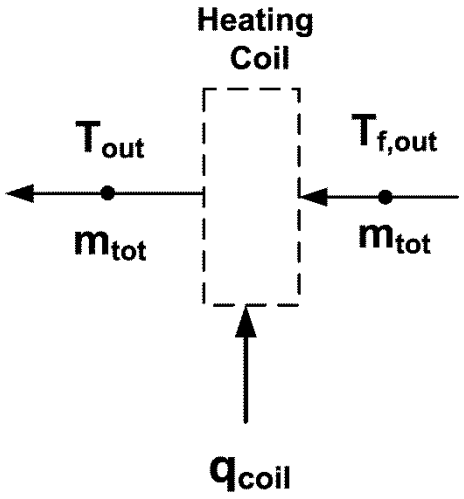

Figure 6.3: Energy and Mass Flows for the Heating Coil

It was assumed the system operates at quasi-steady state and the mass flow of air entering the coil was equal to the mass flow of air exiting the coil in a given timestep. The energy entering the coil was the heating energy input, q_{coil}, and the energy associated with the air flow entering the coil after the FPTU fan. Heating energy is often provided by electric resistance or hot water. The energy exiting the coil was carried by air leaving the coil and supplied to the zone. Applying an energy balance to the heating coil yielded:

$$m_{tot}c_pT_{out} = q_{coil} + m_{tot}c_pT_{f,out} \quad (6.8)$$

Many times, the variable of interest is q_{coil}, the heating energy input, so the above equation can be rearranged to solve for q_{coil}:

$$q_{coil} = m_{tot}c_p\left(T_{out} - T_{f,out}\right) \quad (6.9)$$

6.1.3 FPTU Fan Analysis The mass and energy flows into and out of the FPTU fan are shown in Figure 6.4.

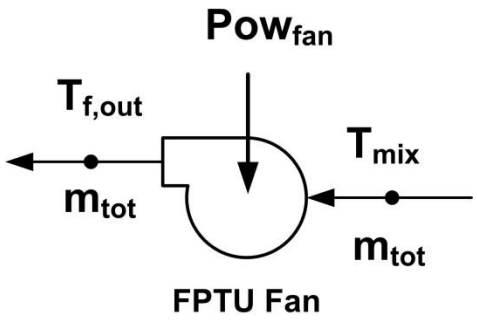

Figure 6.4: Mass and Energy Balance on the Series FPTU Fan

It was assumed that all of the fan motor and controller power is converted to heat energy in the airstream. This fraction of electric power dissipating into airstreams as heat energy can be varied by the user in EnergyPlus (2013). With a series FPTU, the electric motor is located in the primary airstream. With an ECM motor, the controller is also in the airstream, so for an ECM, it should be expected that all the energy converted for the fan motor and controller goes into the airstream. With a SCR controlled fan motor, the SCR controller is typically not located in the primary airstream, but in the plenum airstream. Estimates of the power dissipated by a SCR controller are 1.5 W/amp of current flowing through the controller (Roman and Heiligenstein 2002). Table 6.1 shows the estimated percentage of total power that a SCR controller consumes for a 0.5 horsepower (373 W) PSC fan motor from one manufacturer. The power used by the SCR controller ranged between 0.57% to 0.83% of the total power of the motor. Calculations were run for fan motors ranging from 0.167 horsepower (124 W) to 1.0 horsepower (746 W) with a similar range in percentages of the total power. Thus, with SCR controlled fan motors, assuming that all the fan power is dissipated into the primary airstream introduces less than a 1% error in the heat energy added by the fan.

The airflow out of the fan was assumed to be equal to the airflow into the fan and both were equal to m_{tot}. For constant properties, an energy balance on the fan yielded:

$$m_{tot} c_p T_{f,out} = m_{tot} c_p T_{mix} + Pow_{fan} \tag{6.10}$$

Table 6:1 – SCR Power Consumption for a 0.5 hp (373 W) FPTU Series Fan Motor

SCR Voltage	Airflow ft^3/min (m^3/s)	Current (Amps)	Power Watts	SCR Power Watts	SCR Power/ Total Power
277	2515 (1.19)	3.28	894	4.92	0.55%
277	2435 (1.15)	2.89	803	4.335	0.54%
277	2322 (1.10)	2.66	740	3.99	0.54%
277	2047 (0.97)	2.27	642	3.405	0.53%
240	2136 (1.01)	3.32	770	4.98	0.65%
240	2136 (1.01)	3.07	719	4.605	0.64%
240	2077 (0.98)	2.78	656	4.17	0.64%
240	1879 (0.89)	2.45	602	3.675	0.61%
208	1691 (0.80)	3.1	615	4.65	0.76%
208	1762 (0.83)	2.95	595	4.425	0.74%
208	1703 (0.80)	2.71	566	4.065	0.72%
208	1564 (0.74)	2.25	476	3.375	0.71%
140	1019 (0.48)	2.17	409	3.255	0.80%
140	1079 (0.51)	2.14	409	3.21	0.78%
142	1098 (0.52)	2.06	407	3.09	0.76%
146	877 (0.41)	1.93	397	2.895	0.73%

The power of the fan, Pow_{fan}, can be estimated using models from Chapters 2 and 3 and is discussed later in this chapter. The procedure for estimating power depended on whether the fan had a SCR controlled PSC motor or an ECM. The power multiplied by each time step and summed over the entire year of a simulation would yield the energy use of the FPTU fan.

The temperature increase of the air due to the fan, ΔT_{fan}, can be evaluated by rearranging Equation 6.10.

$$\Delta T_{fan} = T_{f,out} - T_{mix} = \frac{Pow_{fan}}{m_{tot} C_p} \tag{6.11}$$

Equation 6.11 provided a means of quantifying the impact of the fan power on the temperature rise of the air.

6.1.4 Mixer The remaining component in the FPTU was the mixer (See Figure 6.5).

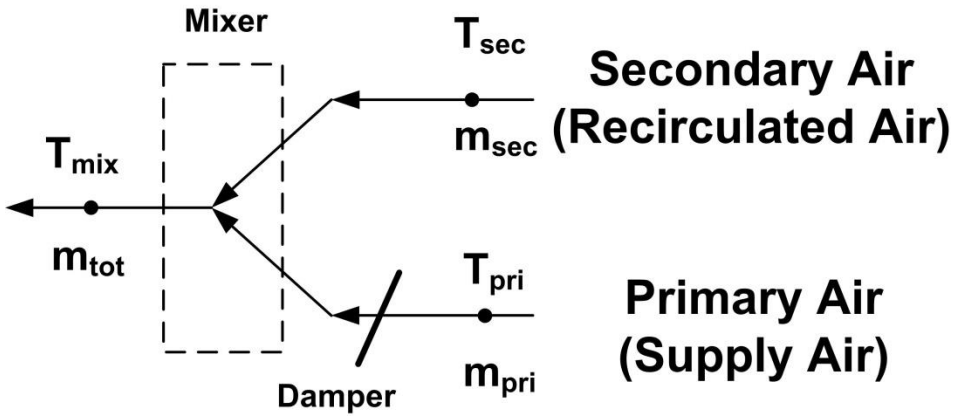

Figure 6.5: Energy and Mass Flows for the Series FPTU Mixer

Mixing of the primary and secondary airstreams occurred in the main housing of the FPTU immediately prior to the air entering the fan. As with the other components, an energy and mass balance can be applied to the mixing process. The result of the mass balance yielded the same equation as Equation 6.3. The mixer was assumed to perform adiabatic mixing; therefore, no heat energy was lost to or gained from the surroundings. Applying an energy balance to the mixer yielded the following:

$$m_{tot}\, c_p T_{mix} = m_{pri}\, c_p T_{pri} + m_{sec}\, c_p T_{sec} \tag{6.12}$$

The variables that would be calculated from Equation 6.12 depended on whether the FPTU was in cooling or heating mode. When the FPTU was in heating mode, the primary airflow would be set at a prescribed minimum needed to satisfy fresh air requirements (ASHRAE 2013). The minimum primary air was also used during dead band operations and when the estimated cooling load in the zone was smaller than the amount of cooling provided by FPTU when the primary air was at its minimum value. Another time when the primary airflow was a fixed value was when the cooling load requirement in the zone is higher than the cooling provided by the FPTU. In this case, the FPTU would reach its maximum airflow and remain constant even if more cooling was required. In all other cooling cases, the primary airflows fell between these two values and the energy and mass balances on each component had to be utilized.

6.1.5 Estimating Fan Power Making an accurate estimate of the fan energy use in a series FPTU was important because the fan runs continuously and the fan power was used for estimating the temperature increase of the air across the fan. The fan energy required estimating the fan power, Pow_{fan}, which can be done with either measured field data or a model. For a fixed

airflow fan, EnergyPlus (2013) had a simple fan power model that related the power to the mass flow rate of the air through the fan, m_{tot}, the pressure differential across the fan, ΔP_{fan}, the fan/motor combined efficiency, η_{tot}, and the density of the air, ρ_{air}.

$$Pow_{fan} = \frac{m_{tot}\Delta P_{fan}}{\eta_{tot}\,\rho_{air}} = \frac{Q_{tot}\Delta P_{fan}}{\eta_{tot}} \tag{6.13}$$

The quantity Q_{tot} in Equation 6.13 is the volumetric flow rate of the air which is usually expressed in ft^3/min or m^3/s. This type of model required knowledge of the pressure differential across the fan and the fan/motor efficiency, which were two quantities often not known to the modeler. As discussed in Chapters 2 and 3, fan/motor performance data from several manufacturers demonstrated that these two variables cannot be treated independently for fans having either PSC motors with SCR controllers or ECMs. EnergyPlus (2013) allows the user to independently input these two variables. Alternative approaches to characterizing fan/motor performance were developed in Chapters 2 and 3 and depended on whether the FPTU had a PSC fan motor controlled by a SCR or had an ECM fan motor. Utilization of these models in the mass and energy balance approach is discussed below.

6.1.6 PSC Motor with a SCR Controller The PSC fan/motor data was analyzed in Chapter 2 and a short summary presented here. Data were analyzed from three manufacturers covering a range of FPTU fan motor sizes from 0.125 to 1 hp (93 to 746 W). The fan/motor efficiency was dependent on the total pressure across the fan. The data was fit with a simple linear model:

$$\eta_{tot} = C_1 * \Delta P_{fan} \tag{6.14}$$

Where, C_1 was 32.06 %/(in w.g.) in IP units or 0.129 %/Pa in SI units. Equation 6.14 can be rearranged to show that the efficiency divided by the pressure differential across the fan can be treated as a constant for a PSC motor with SCR control.

$$\frac{\eta_{tot}}{\Delta P_{fan}} = C_1 \tag{6.15}$$

Equation 6.15 can be substituted into Equation 6.13 and simplified to give an expression for the power solely in terms of air mass flow, m_{tot}, the density of the air, ρ_{air}, and C_1:

$$Pow_{fan} = \frac{m_{tot}}{C_1\,\rho_{air}} = \frac{Q_{tot}}{C_1} \tag{6.16}$$

The correct units for C_1 would need to be used in the above expression and were different in the IP or SI system. If the power was desired to be in Watts, then Equation 6.16 can be rewritten with conversion constants to allow the user to input the volumetric flow and C_1 in ft^3/min and

%/(in w.g) in Equation 6.17 or in m^3/s and %/Pa in Equation 6.18, respectively, to get the power in Watts.

In IP Units:

$$Pow_{fan} = \frac{11.75 * Q_{tot}}{C_1} \quad (6.17)$$

In SI Units:

$$Pow_{fan} = \frac{100 * Q_{tot}}{C_1} \quad (6.18)$$

Another approach was also developed in Chapter 2 was to correlate airflow and power data. A simple linear best fit of the power versus airflow data provided the following (O'Neal et al. 2015a):

$$Pow_{fan} = C_2 * Q_{tot} \quad (6.19)$$

Where C_2 was 0.372 W/(ft^3/min) in IP units and 788 W/(m^3/s) in SI units. Equations 6.16 through 6.19 provide a straightforward way for a building simulation user to estimate the power used by a PSC fan motor controlled with a SCR in a series FPTU.

To illustrate the use of Equations 6.16 through 6.19, consider a series FPTU fan that is producing 1000 ft^3/min (0.472 m^3/s). The value of C_1 would be either 32.06 %/(in w.g.) in IP units or 0.129 %/Pa in SI units. Using Equations 6.17 for IP and 6.18 for SI units, we get the following fan power starting with airflow in IP units:

$$Pow_{fan} = \frac{11.75 * (1000)}{32.06} = 366.5\ W \quad (6.20)$$

Or starting with airflow in SI units:

$$Pow_{fan} = \frac{100 * (0.472)}{0.129} = 365.9\ W \quad (6.21)$$

The small differences between the two are due to round off errors in the coefficients.

Using Equation 6.19 to calculate the fan motor power provided an estimate of 372 W for delivering an airflow rate of 1000 ft^3/min (0.472 m^3/s). While the coefficient, C_1, in Equation 6.16 was developed from a fit of the fan/motor efficiency versus fan total pressure and the coefficient, C_2, in Equation 6.19 was developed from a regression of the fan air flow versus fan/motor power. All of the power calculations agreed to within about 1.5% of each other. As illustrated above, the calculation of fan motor power was very straightforward when the FPTU fan was powered by a PSC motor.

6.1.7 ECM Fan/Motor Analysis For an ECM fan/motor combination, the simple approach of Equation 6.13 became problematic. The data for fan/motor total efficiency for an ECM fan motor showed dependence on both the pressure differential across the fan and fan speed. Thus, unless a modeler knew both the total pressure across the fan and the fan speed, it would be difficult to use Equation 6.13 directly. In addition, some FPTUs vary airflow to meet the load requirements in the zone. In this case the fan efficiency and pressure could vary across a wide range differential. EnergyPlus (2013) did not allow application of a variable speed fan motor in a series FPTU. For a fixed airflow application with an ECM fan motor, it was shown in Chapter 3 that the power was dependent on the capacity factor of the ECM FPTU. The capacity factor quantified the amount of additional airflow capacity the FPTU fan had at its maximum ECM setting compared to the design airflow requirements of the zone. An ECM FPTU that was sized so that its maximum capacity just met the design airflow requirement in the space would use more power than one that had airflow capacity above the design airflow, but whose speed was lowered so the airflow would just meet the design airflow requirements. Thus, the building simulation user needs to know something about the maximum airflow output of an ECM FPTU relative to the size of the design requirements in the space.

Calculation of the fan power for an ECM fan operating at a fixed airflow required several steps. First, the design airflow requirement for the space had to be determined. Usually, this was calculated or estimated by a building simulation program. Second, the user must decide how large a FPTU fan would be used in the zone. The airflow capacity of the FPTU fan, Q_o, divided by the design airflow requirements in the zone, Q_d, can be used to calculate the capacity factor, x_o

$$x_o = \frac{Q_o}{Q_d} - 1 \tag{6.22}$$

In Chapter 3, the power requirement, $Pow_{fan}(Q_d)$, for an ECM FPTU fan with larger airflow capacity than required for the design airflow, Q_d can be calculated from:

$$Pow_{fan}(Q_d) = f_{pl} * C_3 * Q_d * (1 + x_o) \tag{6.23}$$

The first term on the right hand side was the part load power fraction and was given by a third degree polynomial fit of part load data discussed in Chapter 3:

$$f_{pl} = a_1 + a_2 * \left(\frac{1}{1+x_o}\right) + a_3 * \left(\frac{1}{1+x_o}\right)^2 + a_4 * \left(\frac{1}{1+x_o}\right)^3 \tag{6.24}$$

The coefficients in Equation 6.24 are given in Table 6.2.

Table 6.2 - Part Load Power Fraction Coefficients for Equation 6.24

Coefficients	Value
a_1	0.061715
a_2	0.093022
a_3	-0.11627
a_4	0.961538

The constant, C_3, was 0.38 W/(ft^3/min) in IP units or 805 W/(m^3/s) in SI units and was based on a simple linear regression of ECM FPTU data from four manufacturers operating at maximum airflow. The term, x_o, was the capacity factor of the ECM FPTU and quantified the maximum airflow capacity the FPTU had relative to the design airflow requirement. Equations 6.22 through 6.24 can be used to estimate the power of an ECM FPTU operating at a fixed airflow. It is important for a modeler to estimate the capacity factor of the ECM FPTU relative to the design airflow requirements of the space. Discussions with manufacturers indicated that a typical ECM FPTU field installation could be expected to have a capacity factor of 0.25 or more. This size capacity factor would mean the FPTU had a maximum airflow capacity 25% larger than the design airflow requirement.

6.1.8 System Level Calculation Procedure Figure 6.6 shows the basic logic or flow of the calculation procedure for estimating the energy use of a fixed airflow series FPTU. The system operates with the zone being maintained at a certain set-point temperature, T_Z, and with a sensible load, q_{zs}, and latent load, q_{zl}. These data are provided for every hour of the year. The total airflow out of the FPTU, m_{tot}, is maintained at a constant level for operations in heating, cooling, and deadband modes. When the system is in heating mode the primary airflow is set to its minimum airflow which may vary from 10% to 30% of the design airflow (Zhang et al 2014). The amount of secondary airflow that is required to maintain the constant airflow out of the FPTU is then calculated, along with the supplemental heating energy from the heating coil for satisfying the zone heating load. The solution continues throughout the FPTU. In cooling mode, the primary airflow is calculated to match the sensible load in the zone. The primary airflow is limited by the minimum airflow at minimum cooling and the design airflow of the FPTU at maximum cooling requirements. The secondary airflow is used in cooling mode to make up the remainder of air needed to maintain constant total airflow when the system is on.

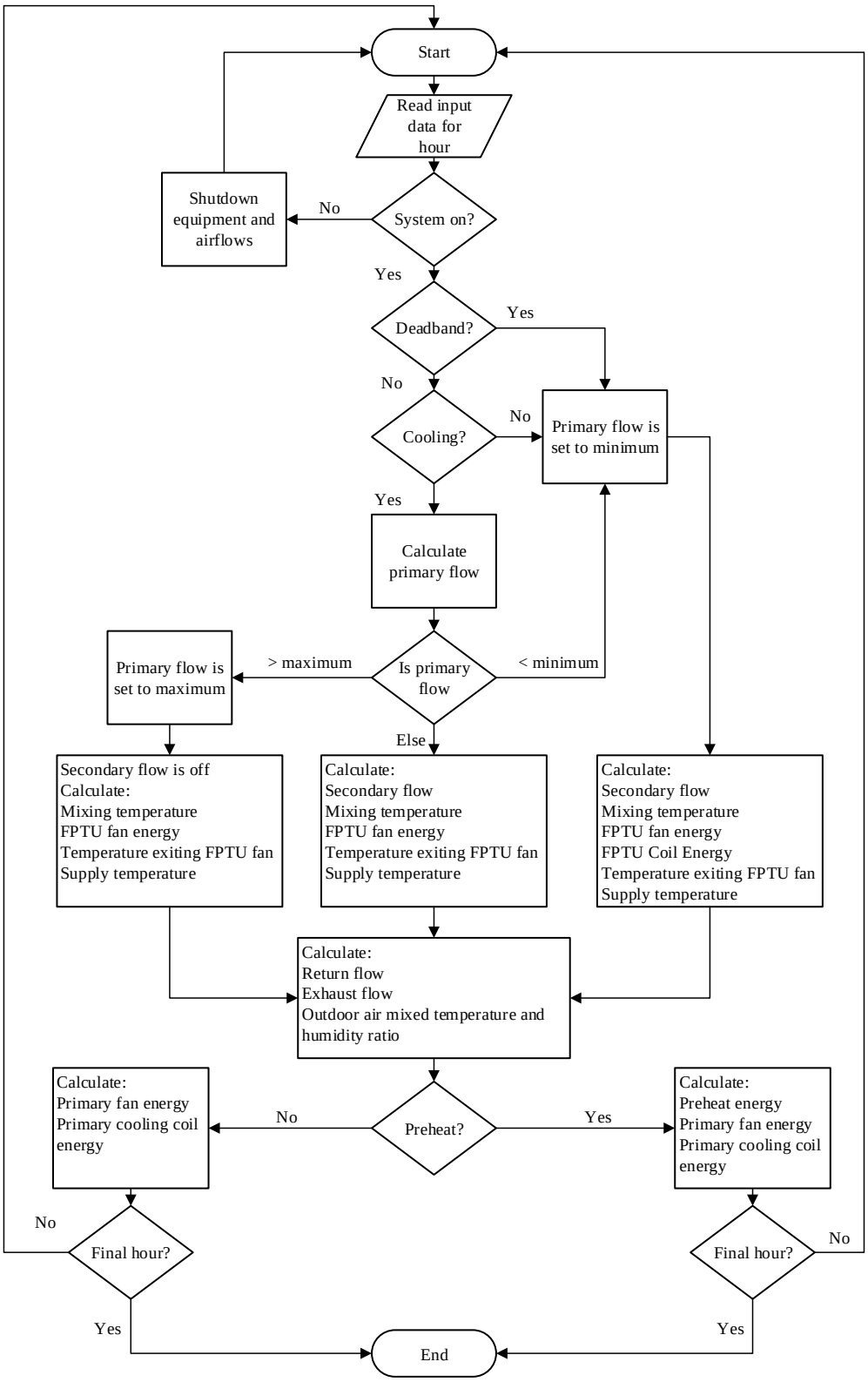

Figure 6.6: Series Fixed Airflow FPTU Controller Routine

The solution then proceeds throughout the FPTU. A deadband is defined to account for the transition between heating and cooling modes. The operation in deadband is similar to the operation in heating mode except for the heating coil. When the system is in deadband, the primary airflow is set to its minimum value, and the secondary airflow is calculated from the difference between the total airflow and the primary airflow. Unlike the operation in heating mode, however, the heating coil is off in deadband region. Operations in heating, cooling, and deadband modes merge in solving for the return air loop of the complete VAV system. The temperature of the return air mix with outdoor air is used to determine whether or not preheating is required. If the temperature is below the primary air temperature then the preheating coil is used to heat the mixed air to the primary air temperature. The procedure then calculates the power consumption of the primary fan and proceeds to calculate the cooling energy required at the primary cooling coil. If there is another hour then the procedure loops back to the start, otherwise the procedure is completed.

Series FPTUs can be applied in systems where the primary airflow can be as low as 45°F (7.2°C) such as that provided by some chilled water coils and as high as 55°F (12.8°C). The variation in primary air temperatures often requires inclusion of secondary airflow at the maximum cooling. If the primary air temperature was in the 45 to 48°F (7.2 to 8.9°C) range, then at maximum cooling, the discharge temperature from the FPTU might be set to at least 51 to 52°F (10.6 to 11.1°C) to prevent condensation on the registers or the feeling of cold drafts from too cold air being discharged into the zone. If the cooling coil produced primary air temperatures at or near 55°F (12.8°C), then no mixing of secondary air would be required at maximum cooling because the discharge temperature was high enough for that condition. While EnergyPlus (2013) allowed the user to input a maximum airflow that was greater than the maximum primary airflow, it provided no guidance to the user on the minimum discharge temperatures needed for the FPTU nor does it provide a check to ensure discharge temperatures are high enough to prevent condensation at the registers.

The total airflow rate (m_{tot}) from a fixed airflow series FPTU was determined by using the zone design load (q_{z_design}) and the difference between the zone set-point temperature (T_z) and the minimum discharge temperature (T_{out}) at design conditions:

$$m_{tot} = \frac{q_{z\_design}}{c_p * (T_z - T_{out})} \tag{6.25}$$

The selection of the minimum discharge temperature was dependent on the temperature of the air provided in the primary airstream. For example, in systems with a primary air temperature at or close to 55°F (12.8°C), the minimum discharge temperature at the design condition was equal to the primary air temperature if the heating effect caused by the FPTU fan was not considered. With the heating effect, the difference between the FPTU outlet discharge temperature, T_{out}, and the mixed air temperature, T_{mix}, in Figure 6.2 should be less than 1°F (0.6°C). If a primary air temperature in the range of 45 to 48°F (7.2 to 8.9°C) was used, the selection of the minimum discharge temperature from the FPTU needed to be at a value that ensured there was no condensation on the supply registers and grilles. The minimum discharge temperature at the design cooling condition should be equal to or greater than 51°F (10.6°C) when a primary air temperature lower than 48°F (8.9°C) was used in a VAV system with series FPTUs.

If desired, the volumetric flow rate (often in ft^3/min or m^3/s) can be determined from the air mass flow rate and density, ρ_{air}

$$Q_{tot} = \frac{m_{tot}}{\rho_{air}} \tag{6.26}$$

It should be noted that once the total airflow rate was sized for a fixed airflow series FPTU, the airflow remained constant and independent of the zone thermal load.

For demonstration purposes, the performance of a series FPTU was estimated by using the mass and energy balance approach discussed earlier and the empirical curves for ECM fan/motor power consumption developed in Chapter 3. As a first step, input data were created, including zone sensible loads, zone set-point temperature, and primary air temperature. To demonstrate the operation in all modes of heating, cooling, and deadband, the zone sensible load was allowed to range from -40,000 to 40,000 Btu/h (-11.73 to 11.73 kW) by using an arbitrary incremental change of 479 Btu/h (0.14 kW), with negative values indicating heating loads and positive values indicating cooling loads. At each zone sensible load, a constant zone set-point temperature of 78°F (25.6°C) was maintained. Also, two primary air temperatures of 55°F (12.8°C) and 45°F (7.2°C) were used for the series FPTU performance prediction. The higher primary air temperature of 55°F (12.8°C) represents a VAV system that uses a direct expansion (DX) coil as the primary cooling coil, while the lower primary air temperature of 45°F (7.2°C) would represent a VAV system that uses a chilled water coil as the primary cooling coil. In addition, a deadband ranging from -4,000 to 4,000 Btu/h was arbitrarily defined and used to help illustrate

series FPTU operation in the deadband region. If the zone sensible load fell into the deadband range, the series FPTU was then considered to be operating in the deadband mode. It should be noted that the above input parameters, namely zone sensible loads, zone set-point temperature, primary air temperature, and deadband range, were user-defined parameters and can be modified for different applications.

The airflow, discharge temperature, and supplemental heating energy for a fixed airflow series FPTU were plotted against the zone sensible load and are shown in Figures 6.7 to 6.9, respectively. Figure 6.7 showed the primary and secondary air variations with the zone sensible load for cases with 55°F (12.8°C) and 45°F (7.2°C) primary air. In both cases, the primary airflow was allowed to decrease to a minimum of 20% of the design primary airflow rate when in the heating and deadband modes, secondary air makes up the remainder of the total airflow rate. While in cooling mode, the primary airflow was increased with the increasing zone sensible cooling load until the design airflow rate was reached for the 55°F (12.8°C) primary air case. For this case, the secondary airflow was decreased based on mass and energy balances until reaching zero at maximum cooling because constant total airflow was maintained over the entire range of the zone sensible cooling load.

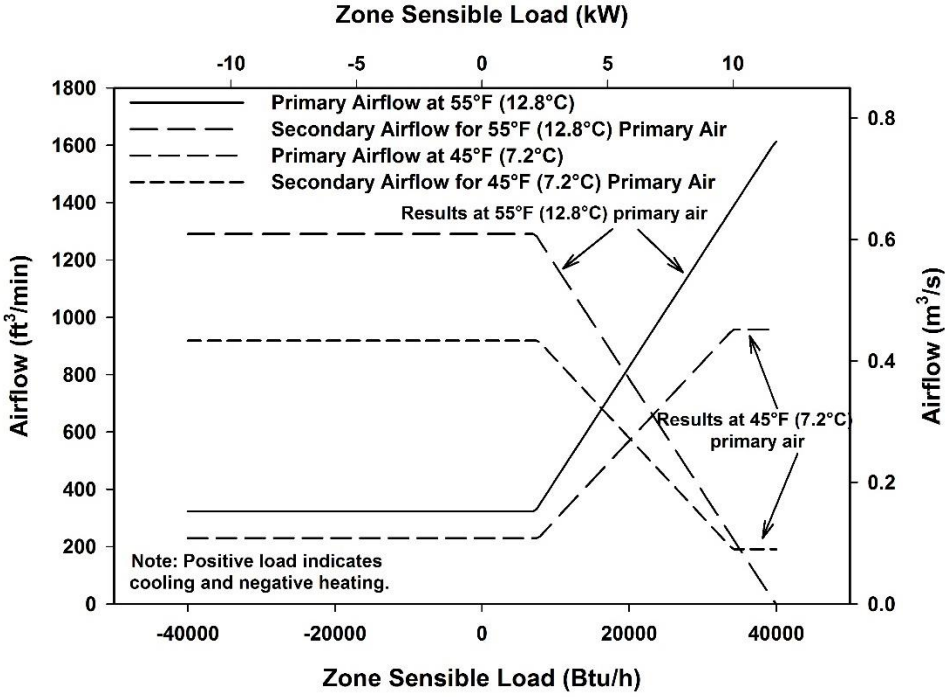

Figure 6.7: Primary and Secondary Airflows for a Fixed Airflow Series FPTU

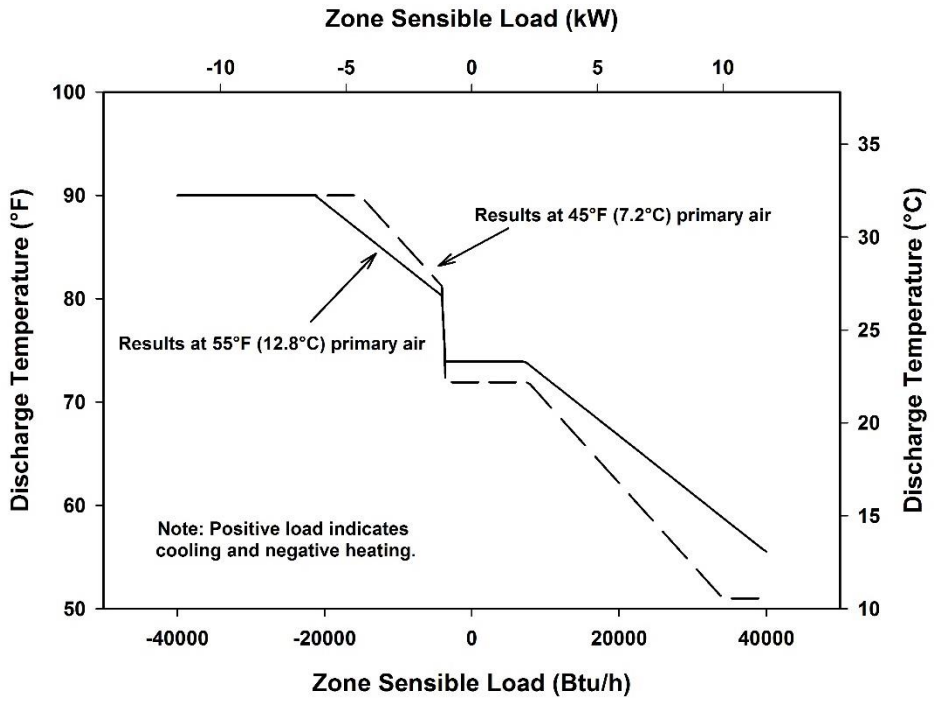

Figure 6.8: Discharge Temperature for a Fixed Airflow Series FPTU

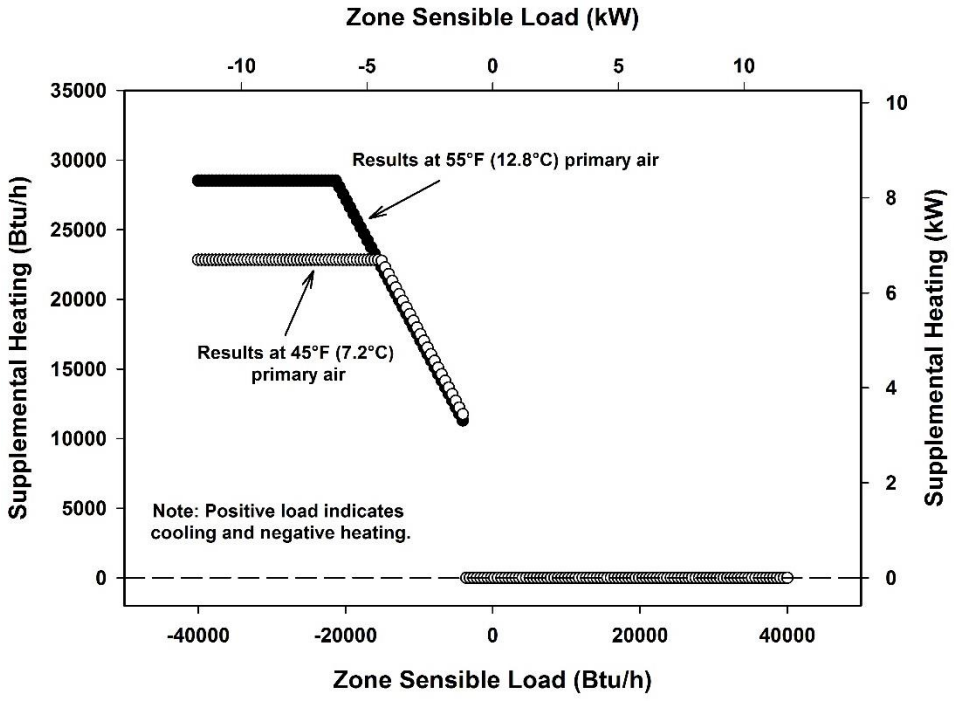

Figure 6.9: Supplemental Heating Energy for a Fixed Airflow Series FPTU

Lowering the primary air temperature to 45°F (7.2°C) resulted in lower total airflow rates in both primary and secondary air for both heating and cooling. Rather than continuously increasing the primary airflow to the design airflow rate at maximum cooling, the primary air at 45°F (7.2°C) required mixing of secondary air at maximum cooling to maintain high enough air discharge temperatures from the FPTU to avoid condensate on the air registers when the primary air temperatures are in the lower temperature range for chilled water coils-typically from 45 to 48°F (7.2 to 8.9 °C). For the example of 45°F (7.2°C) primary air in Figures 6.8 to 6.10, the minimum discharge temperature was assumed to be 51°F, which was obtained by blending enough secondary air with primary air to achieve the mixed temperature.

Figure 6.8 showed the discharge temperature resulting from using 55°F (12.8°C) and 45°F (7.2°C) primary air over the entire range of zone sensible load. At the high end of the heating load, the discharge temperature was limited to 90°F (32.2°C) because a higher discharge temperature could increase the zone temperature stratification (Hydeman and Eubanks, 2014; Faris and Int-Hout, 2014). As the heating load decreased, the discharge temperature was decreased proportionally. A sharp temperature drop occurred at the lower limit of the deadband due to switching off the heating coil. The discharge temperature was maintained constant in the deadband and then decreased as zone cooling load increased. Figure 6.9 showed that at any given zone sensible load, the discharge temperature resulting from using 45°F (7.2°C) primary air was higher in heating mode and lower in cooling mode compared with a discharge temperature with 55°F (12.8°C) primary air. The use of lower primary air temperature resulted in a lower design airflow rate as was shown earlier in Figure 6.8. To deliver the same amount of heating or cooling energy to the zone with a lower airflow rate, the discharge temperature has to be increased in heating mode and decreased in cooling mode with the zone set-point temperature being a constant.

Figure 6.9 showed the supplemental heating energy use for 55°F (12.8°C) and 45°F (7.2°C) primary air. The heating coil only operated in heating mode and remained off in deadband and cooling modes. At the high end of the heating load, the supplemental heating energy was constant because the maximum discharge temperature of 90°F was reached. The system using 55°F (12.8°C) primary air provided a higher supplemental heating capacity than the system using 45°F (7.2°C) primary air due to a higher airflow rate. As the heating load decreased, the

supplemental heating energy continuously decreased until reaching the lower limit of the deadband.

The logic for the FPTU performance calculations depended on which mode of operation it was in and what primary air temperature was provided to the FPTU. There were four distinct modes of operation: off, heating, cooling, and deadband. The logic for each was described below:

1. The entire system is not operating.

For this mode the primary and secondary airflows, the fan, and the central air handler were not running, and temperatures throughout the system were set to the zone set-point temperature.

2. The system is operating in heating mode.

a. The discharge temperature that was required to satisfy the zone load was calculated based on the energy balance performed on the zone using Equation 6.27.

$$T_{out} = T_z - \frac{q_{zs}}{m_{tot} c_p} \tag{6.27}$$

If the calculated discharge temperature was greater than 90°F (32.2°C), then the discharge temperature was set to 90°F (32.2°C).

b. The primary airflow was set to the minimum ventilation level (20% of design).

$$m_{pri} = m_{min} \tag{6.28}$$

c. The secondary airflow was calculated from the mass balance performed on the mixer.

$$m_{sec} = m_{tot} - m_{pri} \tag{6.29}$$

d. The temperature of the air leaving the mixer was calculated based on the energy balance performed on the mixer. Equation 6.12 was rearranged to solve for T_{mix}.

$$T_{mix} = \frac{m_{pri}\, c_p T_{pri} + m_{sec}\, c_p T_{sec}}{m_{tot}\, c_p} \tag{6.30}$$

e. The temperature of the air leaving the fan was calculated based on the energy balance performed on the fan as shown in Equation 6.11, which can be rearranged into Equation 6.31.

$$T_{f,out} = \frac{Pow_{fan}}{m_{tot} c_p} + T_{mix} \tag{6.31}$$

f. The energy input into the heating coil was calculated from the energy balance performed on the heating coil as shown in Equation 6.9.

$$q_{coil} = m_{tot} c_p \left(T_{out} - T_{f,out}\right) \tag{6.32}$$

3. The system is operating in cooling mode

The operation in cooling mode was similar to the operation in heating mode except for the calculation of primary airflow m_{pri}. As a first step, the discharge temperature that was required to satisfy the zone load was calculated according to Equation 6.27. Then, the primary airflow m_{pri} in cooling mode was determined by substituting secondary airflow m_{sec} from Equation 6.3 into Equation 6.5 and rearranging to solve for $m_{pri,}$ as was shown in Equation 6.33. Note that because the system was in cooling mode, the energy use of the heating coil was zero ($q_{coil} = 0$).

$$m_{pri} = m_{tot}\frac{T_{out}-T_{sec}}{T_{pri}-T_{sec}} - \frac{Pow_{fan}}{C_p(T_{pri}-T_{sec})} \quad (6.33)$$

Once the primary airflow m_{pri} was quantified, the logic for the performance calculation in cooling mode was the same as the steps from c to e in the heating mode.

It was important to recognize that the calculated primary airflow, $m_{pri\ ,}$ was constrained between its minimum, which typically ranged from 10 to 30% of the design primary airflow and its maximum (or design) amount. The total airflow from the FPTU will depend on the temperature of the primary air provided to the FPTU. For the case of higher primary air temperatures, such as 55°F (12.8°C), the maximum amount of primary air can be 100% of the design airflow m_{tot}. In this case, the secondary air was set to zero at the design cooling load in the zone as shown in Figure 6.8. If the calculation of primary airflow resulted in a value smaller than the minimum or larger than the maximum, the logic needed to reset the primary airflow to the minimum or maximum accordingly and then proceeded with the calculations in steps from c to e in the heating mode.

When lower primary air temperatures were provided to the FPTU, then secondary air needed to be blended in with the primary air to provide a high enough outlet (or discharge) temperatures to eliminate condensation on registers. The amount of secondary air needed will depend on the temperature and amount of the primary air. The desired discharge air temperature will allow for calculation of the total amount of airflow, m_{tot}, from the FPTU using Equation 6.33. The amount of secondary air can then be calculated using the mass balance from the mixing equation of Equation 6.3. The minimum limit on the primary air remained the same as with the case with a higher primary air temperatures.

4. System is operating in deadband mode

If the zone sensible load was within the prescribed deadband range, then the system was in deadband operation. For Figures 6.8 through 6.10, the deadband was assumed to vary from -4000 to 4000 Btu/h (-1.2 to 1.2 kW). In the deadband mode, the logic for the performance calculation was similar to the operation in heating mode except for the heating coil being switched off. Unlike the operations in heating and cooling modes where the purpose of the FPTU was to satisfy the zone load by maintaining a specific discharge temperature, the discharge temperature in deadband was not controlled and was a direct result of mixing the minimum primary air and maximum secondary air. In a simulation program, the deadband is often specified by the user. Thus, no method of calculating the deadband was provided here.

6.2. Parallel FPTU

A parallel FPTU can be decomposed into its major components: mixer, fan/motor, and heating coil. Figure 6.10 shows a control volume around a traditional parallel FPTU.

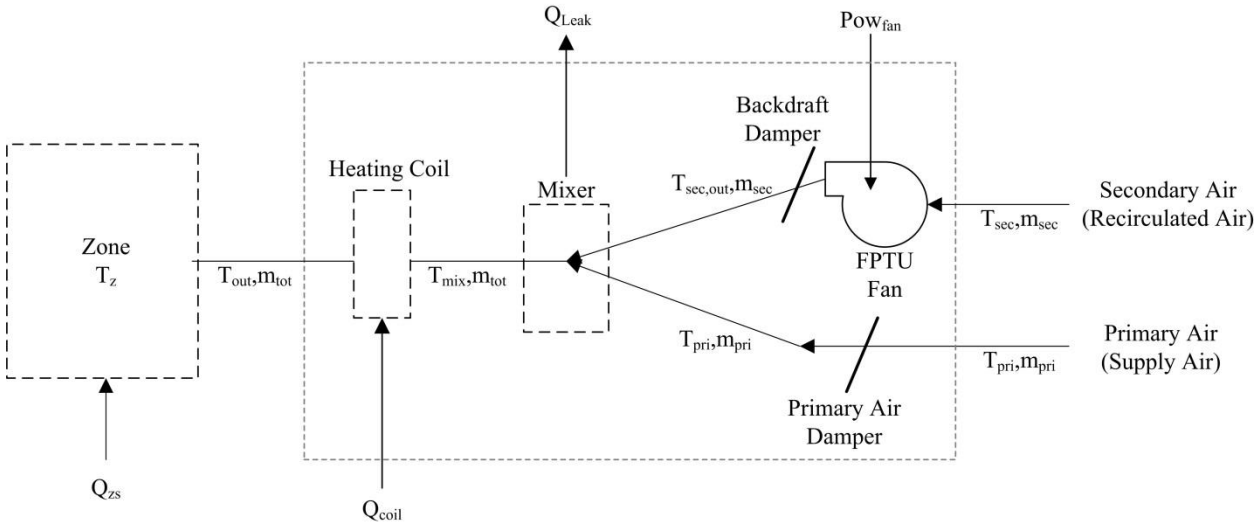

Figure 6.10 Traditional Parallel FPTU with Heating Coil Located after the Mixing of the Primary and Secondary Airflows

An analysis can be performed on each component in the FPTU to estimate overall airflows (or mass flows) into and out of the FPTU as well as the energy used by the FPTU fan/motor for each time step of a simulation. The large dashed box in the right two-thirds of the figure was the control volume for the FPTU. Each FPTU component can be treated as a smaller control volume with mass and energy inputs and outputs.

An alternate configuration of the traditional parallel FPTU moved the heating coil to the secondary air inlet as shown in Figure 6.11.

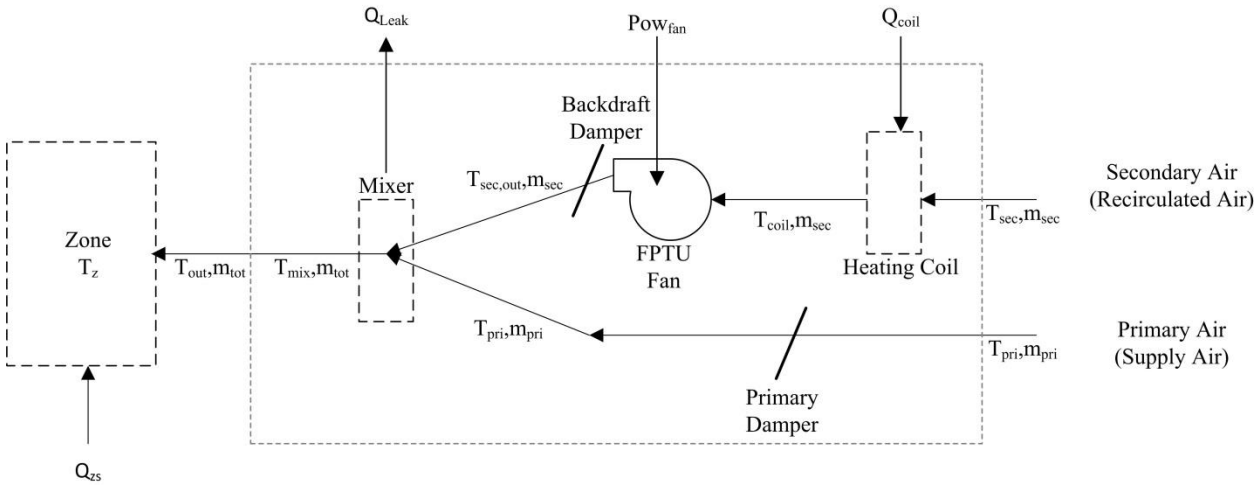

Figure 6.11: Parallel FPTU in Alternate Configuration where the Heating Coil is Located in the Secondary Airstream

One advantage this configuration provided over the traditional configuration of Figure 6.10 was that the heating coil was outside the primary airstream where it would add to the pressure drop of the primary airstream whenever the primary air handler is operating. This pressure drop would have to be overcome by an increase in static pressure of the central air handling unit. One potential disadvantage of the alternative configuration was that the fan motor was located downstream of the heating coil and would be subjected to higher air temperatures than in the traditional configuration in the heating mode.

6.2.1 Parallel FPTU Model For the control volume around the entire FPTU in Figures 6.10 or 6.11, energy was input to the FPTU via electrical energy to the fan, heat energy to the heating coil, and energy associated with the supply and secondary airstreams. The only mass and energy leaving the FPTU was with the airstream at the discharge of the FPTU and leakage from the housing. Unlike series FPTUs that operate at a negative pressure with respect to the plenum, parallel FPTUs operate at a positive pressure. The primary air provided to the parallel FPTU has already been conditioned by the central cooling coil. Thus, air leaking from the parallel FPTU operating in the cooling mode is colder than the return air in the plenum and will reduce the temperature of the plenum air. As has been discussed in Chapter 5, parallel units can leak conditioned air from the housing through seams, penetrations, and the backdraft damper.

The FPTU consists of three major components: mixer, fan, and heating coil. A mass and energy balance must be performed on each of the components to estimate temperatures and airflows to determine the performance of the FPTU.

The basic assumptions used in developing the MEB models of series FPTUs were also applied to parallel FPTUs. First, the system was assumed to operate at quasi-steady state during each time step. Second, the thermo-physical properties were assumed constant. Third, the energy input to the fan motor was assumed to be completely converted into the heat energy in the airstream. Fourth, the FPTU operated with a minimum amount of primary air to ensure enough fresh air into the zone.

The mass and energy balances shown previously in Equations 6.1 and 6.2 for a series FPTU were also applied here for a parallel FPTU. For the control volumes shown in Figures 6.10 or 6.11, the mass entering the system included the primary (supply) air, m_{pri}, from the central air handler and the secondary airstream, m_{sec}. The mass exiting the control volume was total airflow, m_{tot}, and leakage, m_{leak}. Applying conservation of mass to the control volume yielded the mass balance shown below.

$$m_{tot} + m_{leak} = m_{pri} + m_{sec} \tag{6.34}$$

Leakage was included in the modeling of parallel units because the housing is at a positive pressure with respect to the plenum air pressure. Characterizing leakage and it impact on parallel FPTUs is discussed later. The energy transfer into the control volume included the energy provided by the supply and secondary airstreams, energy input into the heating coil, the energy

leaving by leakage, and the power input into the fan. When these were substituted into the conservation of energy equation for the whole FPTU, it yielded the following:

$$m_{tot}h_{out} + m_{leak}h_{leak} = q_{coil} + Pow_{fan} + m_{pri}h_{pri} + m_{sec}h_{sec} \quad (6.35)$$

Equations 6.34 and 6.35 provided the basic equations that described the overall mass and energy balance for parallel FPTU. The unknowns in these equations varied depending on the mode of operation (heating, cooling, or deadband) of the FPTU. Solving for the unknowns in these equations required applying mass and energy balances to each of the components in the FPTU. The process typically started from the left at the FPTU discharge to the zone and moved to the right to the primary and secondary air inlets.

With a parallel FPTU, the fan was on when the FPTU was in the heating mode. For cooling operation, the FPTU fan was off and the primary air damper was used to vary the amount of supply air that flowed through the FPTU. The term m_{tot}, shown in Equations 6.34 and 6.35, was the total airflow delivered to the space. In heating operations, the total airflow was the sum of the supply and secondary airflows minus leakage. In cooling operations, the total airflow was just the primary airflow minus the leakage. The total airflow was a fixed value in heating mode if the secondary airflow was fixed. In cooling mode, the total airflow was determined from the load in the zone and equaled the primary airflow minus the leakage airflow in either Figure 6.12 or 6.13. Additional primary air must be provided that was equal to the amount of air leaking out of the FPTU cabinet to ensure the proper amount of discharge air, m_{tot}, was delivered to the zone to satisfy the cooling load. The primary airflow in the FPTU should not drop below a certain percentage (typically 20 to 30%) of the airflow needed at the design cooling load (ICC 2010, ASHRAE 2013). This minimum amount of primary air was used to maintain fresh air requirements in the zone. A recent study found that minimum primary airflows as low as 10% might still provide acceptable indoor air quality in some applications in California (Zhang et al 2014).

The terms in the left hand side of Equation 6.35 represented the energy leaving the FPTU in the airstream either carried by the discharge airflow or by the leakage airflow. The energy input into the FPTU included heat energy input in the heating coil, power input to the fan (which was assumed to be converted into heat energy in the airstream), and energy being carried into the FPTU by both the supply and secondary airstreams. If the temperature differences between the

entering and exiting airstreams were small enough, then the air properties can be assumed to be constant and the enthalpies, *h*, can be rewritten as the product of specific heat, $c_{p,}$ and temperature, *T*. Equation 6.35 can be rewritten as shown below. Because the assumption of constant density was used, all air flow rates were considered to be mass flows unless otherwise stated.

$$m_{tot}c_pT_{out} + m_{leak}c_pT_{mix} = \mathrm{q}_{coil} + Pow_{fan} + m_{pri}\,c_pT_{pri} + m_{sec}\,c_pT_{sec} \qquad (6.36)$$

Both sides can be divided by the specific heat, c_p

$$m_{tot}T_{out} + m_{leak}T_{mix} = m_{sec}T_{sec} + m_{pri}T_{pri} + \frac{Pow_{fan}}{c_p} + \frac{q_{coil}}{c_p} \qquad (6.37)$$

6.2.2 Energy Balance of the Alternate Configuration In the alternate FPTU configuration in Figure 6.11, the heating coil location changed from the FPTU outlet to the secondary airstream inlet. A mass balance on the control volume in Figure 6.11 yielded the same result as was derived for the traditional configuration as shown in Equation 6.34. An energy balance on the control volume also yielded the same result as the traditional configuration as shown in Equation 6.35. From a simple mass and energy balance on the FPTU alone, the change in the location of the heating coil provided no change in the basic equations.

There were some differences between the two configurations. First, from a larger system standpoint, moving the heating coil out of the primary airstream reduces the static pressure required by the central air handler which provides the supply airflow to the FPTU. The additional pressure drop across the heating coil would depend on the characteristics of the coil (number of rows of the coil, airflow, fin density, etc.) and the amount of airflow through the coil. This pressure drop would require additional work by the central air handler and must be included in a simulation to properly handle the traditional configuration. A second difference was the temperature of the air leaking into the plenum. Because the supplemental heating for the alternative configuration was located upstream of any leakage locations in the FPTU, heated air can leak from the FPTU into the plenum. The leakage of this heated air would also reduce the overall heating provided to the zone once the heating coil discharge temperature reaches its maximum value. For the alternative configuration, the pressure drop of the heating coil in the secondary airstream must be included in heating operations when the FPTU fan was on.

6.2.3 Zone Analysis Analysis of an FPTU often starts at the zone. Typically, the zone load is known and either the discharge temperature, T_{out}, or the total airflow, m_{tot}, needs to be calculated. Either required an energy and mass balance on the zone. The zone control volume was represented by the control volume on the far left side of either Figures 6.10 or 6.11. The control volume was identical in either figure. An energy and mass balance on the zone yielded the following:

$$q_{zs} = m_{tot} c_p (T_z - T_{out}) \tag{6.38}$$

In cooling mode, the outlet temperature was known and the total airflow needed to be calculated. There was no secondary air and all air was provided by the primary airstream at the primary air temperature. Thus, T_{out} was equal to T_{pri} in Figures 6.10 or 6.11. Equation 6.38 can be rewritten to calculate the required airflow to satisfy the zone load:

$$m_{tot} = \frac{q_{zs}}{c_p (T_z - T_{out})} \tag{6.39}$$

In heating mode, the airflow was fixed because the airflow was constant from the fan in the secondary airstream and the primary air was fixed at its minimum value. For this case, the outlet air temperature can be calculated from the following:

$$T_{out} = \frac{q_{zs}}{m_{tot} c_p} + T_z \tag{6.40}$$

6.2.4 Heating Coil An energy balance can be applied to the heating coil in the traditional location in Figure 6.10. The energy entering the coil was the energy input, q_{coil}, either from electric resistance or hot water and the energy from the air entering the coil from the discharge of the FPTU fan. The energy exiting the coil was carried by the air leaving the coil and used to condition the zone. The variable of interest was the heating energy input. An energy balance yielded:

$$q_{coil} = m_{tot} c_p (T_{out} - T_{mix}) \tag{6.42}$$

The analysis for the heating coil for the alternative configuration was very similar to that for the traditional configuration. However, the airflow in and out of the heating coil was just the secondary airflow for the alternative configuration and not the total airflow. The temperature into the coil was the secondary air temperature, T_{sec}, and the outlet temperature from the coil is T_{coil} (See Figure 6.11). The coil energy balance yielded:

$$q_{coil} = m_{sec} c_p (T_{coil} - T_{sec}) \tag{6.44}$$

These two equations represented the energy balance on the heating coil for either the traditional or alternate configurations.

6.2.5 Fan The FPTU fan was located in the same place for both the traditional and alternative configurations. However, because of the presence of the heating coil in the airstream before the fan in the alternate configuration, the terminology would be slightly different. The amount of electrical energy input to the fan for a given time step was represented by POW_{fan}. In addition, energy was being carried into the fan from the secondary airstream. For the traditional configuration (Figure 6.10), the airstream temperature of the air at the inlet of the fan was T_{sec}. For the alternative configuration, the airstream temperature of the air at the fan inlet was given by T_{coil} which was the outlet temperature of the heating coil. The energy exiting the fan was carried by the air leaving the fan and entering the mixer. The exiting temperature was given by $T_{sec,out}$ for both configurations (Figures 6.10 and 6.11). It was assumed that all of the power input to the fan was converted into heat energy. For constant properties, the temperature increase of the air due to the fan can be evaluated with a mass and energy balance. Performing an energy balance on the fan and solving for the power input yielded the following for the traditional configuration:

$$POW_{fan} = m_{sec} c_p \left(T_{sec,out} - T_{sec}\right) \tag{6.43}$$

For the alternative configuration, the energy input to the fan was given by:

$$POW_{fan} = m_{sec} c_p \left(T_{sec,out} - T_{coil}\right) \tag{6.44}$$

6.2.6 Mixer An important variable needed in the modeling of the FPTU was the mixing temperature, T_{mix} of the secondary and primary airflows. To solve for the mixing temperature, a mass and energy balance can be performed on the mixer shown in Figure 6.12.

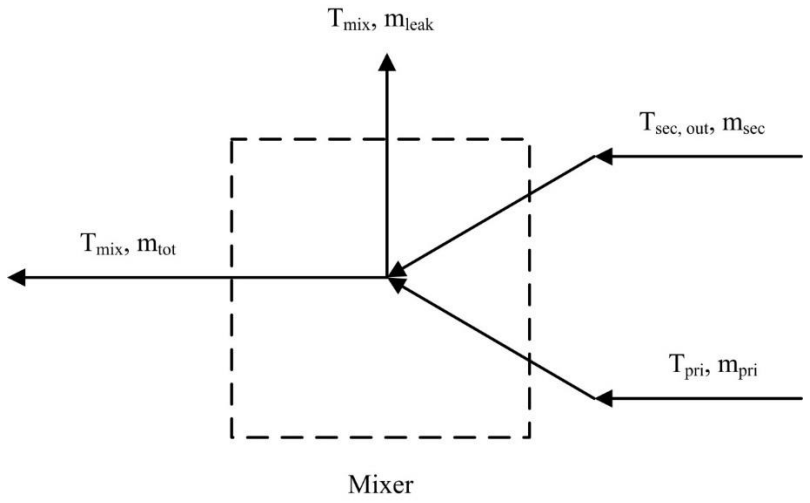

Figure 6.12: Parallel Mixer

Mass flows into the mixer included the primary and secondary airflows. If the leakage was assumed to occur in the region of the mixing in the main chamber of the FPTU, then the total airflow leaving the FPTU was just the sum of the total airflow in minus the leakage out of the FPTU.

$$m_{tot} = m_{pri} + m_{sec} - m_{leak} \tag{6.45}$$

The relationship between the primary airflow and the supply airflow from the air handler depended on the amount of leakage in the FPTU, which was discussed in the next section. The energy entering the mixer was from the primary and secondary airstreams when in heating mode. In cooling operations, there was no secondary airflow; therefore, the mixing temperature was equal to the primary air temperature. The energy exited the mixer in the total airstream and moved to the heating coil. The mixer was assumed to perform adiabatic mixing; no heat energy was lost to the surroundings. Performing an energy balance on the mixer to solve for the energy in the airstream leaving the mixer yielded the following:

$$m_{tot} c_p T_{mix} = m_{pri}\, c_p T_{pri} + m_{sec} c_p T_{sec,out} - m_{leak} c_p T_{mix} \tag{6.46}$$

Leakage from the FPTU was assumed to occur at the mixed temperature of the primary and secondary airstreams. In cooling, there was no secondary airstream, so the mixed air temperature would be the same as the primary air temperature. With the mass and energy equations, we should have two equations and two unknowns that can be solved to give values for m_{pri} and T_{mix} as long as we know the amount of leakage, which was discussed in the next section. The solution can proceed for the contribution of the fan. The fan models from Chapter 2 and 3

can be used for direct calculation of fan power. With the fan power calculated, Equation 6.43 or 6.44 can be solved for the temperature leaving the fan and entering the mixer, $T_{sec,\,out.}$ The final step was to solve for the energy input of the heating coil in either Equation 6.41 or 6.42. All other variables in the equation have been calculated so the value of q_{coil}, can be calculated.

6.2.7 Leakage When supply air was provided by the central air handler to a FPTU, the cabinet operated at a higher pressure than the air surrounding the FPTU in the plenum. As a consequence, there was the potential for air to leak from the FPTU to the surrounding plenum space.

As was discussed in Chapter 5, the data of Edmondson et al (2011b) was reanalyzed in Chapter 5 and presented as a percentage (or fraction) of the primary airflow:

$$f_{leakc} = \frac{m_{leak}}{m_{pri}} \tag{6.47}$$

The data from Edmondson et al (2011b) focused on FPTUs with ECM fan motors. Units were tested over a range of downstream static pressures, upstream static pressures, and supply airflows. In all of their tests, the FPTU fan in the secondary airstream was off and only primary air was flowing through the FPTUs. Figure 6.13 shows a sample plot of the fraction (or percentage) leakage as a function of primary airflow. The leakage fraction term had a "c" designation to indicate that this was a cooling leakage. As discussed later, the leakage in heating may be different than that for cooling. The FPTUs tested were divided into three leakage classifications: low, medium, and high. The percentage leakage was relatively flat for the high leakage case and slightly increased for the low and medium leakage cases.

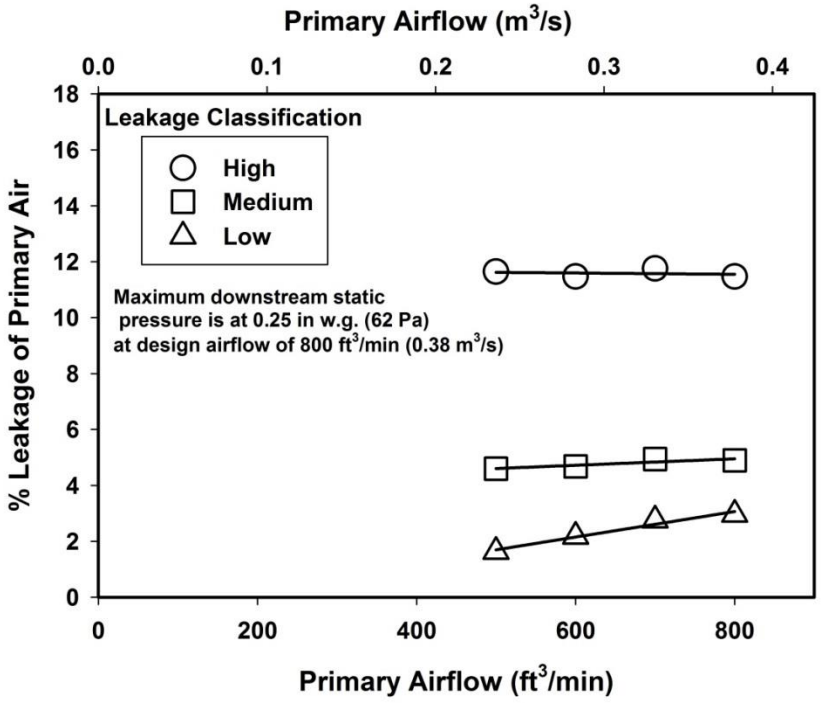

Figure 6.13: Percentage Leakage as a Function of Primary Airflow for Three Leakage Classifications from Chapter 4

The leakage data in Figure 6.13 was collected under conditions when the FPTU fan was off, the backdraft damper was closed, and only primary air was used in the FPTU. This condition simulated cooling operations for a parallel FPTU. Thus, these data were directly applicable to the cooling mode operation when simulating a FPTU. With the secondary airflow equal to zero, the cooling leakage fraction in Equation 6.47 can be substituted into the mass balance for the FPTU in Equation 6.45 to yield:

$$m_{tot} = m_{pri} - m_{leak} = m_{pri}(1 - f_{leakc}) \tag{6.48}$$

The total airflow, m_{tot}, was calculated from the cooling load on the zone. Equation 6.48 can be rearranged to provide an estimate of the amount of primary air needed when there was leakage:

$$m_{pri} = \frac{m_{tot}}{1-f_{leakc}} \tag{6.49}$$

The above equation clearly showed that additional primary air was needed in cooling operations to provide the same amount of total airflow (m_{tot}) to the zone when there was leakage from the FPTU. This additional air had to be provided by the main air handler and meant leakage created

a direct energy penalty on the air handler because it had to provide the additional air to the FPTU.

Besides the direct energy impact of leakage in cooling mode on the air handler, there were also indirect impacts. Leakage from the FPTU in cooling mode introduced cold primary air into the return airstream and would decrease the air temperature in the plenum. If the FPTU shared a common plenum with other FPTUs and some of those were in heating or deadband operations, then the colder plenum air would reduce the heating benefit from blending plenum (secondary) air with the primary air and would require additional heating when supplemental heating was used. Most of the return air was eventually mixed with outdoor air that was then sent to though the air handler and primary cooling coil. Because leakage during cooling operation reduced the return air temperature, it should reduce the temperature of the air that was returned to the primary cooling coil. This could reduce the load on the cooling coil. With the alternative FPTU configuration where the heating coil was located at the secondary inlet, leakage during heating operations would provide warm air to the plenum space. Quantifying the penalty or benefit of these indirect impacts of leakage required a full air conditioning system model that goes beyond the scope of this study.

While Edmondson et al (2011) identified three potential leakage paths (backdraft damper, seams, and cabinet penetrations), they made no attempt to quantify the contributions from each of these sources. If the largest contributor for leakage was the backdraft damper, then the data from either Edmondson et al (2011) or Furr et al (2008) would overestimate the leakage when the parallel FPTU was in the heating mode. Likewise, if building codes required taping all seams on the FPTU, then leakage from seams might be minimal. If the major leakage contributors in a FPTU were at the seams and/or penetrations, then the percentage (or fraction) leakage might remain relatively constant whether the FPTU was in the heating or cooling mode. Without definitive leakage data during heating operation, we are proposing to use a simple fraction (or percentage), f_{leakh}, to describe the leakage in a way similar to what was used for cooling.

$$f_{leakh} = \frac{m_{leak}}{m_{pri} + m_{sec}} \tag{6.50}$$

Equation 6.50 includes the primary and secondary airflows in the denominator because both flows were active during heating operations. This equation can be substituted back into the mass balance (Equation 6.45) for the mixing to yield:

$$m_{tot} = m_{pri} + m_{sec} - m_{leak} = (m_{pri} + m_{sec})(1 - f_{leakh}) \quad (6.51)$$

If the leakage was due to seams and penetrations, then the fraction of leakage for heating could be assumed to be the same as that used for cooling. However, if the leakage was due entirely to the backdraft damper, then the fraction leakage in heating should be set to zero or have a smaller value than that for cooling.

6.2.8 Estimating Fan Power Accurate estimating the fan energy use in a parallel FPTU is still important even if the fan was only operating during heating operations. In cooler climates the fan may still be used significantly in some zones. Thus, the fan energy consumption needed to be captured in any model and needed to include the fan power and the temperature increase of the air across the fan/motor. The fan motor energy required estimating the fan motor power, POW_{fan}, either with measured data or a model. The fan power models for both PSC/SCR and ECMs were the same as that used for the series FPTUs discussed earlier in this chapter. In a series, the FPTU fan was on whenever the system was on. In contrast, the fan in a parallel FPTU only operated during heating or deadband mode.

6.2.9 System Level Calculation Procedures For demonstration purposes, the performance of a parallel FPTU was estimated by using the mass and energy balance approach discussed earlier and the empirical curves for ECM fan/motor power consumption developed in Chapter 3. As a first step, a series of input data were created, including zone sensible loads, zone set-point temperature, primary air temperature, secondary air temperature, and primary air leakage fraction. To show the operation in all modes of heating, cooling, and deadband, the zone sensible load was allowed to vary from -40,000 to 40,000 Btu/h (-11.73 to 11.73 kW) by using an arbitrary incremental change of 479 Btu/h (0.14 kW), with negative values indicating heating loads and positive values indicating cooling loads. At each zone sensible load, a constant zone set-point temperature of 78°F (25.6°C) was maintained with a primary air temperature of 55°F (12.8°C) and secondary air temperature of 78°F (25.6°C), both of which were assumed to be constant throughout the calculation. Also, a deadband sensible load ranging from -4,000 to 4,000 Btu/h was assumed and used to illustrate deadband operation with the parallel FPTU. In addition, four primary air leakage fractions of 0, 2.5%, 5%, and 12% were used in the performance prediction of the parallel FPTU. While these percentages were applied to both cooling and heating operations, if the primary source of air leakage is through the backdraft damper, then the heating leakage will be much smaller than the leakage for cooling operations.

At each leakage level, the amount of supply air that was required to satisfy the zone load was determined. The performance impact of primary air leakage was evaluated by comparing the amount of supply air at different leakage levels. It should be noted that the above input parameters, namely zone sensible loads, zone set-point temperature, primary air temperature, secondary air temperature, and primary air leakage fraction, are user-defined parameters and can be modified for different applications and systems. For example, the secondary air temperature T_{sec} is defined based on the zone set-point temperature T_z and a temperature differential, ΔT, as shown below:

$$T_{sec} = T_z + \Delta \mathrm{T} \tag{6.52}$$

The value of ΔT could be negative or positive. In cooling operation, leakage of cold air into the plenum should reduce the secondary air temperature for either the traditional or alternative parallel FPTU configuration. In that case ΔT would be negative. In heating mode for the alternative FPTU, leakage of warm conditioned air could make ΔT a positive value. The overall air conditioning system model in a building simulation program would have to be used to estimate ΔT. We would anticipate that ΔT might vary from a range of -4 to 4 °F (-2 to 2°C).

Figure 6.14 shows the basic logic or flow of the calculation procedure for modeling the performance of a parallel FPTU. The calculation began with reading the input data, then determined the operating mode based on the zone sensible load and control sequence. There were four different operating modes:

1. If the FPTU was off, all temperatures throughout the system were set at the zone set-point temperature with no primary or secondary airflows.
2. If the zone sensible load was in the deadband range (assume to vary from -4,000 to 4,000 Btu/h (-1.2 to 1.2 kW)), the FPTU was assumed to operate with the primary air set to its minimum value. For this illustration, a minimum value of 20% was assumed with the secondary air making up the rest of the total airflow. The heating coil was turned off in deadband mode.
3. In heating mode, the primary and secondary air setting was the same as the operation in deadband mode except for the heating coil control. The heating coil was active in heating mode to provide supplemental heating to the zone.
4. In cooling mode, the zone sensible load was satisfied by varying the amount of primary air that was delivered to the zone without providing secondary air. The amount of

primary air was constrained between the minimum (assumed to be 20% of the design airflow) and the maximum, which was 100% of the design airflow. The FPTU fan was turned off as well as the heating coil.

A portion of the return air from the zone and plenum space was exhausted to the outdoors. The remaining air was mixed with outdoor air. The temperature of this mixture was used to determine whether or not preheating was required. If the temperature was below the primary air temperature then the preheating coil was used to heat the mixed air to the primary air temperature. The power consumption of the primary fan was then calculated based on the primary airflow through the fan and the fan static (or total) pressure. The cooling energy required at the primary cooling coil was then calculated. The process then looped back to the start for the next time step until the simulation was completed.

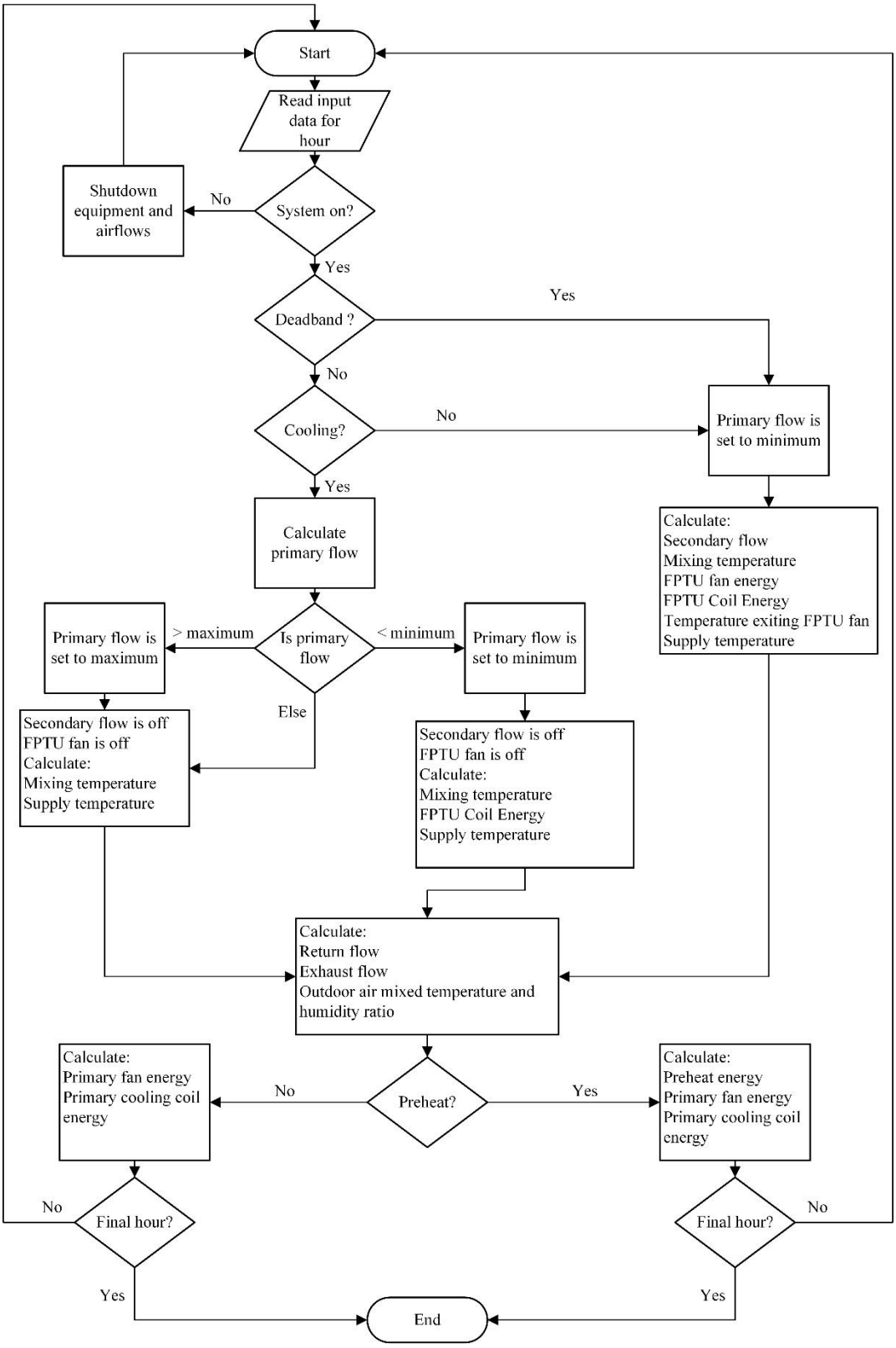

Figure 6.14: Parallel FPTU Controller Routine

6.3. Sample Results

The calculation procedure shown in Figure 6.16 was implemented in EES to perform the system scale calculation. Results of airflow, discharge temperature, and supplemental heating rate from a traditional FPTU were calculated and plotted against the zone sensible load as shown in Figures 6.17 to 6.19, respectively. The results for the alternative parallel FPTU configuration were the same as those for a traditional configuration except for the supplemental heating operations, which was shown in Figure 6.20.

Figure 6.15 showed the variation in primary and secondary airflows with changes in the zone sensible load for a traditional parallel FPTU at four leakage levels of 0, 2.5%, 5%, and 12%. The zero leakage represented an ideal condition. The leakage levels of 2.5%, 5%, and 12% were based on the results from Chapter 5 and represented the scenarios with low, medium, and high leakages. The same leakage ratios were applied in heating, cooling, and deadband modes. Currently, there were no data available on leakage for heating operations when the FPTU fan was on. More data are needed to confirm if leakage in heating operations are nearly as large as those in cooling.

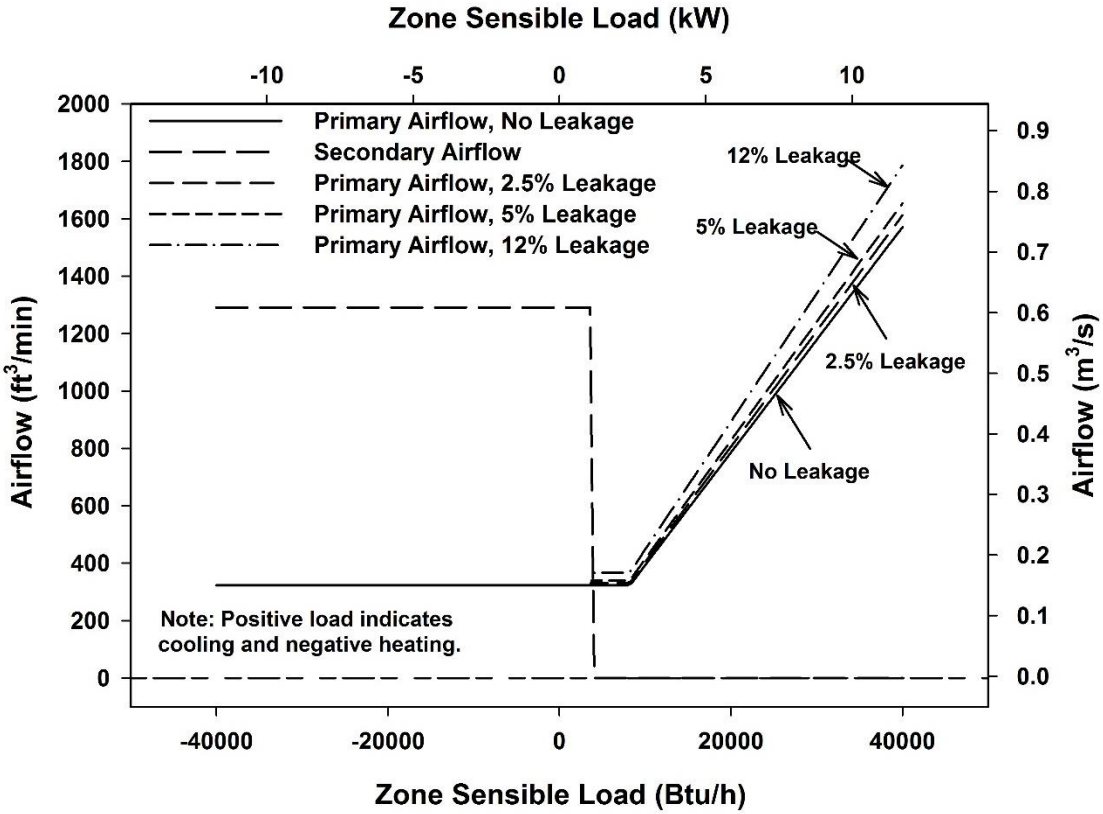

Figure 6.15: Primary and Secondary Airflows for a Traditional Parallel FPTU with Different Levels of Leakage

In Figure 6.15, the primary airflow was set at a minimum of 20% of the total design airflow when operating in either heating or deadband modes with the secondary air making up the remainder of the total airflow rate. At the upper limit of the deadband, the FPTU fan was switched off which resulted in the sharp decrease in the secondary airflow. In cooling mode, the FPTU fan remained off and no secondary air was provided. After the deadband region, the primary air maintained its minimum value at the low end of the cooling load range because the amount of cooling required by the zone was smaller than the cooling that could be provided at the minimum primary airflow. The primary airflow was constrained by its minimum (assumed to be 20% of design for this example) for the ventilation purposes. In this case, the required amount of primary air for satisfying the zone load was lower than this minimum value. As the zone cooling load increased, the primary airflow increased proportionally until the total design airflow rate was reached at the maximum cooling load.

Figure 6.15 also showed that the impact of leakage differs in heating and cooling modes for the traditionally configured parallel FPTU. For example, the primary and secondary air remained the same regardless of leakage levels in heating mode. In contrast, the primary air supplied to the FPTU needed to be increased with increasing leakage rates in cooling mode to compensate for leakage airflow from the FPTU to meet the necessary cooling requirement of the zone. In heating mode, the FPTU fan provided a constant amount of secondary airflow and was independent of leakage. Likewise, in heating, the primary was set at a prescribed level and shouldn't change with leakage. However, the heating provided to the zone was dependent on the amount of total airflow to the zone. With leakage, the total amount of airflow to the zone was smaller than it would be without leakage. Thus, even though leakage did not directly affect the primary and secondary airflows in heating mode, it did decrease the amount of air delivered to the zone. Consequently, with leakage, the discharge temperature from the FPTU reached its maximum temperature of 90°F (32.2°C) at smaller zone heating loads. Once this maximum temperature was reached, the maximum heating capacity of the FPTU was attained. As the heating requirements of the zone increased, the FPTU would be unable to meet the load.

Rather than maintaining airflow by varying discharge temperature in heating mode, the zone cooling load was satisfied by varying the primary airflow rate with a fixed temperature. In the ideal case of zero leakage, the primary airflow rate was equal to the amount of airflow that was

required to match the zone cooling load. However, in scenarios with leakage, higher primary airflow rates were required at the same zone cooling load to compensate for the air loss due to leakage from the FPTU to the plenum space. For example, at the zone sensible load of 20,000 Btu/h, Figure 6.15 shows that the supply airflow rate was increased by 2.6% from 786 to 806 ft^3/min (0.37 to 0.38 m^3/s) relative to the no leakage case as a result of introducing 2.5% primary leakage. The increases in supply airflow rate at the same zone sensible load were even greater at higher leakage levels of 5% and 12%, showing 5.3% and 13.6% increases, respectively, relative to the supply airflow rate without leakage.

Figure 6.16 showed the FPTU discharge air temperature with 55°F (12.8°C) primary air over a range of zone loads. At higher heating loads, the discharge temperature was limited at 90°F (32.2°C) because a higher discharge temperature could increase the zone temperature stratification (Hydeman and Eubanks, 2014; Faris and Int-Hout, 2014). As the heating load decreased, the discharge temperature was decreased proportionally. A sharp temperature drop occurred at the lower limit of the deadband due to switching off the heating coil. The discharge temperature was maintained at a constant of 74°F (23.3°C) in the deadband region. In cooling mode, the discharge temperature was the same as the primary air temperature given the fact that the FPTU fan was turned off, and consequently no secondary air was provided. In addition, the performance impact of leakage from the FPTU to the plenum space in heating mode was reflected in terms of discharge temperature, with showing higher discharge temperatures at greater leakage levels for the same heating load. For example, Figure 6.18 showed that at the heating load of 10,000 Btu/h (2.93 kW), the discharge temperature increased by 0.8°F (0.4°C) from 83.6 to 84.4°F (28.7 to 29.1°C) as a result of increasing the leakage ratio from 0 to 12%. The increase in discharge temperature was the result of the lower total airflows to the space from increased leakage. With lower airflows, the discharge temperatures had to be elevated to meet the heating load in the zone.

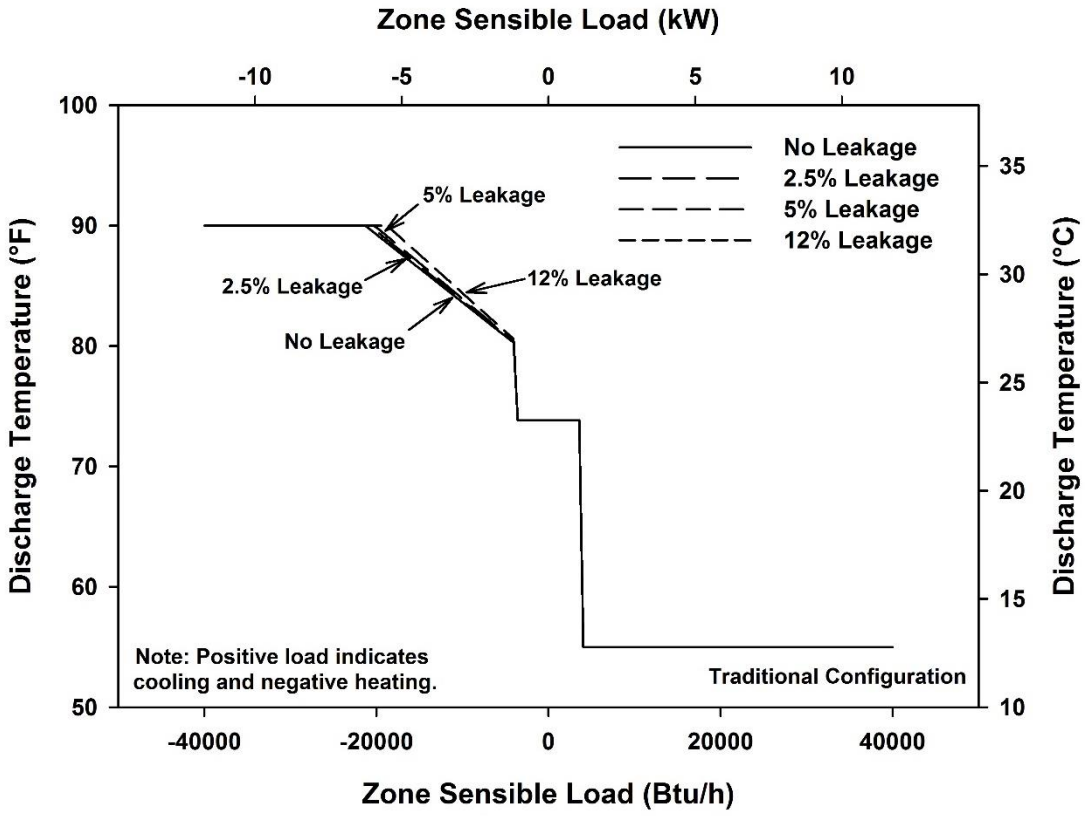

Figure 6.16: Discharge Air Temperature for a Traditional Parallel FPTU with Different Levels of Leakage

Figure 6.17 showed the supplemental heating rate for a traditional FPTU as a function of the zone heating load. Leakage reduced the maximum supplemental heating provided by the FPTU at higher heating loads. This reduction occurred because there was reduced airflow through the heating coil. With a reduced airflow, a fixed maximum discharge temperature of 90°F (32.2°C), and a fixed zone temperature, q_{coil} in Equation 6.43 had to decrease. At lower heating loads, the supplemental heating rate decreased proportionally with decreasing heating load until reaching the deadband region. At that point, the heating coil was turned off, and the supplemental heating rate became zero. The heating coil only operated in heating mode and remained off in the deadband and cooling modes. In addition to increasing the discharge temperature as shown in Figure 6.16, Figure 6.17 showed that the leakage in heating mode decreased the supplemental heating rate for the same zone load. For instance, at the zone heating load of 10,000 Btu/h (2.93 kW), a decrease of 5.1% in the supplemental heating rate from 17,375 to 16,490 Btu/h (5.09 to 4.83 kW) was observed as a result of increasing the leakage from 0 to 12%.

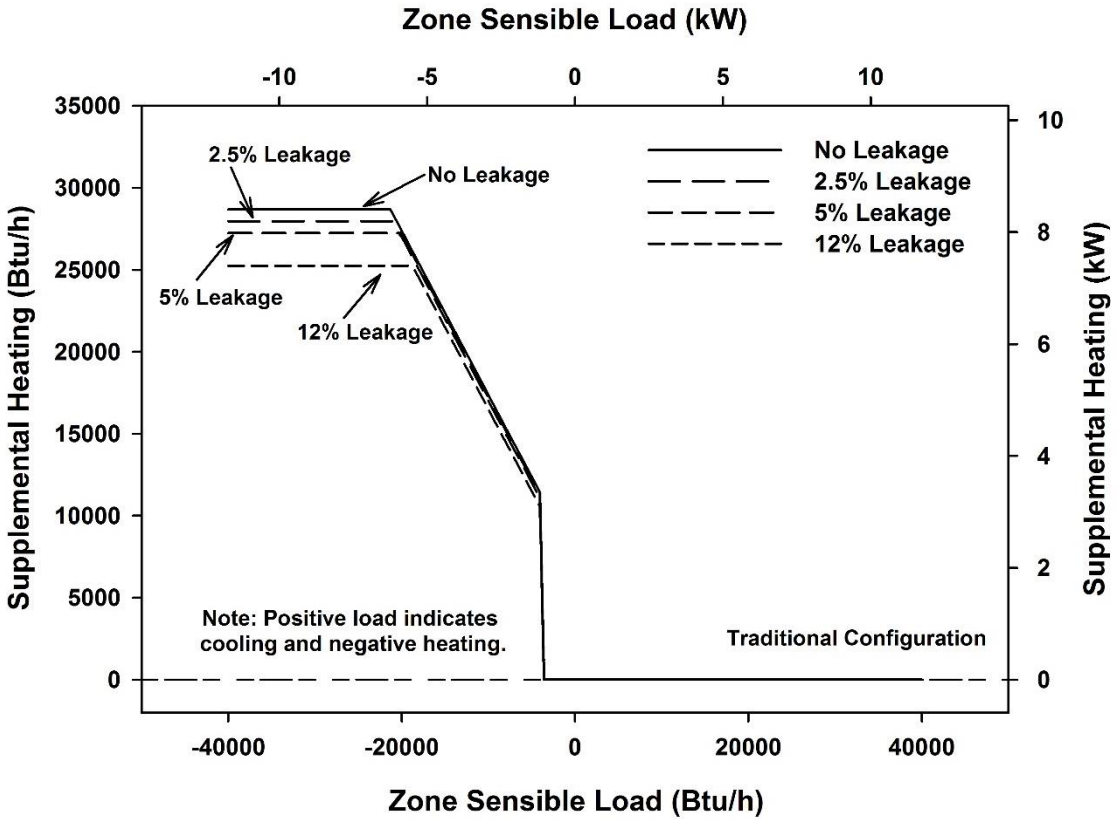

Figure 6.17: Supplemental Heating Energy for a Traditional Parallel FPTU with Different Levels of Leakage

The decrease in supplemental heating rate became even greater and was in the same proportion as the air leakage when the zone was calling for maximum heating. For example, the maximum supplemental heating rate (or heating capacity) decreased by 717 Btu/h (0.21 kW) from 28,685 to 27,968 Btu/h (8.41 to 8.20 kW) with a 2.5% leakage rate. Greater decreases in the heating capacity occurred at higher leakage ratios. At 12% leakage, the reduction was 3442 Btu/h (1.01 kW) compared to the zero leakage case. At lower zone heating loads, the discharge temperature and supplemental heating varied proportionally with the zone heating load.

As discussed above, the impact of leakage on the cooling performance of the alternative configuration was the same as that for the traditional configuration. However, there was a difference in heating operations. Figure 6.18 shows the supplemental heating rate for a parallel FPTU with the alternate configuration where the heating coil was located at the secondary inlet (See Figure 6.11). Figure 6.18 indicates the leakage impact on the supplemental heating rate for an alternate FPTU was different from that for a traditional FPTU shown in Figure 6.17.

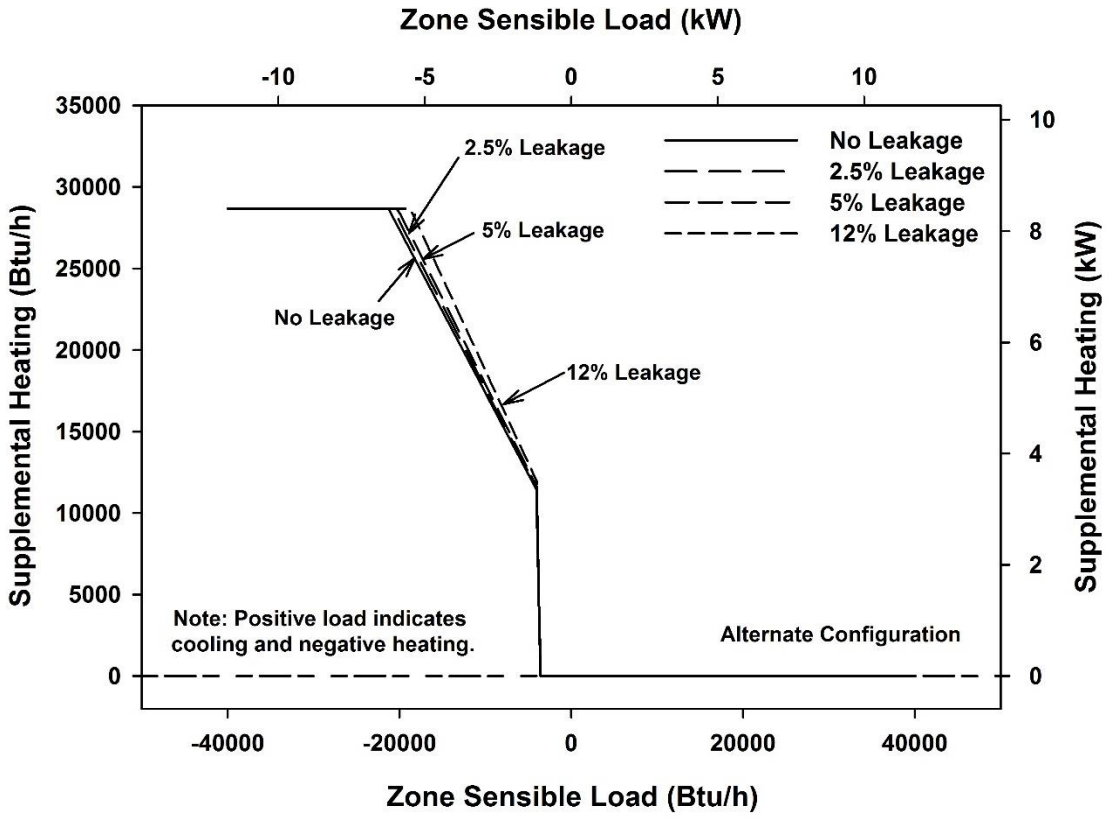

Figure 6.18: Supplemental Heating Energy for an Alternate Parallel FPTU with Different Levels of Leakage

Comparisons of the two figures showed that the maximum supplemental heating (or heating capacity) provided by the alternative configuration remained the same regardless of the leakage. Figure 6.18 showed the supplemental heating at the coil, which was different than the actual heating provided to the zone. For the zero leakage case, these two values would be same in Figure 6.18. However, with leakage, some of the heated air from the supplemental airstream leaks out of the FPTU and does not make it to the zone. Leakage decreased the maximum supplemental heating that was used by a traditionally configured FPTU. For the traditionally configured FPTU, the amount of supplemental heating would equal to the heating provided to the zone because leakage occurred upstream of the heating coil. For the alternative configuration, increases in leakage increased the amount of supplemental heating but the heating provided to the zone was less than the energy input to the heating coil because a portion of that conditioned air leaked from the FPTU into plenum. The differences in supplemental heating at the same heating load can be illustrated for the two configurations. At a zone heating load of 10,000 Btu/h (2.93 kW) the supplemental heating rate increased by 7.8% from 17,375 to 18,738

Btu/h (5.09 to 5.49 kW) as the leakage was increased from 0 to 12% for the alternative configuration. In contrast, for the same zone load and range in leakage levels, the supplemental heating rate for a traditional FPTU decreased 5.1% as shown in Figure 6.17.

The difference in supplemental heating rate responding to various levels of leakage was caused by the different heating coil locations between the traditional and alternate FPTUs. For the traditional FPTU where the heating coil was located at the total airflow outlet, 100% of the energy input into the heating coil was used to satisfy the zone load because the leakage occurred before the air flows through the heating coil. However, for the alternate FPTU where the heating coil was located at the secondary airflow, a portion of the energy input into the heating coil was lost to the plenum space because the leakage occurred downstream of the heating coil. Therefore, greater energy was required to meet the zone heating load as the leakage was increased.

The logic for the FPTU performance calculations began with sizing a parallel FPTU. The total volumetric flow rate from a parallel FPTU was estimated by using the zone design load (q_{design}) and the difference between the zone set-point temperature (T_z) and the primary air temperature (T_{pri}) at the design condition. Based on the assumption of constant air density throughout the system in this study, the mass flow rate was used instead of volumetric flow rate, as was shown below.

$$m_{design} = \frac{q_{z\_design}}{c_p \cdot (T_z - T_{pri})} \quad (6.53)$$

It should be noted that this design mass flow rate was the sum of primary and secondary airflow rates without considering the leakage airflow:

$$m_{design} = m_{pri} + m_{sec} \quad (6.54)$$

If desired, the volumetric flow rate (often in ft^3/min or m^3/s) could be determined from the air mass flow rate and density, ρ_{air}

$$m_{design} = \rho_{air} \cdot V_{design} \quad (6.55)$$

Once the design airflow rate was determined, it remained a constant throughout the calculation.

The FPTU performance calculations depended on which mode of operation it was in and which configuration the FPTU had, specifically the traditional configuration shown in Figure 6.10 or the alternate configuration shown in Figure 6.11. There were four distinct modes of operation: off, heating, cooling, and deadband. The logic for each mode was described below.

The difference in calculations between traditional and alternate configurations was only in the heating mode because the heating coil remained off in both cooling and deadband mode.

1. System is off

For this mode the primary and secondary airflows, the FPTU fan, the heating coil, and the central air handler were not running, and temperatures throughout the system were set to the zone set-point temperature.

2. System is in heating mode

a. Primary airflow was set to the minimum ventilation level:

$$m_{pri} = m_{min} \tag{6.56}$$

b. Secondary airflow was calculated:

$$m_{sec} = m_{design} - m_{pri} \tag{6.57}$$

c. As shown earlier in Equation 6.50, this study used a fraction of primary and secondary airflow to quantify the leakage airflow. After both primary and secondary airflows were determined, the leakage airflow in heating mode could be calculated by re-arranging Equation 6.50:

$$m_{leak} = (m_{pri} + m_{sec}) \cdot f_{leakh} \tag{6.58}$$

d. Then, the actual amount of air delivered to the zone was the sum of primary and secondary airflow with the subtraction of leakage airflow:

$$m_{tot} = m_{pri} + m_{sec} - m_{leak} \tag{6.59}$$

e. The outlet temperature that is required to meet the zone load was calculated by using the actual amount of air delivered to the zone. If the calculated temperature was greater than 90°F (32.2°C) then the system was at maximum heating and outlet temperature was set to 90°F (32.2°C):

$$T_{out} = T_z - \frac{q_{zs}}{m_{tot} c_p} \tag{6.60}$$

The following calculation procedures varied with traditional and alternate configurations. For a parallel FPTU with the traditional configuration:

f. The secondary air temperature at the FPTU fan outlet and the mixer inlet was calculated:

$$T_{sec,out} = \frac{Pow_{fan}}{m_{sec} c_p} + T_{sec} \tag{6.61}$$

g. The temperature of the mixed air was calculated:

$$T_{mix} = \frac{m_{pri}\, c_p T_{pri} + m_{sec}\, c_p T_{sec,out}}{m_{design} c_p} \quad (6.62)$$

h. The heating energy input into the coil was calculated:

$$q_{coil} = m_{tot} c_p (T_{out} - T_{mix}) \quad (6.63)$$

For a parallel FPTU with the alternate configuration, steps f through g were different:

f. The temperature of the mixed air was calculated:

$$T_{mix} = T_{out} \quad (6.64)$$

g. The secondary air temperature at the FPTU fan outlet and the mixer inlet was calculated:

$$T_{sec,out} = \frac{m_{design} c_p T_{mix} - m_{pri}\, c_p T_{pri}}{m_{sec} c_p} \quad (6.65)$$

h. The heating coil outlet temperature was calculated:

$$T_{coil} = T_{sec,out} - \frac{Pow_{fan}}{m_{sec} c_p} \quad (6.66)$$

i. The heating input from the coil was calculated:

$$q_{coil} = \mathrm{m}_{sec} c_p (T_{coil} - T_{sec}) \quad (6.67)$$

3. <u>System is in cooling mode</u>

a. The heating coil was shut off:

$$q_{coil} = 0 \quad (6.68)$$

b. Secondary air was set to zero:

$$m_{sec} = 0 \quad (6.69)$$

c. The amount of primary air that is delivered to the zone in order to match the zone load was calculated:

$$m_{tot} = \frac{q_{zs}}{C_{p*}(T_Z - T_{pri})} \quad (6.70)$$

d. Due to the leakage effect, the amount of primary air delivered to the parallel FPTU should be higher than the amount of primary air m_{tot} required for satisfying the zone load, as shown previously in Equation 6.49. Therefore, the amount of primary air that was required to compensate for the leakage effect could be calculated from re-arranging Equation 6.49:

$$m_{pri} = m_{tot}/(1 - f_{leakc}) \quad (6.71)$$

It was important to recognize that the calculated primary airflow m_{pri} was constrained between the minimum, which typically ranged from 10 to 30% of the design total

airflow and assumed to be 20% in this study, and the maximum, which was 100% of the design total airflow. If the calculation of primary airflow resulted in a value smaller than the minimum or larger than the maximum, the logic reset the primary airflow to the minimum or maximum accordingly.

4. System is in deadband mode

In the deadband mode, the logic for the performance calculation was similar to the operation in heating mode except for the heating coil being switched off. Unlike the operations in heating and cooling modes where the purpose of the FPTU was to satisfy the zone load, the discharge temperature in deadband was not controlled and was a direct result of mixing the minimum primary air and maximum secondary air. In a simulation program, the deadband was often specified by the user. Thus, no method of calculating the range of the deadband was provided here.

6.4. Summary

This chapter provided the basic equations needed to characterize a fixed airflow series and parallel fan powered terminal unit using a mass and energy balance approach. The approach follows closely that used in EnergyPlus (2013) for modeling FPTUs. A step-by-step process of how the basic equations should be used for each FPTU mode of operation was provided for both types of FPTUs. The methodology developed in this paper can be implemented into building simulation models that use a mass and energy balance approach.

A simplified approach was used to allow estimation of fan power based on correlations developed in Chapters 2 and 3 for constant airflow fans in either PSC/SCR and ECM FPTUs. The ECM model allows the user to capture the energy and power savings of FPTUs with larger airflow capacities whose fan speeds are lowered to meet the design load.

The parallel FPTU model allowed the user to include leakage. The leakage model was based on cooling operations when the FTPU fan was off and the backdraft damper closed. Thus, the parallel model should provide excellent results for cooling operations. The leakage model would be expected to overestimate leakage in heating and the deadband operations because the FPTU fan would be running under these conditions and there would be no leakage through the backdraft damper. If the primary source of leakage in parallel FPTUs was through the backdraft damper, then leakage in heating mode would be significantly less than in cooling mode.

CHAPTER 7

VARIABLE AIRFLOW SERIES AND PARALLEL FPTU PERFORMANCE MODELS

The purpose of this chapter was to outline the development of variable airflow series and parallel FPTU models that utilized ECM fan/motor combinations. These models included the ECM fan/motor model developed in Chapter 3 combined with a mass and energy balance approach compatible with EnergyPlus (2013). Both the traditional location of the heating coil at the discharge of the FPTU and an alternate configuration where the heating coil was at the inlet to the secondary airflow stream were included in the parallel FPTU model development. The power and airflow needed for the FPTU to match the thermal load in the zone was estimated by the model, which can be used to characterize the annual performance of a FPTU. The variable airflow series FPTU was discussed first, then the parallel FPTU.

7.1. Series FPTUS

As was done in the previous chapter, a series FPTU can be decomposed into its major components: mixer, fan/motor, and heating coil. Figure 7.1 shows a control volume around a series FPTU.

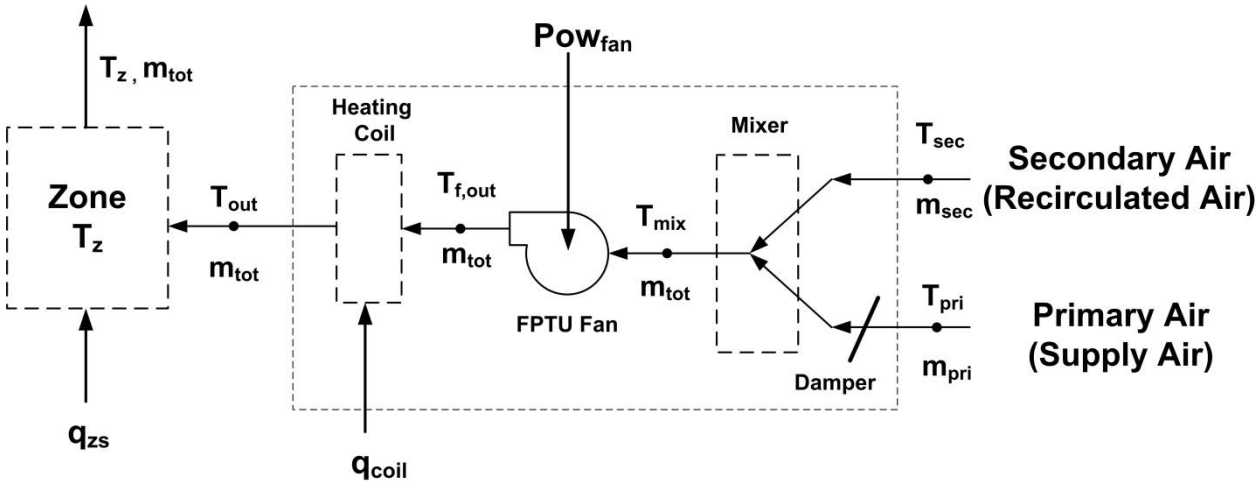

Figure 7.1: Mass and Energy Flows into and out of a Series FPTU

Mass and energy enter and can leave the FPTU in several locations. Mass was carried into the FPTU via the primary and secondary airstreams and out via the discharge airstream at the outlet. Energy was input to the FPTU via electrical energy to the fan, heat energy to the heating coil, and the energy carried in by the primary and secondary airstreams. The only energy leaving the series FPTU was with the airstream at the discharge of the FPTU. The approach outlined below incorporated an empirical model from Chapter 3 for the ECM fan/motor combination to

estimate the fan power. As with the fixed airflow case, the analysis below was dependent on the same basic assumptions. First, we assume the FPTU was operating in quasi-steady state during each time step. Second, we assumed the thermo-physical properties are constant. Third, the energy input to the fan motor was assumed to be completely converted into the heat energy in the airstream. Fourth, the FPTU would always operate with a minimum amount of primary air to ensure enough fresh air into the zone. The impact of these assumptions was discussed in detail in Chapter 6.

For the FPTU control volume shown in Figure 7.1, the mass flow into the control volume included the primary, m_{pri}, and secondary, m_{sec} airstreams. The only mass out of the control volume was the total airflow, m_{tot}. Application of a mass balance to the control volume yielded the following:

$$m_{tot} = m_{pri} + m_{sec} \tag{7.1}$$

The value of m_{pri} is often an unknown that must be estimated using the analysis discussed below. Two exceptions were when the series FPTU was operating under minimum or maximum primary flow conditions.

The energy transfer into the control volume included the energy carried by the two airstreams, the rate of energy input in the heating coil, q_{coil}, and the power input to the fan, Pow_{fan}. The general energy balance for the control volume can be written as:

$$m_{tot}h_{out} = q_{coil} + Pow_{fan} + m_{pri}h_{pri} + m_{sec}h_{sec} \tag{7.2}$$

Equations 7.1 and 7.2 provided the foundation for the analysis of the FPTU and HVAC system. The unknowns in these equations varied depending on the mode of operation (heating, cooling, or deadband) of the FPTU. Solving for the unknowns required applying mass and energy balances to each of the components in the FPTU. The process typically started from the left in Figure 7.1 at the discharge to the zone and moved to the right to the primary and secondary air inlets.

For the case of a variable airflow ECM fan/motor that matched the airflow requirements of the zone, the total airflow must be calculated based on the load in the zone for that time step. The temperature of the discharge air also has to be high enough to ensure there was no condensation on the registers. An additional consideration was that the primary (and total) airflow cannot drop below a specified percentage of the design airflow. With constant air properties, Equation 7.2 can be rewritten in terms of temperatures and specific heats.

$$m_{tot}\, c_p T_{out} = q_{coil} + Pow_{fan} + m_{pri}\, c_p T_{pri} + m_{sec}\, c_p T_{sec} \quad (7.3)$$

Proceeding with the analysis required decomposing the FPTU into its components and performing mass and energy balances on each component as described below.

7.1.1 Zone Analysis A mass and energy balance can be performed on the zone which was located to the far left of Figure 7.1. If there was no air leakage into or out of the zone, then the airflow into the zone, m_{tot}, was the same as that leaving the zone, m_{tot}. Energy was carried into and out of the zone via the total airflow. The sensible load in the zone due to people, equipment, etc. was represented by q_{zs}. An energy balance on the zone yielded:

$$q_{zs} = m_{tot} c_p (T_z - T_{out}) \quad (7.4)$$

The way that Equation 7.4 was used in an analysis depended on whether the FPTU fan was fixed or variable airflow and whether the system was in heating or cooling model. For example, for a fixed airflow application, m_{tot} was known whether in heating or cooling mode. Given the zone load (q_{zs}), specific heat (c_p), and zone set point temperature (T_z) were also known, then it was possible to calculate the required discharge temperature, T_{out}, to satisfy the zone load.

$$T_{out} = \frac{q_{zs}}{m_{tot} c_p} + T_z \quad (7.5)$$

Unlike the fixed airflow series FPTU where m_{tot} was constant, m_{tot} varied with the cooling load in a variable airflow FPTU. Thus, m_{tot} and q_{zs} were not independent in Equation 7.5. Looking at Equation 7.4, both T_{out} and m_{tot} were unknowns. One approach to solving Equations 7.4 and 7.5 was to use an iterative technique to simultaneously solve the energy balances for the zone, fan, and mixer. Other approaches involved specifying a relationship between either T_{out} or m_{tot} with the cooling load. Specific approaches to obtaining solutions for Equation 7.4 are discussed later in this chapter along with temperature constraints that a modeler should use to provide realistic solutions.

7.1.2 Heating Coil Analysis The energy and mass flow into and out of the heating coil were shown in Figure 7.1. Because we assumed the system operated at quasi-steady state, the mass flow of air entering the coil was equal to the mass flow of air exiting the coil in a given time step. The energy entering the coil was the heating energy input, q_{coil}, either from electric resistance or hot water and the energy associated with the air flow entering the coil after exiting the FPTU fan. The energy exiting the coil was carried by air leaving the coil and supplied to the zone. Applying an energy balance to the heating coil yielded:

$$m_{tot}c_pT_{out} = q_{coil} + m_{tot}c_pT_{f,out} \quad (7.6)$$

Often the variable of interest is q_{coil}, the heating energy input, so the above equation can be rearranged to solve for q_{coil}:

$$q_{coil} = m_{tot}c_p\left(T_{out} - T_{f,out}\right) \quad (7.7)$$

The upper limit for T_{out} in heating applications was usually limited to 15°F (8.3°C) above the zone set-point temperature or a fixed value 90°F(32.2°C) to help reduce temperature stratification in the zone (Hydeman and Eubanks, 2014; Faris and Int-Hout, 2014).

7.1.3 FPTU Fan Analysis The mass and energy flows into and out of the FPTU fan are shown in Figure 7.1. All of the fan motor and controller power was assumed to be converted to heat energy in the airstream. This fraction was a user input in EnergyPlus (2013) and could be varied by the user. For an ECM FPTU, all the energy converted from the fan motor and controller was assumed to go into the airstream.

For a mass balance, the airflow out of the fan was equal to the airflow into the fan and both were equal to m_{tot}. For constant properties, an energy balance on the fan yielded:

$$m_{tot}c_pT_{f,out} = m_{tot}c_pT_{mix} + Pow_{fan} \quad (7.8)$$

The power, Pow_{fan}, of an ECM fan/motor operating at either fixed or variable airflow can be estimated using models from Chapter 3. The power multiplied by each time step and summed over the entire year of a simulation would yield the energy use of the FPTU fan.

The temperature increase of the air due to the fan, ΔT_{fan}, can be evaluated by rearranging Equation 7.8.

$$\Delta T_{fan} = T_{f,out} - T_{mix} = \frac{Pow_{fan}}{m_{tot}c_p} \quad (7.9)$$

Equation 7.9 provided a means of quantifying the impact of the fan power on the temperature rise of the air.

7.1.4 Estimating Fan Power Making an accurate estimate of the variable airflow fan energy use in a series FPTU was important because the fan runs continuously and the fan power was used for estimating the temperature increase of the air across the fan. An ECM FPTU that was sized so that its maximum capacity just met the design airflow requirement in the space would use more power than one that had additional capacity, but whose speed was lowered so its airflow would just meet the design airflow requirements. Thus, the building simulation user

should know something about the maximum airflow output of an ECM FPTU relative to the size of the design requirements in the space.

The model described below was based on the variable airflow fan model developed in Chapter 3. Calculation of the fan power for a variable airflow ECM FPTU required several steps. First, the design airflow requirement for the space must be determined. Usually, this was calculated or estimated by a building simulation program. Second, the user must decide how large a FPTU fan will be used in the zone. The volumetric airflow capacity of the FPTU fan, Q_o, divided by the design airflow requirements in the zone, Q_d, can be used to calculate the capacity factor, x_o:

$$x_o = \frac{Q_o}{Q_d} - 1 \tag{7.10}$$

The fan power , $Pow_{fan}(Q)$, for an ECM FPTU operating at a given volumetric airflow, Q, with a capacity factor, x_o, and had a design airflow capacity, Q_d, can be calculated with the following:

$$Pow_{fan}(Q) = f_{pl} * C_3 * Q_d * (1 + x_o) \tag{7.11}$$

The constant, C_3, was 0.38 W/(ft^3/min) in IP units or 805 W/(m^3/s) in SI units and was based on a simple linear regression. The part load power fraction for variable airflow operation, f_{plv}, is given by the following:

$$f_{pl} = a_1 + a_2 * \left(\frac{Q}{Q_d(1+x_o)}\right) + a_3 * \left(\frac{Q}{Q_d(1+x_o)}\right)^2 + a_4 * \left(\frac{Q}{Q_d(1+x_o)}\right)^3 \tag{7.12}$$

The coefficients in Equation 7.12 were given in Table 7.1. The fan power, Pow_{fan}, had to be recalculated every time step of a simulation. While x_o was fixed once the size of the FPTU was selected, the airflow, Q, varied with the cooling load in the space each time step of a simulation.

Table 7.1 – Part Load Power Fraction Coefficients for Equation 7.12

Coefficients	Value
a_1	0.061715
a_2	0.093022
a_3	-0.11627
a_4	0.961538

The above equations can be used to estimate the power of a variable airflow ECM FPTU. With constant air properties, the volumetric flow rates in Equations 7.10 through 7.12 can be replaced by their mass flow counterparts. It is important for a modeler to estimate the size of an ECM FPTU relative to the design airflow requirements of the space. Discussions with manufacturers indicated that a typical ECM FPTU field installation could be expected to have 25% or more capacity above the design airflow requirement.

The capacity of the ECM FPTU impacted the estimated power use of the ECM fan motor. To illustrate, consider three ECM FPTUs that could be applied to a zone with cooling design airflow of 1000 ft^3/min (0.472 m^3/s). One has a maximum capacity of 1000 ft^3/min (0.472 m^3/s); the second has a capacity of 1200 ft^3/min (0.566 m^3/s) and the third a capacity of 1400 ft^3/min (0.661 m^3/s). These three corresponded to capacity factors of 0%, 20%, and 40%. Equations 7.10 through 7.12 were used to estimate the power use of the three different sized FPTUs as they followed the airflow requirements in the zone from 1000 ft^3/min (0.472 m^3/s) down to a minimum of 200 ft^3/min (0.094 m^3/s). The results in Figure 7.2 show how ECM FPTUs with different capacity factors follow the airflow requirements in the zone from the design airflow all the way down to the minimum primary airflow.

The units with capacity factors of 20% and 40% provided substantial savings at the higher airflow rates over the ECM unit that was just sized to meet the design airflow. However, at airflows below about 400 ft^3/min (0.189 m^3/s), the unit just sized to meet the design airflow has a smaller power use.

With the fan/motor model outlined above, the power during a given time step can be calculated for a series FPTU with a variable airflow ECM fan/motor combination. Once the power of the fan was known, then the temperature change across the fan can be calculated with Equation 7.9.

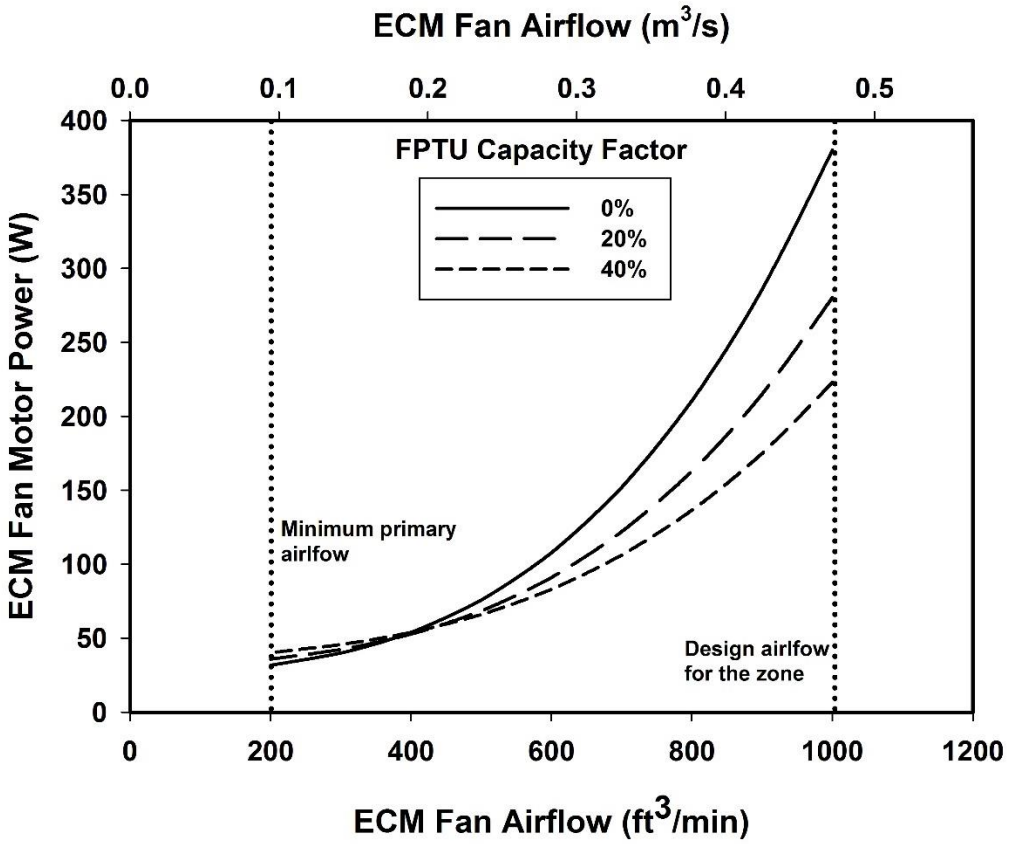

Figure 7.2: Part Load Power Use of Three Different Sized ECM FPTUs

7.1.5 Mixer The remaining component needing analysis in the FPTU was the mixer, which was located on the right side of the FPTU control volume in Figure 7.1. The mixing of the primary and secondary airstreams occurred in the main housing of the FPTU immediately prior to the air entering the series FPTU fan. As with the other components, an energy and mass balance can be applied to the mixing process. The result of the mass balance yielded the same equation as Equation 7.3 and was not repeated here. The mixer was assumed to perform adiabatic mixing; therefore, no heat energy was lost to the surroundings. Applying an energy balance to the mixer yielded the following:

$$m_{tot}\, c_p T_{mix} = m_{pri}\, c_p T_{pri} + m_{sec}\, c_p T_{sec} \tag{7.13}$$

The variables that would be calculated from Equation 7.13 depended on whether the FPTU was in cooling or heating mode. When the FPTU was in heating mode, the primary airflow would be set at a prescribed minimum needed to satisfy fresh air requirements (ASHRAE 2013). The minimum primary air was also used during deadband operations and when the estimated cooling load in the zone was smaller than the amount of cooling provided by FPTU when the primary air

was at its minimum value. Another example of the primary airflow being at a fixed value was when the cooling load requirement in the zone was higher than the maximum cooling provided by the FPTU. In this case, the FPTU would reach its maximum airflow and remain constant even if more cooling was required. In all other cooling cases, the primary airflows fell between these two values and the energy and mass balances on each component had to be utilized. The process is described later and depends on the operational mode of the FPTU.

7.1.6 Calculation Models for Cooling The energy balance on the zone represented by Equations 7.4 and 7.5 was the normal starting point for analyzing the cooling performance of a series FPTU. If the series unit had constant airflow, then the total airflow, m_{tot}, was a fixed quantity and the outlet air temperature, T_{out}, needed to satisfy the cooling load in the zone can be easily calculated with Equation 7.5. The calculation procedure would then proceed to determine the temperature increase across the fan with Equation 7.9 using an appropriate fan model. The desired amount of secondary air could then be calculated with the mixer energy and mass balance (Equations 7.1 and 7.13) to estimate the mixed air temperature before the fan.

With variable airflow ECM fans in a series FPTU, the modeling process becomes more complex. With a fixed airflow series ECM, the outlet air temperature of the FPTU was achieved by mixing increasing amounts of secondary air with decreasing amounts of primary air as the cooling load decreased. At first glance, for a variable airflow series FPTU, it would be tempting to use only primary air during most of the cooling operations to satisfy the cooling load in the zone. The ECM fan/motor would run at full airflow at maximum cooling. The airflow would then be decreased as the cooling load decreased until the minimum amount of primary air was reached. Secondary air could then be used for zone cooling loads that were below the load satisfied with the minimum amount of primary air. Solving this scenario was rather straightforward, but required an iterative solution. Neither the m_{tot} or T_{out} were known in the zone energy balance in Equation 7.4. While T_{out} was near the primary air temperature, it was slightly higher than the primary air temperature by the amount of the temperature increase across the fan, ΔT_{fan}. As the airflow from the FPTU was lowered, the power of the fan dropped and, consequently, ΔT_{fan} dropped. What this meant for a building simulation user was that for a variable airflow series FPTU application, an iterative solution must be used to solve for m_{tot} and T_{out} simultaneously. For example, the airflow can be guessed, then T_{out} estimated from Equation 7.5. If no secondary air was used for cooling operations and only primary air was used, then the

mixing temperature before the fan would be T_{pri} and the temperature at the outlet of the fan would be $T_{pri} + \Delta T_{fan}$. If the fan outlet temperature didn't match the T_{out} calculated from the zone energy balance, then another airflow must be guessed until there was convergence on T_{out}. If a modeler was trying to simulate a building with dozens of variable airflow series FPTUs, then the cost in computational time could be large. Besides the iteration issue, there are field application issues with only using primary air to provide cooling to the zone. For cooling coils fed by a chilled water system, the primary air temperature is low enough that condensation can occur on the registers. Likewise, near the deadband region when cooling loads are small, use of only primary air can create cold draft conditions for occupants. As a consequence, secondary air is usually blended in with the primary air for cooling applications of variable airflow series FPTUs.

In field applications of variable airflow series FPTUs, the comfort constraints affect how the primary airflow and ECM are modulated to meet the cooling load in the zone. For a system with a chilled water cooling coil, the primary air temperatures may range from 45 to 48°F (7.2 to 8.9°C). In this case, the FPTU discharge air temperatures are usually set at 51°F (10.6°C) or higher at maximum cooling to ensure there is no condensation at the registers. Likewise, the discharge air temperatures are gradually increased to at least 60°F (15.6°C) as the cooling load decreases and enters the deadband region. The mixing helps reduce cold drafts from the registers when there are minimal cooling requirements in the zone. For direct expansion cooling coils, the discharge temperature at full cooling can be expected to be near 55°F (12.8°C) with minimal secondary air. However, even with direct expansion coils, the discharge temperature of the FPTU has to be adjusted to be at least 60°F (15.6°C) in the deadband region for the same reason mentioned above for chilled water cooling coils. In both the chilled water and direct expansion coil systems, the discharge temperature of the FPTU increases as the cooling load decreases.

For a variable airflow FPTU, a modeler needs to specify the discharge temperature at full load cooling conditions to ensure no condensation and in the deadband region to reduce cold drafts. There were two possible modeling approaches that could be used to approximate FPTU performance between full cooling and the deadband region. In the first approach, the total and primary airflow profiles were specified between full cooling and the deadband region. For the second approach, the discharge temperature profile was specified between full cooling and the

deadband region. In both cases, the end-points (full cooling and deadband) were specified, but the operations in between the end-points were slightly different. Each is discussed below.

The first approach to modeling cooling operations was for the user to specify that the total and primary airflows were linear with respect to the cooling load. For this case, the total airflow can be represented with the following:

$$m_{tot} = \gamma q_{zs} + \delta \tag{7.14}$$

Both γ and δ were constants. The total airflow needed at full cooling was estimated based on the desired discharge temperature and was calculated from the zone energy balance in Equation 7.4. In the deadband region, the primary airflow was set at its minimum, and the amount of total airflow was calculated to provide the desired discharge temperature. The secondary airflow was calculated by subtracting the amount of primary airflow from the total airflow. These calculations at full cooling and the deadband region provided the end points to the line for total airflow which was defined by Equation 7.14. The primary airflow was assumed to linearly vary from full cooling down to its minimum value. Once the primary airflow was at its minimum value, it was held constant in the deadband and heating regions. With a linear variation in m_{tot} with respect to the cooling load, the discharge temperature can be solved by substituting Equation 7.14 into Equation 7.5 to show how the FPTU discharge temperature, T_{out}, varied with zone cooling load:

$$T_{out} = \frac{q_{zs}}{c_p(\gamma q_{zs} + \delta)} + T_z \tag{7.15}$$

The zone load appeared in the numerator and denominator of the first term on the right hand size of the equation. The form of Equation 7.15 meant that the outlet temperature, T_{out}, was not linear with the zone load.

A second possible modeling approach was to specify a simple linear decrease in discharge temperature from the deadband region to full cooling as the cooling load increases. For example, with a chilled water system, at full cooling, the temperature was specified at a high enough value to ensure no condensation on the registers. At the minimum load corresponding to the upper end of the deadband, the discharge temperature was specified to be high enough to reduce cold drafts. A simple linear regression can then be used to estimate the coefficients α and β in Equation 7.16. Unlike the first modeling approach where T_{out} was non-linear with q_{zs}, this equation then provided a linear variation in outlet temperature with the cooling load, $q_{zs.}$

$$T_{out} = \alpha q_{zs} + \beta \quad (7.16)$$

With a discharge temperature known at a given zone cooling load, the required total airflow can be determined. The FPTU fan power, air temperature rise across the FPTU fan ΔT_{fan}, the mixed air temperature before the fan, and secondary airflow can then be calculated. These calculations can be done without needing to iterate to find a solution. A curious artifact of a linear discharge temperature profile with the cooling load was the shape of the total and secondary airflows with respect to cooling load. If Equation 7.16 was substituted into the energy balance equation (Equation 7.4) for the zone and the terms rearranged to solve for m_{tot}, the following expression emerged:

$$m_{tot} = \frac{1}{c_p}[(T_z - \beta)q_{zs} - \alpha q_{zs}^2] \quad (7.17)$$

This equation showed that the total airflow, m_{tot}, had a quadratic relationship with the cooling load, q_{zs}. This equation was only applicable from maximum cooling down to the top end of the deadband region. If the primary air was assumed to linearly decrease from a maximum at full cooling to its minimum value (typically 10 to 30% of maximum), then the secondary air also was quadratic with respect to the cooling load. FPTUs have a sensor that allows for measurement of primary air but not secondary air. Any estimates of the secondary airflow have to be inferred from primary and total airflow measurements and application of energy and mass balances throughout the system.

Both approaches accomplish the same goal of providing high enough air temperatures at maximum cooling to prevent condensation on the registers and high enough air temperatures in the deadband region to prevent cold drafts. Both approaches also eliminated the need to iterate every time step to obtain a solution for the performance of the FPTU. We anticipated that either approach should provide comparable estimates of the FPTU cooling performance. Both approaches are discussed below with illustrations using a direct expansion cooling coil providing higher primary air temperatures and a chilled water system with lower primary air temperatures. The step-by-step implementation of the equations was also provided.

7.1.7 Performance Modeling of Series FPTU with Variable Airflow The performance of a variable airflow series FPTU was estimated by using the component models of the heating coil and mixer that were derived from the mass and energy balances along with the variable speed fan model. As mentioned above, two modeling approaches can be used for estimating cooling performance of the FPTU. We called one the "airflow control approach" and the second the

"discharge temperature control approach." The airflow control approach increased the total and primary airflows linearly as the zone cooling load increased. The discharge temperature control approach decreased the discharge temperature in cooling mode proportionally with increasing the zone cooling load. It should be noted that in both approaches airflows and temperatures were subject to restrictions that were imposed by the mass and energy balances. Detailed information on each modeling approach was provided in this section, along with example results to demonstrate the airflow and temperature trends in each approach.

7.1.8 Airflow Control Approach In this approach, the total and primary airflows were varied linearly with the zone cooling load to maintain the prescribed zone set-point temperature. The logic for the performance calculations began with sizing a series FPTU. The total volumetric flow rate from a series FPTU was estimated by using the zone design load q_{design} and the difference between the zone set-point temperature T_z and the discharge temperature $T_{out,design}$ at the design condition. Based on the assumption of constant air density throughout the system, the mass flow rate was used instead of volumetric flow rate, as was shown below:

$$m_{tot,design} = \frac{qz_{\_design}}{c_p \cdot (T_z - T_{out,design})} \tag{7.18}$$

The outlet discharge temperature at design, $T_{out,design}$, varied on whether the system had a direct expansion or chilled water cooling coil. The discharge temperature can be expected to be slightly higher than the primary air temperature even when the FPTU was only using primary air, which would be the case for a direct expansion cooling coil application. There was a small temperature increase across the FPTU fan which can be expected to be from about 0.2 to 1.0°F (0.1 to 0.6°C) based on the ECM fan/motors evaluated in Chapter 3. The selection of the design discharge temperature was dependent on the primary air temperature. For example, in systems with a primary air temperature at or close to 55°F (12.8°C), the discharge temperature at the design condition was typically a little higher than the primary air temperature because of temperature increase across the fan. When a lower primary air temperature in a range of 45 to 48°F (7.2 to 8.9°C) was used, the discharge temperature at the design condition should be equal to or greater than 51°F (10.6°C) with a purpose of preventing condensation on supply registers and air diffusers. Once the design airflow rate was determined, the sum of primary and secondary airflows at any given zone load was capped by the design airflow. If desired, the volumetric airflow rate (often in ft^3/min or m^3/s) can be determined from the air mass flow rate and air density ρ_{air}

$$Q_{tot,design} = \frac{m_{design}}{\rho_{air}} \tag{7.19}$$

The next step was to determine the total airflow and zone load range in deadband according to the user-defined deadband discharge temperature $T_{out,deadband}$. In deadband mode, both primary and secondary airflows were constant and independent of zone loads. Consequently, the total airflow and discharge temperature were also constants. The primary airflow in the deadband region had a known minimum value which was typically 10 to 30% of the design airflow.

$$m_{pri,deadband} = m_{min} \tag{7.20}$$

To estimate the deadband total airflow, which was the sum of primary and secondary air, the secondary airflow needed to be estimated. The mixing of the secondary and primary airflows must provide the desired discharge temperature from the FPTU, $T_{out,deadband}$. With a known amount of primary air, the secondary air $m_{sec,deadband}$ can be calculated:

$$m_{sec,deadband} = m_{pri,deadband} \cdot \frac{T_{mix,deadband} - T_{pri}}{T_{sec} - T_{mix,deadband}} \tag{7.21}$$

where $T_{mix,deadband}$ was the mixing temperature of primary and secondary air and was also an unknown. The mixing temperature $T_{mix,deadband}$ can be determined from the $T_{out,deadband}$ and the temperature rise across the FPTU fan because the heating coil was not operating in the deadband region:

$$T_{mix,deadband} = T_{out,deadband} - \frac{Pow_{fan,deadband}}{m_{tot,deadband} \cdot C_p} \tag{7.22}$$

where $Pow_{fan,deadband}$ was the FPTU fan power in the deadband region, and $m_{tot,deadband}$ was the total airflow rate delivered by the FPTU fan, both of which varied with the secondary airflow rate in Equation 7.21. Therefore, an iterative solution was required to determine the mixing temperature, $T_{mix,deadband}$, and the amount of secondary air, $m_{sec,deadband}$, in the deadband region. This iteration was only required to be performed once for each FPTU in the HVAC system to determine the secondary and total airflow requirements in the deadband region. Once these values were calculated, they were used as the end-point of the airflow requirements in the deadband region.

With the results of $m_{pri,deadband}$ and $m_{sec,deadband}$, the total airflow in deadband $m_{tot,deadband}$ can be calculated as:

$$m_{tot,deadband} = m_{pri,deadband} + m_{sec,deadband} \quad (7.23)$$

In addition, the zone cooling load representing the upper limit of the deadband was:

$$q_{cooling,deadband} = m_{tot,deadband} \cdot C_p \cdot (T_z - T_{out,deadband}) \quad (7.24)$$

Similarly, the zone heating load representing the lower limit of the deadband was:

$$q_{heating,deadband} = m_{tot,deadband} \cdot C_p \cdot (T_z - T_{out,heating}) \quad (7.25)$$

where $T_{out,heating}$ was the prescribed discharge temperature in heating mode. Determining the upper limit of the deadband and its corresponding airflows of $m_{pri,deadband}$ and $m_{tot,deadband}$ provided the starting point for linearly varying the primary and total airflow over the entire zone cooling range.

After determining the airflows and load limits in deadband, the FPTU performance calculations depended on which mode of operation it was in. There were four distinct modes of operation: off, deadband, heating, and cooling. The logic for each mode is described below:

1. Off mode

   For this mode, the primary and secondary airflows, the FPTU fan, and the heating coil were not operating. Therefore, temperatures throughout the system were set to the zone set-point temperature.

2. Deadband mode

   If the zone load was in the range that was defined by the lower limit of $q_{heating,deadband}$ and the higher limit of $q_{cooling,deadband}$, the FPTU was in deadband mode. In this mode, the heating coil was switched off.

   $$q_{coil} = 0 \quad (7.26)$$

   The secondary airflow m_{sec}, primary airflow m_{pri}, and the total airflow m_{tot} were set to the values that were determined from the iterative approach earlier.

   $$m_{sec} = m_{sec,deadband} \quad (7.27)$$

   $$m_{pri} = m_{pri,deadband} \quad (7.28)$$

   $$m_{tot} = m_{tot,deadband} \quad (7.29)$$

   The discharge temperature was set to the user-defined value.

$$T_{out} = T_{out,deadband} \tag{7.30}$$

3. Heating mode

   If the zone load was smaller than the lower limit of $q_{heating,deadband}$, the FPTU was in heating mode.

   a. The primary airflow was set to the minimum ventilation level.

   b. The heating discharge temperature $T_{out,heating}$ was set to 90°F (32.2°C).

   c. Estimate the total airflow rate that was required to meet the zone heating load by using the temperature difference between the heating discharge temperature of 90°F (32.2°C) and the zone set-point temperature.

$$m_{tot} = \frac{q_{zs}}{C_p \cdot (T_z - T_{out,heating})} \tag{7.31}$$

   The total airflow rate delivered to the zone m_{tot} was constrained between the minimum value, which was the total airflow in deadband, and the maximum value, which was the design airflow rate $m_{tot,design}$. If the calculation resulted in a value smaller than the minimum value or greater than the maximum value, the total airflow rate m_{tot} was reset to the minimum or maximum value accordingly.

   d. The secondary airflow rate was calculated:

$$m_{sec} = m_{tot} - m_{pri} \tag{7.32}$$

   e. The temperature of the mixed air was calculated:

$$T_{mix} = \frac{m_{pri} T_{pri} + m_{sec} T_{sec}}{m_{tot}} \tag{7.33}$$

   f. The temperature at the FPTU fan outlet with the fan temperature rise was calculated:

$$T_{f,out} = T_{mix} + \frac{Pow_{fan}}{m_{tot} C_p} \tag{3.34}$$

   g. The energy input to the heating coil was calculated according to Equation 7.7.

4. Cooling mode

   If the zone load was greater than the higher limit of $Q_{cooling,deadband}$, the FPTU is in cooling mode.

   a. In cooling mode, the heating coil was switched off.

   b. The primary and total airflow at the design cooling load was determined.

   The logic in this mode linearly increased the primary and total airflows from the values in deadband to the values at the design cooling load as the zone cooling load increased.

The total airflow at the design cooling load $m_{tot,design}$ was known from the previous sizing calculation, while the primary airflow at the design cooling load $m_{pri,design}$ varied with the primary air temperature. In systems with a primary air temperature at or close to 55°F (12.8°C), the secondary airflow could be zero at the design load, which meant the primary airflow should be equal to the design airflow at the design cooling load. However, for systems with a primary air temperature in a range of 45 to 48°F (7.2 to 8.9°C), the minimum secondary airflow cannot go to zero because a certain amount of warmer secondary air was required to maintain the prescribed value $T_{out,design}$ for preventing condensation on supply registers and air diffusers. In this case, the secondary airflow at the design cooling load was calculated as

$$m_{sec,design} = m_{tot,design} \cdot \frac{T_{mix,design} - T_{pri}}{T_{sec} - T_{pri}} \tag{7.35}$$

where $T_{mix,design}$ was the mixing temperature at the design cooling load and can be calculated from the user-defined $T_{out,design}$ along with the FPTU fan power consumption

$$T_{mix,design} = T_{out,design} - \frac{Pow_{fan}}{m_{tot,design} \cdot C_p} \tag{7.36}$$

Then, the primary airflow at the design cooling load $m_{pri,design}$ can be calculated as

$$m_{pri,design} = m_{tot,design} - m_{sec,design} \tag{7.37}$$

c. The secondary airflow rate as a function of zone cooling load was derived.

Once the primary airflow at the design cooling load was known, the minimum primary airflow $m_{pri,deadband}$ and the maximum primary airflow $m_{pri,design}$ can be connected by using a straight line, which correlated the minimum cooling load $q_{cooling,deadband}$ and the maximum cooling load $q_{zs,design}$ respectively. Therefore, at any given zone cooling load, the corresponding primary airflow can be interpolated from the straight line

$$\frac{m_{pri,deadband} - m_{pri,design}}{q_{cooling,deadband} - q_{zs,design}} = \frac{m_{pri,deadband} - m_{pri}}{Q_{cooling,deadband} - q_{zs}} \tag{7.38}$$

In a similar approach, a straight line can be drawn between the minimum total airflow $m_{tot,deadband}$ at $q_{cooling,deadband}$ and the maximum total airflow $m_{tot,design}$ at $q_{zs,design}$. Hence, the total airflow at any given zone cooling load can be interpolated from the straight line

$$\frac{m_{tot,deadband}-m_{tot,design}}{q_{cooling,deadband}-q_{zs,design}} = \frac{m_{tot,deadband}-m_{tot}}{q_{cooling,deadband}-q_{zs}} \quad (7.39)$$

It was important to know that the total and primary airflows were bounded by the prescribed airflow limits. For example, the total airflow at any zone cooling load cannot go above the design airflow. Similarly, the calculated primary airflow cannot be greater than the total airflow at any zone cooling load.

d. The secondary airflow at any given zone load was calculated.

After the primary and total airflows were determined, the secondary airflow can be readily calculated as

$$m_{sec} = m_{tot} - m_{pri} \quad (7.40)$$

7.1.9 Sample Results For demonstration purposes, the performance of a series FPTU was estimated by using the mass and energy balance approach and the empirical curves for ECM fan/motor power consumption. As a first step, a series of input data were created, including zone sensible loads, zone set-point temperature, zone design load, primary air temperature, and secondary air temperature. The series FPTU was sized by using a design zone cooling load of 39000 Btu/h (11.43 kW). In order to show the operation in heating, cooling, and deadband operations, the zone sensible load was allowed to vary from -40,000 to 40,000 Btu/h (-11.73 to 11.73 kW) by using an arbitrary incremental change of 479 Btu/h (0.14 kW), with negative values indicating heating loads and positive values indicating cooling loads. At each zone sensible load, a constant zone set-point temperature of 78°F (25.6°C) was maintained. Also, two primary air temperatures of 55°F (12.8°C) and 45°F (7.2°C) were used for the series FPTU performance prediction with a constant secondary air temperature being 82°F (29.4°C). The higher primary air temperature of 55°F (12.8°C) represents a VAV system that uses a direct expansion (DX) coil as the primary cooling coil, while the lower primary air temperature of 45°F (7.2°C) would represent a VAV system that uses a chilled water coil as the primary cooling coil. It should be noted that the above input parameters, namely zone sensible loads, zone set-point temperature, zone design load, primary air temperature, and secondary air temperature, are user-defined parameters and can be modified for different applications and systems. For example, the secondary air temperature T_{sec} is defined based on the zone set-point temperature T_z and a temperature increase ΔT.

$$T_{sec} = T_z + \Delta T \quad (7.41)$$

A typical input for the temperature increase ΔT is in a range of 0 to 4 °F (0 to 2°C).

The system level calculation began with reading the input data, then determined the operating mode based on the zone sensible load. In each operating mode, namely off, deadband, heating, and cooling, the series FPTU operated in the way as described earlier. Results from each mode merged in solving for the return air loop of the complete VAV system. The mixing temperature of the return air and the outdoor air was used to determine whether or not preheating was required. If the mixing temperature was below the primary air temperature then the preheating coil was used to heat the mixed air to the primary air temperature. The procedure then calculated the power consumption of the primary fan and proceeded to calculate the cooling energy required at the primary cooling coil. If there was another hour then the procedure looped back to the start. Otherwise, the procedure was completed.

By using the system level calculation procedure as discussed above, results of airflow and discharge temperature from a series FPTU were calculated and plotted against the zone sensible load in Figures 7.3 to 7.6. Figures 7.3 and 7.4 showed the primary, secondary, and total airflow variations with the zone sensible load for cases with 55°F (12.8°C) and 45°F (7.2°C) primary air.

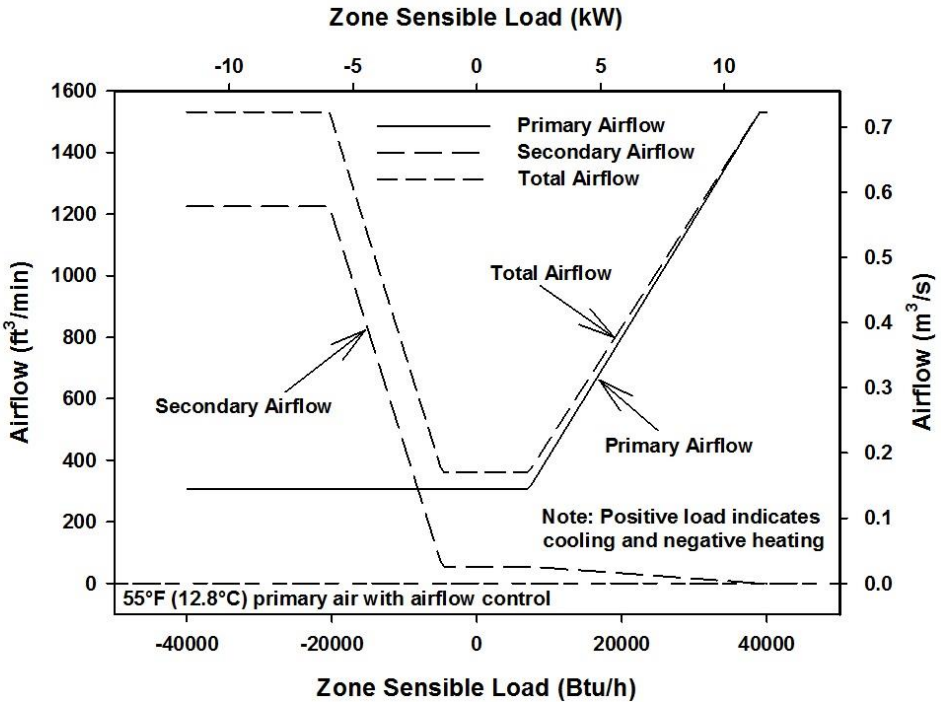

Figure 7.3: Airflow Results with 55°F (12.8°C) Primary Air by Using Airflow Control Approach

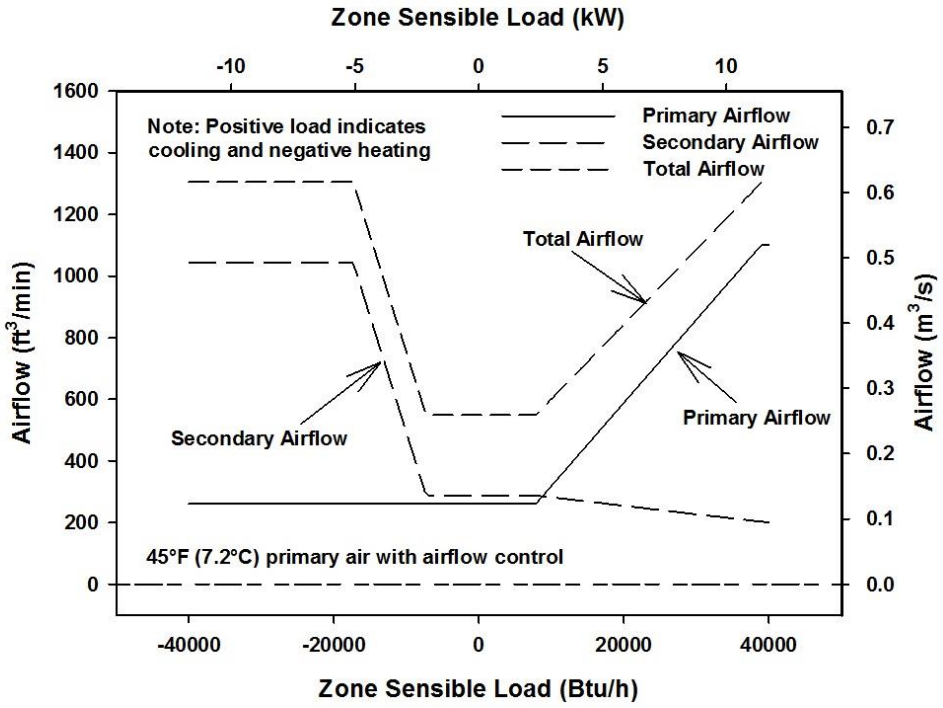

Figure 7.4: Airflow Results with 45°F (7.2°F) Primary Air by Using Airflow Control Approach

In heating mode, the primary airflow was set to the minimum, which was assumed to be 20% of the design airflow for these sample calculations. The secondary and total airflow varied with the zone heating load. When the zone heating load exceeded the maximum supplemental heating capacity, the secondary and total airflow were maintained as constant regardless of zone load. As the zone heating load decreased, the secondary air was decreased proportionally until reaching the lower end of the deadband. In deadband region, both primary and secondary airflows were maintained constant, with the primary airflow was held at 20% of the design airflow. The secondary airflow in the deadband region depended on the user-defined discharge temperature $T_{out,deadband}$. For the case of 55°F (12.8°C) primary air, the user-defined discharge temperature was 60°F (15.6°C). For the case of 45°F (7.2°C) primary air, a higher user-defined discharge temperature of 65°F (18.3°C) was selected. Once the user-defined deadband discharge temperature was determined, the secondary airflow in the deadband region could be calculated by using Equation 7.21. In this example, the secondary airflow rates in the deadband region were 55 ft^3/min (0.03 m^3/s) and 287 ft^3/min (0.14 m^3/s) for cases with 55°F (12.8°C) and 45°F (7.2°C) primary air, respectively.

In cooling mode, the primary and total airflows were increased linearly with increasing zone cooling load until reaching the design or maximum airflow. The secondary airflow decreased linearly as the zone cooling load increased. For the case of 55°F (12.8°C) primary air, the secondary air was decreased from 55 ft^3/min (0.03 m^3/s) in the deadband region to zero at the design cooling load. The primary air was increased from the assumed minimum of 20% at the deadband to the maximum of 100% of the design airflow rate at the design cooling load. For the case of 45°F (7.2°C) primary air, rather than continuously increasing the primary airflow to the design airflow at the design cooling load, the primary air at 45°F (7.2°C) required mixing of secondary air at the higher end of the cooling load range to maintain a high enough air discharge temperature from the FPTU to avoid condensation on the registers. For the example of 45°F (7.2°C) primary air in Figure 7.4, a secondary airflow rate of 200 ft^3/min (0.09 m^3/s) was maintained at the design cooling load with the purpose of maintaining a discharge temperature of 51°F (10.6°C).

Figures 7.5 and 7.6 show the discharge temperatures resulting from using 55°F (12.8°C) and 45°F (7.2°C) primary air over the entire range of the zone sensible load.

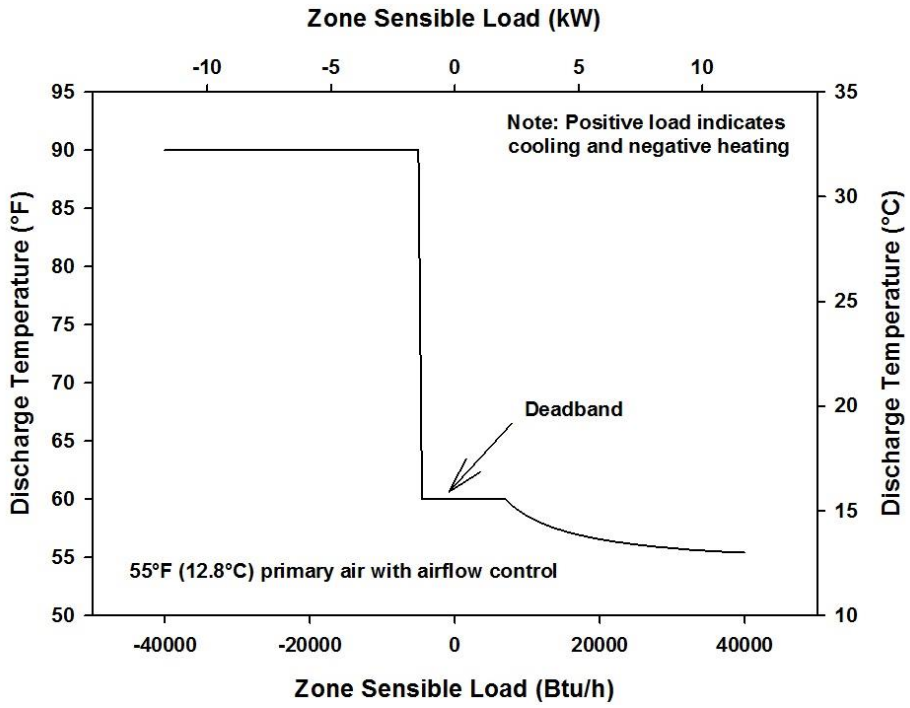

Figure 7.5: Discharge Temperature with 55°F (12.8°C) Primary Air by Using Airflow Control Approach

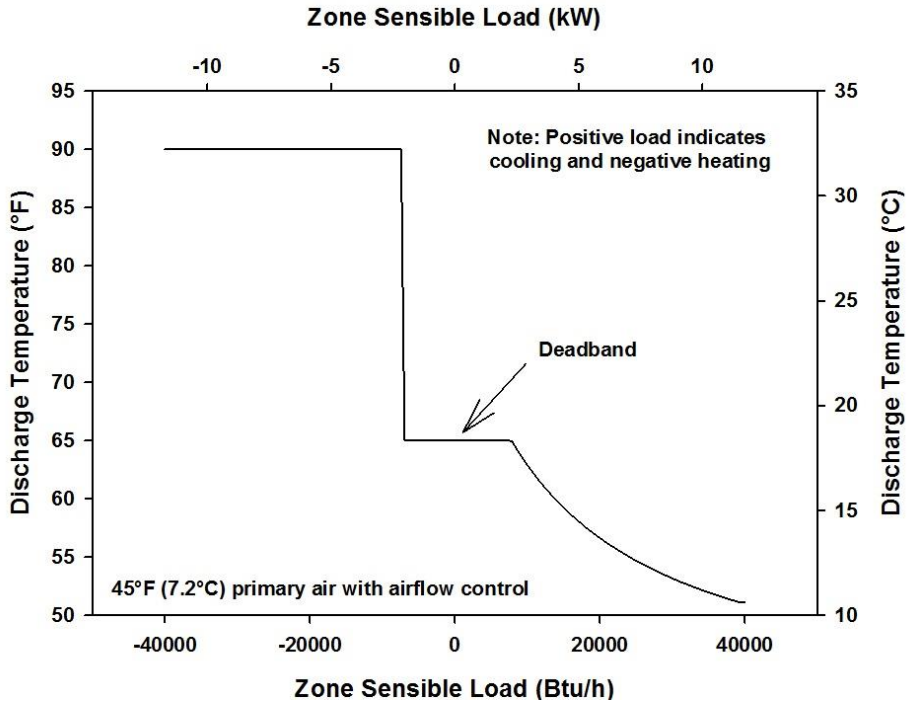

Figure 7.6: Discharge Temperature with 45°F (7.2°C) Primary Air by Using Airflow Control Approach

In heating mode, the discharge temperature in both cases was limited to 90°F (32.2°C). With a constant discharge temperature of 90°F (32.2°C), the zone heating load was satisfied by varying the amount of total airflow delivered to the zone, as was shown in Figures 7.3 and 7.4. The constant discharge temperature of 90°F (32.2°C) was maintained until the lower limit of the deadband region was reached. A sharp temperature drop then occurred due to switching off the heating coil. The discharge temperature in the deadband region was constant and was a user-defined input parameter that was used to determine the deadband secondary airflow rate. In this example, 60°F (15.6°C) and 65°F (18.3°C) were selected for cases with 55°F (12.8°C) and 45°F (7.2°C) primary air temperatures, respectively. As a result of increasing the zone cooling load, the discharge temperature continuously decreased in a nonlinear manner regardless of primary air temperatures. Capturing this nonlinear variation in discharge air temperature with respect to the zone cooling load is important to control and/or application engineers, who can use this nonlinear relation to develop airflow control sequences for better thermal comfort.

7.1.10 Discharge Temperature Control Approach The discharge temperature control modeling approach had the same operating sequences in the off, deadband, and heating regions as the airflow control modeling approach that was discussed earlier. The only difference was the

operations in the cooling region. Recall that in the airflow control modeling approach, the primary and total airflows increased linearly with increasing zone cooling loads. In contrast, with the temperature control modeling approach, the discharge temperature decreased linearly by adjusting the mixing ratio of primary and secondary air as the zone cooling load increased. Similar to the airflow approach, the logic of the performance calculation of the temperature control approach began with sizing a series FPTU, followed by determining the airflows and load limits in the deadband region. The calculation then depended on the operational mode of the FPTU. Because the temperature control approach had the identical operating sequence in off, deadband, and heating regions as in the airflow control approach, there was no need to repeat the logic in these modes. The logic for cooling mode is described below.

When the series FPTU was in cooling mode:

a. The heating coil was switched off.

b. The discharge temperature as a function of zone cooling load was determined.
In temperature control modeling approach, the discharge temperature was linearly decreased from the highest value, which was the discharge temperature in deadband $T_{out,deadband}$, to the lowest value, which was the discharge temperature at the design condition $T_{out,design}$, as the zone cooling load increased. By correlating $T_{out,deadband}$ and $T_{out,design}$ with the lower and higher limits of cooling range respectively, the discharge temperature can be correlated with the zone cooling load through a straight line. Therefore, a unique discharge temperature at any given zone cooling load can be determined from the following:

$$\frac{T_{out,design}-T_{out,deadband}}{q_{zs,design}-q_{cooling,deadband}} = \frac{T_{out,deadband}-T_{out}}{q_{cooling,deadband}-q_{zs}} \quad (7.42)$$

If the calculated T_{out} is lower than the $T_{out,design}$, as a result of a greater q_{zs} than $q_{zs,design}$, T_{out} will be reset to the value of $T_{out,design}$.

c. The total airflow rate was calculated.
Once the discharge temperature at any given zone cooling load was determined, the total airflow m_{tot} that was required to meet the zone load can be calculated:

$$m_{tot} = \frac{Q_{zs}}{C_p \cdot (T_z - T_{out})} \quad (7.43)$$

As before, if the calculated m_{tot} was greater than the design airflow $m_{tot,design}$, the m_{tot} would be reset to the value of $m_{tot,design}$.

d. The mixing temperature of primary and secondary airflow was calculated.

The mixing temperature can be calculated:

$$T_{mix} = T_{out} - \frac{Pow_{fan}}{m_{tot} \cdot C_p} \quad (7.44)$$

e. The primary and secondary airflow was calculated.

The primary airflow can be calculated:

$$m_{pri} = m_{tot} \cdot \frac{T_{mix} - T_{sec}}{T_{pri} - T_{sec}} \quad (7.45)$$

The secondary airflow can then be calculated:

$$m_{sec} = m_{tot} - m_{pri} \quad (7.46)$$

7.1.11 Sample Results from the Model As before, the series FPTU performance was estimated by using the temperature control modeling approach, and results were plotted against the zone sensible load in Figures 7.7 to 7.10 for demonstration purpose. The input parameters, such as zone sensible loads, zone set-point temperature, zone design load, primary air temperature, and secondary air temperature remained the same as were used in the airflow control modeling approach.

Figures 7.7 and 7.8 showed the primary, secondary, and total airflow variations responding to zone sensible load changes for cases with 55°F (12.8°C) and 45°F (7.2°C) primary air, respectively.

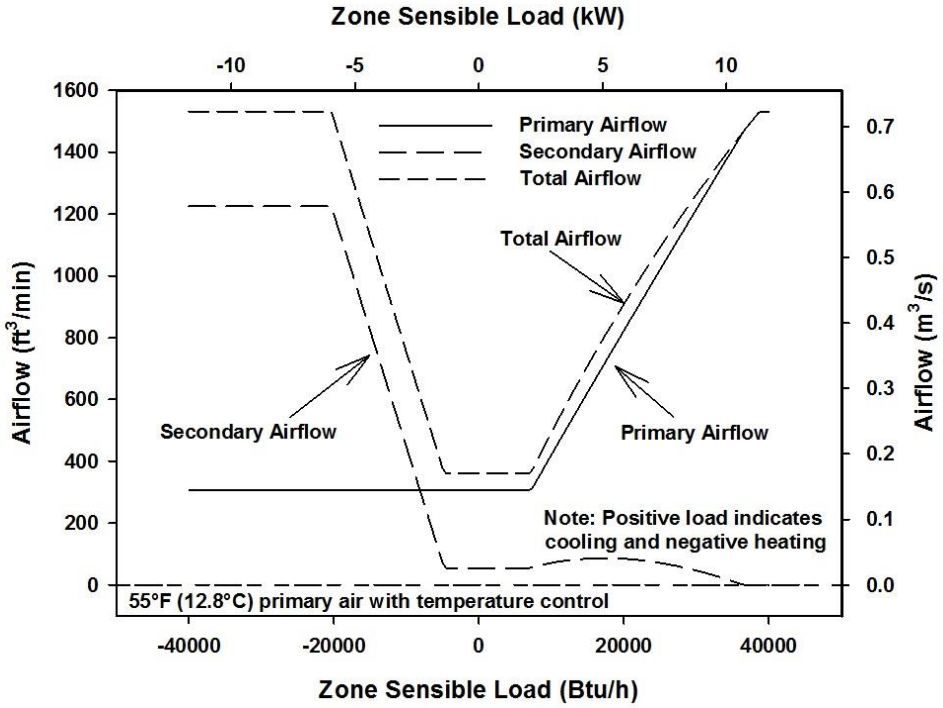

Figure 7.7: Airflow Results with 55°F (12.8°C) Primary Air by Using Temperature Control Approach

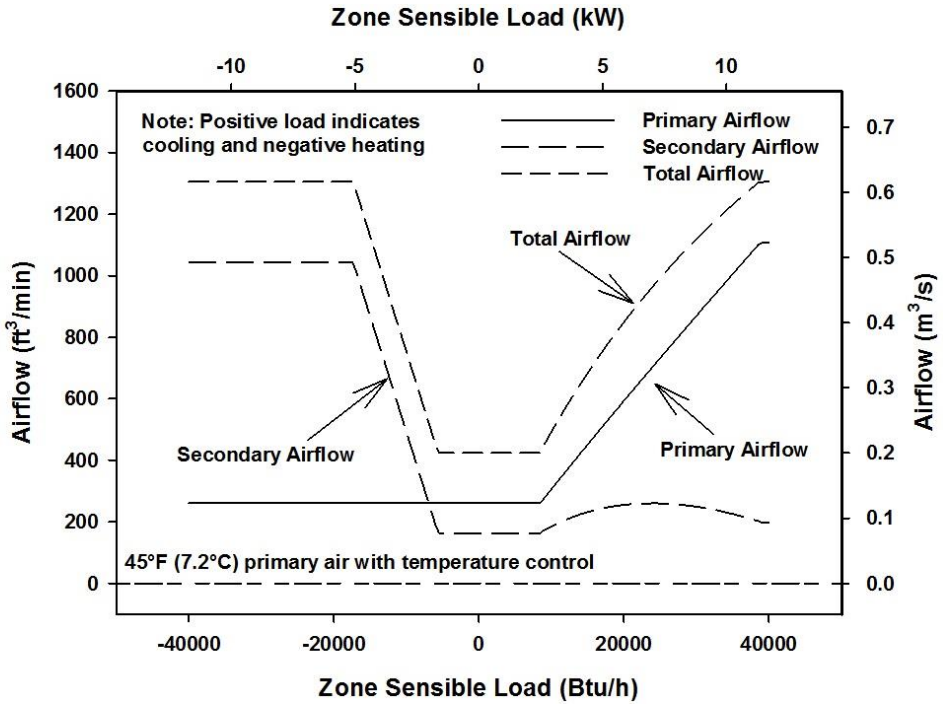

Figure 7.8: Airflow Results with 45°F (7.2°C) Primary Air by Using Temperature Control Approach

Comparing these two figures with Figures 7.3 and 7.4, the main difference were in the shapes of the total and secondary airflows with respect to the zone cooling load. Unlike the linear decrease in secondary air in cooling mode as shown in Figures 7.3 and 7.4, the total and secondary airflow variations were nonlinear with respect to the zone cooling load. As discussed earlier, these nonlinear trends resulted from the application of the energy and mass balance equations with a linear discharge temperature profile. The secondary airflow in both Figures 7.7 and 7.8 first increased from the deadband region with increasing zone cooling load and then decreased until the zone cooling load reached the maximum of 40,000 Btu/h (11.72 kW). The secondary airflow rates at the higher end of the cooling load range depended on the value of the primary air temperature. In the case of 55°F (12.8°C) primary air temperature, the secondary airflow reached its minimum of zero at the design cooling load of 39,000 Btu/h (11.43 kW) and maintained this minimum value to the maximum load of 40,000 Btu/h (11.72 kW). For the case of 45°F (7.2°C) primary air temperature, a non-zero secondary airflow rate was maintained over the entire cooling load range. This distinct performance difference was caused by the need to mix warmer secondary air with the primary air at high cooling loads to prevent condensation when the primary air temperature is in a range of 45 to 48°F (7.2 to 8.9°C). The nonlinear variation in the secondary airflow also resulted in nonlinear variations in the total airflow. Whether the secondary airflow in the field varied like that in Figures 7.3 and 7.4 or Figure 7.7 and 7.8 can't be known directly, because the secondary air was neither directly controlled nor measured. In both sets of plots, the secondary air was inferred from the mass and energy balances.

Figures 7.9 and 7.10 showed the results of discharge temperature over a range of zone sensible loads with respect to 55°F (12.8°C) and 45°F (7.2°C) primary air temperatures.

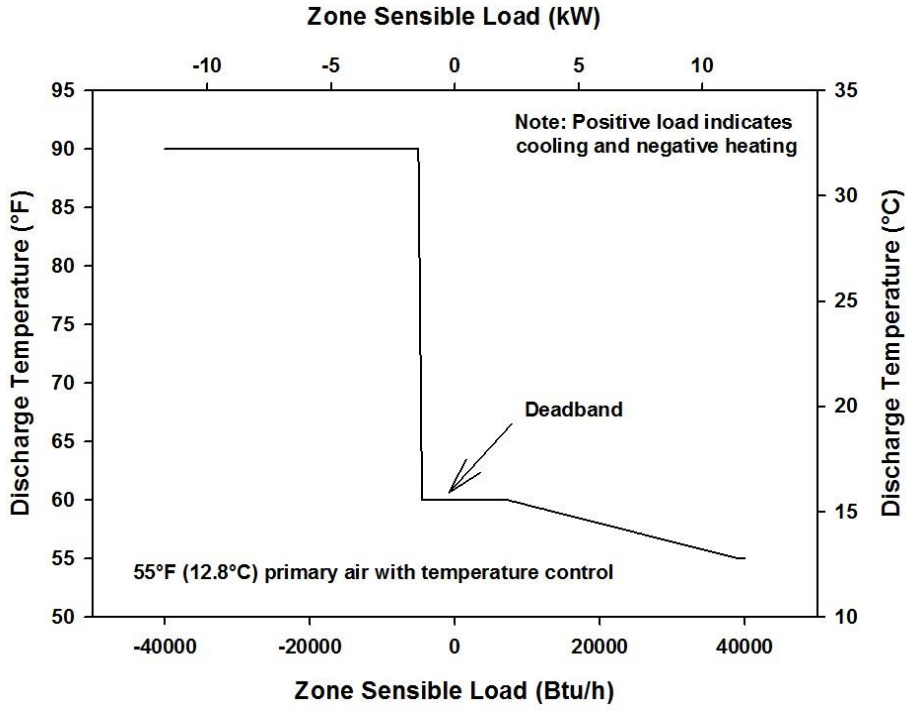

Figure 7.9: Discharge Temperature with 55°F (12.8°C) Primary Air by Using Temperature Control Approach

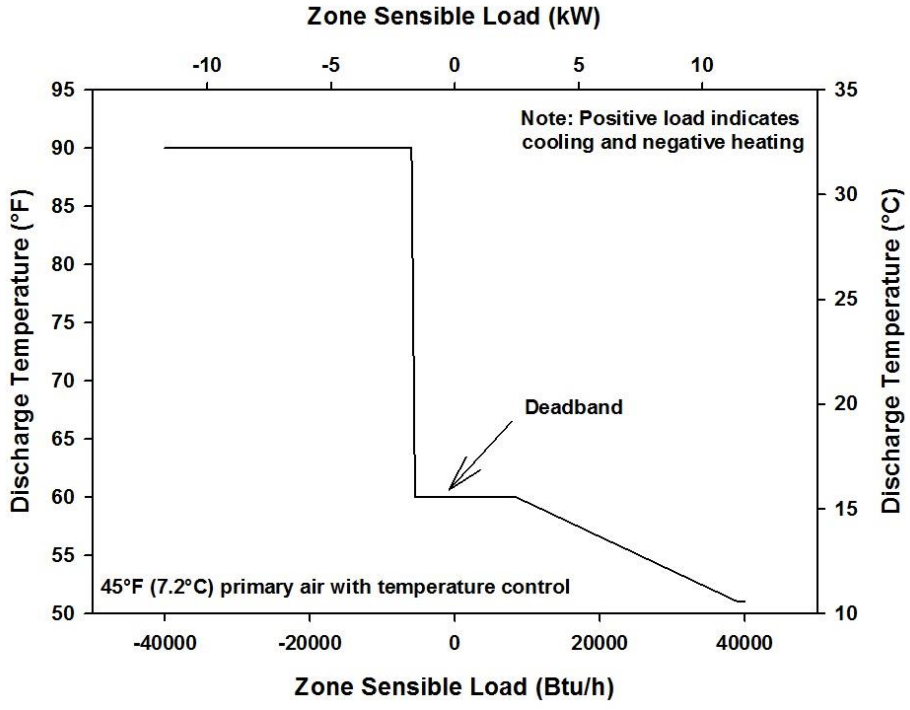

Figure 7.10: Discharge Temperature with 55°F Primary Air by Using Temperature Control Approach

The discharge temperature was constant in both heating and deadband modes regardless of the primary air temperature, with the temperature being 90°F (32.2°C) in heating mode and a user-defined value of 60°F (15.6°C) in deadband mode. Compared with Figures 7.5 and 7.6, the discharge temperature in Figures 7.9 and 7.10 decreased proportionally from 60°F (15.6°C) in the deadband region to the design discharge temperature as the zone cooling load increased, which was consistent with the described logic of temperature control modeling approach. At cooling loads above the design cooling load of 39,000 Btu/h (11.43 kW), the discharge temperature was a constant of 55°F (12.8°C) for 55°F (12.8°C) primary air and 51°F (10.6°C) for 45°F (7.2°C) primary air without further decreases.

7.2. Parallel FPTUs

Figure 7.11 shows a traditional parallel FPTU with its major components: mixer, fan/motor, and heating coil. An analysis needed to be performed on each component in the FPTU to estimate overall airflows (or mass flows) into and out of the FPTU as well as the energy used by the FPTU fan/motor for each time step of a simulation.

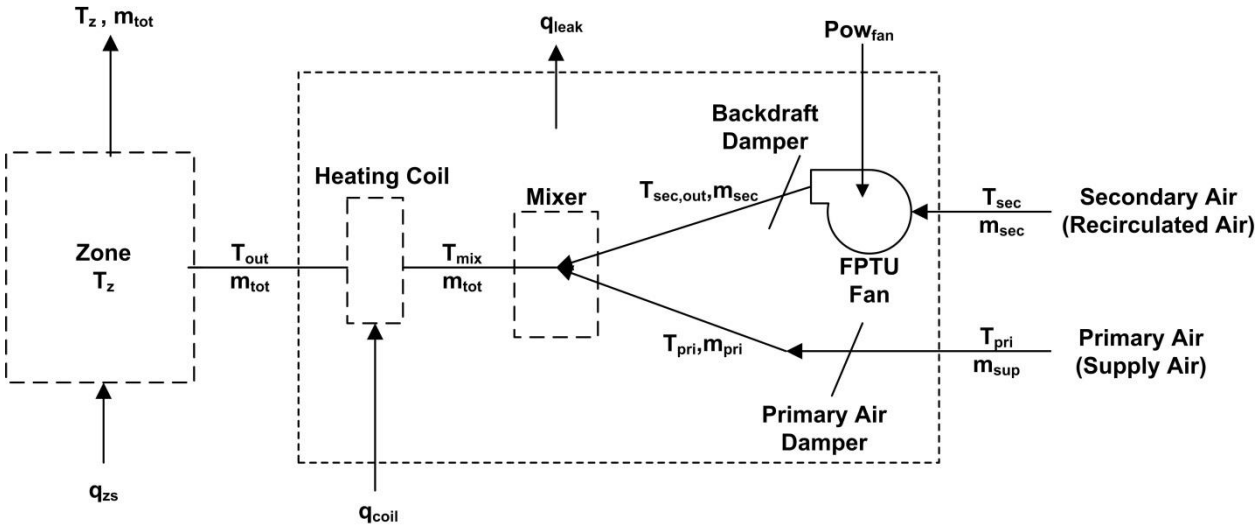

Figure 7.11: Traditional Parallel FPTU with Heating Coil Located after the Mixing of the Primary and Secondary Airflows

An alternate configuration of the traditional parallel FPTU moved the heating coil to the secondary air inlet as shown in Figure 7.12. This configuration provided an advantage over the traditional configuration of Figure 7.11 in that the heating coil is outside the primary airstream

where it adds to the pressure drop of the primary airstream. The added pressure drop had to be overcome by a slight pressure increase produced by the central air handling unit providing the primary air. One potential disadvantage of the alternate configuration was that the fan motor was located downstream of the heating coil and would be subjected to a higher air temperature than in the traditional configuration when the heating coil is engaged.

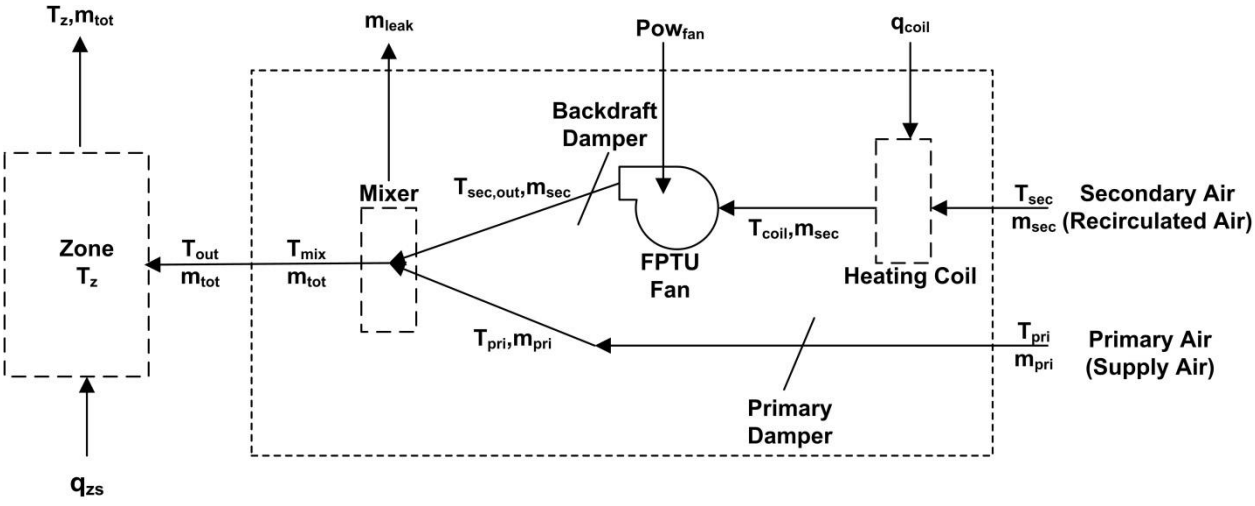

Figure 7.12: Parallel FPTU in Alternate Configuration where the Heating Coil is Located in the Secondary Airstream

For the control volume around the FPTU, energy was input to the FPTU via electrical energy to the fan, heat energy to the heating coil, and energy associated with the primary and secondary airstreams. The only mass and energy leaving the FPTU was with the airstream at the discharge of the FPTU and leakage from the housing.

The same basic assumptions used to develop the MEB models of the fixed airflow parallel FPTU in Chapter 6 were also applied here. First, the systems in Figure 7.11 and Figure 7.12 were assumed to operate at quasi-steady state during each time step. Second, the thermo-physical properties were assumed constant. Third, the energy input to the fan motor was assumed to be completely converted into the heat energy in the airstream. Fourth, the FPTU always operated with a minimum amount of primary air to ensure enough fresh air into the zone.

For the control volume shown in Figure 7.11, the mass balances entering the system included the primary and secondary airstreams. The only mass exiting the control volume was in the total airflow. A mass balance on the control volume yielded:

$$m_{tot} + m_{leak} = m_{pri} + m_{sec} \quad (7.47)$$

Leakage must be included because the housing was at a positive pressure with respect to the plenum air pressure for parallel units.

The energy transfer into the control volume included the energy provided by the primary and secondary airstreams, energy input into the heating coil, the energy leaving by leakage, and the power input into the fan:

$$m_{tot}h_{out} + m_{leak}h_{leak} = q_{coil} + Pow_{fan} + m_{pri}h_{pri} + m_{sec}h_{sec} \quad (7.48)$$

Equations 7.47 and 7.48 provided the basic equations that described the overall mass and energy balances for the parallel FPTU. The unknowns in these equations varied depending on the mode of operation (heating, cooling, or deadband) of the FPTU. Solving for the unknowns required applying mass and energy balances to each of the components in the FPTU. The process typically started from the left at the FPTU discharge to the zone and moved to the right to the primary and secondary air inlets.

For cooling operations, the FPTU fan was off and the primary air damper was used to vary the amount of primary air that flows through the FPTU. The term m_{tot}, shown in Equations 7.47 and 7.48, was the total airflow delivered to the space. In heating operations, the total airflow was the sum of the primary and secondary airflows minus leakage. In cooling operations, the total airflow was the primary airflow minus leakage airflow. The secondary airflow varied to meet the heating load. In cooling mode, the total airflow was determined from the load in the zone. Additional primary air must be provided equal to the amount of air leaking out of the FPTU cabinet, m_{leak}. The primary airflow from the FPTU should not drop below a certain percentage (typically 10 to 30%) of the airflow needed at the design cooling load (ICC 2010, ASHRAE 2013). This minimum amount of primary air was used to maintain fresh air requirements in the zone. Zhang et al (2014) found that minimum primary airflows as low as 10% might still provide acceptable indoor air quality in some applications in California.

The left hand terms of Equation 7.48 were the energy leaving the FPTU in the airstream either by discharge or leakage. The energy input into the FPTU included heat energy input in the heating coil, power input to the fan (which is assumed to be converted into heat energy in the airstream), and energy being carried into the FPTU by both the primary and secondary airstreams. With constant properties assumed, the enthalpies, h, can be rewritten as the product of specific heat, $c_{p,}$ and temperature, T:

$$m_{tot}\, c_p T_{out} + m_{leak} c_p T_{mix} = q_{coil} + Pow_{fan} + m_{pri}\, c_p T_{pri} + m_{sec}\, c_p T_{sec} \quad (7.49)$$

7.2.1 Energy Balance of the Alternate Configuration The alternate configuration (see Figure 7.12) had the heating coil location at the secondary airstream inlet. A mass balance on the control volume yielded the same result as was derived for the traditional configuration in Equation 7.47. Likewise, an energy balance on the alternate configuration FPTU yielded the same energy equation found in Equation 7.49. From a simple mass and energy balance on the whole FPTU, the change in location yielded the same mass and energy equations. The differences between the two configurations was discussed in Chapter 6.

7.2.2 Zone Analysis The analysis of FPTU performance started with an evaluation of the zone, which was on the far left side of the FPTU schematic shown in either Figure 7.11 or Figure 7.12. Typically the zone load was known and either the value of m_{tot} or the value of T_{out} must be calculated. An energy and mass balance on the zone yielded the following:

$$q_{zs} = m_{tot} c_p (T_z - T_{out}) \quad (7.50)$$

During cooling operations, the discharge temperature, T_{out}, was the same as the primary air temperature because all air was provided by the primary airstream. With the cooling load on the zone, q_{zs}, and T_{out} known, Equation 7.50 can be used to solve for the total airflow, m_{tot}. The total airflow decreased as the cooling load decreased, but could not go below the minimum airflow set by fresh air requirements in the zone. During heating and deadband operations, the amount of primary airflow was fixed by the minimum fresh air requirements. In heating, the secondary airflow and temperature were varied to meet the heating requirements in the zone. The secondary airflow temperature was usually not increased more than 15°F (8.3°C) above the zone set-point temperature. When the secondary airflow was at a maximum, then m_{tot} was fixed.

7.2.3 *Heating Coil (Traditional Location)* An energy balance can be applied to the heating coil in the traditional location in Figure 7.11. The energy entering the coil was the sum of energy input, q_{coil}, either from electric resistance or hot water, and the energy from the air entering the coil from the discharge of the FPTU fan. The energy exiting the coil was carried by the air leaving the coil and used to condition the zone. The variable of interest was the heating energy input. An energy balance yielded:

$$q_{coil} = m_{tot} c_p (T_{out} - T_{mix}) \quad (7.51)$$

The analysis for the heating coil for the alternate configuration was similar to that for the traditional configuration. However, the airflow in and out of the heating coil was the secondary

airflow and not the total airflow. The temperature into the coil was the secondary air temperature, T_{sec}, and the outlet temperature from the coil was T_{coil} (See Figure 7.12). The coil energy balance yielded:

$$q_{coil} = m_{sec} c_p (T_{coil} - T_{sec}) \tag{7.52}$$

These two equations represented the energy balance on the heating coil for either the traditional or alternate configurations.

7.2.4 Fan The FPTU fan was located in the secondary airstream for both the traditional and alternate configurations. Because of the presence of the heating coil in the airstream before the fan in the alternate configuration, the terminology was slightly different for each configuration. The electrical energy input to the fan for a given time step was represented by Pow_{fan}. For the traditional configuration (7.11), the temperature of the air at the inlet of the fan was T_{sec}. For the alternate configuration (7.12), the temperature of the air at the fan inlet was given by T_{coil}, the outlet temperature of the heating coil. The energy exiting the fan was carried by the air leaving the fan and entering the mixer. The exit temperature was given by $T_{sec,out}$ for both configurations (Figures 7.11 and 7.12). It was assumed that all of the power input into the fan was converted into heat energy. Assuming constant properties, an energy balance on the fan yielded the following for the power of the fan in the traditional configuration:

$$Pow_{fan} = m_{sec} c_p \left(T_{sec,out} - T_{sec}\right) \tag{7.53}$$

For the alternate configuration, the energy input to the fan was given by:

$$Pow_{fan} = m_{sec} c_p \left(T_{sec,out} - T_{coil}\right) \tag{7.54}$$

7.2.5 Mixer The mixing temperature, T_{mix} from the secondary and primary airflows is an important variable needed in the modeling the FPTU. Mass flows into the mixer included the primary and secondary airflows. If leakage was assumed to occur in the region of the mixing in the main chamber of the FPTU, then the total airflow leaving the FPTU was just the sum of the total airflow in minus the leakage out of the FPTU.

$$m_{tot} = m_{pri} + m_{sec} - m_{leak} \tag{7.55}$$

The energy entering the mixer was from the primary and secondary airstreams when in heating mode. In cooling operations, there was no secondary airflow; therefore, the mixing temperature was equal to the primary air temperature. The energy exited the mixer in the total airstream and moved to the heating coil. The mixer was assumed to perform adiabatic mixing so no heating energy was lost to the surroundings. An energy balance on the mixer yielded:

$$m_{tot}c_pT_{mix} = m_{pri}\,c_pT_{pri} + m_{sec}c_pT_{sec,out} - m_{leak}c_pT_{mix} \quad (7.56)$$

Leakage from the FPTU was assumed to occur at the mixed temperature of the primary and secondary airstreams. In cooling, there was no secondary airstream, so the mixed air temperature would be the same as the primary air temperature. With the mass and energy equations, we should have two equations and two unknowns that can be solved to give values for m_{pri} and T_{mix} as long as we know the amount of leakage. The solution can proceed for the contribution of the fan. Fan models that allowed for direct calculation of fan power were described in Chapter 3. With the fan power calculated, Equation 7.53 or 7.54 can be solved for the temperature leaving the fan and entering the mixer, $T_{sec,\,out.}$ The final step was to solve for the energy input of the heating coil in either Equation 7.51 or 7.52. All other variables in the equation have been calculated so the value of q_{coil}, can be calculated.

7.2.6 Leakage Analysis Leakage data from Edmondson et al (2011b) was analyzed in Chapter 5. Leakage can be represented as a percentage (or fraction) of the primary airflow.

$$f_{leakc} = \frac{m_{leak}}{m_{pri}} \quad (7.57)$$

The leakage fraction term had a "c" designation to indicate that this was a cooling leakage. The leakage in heating can be different than that for cooling. The FPTUs were divided into three leakage classifications: low, medium, and high. Table 7.2 lists the average percentage leakages at two downstream static pressures from the analysis in Chapter 5.

Table 7.2 - Average Leakage Airflow at Two Downstream Static Pressures and the Three Leakage Classifications

Leakage Classification	Leakage as Percent of Primary Airflow	
	@0.25 in w.g. (62 Pa)	@0.50 in w.g. (125 Pa)
Low	2.4%	3.5%
Medium	4.8%	6.2%
High	11.6%	14.8%

The values in Table 7.2 were collected with the FPTU fan off, the backdraft damper closed, and only primary air used in the FPTU. This condition simulated cooling operations for a

parallel FPTU. These data were directly applicable to cooling mode operations when simulating a FPTU. With the secondary airflow equal to zero, the cooling leakage fraction in Equation 7.57 can be substituted into the mass balance for the FPTU in Equation 7.55 to yield:

$$m_{tot} = m_{pri} - m_{leak} = m_{pri}(1 - f_{leakc}) \quad (7.58)$$

The total airflow, m_{tot}, was calculated from the cooling load on the zone. Equation 7.58 can be rearranged to provide an estimate of the amount of primary air needed when there was leakage:

$$m_{pri} = \frac{m_{tot}}{1 - f_{leakc}} \quad (7.59)$$

This equation showed that additional primary air was needed in cooling operations to provide the same amount of total airflow (m_{tot}) to the zone when there was leakage from the FPTU. This additional air had to be provided by the main air handler, which meant leakage created a direct energy penalty on the air handler because it had to provide the additional air to the FPTU.

There were also indirect impacts of leakage on the performance. Leakage in cooling operations introduced cold primary air into the return airstream and decreased the air temperature in the plenum. If the FPTU shared a common plenum with other FPTUs, and some of those were in heating or deadband operations, then the colder plenum air reduced the heating benefit from blending plenum (secondary) air with the primary air and required additional heating when supplemental heating was used. Most of the return air was eventually mixed with outdoor air that was then sent to the air handler and primary cooling coil. Leakage in cooling operation reduced the return air temperature. Thus, it should also reduce the temperature of the air returned to the primary cooling coil and reduce the load on the cooling coil. With the alternate FPTU configuration, leakage during heating operations would provide warm air to the plenum space. Quantifying the penalty or benefit of these indirect impacts of leakage would require a full air conditioning system model.

Without definitive leakage data during heating operations, we proposed to use a simple fraction (or percentage), f_{leakh}, to describe the leakage in a way similar to what was used for cooling.

$$f_{leakh} = \frac{m_{leak}}{m_{pri} + m_{sec}} \quad (7.60)$$

Both the primary and secondary airflows were included in the denominator because both flows were active during heating and deadband operations. This equation can be substituted back into the mass balance (Equation 7.55) for the mixing to yield:

$$m_{tot} = m_{pri} + m_{sec} - m_{leak} = (m_{pri} + m_{sec})(1 - f_{leakh}) \quad (7.61)$$

If the leakage was known to be due to seams and penetrations, then the fraction of leakage for heating should be assumed to be the same as that for cooling. However, if the leakage was due entirely to the backdraft damper, then the fraction leakage in heating should be set to zero or have a smaller value than for cooling.

7.2.7 Estimating Fan Power Estimating FPTU fan energy required estimating the fan power, Pow_{fan}, for each timestep in a simulation. The same model used for estimating fan power for variable airflow ECM FPTUs earlier in this chapter was also used here. Therefore, the model was not repeated here.

7.3. Calculation Procedure for Variable Airflow Parallel FPTUs

The performance of variable airflow parallel FPTUs in both the traditional and alternate configurations were estimated by using the component models of the heating coil and mixer that were derived from the mass and energy balances along with the variable speed fan model described above. In this section, an explanation is provided on how the mass and energy balance equations were implemented to model the parallel FPTU performance in the heating, cooling, and deadband modes. In addition, sample results were generated and graphically presented to illustrate how leakage impacts the performance in each mode.

7.3.1 Logic of FPTU Performance Calculation The logic for the performance calculation began with sizing the airflow of a parallel FPTU. The total volumetric flow rate from a parallel FPTU was estimated by using the zone design load q_{design} and the temperature difference between the zone set-point temperature T_z and the primary air temperature T_{pri}. Based on the assumption of constant air density, the design airflow rate was given by:

$$m_{tot,design} = \frac{qz_{\_design}}{c_p \cdot (T_z - T_{pri})} \quad (7.62)$$

Once the design airflow rate was determined, the sum of primary and secondary airflows at any given zone load was capped by the design airflow. If desired, the volumetric airflow rate (often in ft^3/min or m^3/s) can be determined from the air mass flow rate and air density ρ_{air}

$$Q_{tot,design} = \frac{m_{design}}{\rho_{air}} \tag{7.63}$$

The next step was to determine the secondary airflow and zone load limits in the deadband region based on the user-defined deadband discharge temperature $T_{out,deadband}$ that was constrained by field applications. To avoid over-cooling zones, the discharge temperature of FPTUs in the deadband region had to be adjusted to be at least 60°F (15.6°C), which meant a certain amount of secondary air was required to mix with the primary air to produce a higher discharge temperature than the primary air temperature. In the deadband region, the heating coil was switched off, and the primary airflow was set to its minimum to meet fresh air requirements, which was typically 10 to 30% of the design airflow.

$$m_{pri,deadband} = m_{min} \tag{7.64}$$

With a known value of primary air in the deadband region, the specific amount of secondary air that was needed to maintain a higher discharge temperature than the primary air temperature can be calculated

$$m_{sec,deadband} = m_{pri,deadband} \cdot \frac{T_{mix,deadband} - T_{pri}}{T_{sec,out} - T_{mix,deadband}} \tag{7.65}$$

where $T_{mix,deadband}$ was the deadband mixing temperature and was equal to the user-defined deadband discharge temperature

$$T_{out,deadband} = T_{mix,deadband} \tag{7.66}$$

$T_{sec,out}$ was the air temperature at the FPTU fan outlet, which can be calculated as

$$T_{sec,out} = T_{sec} + \frac{Pow_{fan,deadband}}{m_{sec,deadband} \cdot C_p} \tag{7.67}$$

Because both $m_{sec,deadband}$ and $T_{sec,out}$ were unknown, an iteration procedure was required to solve the $m_{sec,deadband}$ and $T_{sec,out}$ simultaneously. This iteration was only required to be performed once for each FPTU in the HVAC system to determine the secondary airflow requirement in the deadband region. After $m_{sec,deadband}$ was determined, the total airflow in the deadband region $m_{tot,deadband}$ then can then be calculated

$$m_{tot,deadband} = (m_{pri,deadband} + m_{sec,deadband}) \cdot (1 - f_{leakh}) \tag{7.68}$$

where f_{leakh} was the leakage ratio for heating mode. With the known total airflow in the deadband region, the zone cooling load representing the upper limit of the deadband was

$$q_{cooling,deadband} = m_{tot,deadband} \cdot C_p \cdot (T_z - T_{out,deadband}) \tag{7.69}$$

while the zone heating load representing the lower limit of the deadband was

$$q_{heating,deadband} = \ m_{tot,deadband} \cdot C_p \cdot (T_z - T_{out,heating})/2 \qquad (7.70)$$

where $T_{out,heating}$ was the prescribed discharge temperature in the heating mode.

Once the airflows and load limits in the deadband region were determined, the FPTU performance calculations depended on different modes of operation, such as off, deadband, cooling, and heating. While the two FPTU configurations for the heating coil (traditional and alternate) shared the same performance calculations in the off, deadband, and cooling modes, the performance calculation in heating mode was different between the two configurations. The logic for each mode is described below:

1. Off mode

   For this mode, the primary and secondary airflows, the FPTU fan, and the heating coil were not operating. Therefore, temperatures throughout the system were set to the zone set-point temperature.

2. Deadband region

   If the zone load was in the range that was defined by the lower limit of $q_{heating,deadband}$ and the higher limit of $q_{cooling,deadband}$, the FPTU was in the deadband region. In this mode, the heating coil was switched off.

   $$q_{coil} = \ 0 \qquad (7.71)$$

   The secondary airflow m_{sec}, primary airflow m_{pri}, and the total airflow m_{tot} were set to the values that were determined from the iterative approach earlier.

   $$m_{sec} = m_{sec,deadband} \qquad (7.72)$$

   $$m_{pri} = m_{pri,deadband} \qquad (7.73)$$

   $$m_{tot} = m_{tot,deadband} \qquad (7.74)$$

   The discharge temperature was set to the user-defined value.

   $$T_{out} = T_{out,deadband} \qquad (7.75)$$

3. Cooling mode

   If the zone load was greater than the higher limit of $Q_{cooling,deadband}$, FPTUs were in the cooling mode. In this mode, the heating coil was switched off as well as the FPTU fan. Therefore, the secondary airflow in the cooling mode was zero.

   $$m_{sec} = 0 \qquad (7.76)$$

   The total airflow that was required to meet the zone sensible load was calculated as:

$$m_{tot} = \frac{q_{ZS}}{c_p \cdot (T_z - T_{pri})} \quad (7.77)$$

If the calculated m_{tot} was greater than the value of $m_{tot,design} \cdot f_{leakc}$, then the value of m_{tot} was set to the value of $m_{tot,design} \cdot f_{leakc}$, where f_{leakc} was the leakage ratio in the cooling mode. The primary airflow was then calculated as:

$$m_{pri} = \frac{m_{tot}}{1 - f_{leakc}} \quad (7.78)$$

4. Heating mode

If the zone load was smaller than the lower limit of $q_{heating,deadband}$, the FPTU was in the heating mode. In this mode, the primary airflow was set at its minimum to satisfy fresh air requirements, while the discharge temperature and the secondary airflow varied with the zone heating load. The heating mode operation differed between the traditional and alternate configurations for the heating coil. Heating operations also varied with the zone heating loads. If the zone heating load was smaller than twice that of $q_{heating,deadband}$, the total airflow was maintained at the deadband level while the discharge temperature T_{out} was gradually increased to $T_{out,heating}$. When the zone heating load was greater than twice that of $q_{heating,deadband}$, the discharge temperature was maintained at $T_{out,heating}$ while the secondary airflow was gradually increased from the deadband level to the maximum that was restricted by $m_{tot,design}$.

a) When the zone heating load was smaller than twice that of $q_{heating,deadband}$, the secondary and total airflow rates were set to the values in the deadband region as shown in Equations 7.72 and 7.74.

For a parallel FPTU in the traditional configuration:

With a known value of secondary airflow, the air temperature at the FPTU fan outlet can be calculated as

$$T_{sec,out} = T_{sec} + \frac{Pow_{fan}}{m_{sec} \cdot C_p} \quad (7.79)$$

The mixing temperature of primary and secondary air was

$$T_{mix} = \frac{m_{pri} T_{pri} + m_{sec} T_{sec}}{m_{pri} + m_{sec}} \quad (7.80)$$

The discharge temperature that was required to satisfy the zone heating load was

$$T_{out} = T_z - \frac{q_{zs}}{m_{tot} c_p} \quad (7.81)$$

Then, the energy required by the supplemental heating coil was

$$q_{coil} = m_{tot} c_p (T_{out} - T_{mix}) \quad (7.82)$$

For a parallel FPTU in the alternate configuration:

First, the discharge temperature for meeting the zone load was calculated according to Equation 7.81, and assigned the value of discharge temperature to the mixing temperature.

$$T_{mix} = T_{out} \quad (7.83)$$

Then, the secondary air temperature at the FPTU fan outlet was calculated

$$T_{sec,out} = \frac{[(m_{pri}+m_{sec})\cdot T_{mix} - m_{pri}\cdot T_{pri}]}{m_{sec}} \quad (7.84)$$

The secondary air temperature at the FPTU fan inlet was

$$T_{coil} = T_{sec,out} - \frac{Pow_{fan}}{m_{sec}\cdot C_p} \quad (7.85)$$

After the T_{coil} was calculated, the energy required by the supplemental heating coil was

$$q_{coil} = m_{sec} c_p (T_{coil} - T_{sec}) \quad (7.86)$$

b) When the zone heating load was greater than twice of $q_{heating,deadband}$, the discharge temperature was set as a constant

$$T_{out} = T_{out,heating} \quad (7.87)$$

The total airflow that was required to satisfy the zone heating load was calculated

$$m_{tot} = \frac{qzs}{c_p\cdot(T_z - T_{out})} \quad (7.88)$$

The calculated m_{tot} was capped by the design airflow of $m_{tot,design}$. If Equation 7.95 resulted in a value of m_{tot} that was greater than $m_{tot,design}$, then m_{tot} was reset to the value of $m_{tot,design}$.

With a known value of m_{tot}, the secondary airflow can be calculated

$$m_{sec} = \frac{m_{tot}}{1 - f_{leakh}} - m_{pri} \quad (7.89)$$

where f_{leakh} was the leakage ratio in the heating mode.

The calculation then proceeded according to Equations 7.79 to 7.82 for a parallel FPTU in the traditional configuration and Equations 7.83 to 7.86 for a parallel FPTU in the alternate configuration.

7.3.2 System Level Calculation For demonstration purposes, the performance of a parallel variable airflow FPTU was estimated by using the mass and energy balance approach discussed above and the empirical curves for ECM fan/motor power consumption developed in Chapter 3. Simulations were done with Engineering Equation Solver. As a first step, a series of input data

were created, including zone sensible loads, zone set-point temperature, primary air temperature, secondary air temperature, and leakage ratio. The parallel FPTU was sized by using a design zone cooling load of 39,000 Btu/h (11.43 kW). In order to show the operation in heating, cooling, and deadband regions, the zone sensible load was allowed to vary from -40,000 to 40,000 Btu/h (-11.73 to 11.73 kW) by using an arbitrary incremental change of 479 Btu/h (0.14 kW), with negative values indicating heating loads and positive values indicating cooling loads. At each zone sensible load, a constant zone set-point temperature of 78°F (25.6°C) was maintained with a constant primary air temperature being 55°F (12.8°C). The secondary air temperature was assumed to be the same as the zone temperature of 78°F (25.6°C), representing the direct air return from the zone. In addition, FPTU performance calculations were conducted by using four leakage ratios of 0, 2.5%, 5%, and 12% that were maintained constant in all heating, cooling, and deadband regions. The zero leakage case represented an ideal condition. Leakage levels of 2.5%, 5%, and 12% were used for simulating the scenarios with low, medium, and high leakages. At each leakage level, the primary airflow, secondary airflow, total airflow, and supplemental heating energy required to satisfy the zone load were determined. It should be noted that the above input parameters, namely zone sensible loads, zone set-point temperature, zone design load, primary air temperature, secondary air temperature, and leakage ratio, were user-defined parameters and can be modified for different applications and systems.

The system level calculation began with reading the input data and then determining the operating mode based on the zone sensible load. In each operating mode (off, deadband, heating, and cooling) the parallel FPTU operated based on the equations described earlier in this paper. Results from each mode merged in solving for the return air loop of the complete VAV system. The mixing temperature of the return air and the outdoor air was used to determine whether or not preheating was required. If the mixing temperature was below the primary air temperature, then the preheating coil was used to heat the mixed air to the primary air temperature. The procedure then calculated the power consumption of the primary fan and proceeded to calculate the cooling energy required at the primary cooling coil. If there was another hour, then the procedure looped back to the start, otherwise the procedure was completed.

7.3.3 Sample Results from the Model By using the system level calculation procedure as discussed above, results of airflow, discharge temperature, and heating energy use from a parallel FPTU in the traditional configuration were calculated and plotted against the zone sensible loads.

Because the results of airflow and discharge temperature were identical regardless of FPTU configurations, the same results were not repeated for a parallel FPTU in the alternate configuration except for the result of supplemental heating.

Figures 7.13 and 7.14 show the primary, secondary, and total airflow variations with zone sensible loads at different leakage ratios of 0, 2.5%, 5%, and 12%. The ideal case of no leakage was represented as well as cases of low, medium, and high leakage levels.

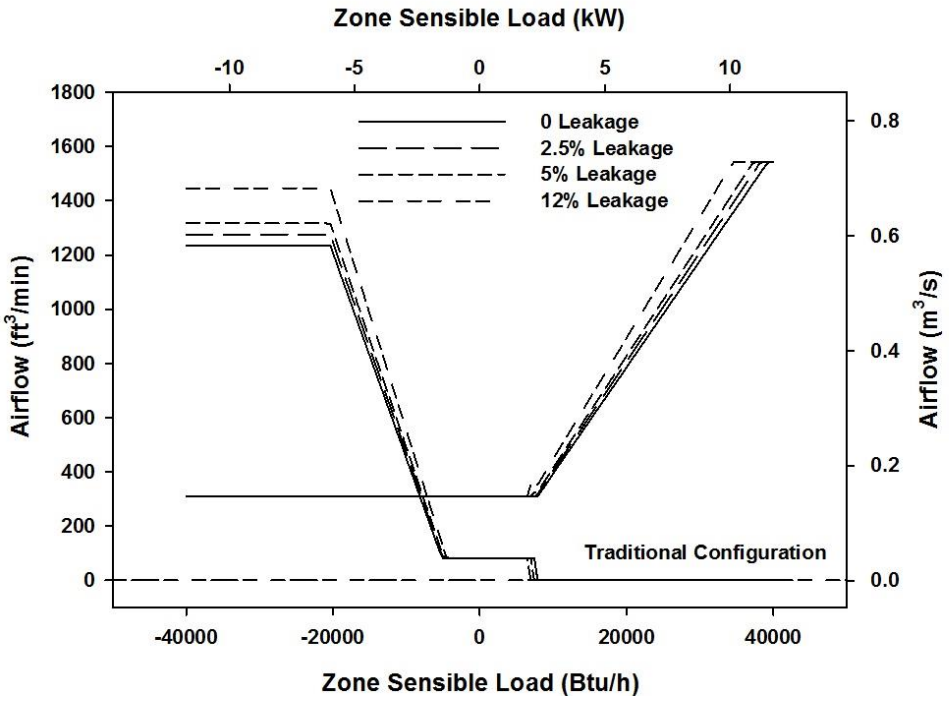

Figure 7.13: Primary and Secondary Airflow Variations with Zone Loads

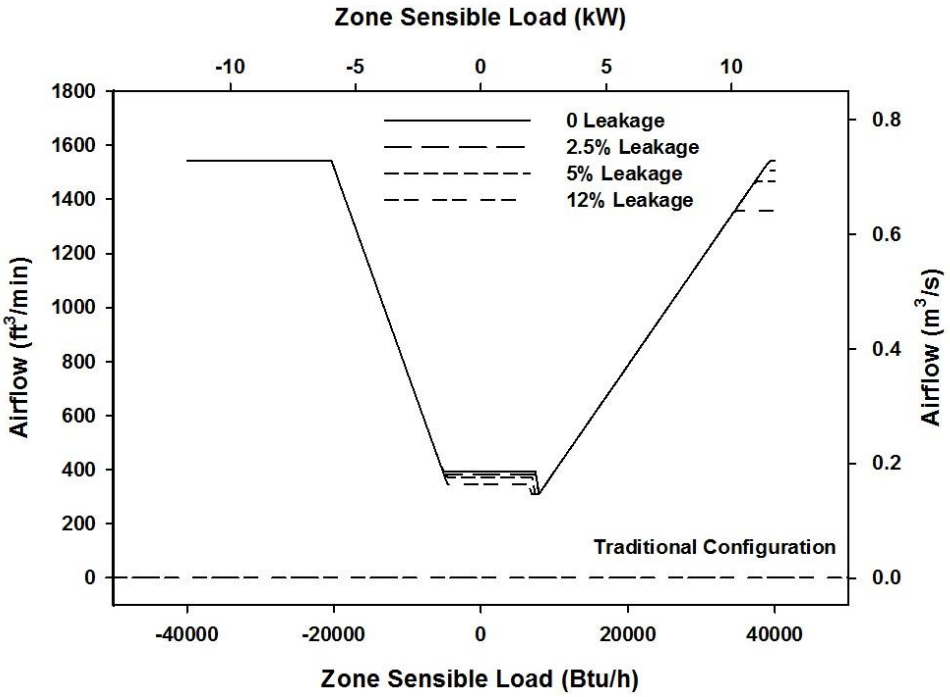

Figure 7.14: Total Airflow Variation with Zone Loads

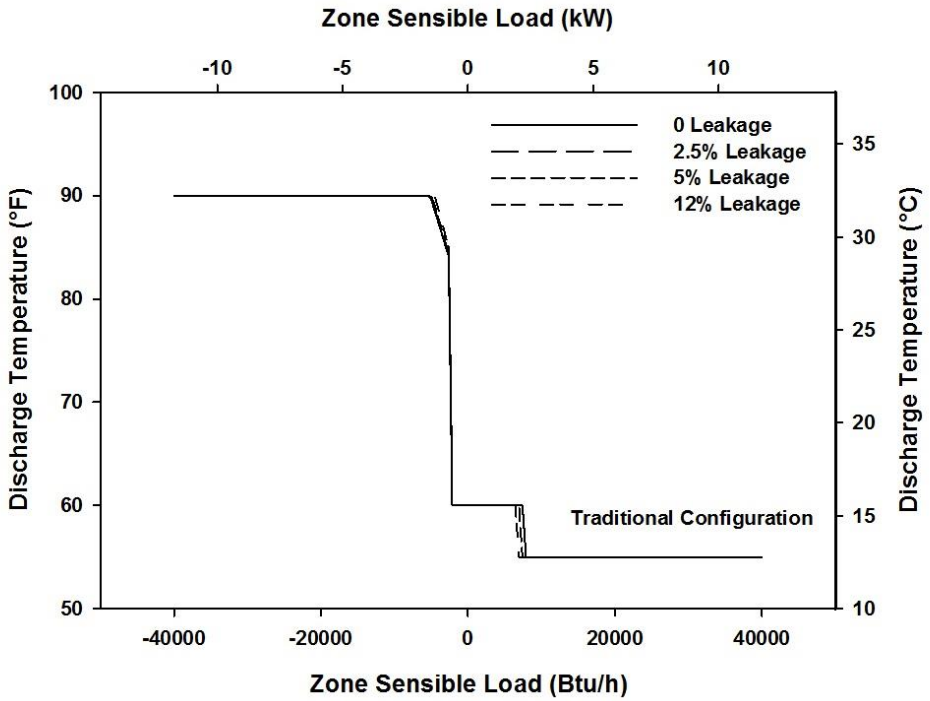

Figure 7.15: Discharge Temperature Variation with Zone Loads

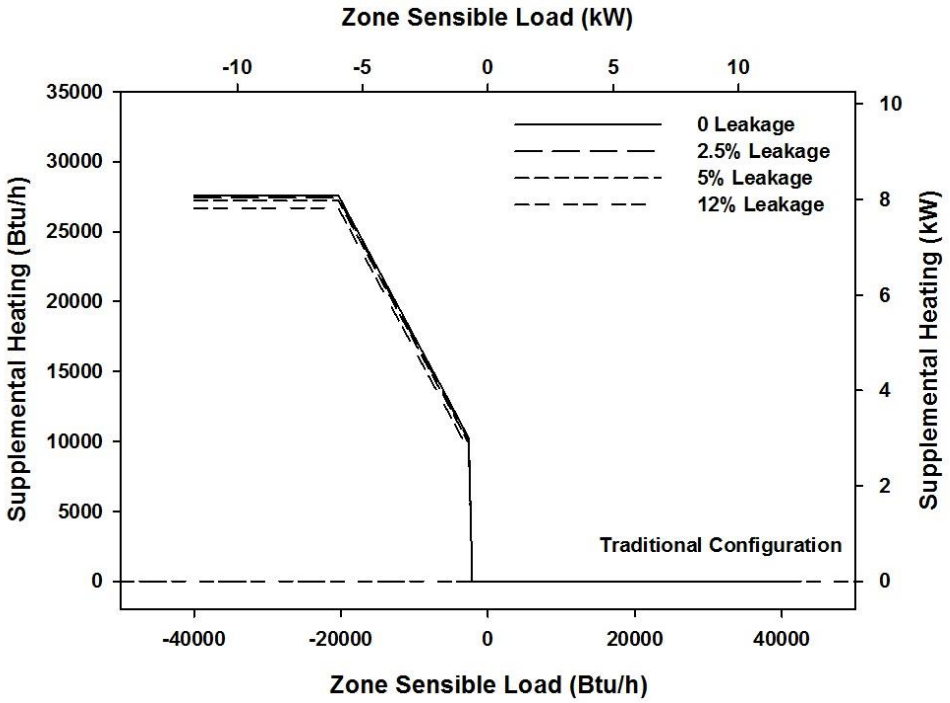

Figure 7.16: Energy Input to the Heating Coil for a Parallel FPTU in the Traditional Configuration

In the higher end of the heating region above the mark of -20,000 Btu/h (5.9 kW), both primary and secondary airflows were constant, with the primary airflow being at its minimum, which was assumed to be 20% of the design airflow in this study, and the secondary airflow made up the rest of the design airflow.

Therefore, the total airflow was also constant, which was reflected by the horizontal line in Figure 7.14 when the zone heating load was greater than 20,000 Btu/h (5.9 kW). As the zone heating load decreased, Figure 7.13 showed that the secondary airflow decreased proportionally until the heating load dropped below twice of $q_{heating,deadband}$, while the primary airflow maintained its minimum value over the entire heating and deadband regions for the ventilation purpose. In the deadband region and the heating region below twice of $q_{heating,deadband}$, the secondary airflow was maintained at the calculated value by using the user-defined discharge temperature, which was 60°F (15.6°C). Because both primary and secondary airflows in the deadband region were constant, the total airflow was also a constant in the deadband region as shown in Figure 7.14. As the transition occurred from heating to cooling, a sharp drop in the secondary and total airflows was observed at the higher limit of the deadband region due to switching off the FPTU fan. Consequently, the secondary airflow became zero and maintained

this value over the entire cooling region. As a result of further increases in the zone cooling load, the primary airflow proportionally increased until it reached the design airflow rate. At higher cooling loads above the design cooling load, the primary airflow maintained its value at the design airflow without further increases.

In addition to airflow variations with zone loads, Figures 7.13 and 7.14 show the impact of air leakage on primary, secondary, and total airflows at four different leakage levels of 0, 2.5%, 5%, and 12%. In heating mode, the primary airflow in Figure 7.13 and total airflow in Figure 7.14 at different leakage levels remained the same, which indicated that both primary and total airflows were independent of leakage levels. The independent relationship between the primary airflow and leakage ratios was caused by the fact that the measurement of primary airflow was made at the primary air inlet port by using a multi-point flow sensor upstream to the location where leakage occured. Therefore, once the minimum value of primary airflow was measured at the inlet port, FPTUs would maintain this minimum value regardless the downstream leakage. The independent relationship between the total airflow and leakage ratios can be explained by using Equation 7.70. In the heating range above twice of $q_{heating,deadband}$, Equation 7.70 showed that the total airflow at a specific zone heating load was dependent on c_p, T_{out}, and T_z, all of which were assumed to be constant in this study, and consequently the total airflow was independent of leakage levels. However, the results in Figure 7.13 showed that the secondary airflow consistently increased with increasing leakage ratio to satisfy the same zone heating load. For example, at a zone heating load of 15000 Btu/h (4.4 kW) the secondary airflow increased by 18.7% from 827 ft^3/min at zero leakage to 982 ft^3/min at 12% leakage as a result of increasing the leakage ratio. This increase in the secondary airflow was modeled by Equation 7.77, where both primary and total airflow were maintained constant in the heating mode. It was important to recognize this impact of air leakage on the secondary airflow behavior because the variable secondary airflow was achieved by adjusting the fan speed in parallel FPTUs. Higher secondary airflow was directly linked to higher fan speeds, and consequently results in greater fan energy consumption.

In the deadband and lower end of heating range below twice of $q_{heating,deadband}$, Figure 7.13 showed that both primary and secondary airflow were maintained constant, resulting in constant total airflow as shown in Figure 7.14. However, the total airflow decreased with increasing the leakage ratio, which was characterized by Equation 7.58. Although the air

leakage did not affect the total airflow in the cooling mode that was calculated according to Equation 7.77, Figure 7.13 showed that higher leakage ratios resulted in higher primary airflows at the same zone cooling load. For instance, at the cooling load of 20,000 Btu/h (5.9 kW), the primary airflow was increased by 13.6% from 786 ft^3/min at zero leakage to 893 ft^3/min at 12% leakage. Because part of the primary air provided to FPTUs was lost to the plenum space due to air leakage, increases in the primary airflow were required to compensate for this air leakage while providing enough cooling to meet the zone load. Figure 7.14 also showed that the air leakage from FPTUs to the plenum space resulted in the delivered airflow that was less than the design airflow at or above the design cooling load, with greater decreases at higher leakage ratios. Of greater importance, the decreases in the delivered airflow reduced the FPTU's cooling capacity because of the fact that the zone cooling load was met by varying the amount of primary air at a constant temperature of 55°F (12.8°C). For example, Figure 7.14 showed that cases with higher leakage ratios reached the maximum cooling capacity, which was represented by the horizontal lines in the higher cooling range in Figure 7.14, at lower zone cooling loads. Based on the above analysis, it can be seen that the air leakage in parallel FPTUs not only increased the FPTU fan power consumption, but also affected the cooling energy use and maximum cooling capacity of parallel FPTUs.

Figure 7.15 showed the discharge temperature variation over the entire zone load range. In the heating range above twice of $q_{heating,deadband}$ the discharge temperature was set at a constant of 90°F, and the zone heating load was satisfied by varying the amount of secondary air. In the lower heating range below twice of $q_{heating,deadband}$, the discharge temperature increased linearly from 84 to 90°F (28.9 to 32.2°C) as the zone heating load increased because the total airflow in this heating range was a constant at the deadband level. Then, a sharp temperature drop occurred at the lower limit of the deadband due to switching off the heating coil. In the deadband region, the discharge temperature was constant at the user-defined temperature 60°F. Another temperature drop occurred at the higher limit of the deadband because of turning off the FPTU fan. Consequently, no secondary air was provided and mixed with the primary air in the cooling region, and the discharge temperature in the cooling range was the same as the primary air temperature that is assumed to be 55°F (12.8°C) in this study.

In addition, the impact of air leakage from parallel FPTUs to the plenum space was reflected in terms of the discharge temperature in the heating range below twice of $q_{heating,deadband}$,

with showing higher discharge temperatures at greater leakage levels for the same heating load. For example, Figure 7.15 showed that at the heating load 4,550 Btu/h, the discharge temperature increased by 1.5°F (0.8°C) from 88.5 to 90°F (31.4 to 32.2°C) as a result of increasing the leakage ratio from 0 to 12%. The increase in the discharge temperature was caused by the fact that the total airflow delivered to the zone in this heating range decreased with increasing the leakage ratio, as shown in Figure 7.14. Therefore, an elevated discharge temperature was required for satisfying the zone load when the total airflow delivered to the zone was reduced.

Figure 7.16 showed the supplemental heating energy for a parallel FPTU in the traditional configuration. The heating coil only operated in the heating mode and remained off in the deadband and cooling regions. At the higher end of the heating range, the heating energy was constant and capped by limiting the 90°F (32.2°C) maximum discharge temperature with the prescribed design airflow as shown in Equation 7.63. Then, the supplemental heating rate decreased proportionally as the heating load decreased until it reached the lower limit of the deadband region. At that point, the heating coil was turned off, and the supplemental heating rate became zero. In addition to increasing the discharge temperature as shown in Figure 7.15, Figure 7.16 showed that the air leakage from parallel FPTUs in the traditional configuration decreased the heating energy use for the same zone load. For instance, at the zone heating load of 10,000 Btu/h, the heating energy decreased by 5.3% as a result of increasing the leakage ratio from 0 to 12%.

The decrease in the heating energy use at higher leakage ratios can be explained by observing Equation 7.63 which shows the energy input to the supplemental heating coil was dependent on the total airflow and the temperature difference between the discharge temperature and the mixing temperature of primary and secondary airflows. At any given zone heating load, the discharge temperature was constant, either calculated from Equation 7.62 or set at a constant of 90°F (32.2°C. In the heating range above twice of $q_{heating,deadband}$, the total airflow was constant as shown earlier in Figure 7.14, and the decrease in the heating energy was caused by the increase in the mixing temperature at higher leakage ratios as shown in Figure 7.17.

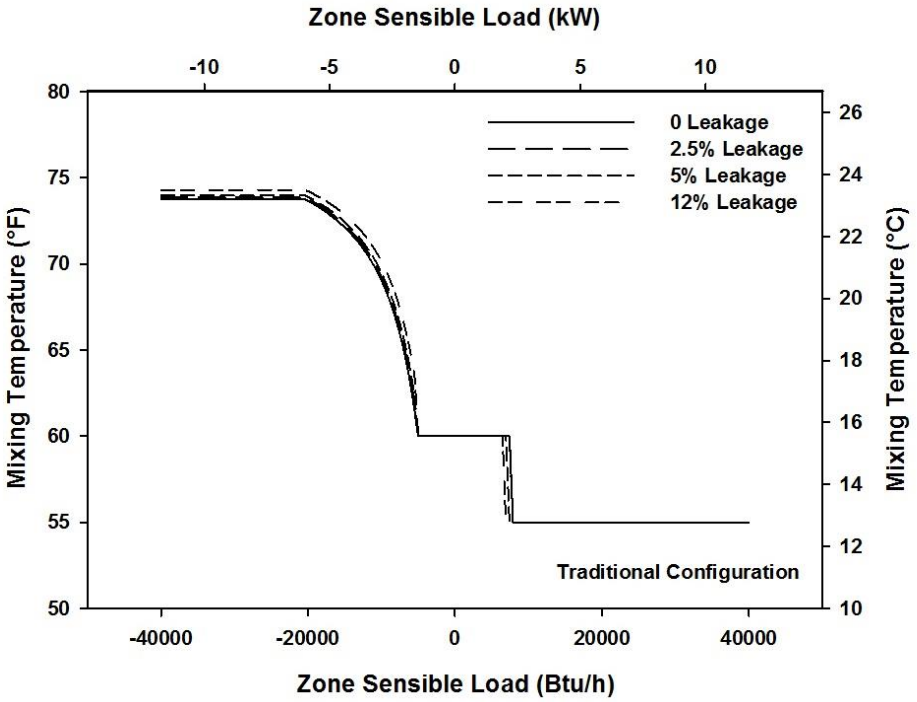

Figure 7.17: Mixing Temperature for a Parallel FPTU in the Traditional Configuration

To maintain the required total airflow for meeting the zone load at higher leakage ratios, increased amount of warmer secondary air was provided to mix with the prescribed minimum amount of primary air. Consequently, the mixing temperature was increased with increasing the leakage ratio. In the heating range below twice of $q_{heating,deadband}$, the mixing temperature was constant and set to the user-defined discharge temperature as shown in Equation 7.50, and the total airflow decreased with increasing leakage ratio. Therefore, less heating energy was used at higher leakage ratios.

As mentioned earlier, the performance results were identical for parallel FPTUs in both traditional and alternate configurations except for the heating energy use. Similar to the result shown in Figure 7.16 for a unit in the traditional configuration, Figure 7.18 showed the heating energy use for a unit in the alternate configuration.

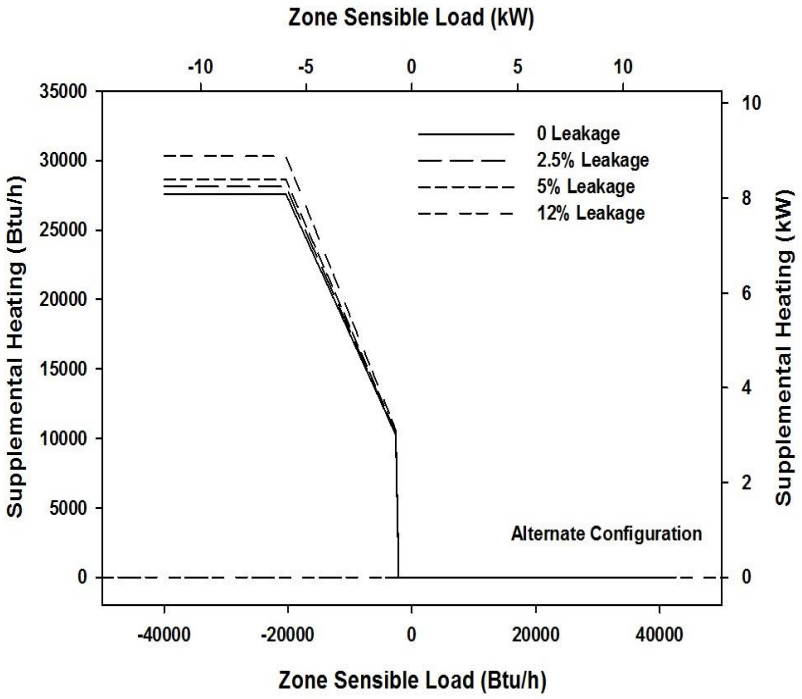

Figure 7.18: Energy Input to the Heating Coil for a Parallel FPTU in the Alternate Configuration

Unlike Figure 7.16 that showed lower heating energy use at higher leakage ratios, Figure 7.18 showed that increases in the leakage ratio resulted in greater heating energy use for parallel FPTUs in the alternate configuration. For example, Figure 7.18 showed that at the same zone heating load of 10,000 Btu/h, the heating energy increased by 7.6% as the leakage ratio was increased from 0 to 12%. The difference in the heating energy use with respect to different leakage ratios between the traditional and alternate configurations was caused by different heating coil locations. For parallel FPTUs in the traditional configuration where the heating coil was located at the total airflow outlet, 100% of the energy input into the heating coil was used to satisfy the zone load because the leakage occurred upstream to the heating coil. However, units in the alternate configuration where the heating coil was located at the secondary air inlet, part of the energy input into the heating coil was lost to the plenum space with the leakage airflow that occurred at the downstream of the heating coil. Therefore, greater energy was required to meet the zone heating load as the leakage ratio was increased.

7.4. Implementing Fixed and Variable Airflow FPTU Improvements in EnergyPlus

Significant improvements in the mass and energy balance approach used in EnergyPlus have been outlined in Chapter 6 for fixed airflow FPTUs and this chapter for variable airflow FPTUs.

Both chapters provided step-by-step methodologies that included integrating such features as improved fan/motor models, leakage model, parallel model with alternate fan/motor location, variable airflow, and mixing secondary with primary avoid condensation on registers or cold drafts in deadband operations.

To investigate how to integrate new features into EnergyPlus, we contacted personnel at one national laboratory (Pacific Northwest National Laboratory) and a member of ASHRAE TC 4.7. We were informed that only experts who are on the Department of Energy development team have the expertise to make substantial changes in EnergyPlus. We were then directed to GARD Analytics which has expertise in building energy modeling, including developed new components for DOE-2, which was the predecessors to EnergyPlus. Their suggestion to our team was one of the following:

1. For fixing a bug or minor issue - Post an "issue" (either directly on github or by posting a helpdesk ticket energyplus-support@gard.com or energyplus.helpserve.com). The issue should describe what's wrong and include example file(s) that illustrate the problems. And if you already have solutions to offer, that's even better. Issues get addressed on a rolling basis, but they all compete with each other for priority.
2. For a large new feature - If it's a large new feature that requires the Department of Energy to allocate significant funding, then a new feature request can be submitted through the following website:
   https://energyplus.uservoice.com/forums/258860-energyplus
   This platform allows users to vote up particular features and the highest vote getters will be considered for funding in the next fiscal year.
3. For large feature coded by a third party – Because there are some independent developers, such as GARD, that have in house capability to develop computer code compatible with EnergyPlus and other building simulation programs, the computer code can be developed and "donated" to the Department of Energy.

Looking at the methodologies developed in this report, we would tentatively estimate that each change should be categorized as shown in Table 7.3. These estimates were based on our limited knowledge of the coding that currently exists in EnergyPlus. None of the current team has ever

seen the original source code of EnergyPlus which was written in C++ and most of the team has never written any code in C++.

Table 7.3 – Classification of the Changes Needed in EnergyPlus as a Result of this Work

Change	Change in EnergyPlus	Type of Change
1	PSC fan motors with SCR control (Chapter 2)	Bug fix/minor issue
2	ECM fan motors (Chapter 3) – Fixed and Variable Airflow	Large New Feature
3	Realistic fan pressure differentials and fan/motor efficiencies (Chapter 4)	Bug fix/minor issue
4	Leakage in parallel FPTUs (Chapter 5)	Uncertain
5	Alternative heating coil location in parallel FPTUs (Chapter 6 and 7)	Large new feature
6	Mixing of secondary air to ensure no condensation on registers or cold drafts (Chapter 6 and 7)	Large new feature
7	Variable airflow ECM FPTUs (Chapter 7)	Large new feature

The two issues that appeared to be bug/fixes or minor issues were changes numbered 1 (PSC fan motors with SCR control) and 3 (realistic fan pressure differentials and fan/motor efficiencies). Given the simplicity of the model of PSC fan motors with SCR control in Chapter 2, it should be a straightforward fix in EnergyPlus. Option 3 should be a change in default values for fan pressure differential and fan/motor efficiencies that the user can access when setting up a run in EnergyPlus. If those default values were constrained to more realistic values than were currently used or recommended in EnergyPlus, then users would not be able to pick either unrealistic fan/motor efficiencies or fan pressure differentials.

EnergyPlus allowed leakage in duct system components, but leakage was not available as an explicit option for a parallel FPTU. A user could potentially try to mimic leakage in the FPTU by specifying leakage in the primary duct attached to the FPTU. However, it was not clear how well this would capture actual leakage in the FPTU. We recommend that the leakage in the FPTU be explicitly included in EnergyPlus. We are estimating that this could be a large new feature, but it could be a simple bug fix depending if the computer code describing the FPTU can be easily altered. Thus, in Table 3, it is listed as uncertain.

All of the other issues appeared to be major fixes to EnergyPlus and would fall under the "large new feature" category. For example, EnergyPlus currently has no provision in it to handle ECM fan/motor combinations (Change 2 in Table 7.3) for either fixed or variable airflow applications in the way they were formulated in Chapter 3. Thus, implementation appeared to

require a major programming effort so users could specify the capacity factor of the FPTU in each zone and then track the load if the ECM was operating in a variable airflow FPTU. Change 7 (variable airflow ECM FPTUs) should be done in conjunction with Change 2. The complexities of the control algorithms for Change 7 would require significant reprogramming compared to the fixed airflow operations that are now in EnergyPlus.

EnergyPlus assumed the heating coil in a parallel FPTU was located at the exit of the FPTU. Its energy and mass balances were setup for a heating coil in the primary airstream, not the secondary airstream. Thus, this change would most likely require significant programming effort to allow the alternative (Change 5) location for the supplemental heating coil.

Mixing secondary air with primary air (Change 6) to maintain high enough discharge temperatures to either prevent condensation on the registers or reduce "cold" drafts to occupants in the zone is not an option that users can specify in EnergyPlus. While the energy balances to accomplish the mixing were relatively straightforward, this option would require specifying minimum discharge temperatures at maximum cooling all the way up to the deadband region. We think this would require a significant programming effort that could potentially be done with Changes 2 and 7.

All of the above changes would also require changes in the EnergyPlus Engineering Manual (2013) which describes the models and inputs needed in the FPTU models. The manual should also be modified to include reasonable ranges of values for the user on such things as fan pressure differential and fan/motor efficiencies so a user not familiar with FPTUs would be able to make realistic estimates of these variables.

7.5. Summary

This chapter has provided the basic equations needed to characterize either variable airflow series or parallel ECM FPTUs using a mass and energy balance approach. Two approaches were outlined for handling the variable airflow cooling operations in a series unit. The first approach, called the airflow control approach, varied the airflow linearly from full cooling to the beginning of the deadband region. The second approach, called the discharge temperature control approach, varied the discharge temperature linearly from full cooling to the beginning of the deadband region. Both should provide similar simulation results and allow the user to eliminate iterating each time step to obtain a solution. Both approaches allowed a user to simulate a FPTU with either a chilled water cooling coil or a direct expansion cooling coil and blend secondary air

to produce conditions that eliminate condensation on the registers at full cooling or cold drafts in the deadband region. A step-by-step process of how the basic equations should be used for each FPTU mode of operation was provided.

For parallel FPTUs, the basic equations for modeling performance were provided. Both the traditional configuration where the heating coil is located at the discharge of the FPTU and the alternate configuration where the heating coil is located at the inlet to the secondary air port were discussed. The FPTU models included leakage as a variable so a user could assess the impact of leakage on the performance of parallel FPTUs. The methodology developed in this chapter can be implemented into building simulation models that use a mass and energy balance approach.

CHAPTER 8

FIXED AIRFLOW MODEL COMPARISON TO THE DAVIS "BLACK BOX" MODEL

This chapter summarized the comparisons of the energy use of a small office building using the fixed airflow series and parallel models from Chapter 6 and the "black box" fixed airflow FPTU model of Davis (2010). The purpose of the comparisons was to assess how different the results from the mass and energy balance (MEB) approach from Chapter 6 were from using the "black box" approach developed by Davis et al (2007). A five zone small office building model developed and used by Davis et al (2007) served to provide the thermal loads that could be used to assess the differences in the modeling approaches. Davis (2015) provided corrected hourly loads data for each zone and city to the Baylor research team to better match the assumptions used in the MEB model.

8.1. Davis Black Box Model

Davis (2010) and Davis et al (2012a and 2012b) developed FPTU models based on the equations from Furr et al (2008a and 2008b) and Edmondson et al (2011a and 2011b). Essentially the equations described the power and airflow of the FPTU fan as a function of variables such as upstream and downstream static pressures, primary airflow, and primary damper setting. Figures 8.1 and 8.2 show depictions of the black box series and parallel FPTU models of Davis.

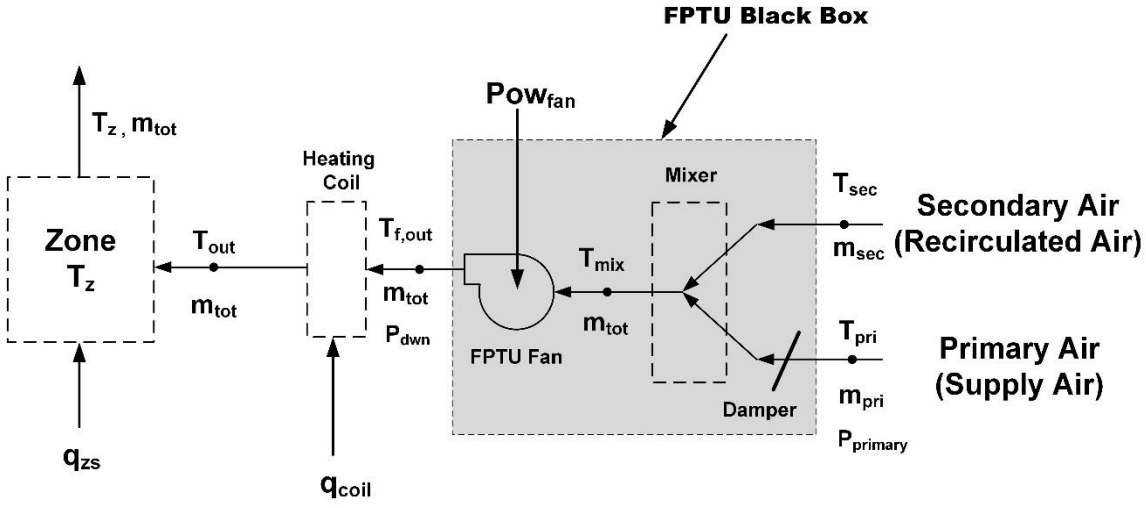

Figure 8.1: Schematic of Series Black Box FPTU Model

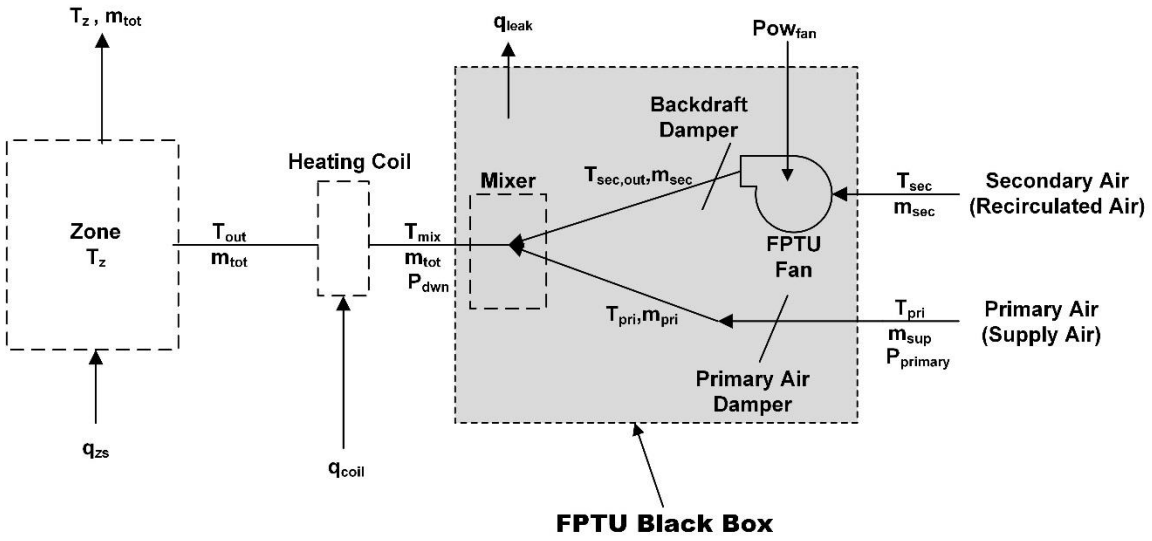

Figure 8.2: Schematic of Parallel Black Box FPTU Model

The greyed out areas in both figures are treated as simple input/output systems (or "black boxes") based on the equations developed by Furr et al (2008a and 2008b) and Edmondson et at (2011a and 2011b). The individual components, such as the fan and mixer inside the FPTU were not modeled directly in either the series or parallel models by Davis. However, the FPTU models could directly handle pressure variations in the duct system which was something often lacking in the mass and energy balance models. The Davis models also included leakage in parallel FPTUs, but did not include any alternative configuration of the heating coil in parallel FPTUs as was done with the MEB models in Chapter 6. Davis only published results from fixed airflow PSC/SCR and ECM FPTUs.

8.2. Davis Building and HVAC System Model

To estimate the potential savings with different FPTU technologies, Davis (2010) modeled a simple five zone office building. The building exterior was exposed to weather and solar effects while the interior, or core zone, was dominated by internal thermal loads. A brief description is provided here, while a more detailed description can be found in Davis et al (2007 and 2009). The DOE-2 building simulation program was used to develop the hourly loads used for the system simulations (Department of Energy, 2003). Davis et al (2009) designed a generic five zone office building with North, East, South, West and Core zone types. The exterior zones were influenced by external weather and solar effects as well as internal loads and infiltration. The interior, or core zone, was dominated by internal thermal loads. These zone types

represented zones typically encountered in applications that use single duct VAV systems based on either series or parallel fan powered terminal units.

Figure 8.3 shows a diagram of the five zone building layout (Davis et al 2007 and 2009). The building was a single story rectangular structure that had a footprint of 122.5 ft x 122.5 ft (37.3 m x 37.3 m). The perimeter zones had 1,612 ft^2 (149.8 m^2) of floor area while the core zone had 8,556 ft^2 (794.9 m^2).

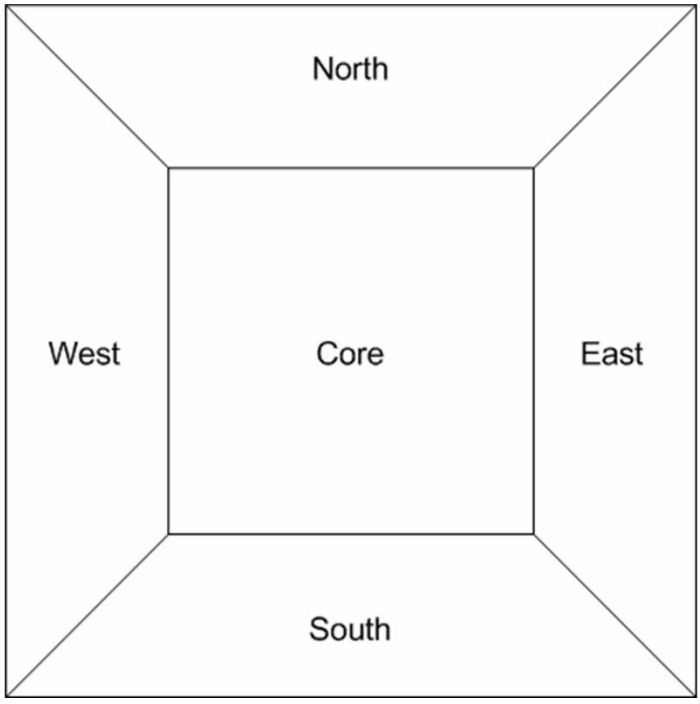

Figure 8.3: Diagram of the Floor Plan of the Building Used as the Basis for the DOE-2 Loads Model

The perimeter zones had walls that were 50% glass with a U-Factor of 0.46 Btu/hr/F°/ft^2 (2.6 W/m^2/°C) and a solar heat gain coefficient of 26%. The wall insulation was R-13 (2.6 m^2°K/W) and the roof insulation was R-15 (2.64 m^2°K/W). The cooling loads due to people in the building were calculated using a factor of 275 ft^2 (25.5 m^2) per person. The lighting and equipment loads were 1.3 Watt/ft^2 and 0.75 Watt/ft^2 (14 Watt/m^2 and 8.1 Watt/m^2) respectively.

The building was operated on a typical office schedule for the entire year and the normal holidays encountered in the U.S. were not included in the operating schedule. Hourly sensible and latent space loads were calculated for all zones for the entire 8,760 hours in a year using the TMY weather data set for the five locations of Chicago, Houston, New York, Phoenix and San Francisco.

After the space loads for each climate were generated, Davis et al (2007) exported the loads to an Excel spreadsheet. The hourly weather data used to generate the hourly loads were also loaded into a separate Excel workbook with each set of weather data located in a separate worksheet. The hourly weather data consisted of a time stamp (as included in the TMY data set), the outdoor ambient dry-bulb temperature, and the outdoor ambient humidity ratio.

The five weather climates consisted of Chicago, Houston, Phoenix, San Francisco, and New York. These climates were chosen because of the variety in range of low and high ambient temperatures, the range in the amount of moisture in air during the cooling months, and variation in the number of hours that the facility would experience of temperature ranges associated with cooling and heating operations.

Davis et al (2009) normalized the hourly loads from DOE-2 to the peak cooling capacity that could be met by the larger FPTUs that had been evaluated by Furr et al (2007) in the laboratory. This normalization of the loads resulted in all zones having the same peak loads and the same size FPTU serving each zone. Their normalization allowed for comparisons to be made between both series and parallel FPTU systems because both types of systems were subjected to the same cooling and heating load profiles. For their project, the system needed to be able to "move" from one city to another without changing the peak loads in each zone. Hourly loads for all zones at all weather locations were generated from DOE-2. The hourly loads were then used to build hourly load profiles for each zone at each geographic location. The hourly load profiles were generated by normalizing each zone load to the annual peak cooling for that zone. By normalizing load calculations for all values in the load profile, a normalized load profile was created for all zones at all geographic locations. This technique allowed modeling of the operation of the facility at various geographic weather locations while maintaining the peak cooling loads within the capacities of the FPTUs studied by Furr et al (2008a and 2008b). This method also reduced potential bias in the simulation results if the VAV terminal units were either over or undersized when moved to different geographic locations. These loads were provided to the Baylor team in the form of a spreadsheet that contained 8760 hours of load and weather data for each city.

Air was returned from each zone, but a portion could be used to provide secondary air to the FPTU. Some of the return air was exhausted to the outdoors. For this analysis, it was assumed that the amount of air outdoor air introduced into the system just equaled the amount of air

exhausted from the system. Outdoor air was needed to provide fresh air to the occupants of the building. Some systems may operate with the exhaust and intake at different values in order to create positive or negative pressure in the system. This mixture of return and outdoor air went through a preheating coil. Heating energy could be added to the air depending on the mixed air temperature, $T_{oa,mix}$. The air was heated when the mixed air temperature below the designated primary air temperature. The air then ran through the primary fan (or air handler), then was cooled if it was above the designated primary air temperature. The cooling coil provided both sensible and latent cooling. After the primary cooling coil, the air was routed through the ductwork to each zone's FPTU.

The diagram of the simple five zone HVAC system was provided in Figure 8.4. Each zone was labeled in the figure and had its own temperature set point and FPTU which supplied conditioned air.

8.3. Comparison Between Two Models

Davis (2015) made some corrections to his model, reran his fixed airflow cases, and provided the results to the Baylor team. The results obtained for both the fixed airflow series and parallel FPTUS using the MEB approach were compared to results from simulation results provided by Davis (2015). The MEB approach was implemented using EES. Davis developed a C++ program (Davis 2010) to implement the simulation of series and parallel FPTUs in a single duct VAV systems that included tracking pressures in the system. Attempts were made to match assumptions used in both programs as closely as possible. A summary of the major assumptions for the series and parallel fixed airflow units is provided in Table 8.1. The models used the same five U.S. cities: Houston, Phoenix, Chicago, New York, and San Francisco.

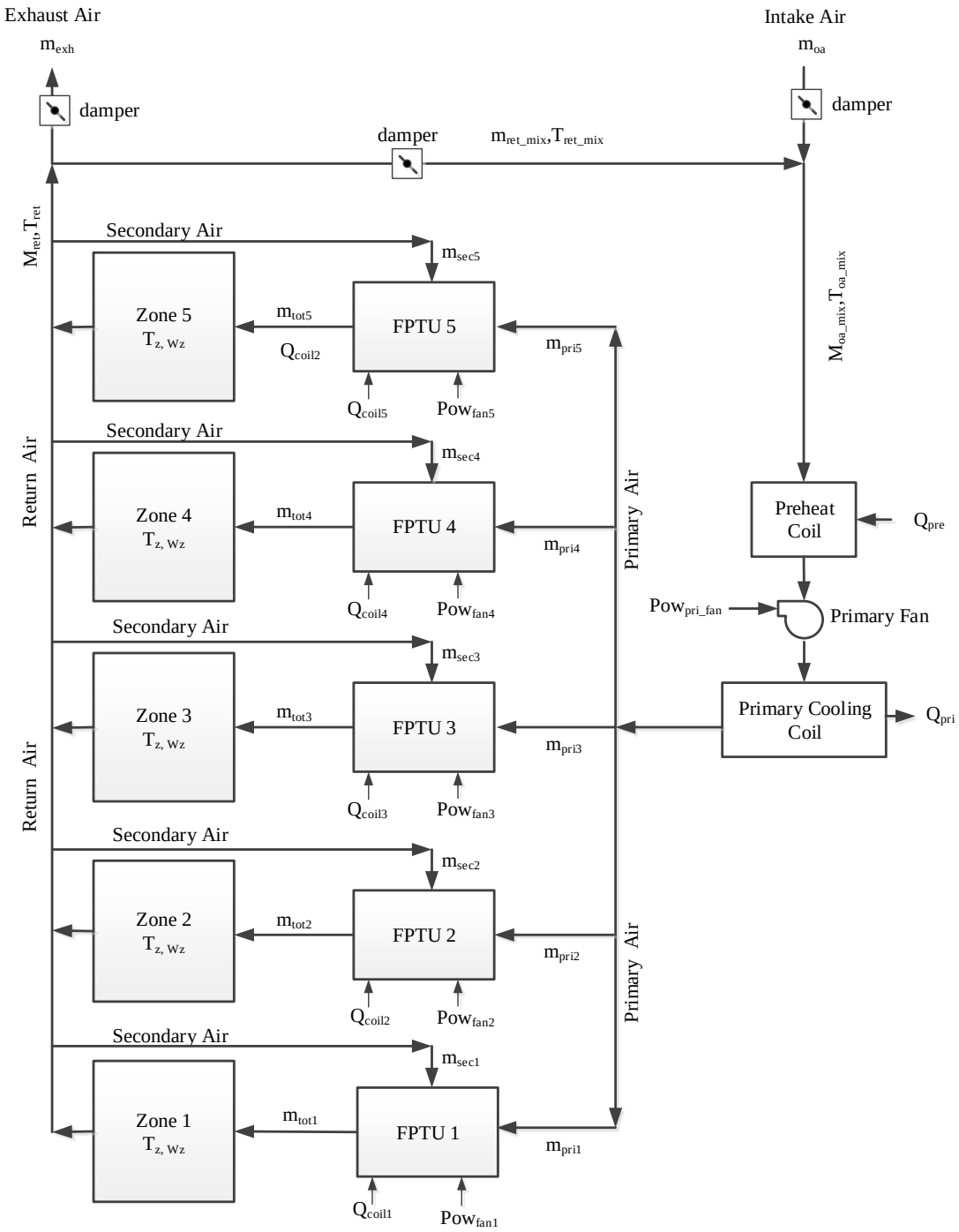

Figure 8.4 Five Zone System Model Diagram

Table 8.1 - Common Model Assumptions Between Davis (2015) and the MEB Model

Variable	Davis Model	MEB Model
Zone Set Point	78°F (25.6°C)	78°F (25.6°C)
Zone Relative Humidity	Based on load data	50%
Exhaust/Intake Percentage	25% of design load	25% of design load
Primary Air Temperature	55°F (12.8°C)	55°F (12.8°C)
Primary Air Relative Humidity	95%	95%
Design Airflow per Zone	1575 cfm	1575 cfm
Coefficient of Performance	3.22	3.22
Primary Fan Efficiency	85%	85%
Primary Air Temperature	55°F (12.8°C)	55°F (12.8°C)
Primary Fan Energy Calculation	AHU model	Fan laws
FPTU Coil Energy	Based on energy	Based on energy*
Annual Hours of Operation	8760	8760
Time Step for Analysis	1 Hour	1 Hour

*Had a maximum operating temperature of 90^{o}F.

The assumptions in Table 8.1 primarily pertain to the components of the five zone model not the individual FPTUs. The zone set point temperature, T_z, was 78°F (25.6°C) for all zones in both heating and cooling operations. The design airflow was set by Davis (2010) so that the same sized FPTU could be used in each zone and location. The MEB model was set so that its zone sizing matched that of Davis. The FPTU heating coil in the MEB model could not go over 90^{o}F (32.2^{o}C), which meant that there could be times when the heating load exceeded the heating capacity of the coil.

The zone relative humidity was used when determining the humidity of the return and outdoor air mix in the five zone model (see top right of Figure 8.4). The exhaust/intake percentages were the amount of return air that was exhausted and the amount of outdoor air that was added to the return air. To be consistent with the Davis model, these were set at 25% of the design airflow for the space and remained constant whenever the HVAC system was on. The primary air temperature was also assumed to be 55°F (12.8°C) to match Davis' assumption. This temperature remained fixed for the yearly simulation. The relative humidity of the air leaving the primary cooling coil remained fixed at 95%. The coefficient of performance (COP) of the chiller was a constant with respect to outdoor temperature and load. It was used to determine the energy used to provide chilled water to the primary cooling coil. The type (centrifugal, reciprocating, etc.) of chiller wasn't specified. The two models used different methods to calculate the primary fan energy but both used a primary fan efficiency of 85%. The Davis

model used a semi-empirical equation to model the primary fan. The MEB model used a general equation based on the fan laws. The temperature at the exit of the preheating coil was set to 55°F (12.8°C). If the temperature of the mixed air was below this value, then the air was heated using the preheat coil up to this designated value. If the mixed air temperature was above this value then no heat was added to the air.

There were some differences between the MEB and Davis approaches. Davis used a specific model for the primary fan, while the MEB approach used the general fan power equation based on the fan laws. Davis also used FPTU fan power models specific to each FPTU based on the semi-empirical fits developed by Furr et al (2008a and 2008b) and Edmondson et all (2011a and 2011b). The MEB fixed airflow approach, as was shown in Chapter 6, used general fan/motor models developed in Chapters 2 and 3.

Each of the tables below reported the same set of energy values, so an explanation of what each value represents was provided here. The "Unit Type" column provided information on whether the unit was a series or parallel FPTU. The "FPTU Fan" column was the total energy used by the five FPTU fans over the entire year. The "FPTU Coil" column was the total amount of supplemental heating energy added to the airstream by the heating coils over the entire year. The "Primary Fan" column was the amount of energy used by the primary fan over the entire year. The "Primary Chiller" column was the estimated annual amount of energy required at the primary chiller plant to provide the primary cooling coil with chilled water. The "Total Plant Energy" (TPE) column was the sum of the second through fifth columns. The last column provided an estimate of the percentage difference between the mass and energy balance (MEB) model and the model used by Davis (2010). The percent difference was calculated by Equation 8.1 with the results from the Davis (2015) model being used as the reference value.

$$\%\ Difference = \frac{TPE_{MEB} - TPE_{Davis}}{TPE_{Davis}} * 100\% \quad (8.1)$$

Where: TPE_{Davis} = total plant energy by Davis model

TPE_{MEB} = total plant energy by MEB model

8.3.1 Series Fixed Airflow The first runs made were for fixed airflow settings for both the PSC/SCR and ECM series FPTUs and are shown in Tables 8.2 and 8.3. For Houston, the Davis and MEB total plant energy were within 2.1 % for the PSC/SCR FPTUs. For the series PSC/SCR FPTUs, the total plant energy from the MEB model was always smaller than from the

Davis model. In all cases, the FPTU fan energy was less than that for the Davis model. Because the MEB model was based on newer fan/motor data than the Davis model, it was possible that the fan/motor efficiencies were higher which would produce a smaller fan/motor energy use. The FPTU coil energy use was also less than that for the Davis model in all cities. The largest difference for the series PSC/SCR FPTUs was for San Francisco for total plant energy use.

Table 8.2 - Series PSC/SCR FPTU Comparisons for Five Cities

Unit Type Series PSC/SCR	FPTU Fan (MWh)	FPTU Coil (MWh)	Primary Fan (MWh)	Primary Chiller (MWh)	Total Plant Energy (MWh)	Difference
MEB Houston	31.7	75.1	3.98	73.9	185	
Davis Houston	33.0	79.1	3.89	73.4	189	-2.1%
MEB Phoenix	31.7	59.7	4.04	54.7	150	
Davis Phoenix	33.0	61.5	3.79	53.7	152	-1/3%
MEB New York	31.7	74.0	3.69	31.8	141	
Davis New York	33.0	76.2	3.02	33.6	146	-3.4%
MEB Chicago	31.7	84.0	3.64	29.3	149	
Davis Chicago	33.0	87.9	2.92	30.8	155	-3.9%
MEB San Francisco	31.7	66.6	3.60	19.7	122	
Davis San Francisco	33.0	68.9	2.68	24.2	129	-5.4%

Table 8.3 - Series Fixed Speed ECM Comparisons

Unit Type Series ECM	FPTU Fan (MWh)	FPTU Coil (MWh)	Primary Fan (MWh)	Primary Chiller (MWh)	Total Plant Energy (MWh)	Difference
MEB Houston	12.2	86.5	3.79	70.6	173	0.6%
Davis Houston	11.3	87.0	3.29	70.3	172	
MEB Phoenix	12.2	70.3	3.84	51.7	138	3.0%
Davis Phoenix	11.3	68.9	3.19	50.4	134	
MEB New York	12.2	86.5	3.53	29.6	132	1.5%
Davis New York	11.3	84.7	2.57	31.1	130	
MEB Chicago	12.2	97.0	3.49	27.4	140	0.0%
Davis Chicago	11.3	97.9	2.49	28.6	140	
MEB San Francisco	12.2	79.3	3.45	17.6	112	-1.8%
Davis San Francisco	11.3	78.2	2.28	21.7	114	

Much of the differences between the two models in San Francisco related to the chiller energy use, which was 18.5% lower with the MEB model. It should also be pointed out that the estimated chiller energy use in San Francisco was smallest of all the cities. It was not clear why there was such a difference in chiller energy use in San Francisco because in the other cities, the chiller energy use was much closer. The majority of the energy use in the two southern climates (Houston and Phoenix) was in supplemental heating and the chiller. For the other three cities, the FPTU fan energy was comparable to and larger than the estimated annual chiller energy.

For the fixed airflow series ECM FPTU, the differences in total plant energy use agreed to within 3% between the two models. For the series ECM FPTUs, the MEB model was higher than the Davis model in every city except San Francisco. As with the PSC/SCR comparisons, the chiller energy use was the major contribution to the differences between the two models. The fan energy use was significantly lower for the ECM FPTU than for the PSC/SCR FPTU. This would imply that the ECM FPTU's airflow capacity was larger than the design airflow and its speed was lowered to just meet the design airflow requirements of the zone. Because the fan in the series FPTU operated continuously while the HVAC system was on, the savings in energy use over the course of the year can be significant. For example, in comparing the Houston data, the ECM FPTU used 6.5% less energy than the PSC/SCR FPTU. For, Chicago, the ECM FPTU used 6.0% less energy than the PSC/SCR FPTU.

Overall, given the difference in assumptions and methodology between the two approaches, there were relatively small differences between the MEB and Davis models in total plant energy. These differences suggested that either the MEB model for the series FPTU found in Chapter 6 or the Davis model should be usable as models to estimate the performance of FPTUs.

8.3.2 Parallel Fixed Airflow – No Leakage The parallel fixed airflow results were compared in the same way as the series fixed airflow results, as shown in Table 8.4 and 8.5 for the PSC/SCR and ECM FPTUs, respectively. For both the PSC/SCR and ECM FPTU cases, the maximum difference between the MEB and Davis model was 4%, which was in Phoenix. In all other cities, the differences between the two approaches was less than 2%. The MEB model tended to have higher energy use for the FPTU fan for both the PSC/SCR and ECM FPTU simulation. We speculated that the differences may have been in the run times estimated by the two models. However, without the detailed hour-by-hour results from the Davis model, it would be difficult to identify any other cause for the differences. While the ECM FPTU had a smaller

fan energy use than its counterpart PSC/SCR FPTU in the same city, the reduced energy use was made up with a higher FPTU coil energy use. This resulted in the total plant energy use being nearly the same whether an ECM FPTU or PSC/SCR FPTU was used.

Table 8.4 - Parallel PSC/SCR (No Leakage) Comparisons

Parallel SCR Totals	FPTU Fan (MWh)	FPTU Coil (MWh)	Primary Fan (MWh)	Primary Chiller (MWh)	Total Plant Energy (MWh)	Difference
MEB Houston	9.60	84.5	3.65	68.1	166	
Davis Houston	7.78	85.0	3.37	68.8	165	0.6%
MEB Phoenix	9.11	68.3	3.68	49.3	130	
Davis Phoenix	7.18	65.9	3.26	48.9	125	4.0%
MEB Chicago	12.0	93.4	3.37	25.9	135	
Davis Chicago	9.12	92.9	2.61	27.6	132	2.3%
MEB New York	10.7	84.0	3.41	27.9	126	
Davis New York	8.65	82.4	2.68	30.0	124	1.6%
MEB San Francisco	11.3	76.3	3.33	15.9	107	
Davis San Francisco	8.80	74.4	2.40	20.5	106	0.9%

Table 8.5 - Parallel ECM (No Leakage) Comparisons

Parallel ECM Totals	FPTU Fan (MWh)	FPTU Coil (MWh)	Primary Fan (MWh)	Primary Chiller (MWh)	Total Plant Energy (MWh)	Difference
MEB Houston	3.70	90	3.65	68.1	166	
Davis Houston	2.57	90	3.50	68.8	165	0.6%
MEB Phoenix	3.51	74	3.68	49.3	130	
Davis Phoenix	2.37	71	3.59	49.0	126	3.2%
MEB Chicago	4.63	101	3.37	25.9	135	
Davis Chicago	3.02	99	2.72	27.6	132	2.3%
MEB New York	4.14	91	3.41	27.9	126	
Davis New York	2.86	88	2.78	30.0	124	1.6%
MEB San Francisco	4.36	83	3.33	15.9	107	
Davis San Francisco	2.91	80	2.50	20.5	106	0.9%

8.4. Summary

The results of both the series and parallel MEB models compared favorably to the results from the Davis (2010) "black box" models. Comparisons were made for a small, five zone office building in five cities: Houston, Phoenix, Chicago, New York, and San Francisco. These locations were used because Davis (2010) used these locations in his original analysis. Simulations were run for both PSC/SCR and ECM FPTUs. The heating and cooling loads in the building were generated by Davis (2007 and 2010) using the original DOE-2 building simulation program and were used as input into the EES model developed here. The two modeling approaches agreed to within 4% in annual energy use for all FPTUs (parallel and series) except for one case in San Francisco for the PSC/SCR series FPTU where the differences were 6%. For that case, the main contributor to the differences in energy use was the chiller energy use, not the FPTU fan or coil. While the two approaches used different ways to model the FPTU, the small differences in total energy use pointed to the fact that both MEB and black box approaches can be used to simulate FPTUs.

CHAPTER 9

ANNUAL PERFORMANCE ESTIMATES OF SERIES AND PARALLEL FPTUS

The performance models of fan-powered terminal units (FPTUs) with fixed and variable airflow operations were developed in Chapters 6 and 7, respectively. For these models to be useful, they need to be integrated into larger HVAC system models. The impact on annual energy use can then be estimated for different FPTU characteristics such as motor types (PSC and ECM), terminal unit types (series and parallel), ECM sizing, fixed and variable airflow operations, and air leakage in parallel units. The purposes of this chapter were to 1) develop a prototype small office building that could be modeled in EnergyPlus and used to generate the thermal loads needed for Engineering Equation Solver (EES), 2) compare the annual energy savings in the small office building that occurred with a range of fixed airflow FPTU options for a simplified VAV system model implemented in both Engineering Equation Solver (EES) and EnergyPlus and 3) use the EES model to estimate the impact of variable airflow FPTUs and leakage in parallel FPTUs on the annual system energy consumption. The energy savings estimates developed in this chapter were for a small office building. They illustrate the use of the models developed in the chapters 6 and 7. Because FPTUs are applied in a wide range of building types and sizes, the savings for a small office building may differ from the savings estimates in a larger building or from a building with a different purpose (healthcare, retail, etc.) where the internal loads may vary dramatically from the small office building modeled in this chapter.

9.1. Building and HVAC System Model Development

A single story office building model with five zones was generated in EnergyPlus. The HVAC system was a single-duct VAV system that could be modeled with either all series or all parallel FPTUs. The modeling work conducted in EnergyPlus served two purposes. First, EnergyPlus provided the zone peak load and hourly loads throughout a year, both of which were required by the EES models. Second, annual energy use estimated by EnergyPlus was used as a comparison to the energy use estimated by the EES models for fixed airflow FPTU applications. These comparisons provided insights into the ability of the simpler EES model to capture major energy uses in a VAV system.

The design load of each zone and the hourly load profile throughout a year in five cities were generated by using EnergyPlus, along with the annual energy use in the HVAC systems as a result of using series and parallel FPTUs. Because EnergyPlus required fan total pressure and efficiency, it did not allow the direct modeling of either PSC/SCR or ECM FPTUs that could be done in the EES model. The FPTU fan power at the design airflow in each zone had to be matched to the EES model by adjusting the fan efficiency and/or the fan total pressure in EnergyPlus. In addition, neither variable airflow FPTU fans nor leakage effects in the parallel units could be captured in EnergyPlus. Therefore, the modeling work conducted in EnergyPlus focused only on fixed airflow series and parallel FPTUs without leakage.

Figure 9.1 showed the geometric model of the office building simulated in EnergyPlus. The building had dimensions of 100 ft × 50 ft × 8 ft (30.5 m x 15.2 m x 2.4 m) with a conditioned floor area of 5000 ft^2 (464 m^2). The building was split into five zones with four exterior zones and one interior zone. The exterior zone depth was 12 ft (3.7 m), and the window-to-wall ratio was 0.29. The properties of building materials and structure of building envelops were directly adopted from one of the commercial prototype building models developed by Pacific Northwest National Laboratory (PNNL). It complied with ASHRAE Standard 90.1-2013. Table 9.1 showed the R values for exterior wall and roof as well as U and solar heat gain coefficient (SHGC) values for exterior windows that were used in this building model.

Table 9.2 showed the internal heat gains from occupancy, lighting, and equipment along with infiltration and ventilation. Thermostat settings of 75°F (23.9°C) for cooling and 73°F (22.8°C) for heating were used for the calculation of peak design load and hourly load. The 2°F (1.1°C) difference between the cooling and heating set point was considered as the deadband. Representative schedules for occupancy, lighting, and equipment were added to capture the variation of internal heat with time.

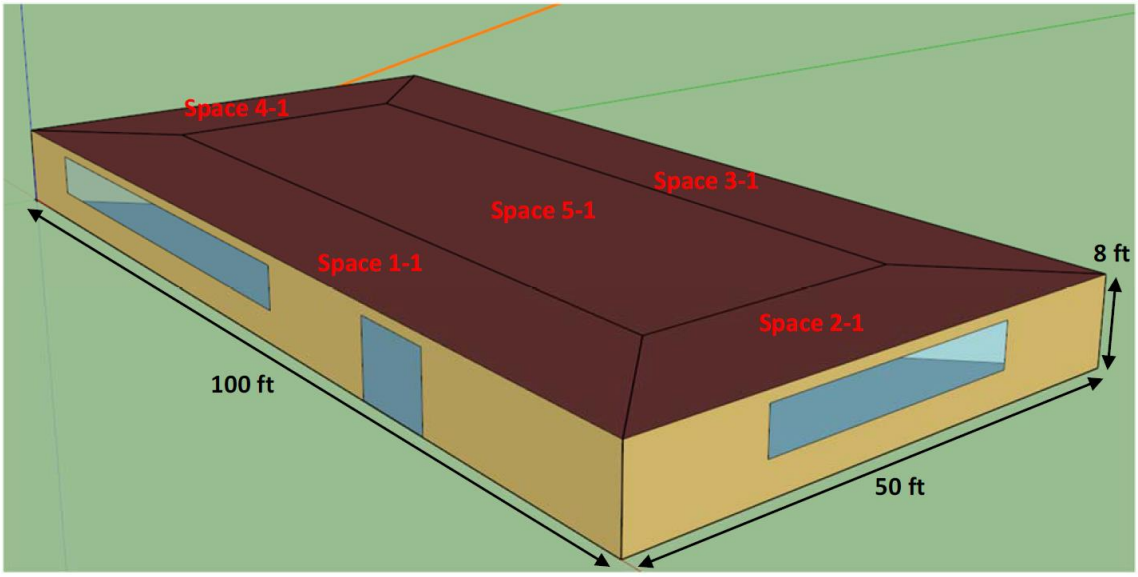

Figure 9.1: Single-Story Office Building Model in EnergyPlus

Table 9.1 - Building Modeling Design Parameters

	Houston TX	Phoenix AZ	San Francisco CA	New York NY	Chicago IL
	Climate Zone 2A	Climate Zone 2B	Climate Zone 3C	Climate Zone 4A	Climate Zone 5A
Exterior wall insulation R value, ft^2-F-h/Btu	9.1	9.1	9.1	13.5	17.4
Exterior roof insulation R value, ft^2-F-h/Btu	35.4	35.4	35.4	46	46
Exterior Window U value, Btu/h -ft^2-F	0.6	0.6	0.55	0.42	0.42
Exterior Window SHGC	0.25	0.25	0.25	0.4	0.4

Table 9.2 - Internal Heat Gain and Infiltration/Ventilation Design Parameters

Item	Value
Occupancy	178 ft^2/person and 120 W/person with schedules
lighting	0.84 W/ft^2 with schedules
Equipment	0.63 W/ft^2 with schedules
Infiltration and ventilation	0.15 ft^3/min per ft^2 of exterior wall area
	400 ft^3/min for space 1-1 and space 3-1 for door opening with schedules
Thermostat	75°F cooling constant 73°F heating constant

A single duct VAV system with either all series or all parallel FPTUs was defined in EnergyPlus by using HVACTemplate:Zone:VAV:FanPowered and VACTemplate:System:VAV through a series of temperature, pressure, fan efficiency, and airflow inputs. Table 9.3 showed the input parameters that were used for modeling VAV systems with series or parallel FPTUs.

Table 9.3 - Input Parameters for Modeling VAV Systems with Series or Parallel FPTUs

Item	Value
Primary supply air minimum flow fraction	0.2
Zone cooling design supply air temperature	55°F
Zone heating design supply air temperature	90°F
Fan delta pressure	0.5 in. w.g.
Fan total efficiency	Calculated based on EES results

The system loop representing a VAV system with series FPTUs in EnergyPlus is shown in Figure 9.1. The supply side consisted of a preheat coil, a system air mixer, a primary cooling coil, and a supply fan. These components were used to model the processes in the central air handling unit. The demand side incorporated all conditioned spaces and zonal equipment loads. Each component in the system loop was defined in EnergyPlus individually and connected by using the nodes represented by the black dots in Figure 9.1. The supply and demand sides were connected by using the zone air splitter and mixer. The primary air was delivered to the zones by the primary supply fan. The amount of primary air was based on the zone load. The primary air was mixed with a pre-determined amount of secondary air. The mixture of primary and secondary air formed the supply air, which was delivered to each zone by the terminal unit.

After mixing of the supply air into the zone, secondary air was drawn back to the series terminal unit for re-circulation while an amount of the air from the zone equal to the primary air was returned to the supply side through the system air mixer, where a certain percentage of the return air was exhausted to the outside and replaced by the outdoor air. The mixture of return and outdoor air went through the primary cooling coil and completed the air loop. While the supply side remained the same for the system with parallel units, the demand side in Figure 9.2 was simply replaced by Figure 9.3.

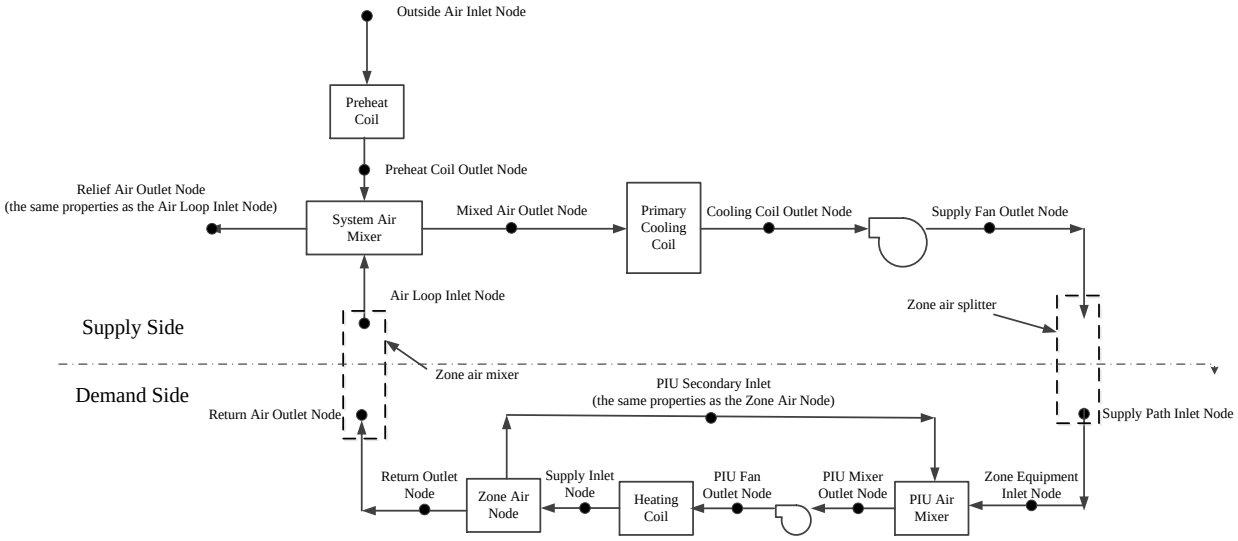

Figure 9.2: VAV System Diagram with Series FPTUs in EnergyPlus

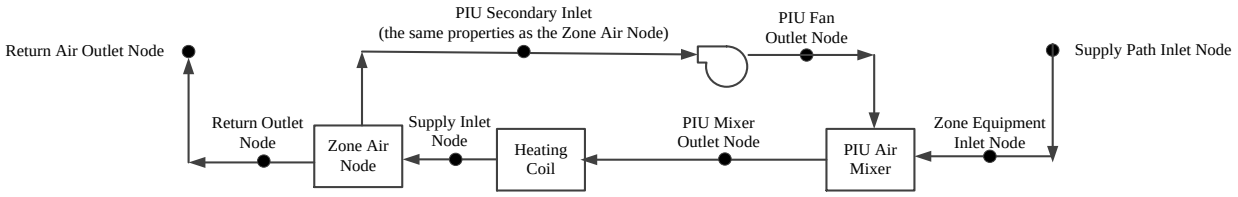

Figure 9.3: Demand Side VAV System Diagram with Parallel FPTUs in EnergyPlus

9.1.1 Design and Hourly Cooling Load Generation After the building model was developed, the data for heating and cooling design days for five U.S. cities (Phoenix AZ, San Francisco CA, Chicago IL, New York NY, and Houston TX) were obtained from ASHRAE *Handbook of Fundamentals* (ASHRAE 2013) as shown in Table 9.4. January 21st was the heating design day and July 21st was the cooling design day. With the information shown in Tables 9.1 through 9.4, the peak zone load was calculated by using EnergyPlus. The load calculation results are summarized in Table 9.5. There was a wide variation in design loads for the five zones in each city shown in this table. The largest cooling loads were in Phoenix for all five zones.

Table 9.4 - Summary of Heating and Cooling Design Day Data

Item	Design Temperatures				
	Houston TX	Phoenix AZ	San Francisco CA	New York NY	Chicago IL
Heating design day	33.8°F DB (1.0°C DB)	38.7°F DB (3.7°C DB)	38.8°F DB (3.8°C DB)	13.8°F DB (-10.1°C DB)	-1.5°F DB (-18.6°C DB)
Cooling design day	95.2°F DB 76.6°F WB (35.1°C DB 24.8°C WB)	110.1°F DB 70°F WB (43.4°C DB 21.1°C WB)	82.9°F DB 63°F WB (28.3 °C DB 17.2 °C WB)	89.8°F DB 72.9°F WB (32.1 °C DB 22.7 °C WB)	91.9°F DB 74.7°F WB (32.3 °C DB 23.7 °C WB)

Table 9.5 - Design Peak Cooling Loads

City	Load calculation, Btu/h(kW)				
	Space 1-1	Space 2-1	Space 3-1	Space 4-1	Space 5-1
Houston TX	14800(4.3)	6810(2.0)	11700(3.4)	8490(2.5)	13100(3.8)
Phoenix AZ	20200(5.9)	8640(2.5)	14200(4.2)	9130(2.7)	14300(4.2)
San Francisco CA	16500(4.8)	7180(2.1)	9230(2.7)	7180(2.1)	12900(3.8)
New York NY	17700(5.2)	8140(2.4)	12000(3.5)	8300(2.4)	12900(3.8)
Chicago IL	18200(5.3)	8310(2.4)	12200(3.6)	8770(2.6)	13000(3.8)

*only sensible load was calculated.

The peak cooling loads were used to size the FPTUs in the EES models. In addition to the peak design loads shown in Table 9.5, the hourly heating and cooling loads throughout a year were determined for each of the cities, which were used as input by the EES models to estimate the energy consumption of VAV systems with series and parallel FPTUs.

9.1.2 Description of the VAV System Calculation in the EES Model The local climate conditions, zone peak design load, and hourly zone loads were imported into the EES models.

The zone peak load was used to size the design airflow requirement in the zone and provide a reference for the airflow capacity of each terminal unit. For the ECM units with a capacity factor above zero, their capacity was found by using the capacity factor to estimate the maximum airflow of the FPTU. The hourly zone loads were used to determine the hourly energy consumption of terminal unit fans, heating coils, preheat coils, primary cooling coils, and primary supply fans. The VAV system calculation in the EES model started with each zone being maintained at a certain set-point temperature of 75°F (23.9°C) with the same zone hourly load and local climates as determined by the EnergyPlus model. These data were provided for every hour of the year. The FPTU models developed in Chapters 6 and 7 were used to characterize the performance of fixed airflow series and parallel units. The zone calculations of airflow and temperature were then merged to solve for the return air loop of the complete VAV system. The mixing temperature of the return air and outdoor air was used to determine whether or not preheating was required. If the temperature was below the primary air temperature of 55°F (12.8°C) then the preheating coil was used to heat the mixed air to the primary air temperature. The procedure then calculated the power consumption of the primary fan and proceeded to calculate the cooling energy required at the primary cooling coil. If there was another hour then the procedure looped back to the start, otherwise the procedure is completed.

9.2. Differences Between EES and EnergyPlus Modeling Methodologies

The annual energy consumption in a typical VAV system with either series or parallel FPTUs was calculated by using EnergyPlus with the TMY3 climate data for Phoenix AZ, San Francisco CA, Chicago IL, New York NY, and Houston TX. The output from EnergyPlus included the annual energy consumption of primary cooling coil, primary supply fan, preheat coil, terminal unit fans, and heating coil. These EnergyPlus results were compared with the EES results that were generated by using the same local climate conditions and hourly zone loads. To provide meaningful interpretation of the comparison results, it was important to know the differences between the EES and EnergyPlus modeling approaches. Table 9.6 summarized the major differences between EES and EnergyPlus models.

Table 9.6 - Summary of Differences between EES and EnergyPlus Models

		EES model	EnergyPlus model
Supply side	Preheat coil location	Primary air stream	Outdoor air stream
	Chiller cooling performance	Constant capacity without limit	Capacity varying with outdoor temperature and limited turndown ratio
	Primary air temperature	Constant at 55°F and 95% RH independent of outdoor temperature	Ranging from 55 to 64°F due to varying the chiller cooling performance
	Primary supply fan power	Constant pressure rise and efficiency	Varying with airflow following the fan laws
	Outdoor air	A fixed fraction of zone supply air	A fixed fraction of primary air
Demand side	Terminal unit fan power	The capacity factor approach	Airflow rate, pressure rise, and efficiency
	Deadband	2% of zone peal load	2°F between heating and cooling set point
	Terminal unit airflow control	Capable of fixed and variable airflow operation	Only fixed airflow
	Air leakage in parallel units	Fixed percentage of primary air	Nor available

9.2.1 ***Preheat Coil Location*** Figure 9.4 showed the system layout for the demand side of the EES model. The preheat coil was located downstream of the mixing of return and outdoor air. At this location, the cold outdoor air was tempered with the return air before entering the preheat coil. This location was chosen to match the simulations by Davis et al (2010) presented in Chapter 8. Unlike the EES model, EnergyPlus placed the preheat coil in the outdoor air stream before mixing with the return air as shown in Figure 9.2. Because of the differences in location of the preheat coil, the EnergyPlus model should require more preheat energy than the one in the EES model. In both cases, the preheat coil heated the air up to the minimum primary temperature. However, with the preheat coil located in the outside air intake, there would be more hours where the outdoor temperature was below the primary air temperature compared to the EES location where return air was mixed with the outdoor air which kept the mixed air temperature above the primary air temperature most of the time in the simulations.

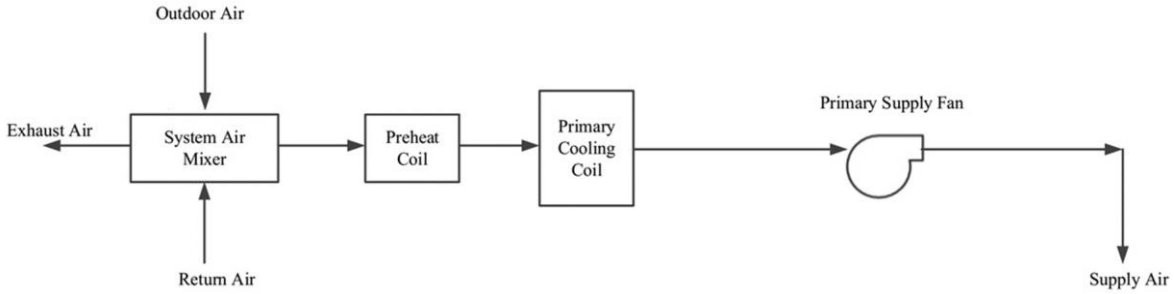

Figure 9.4: Demand Side Layout for the EES Model

9.2.2 Chiller Cooling Capacity and Primary Air Temperature The chiller was modeled as a virtual component in the EES model with unlimited cooling capacity turndown ratio and a constant COP. In EnergyPlus, the chiller performance was constrained by an integrated part load value curve and outdoor air temperature. Therefore, chiller COP and the primary air temperature in EnergyPlus changed with outdoor temperature. In contrast, the EES model assumed a single chiller COP and a fixed primary air temperature, both of which were independent of outdoor air temperature.

9.2.3 Primary Supply Fan Power For the EES model, the user specified a constant fan pressure rise and efficiency for the fan/motor to estimate the power used by the fan motor. In EnergyPlus, the fan laws were used to calculate the fan power as a function of airflow rate. If the primary airflow was at small part load values for significant periods of time during a simulation, then the EnergyPlus model would be expected to estimate lower energy use for the primary fan since power decreased by the third power with the EnergyPlus model.

9.2.4 Outdoor Air The outdoor air calculation was also different for the EES and EnergyPlus models. In EnergyPlus, the outdoor air was calculated as a constant percentage of the primary air that was conditioned by the primary cooling coil. Because the primary air varied with zone loads, the outdoor air also fluctuated even though the outdoor fraction was a constant. Rather than using the primary air for the basis of the outdoor air fraction, the EES model calculated the outdoor air as a percentage of the supply air to each zone. The sum of the required outdoor air in each zone was equal to the total amount that was introduced into the VAV system. Because the zone supply air was constant in the fixed airflow operation, the outdoor air was also constant in the EES calculation approach.

9.2.5 Terminal Unit Fan Power In EnergyPlus, the terminal unit fan power was calculated according to:

$$Pow_{fan} = \frac{m_{tot}\Delta P_{fan}}{\eta_{tot}\,\rho_{air}} = \frac{Q_{tot}\Delta P_{fan}}{\eta_{tot}} \quad (9.1)$$

Where ΔP_{fan} was the pressure rise across the terminal unit fan, η_{tot} was the fan/motor efficiency, and Q_{tot} was the total fan airflow rate. In the EES models, the terminal unit fans driven by PSC motors were calculated by using the airflow rate times a constant efficacy of 0.372 W per ft^3/min determined by results in Chapter 2. The power for ECM fans in the EES model was calculated by using the empirical model developed in Chapter 3:

$$Pow_{fan}(Q) = f_{plv} * C_3 * Q_d * (1 + x_o) \quad (9.2)$$

where Q_d was the design airflow rate, Q was the airflow rate actually delivered, x_o was the capacity factor as defined in Equation 9.3, and f_{plv} was the part load power fraction as calculated in Equation 9.4 with the empirical coefficients in Table 9.7. The constant, C_3 in Equation 9.2 was 0.38 W/(ft^3/min) in IP units or 805 W/(m^3/s) in SI units.

$$x_o = \frac{Q_o}{Q_d} - 1 \quad (9.3)$$

$$f_{plv} = a_1 + a_2 * \left(\frac{Q}{Q_d(1+x_o)}\right) + a_3 * \left(\frac{Q}{Q_d(1+x_o)}\right)^2 + a_4 * \left(\frac{Q}{Q_d(1+x_o)}\right)^3 \quad (9.4)$$

Table 9.7 - Part Load Power Fraction Coefficients for Equation 9.4

Coefficients	Value
a_1	0.061715
a_2	0.093022
a_3	-0.11627
a_4	0.961538

Given the differences between the terminal unit fan power calculations, it was necessary to ensure the fan power calculations in EnergyPlus were consistent with the results from the EES models. The terminal unit fan power in the series and parallel FPTUs were first calculated by using the EES models, and then the calculated fan power results were input into Equation 9.1 to determine the fan/motor total efficiency that could be used in EnergyPlus to provide the same fan power results. In addition, the fan power calculation results with three different capacity factors

of 0, 25%, and 50% were generated in the EES models for both series and parallel units, which were also converted into the equivalent fan/motor efficiencies for the EnergyPlus modeling.

9.2.6 Deadband. The EES models used loads to describe the deadband while EnergyPlus utilized temperature to characterize the equipment operation in deadband. In the EES model, the range of 2% of the zone peak design load was considered as the deadband. In the EnergyPlus model, the 2°F (1.1°C) range between the heating set point temperature of 73°F (22.8°C) and the cooling set point temperature of 75°F (23.9°C) was used to represent the deadband.

9.2.7 Other Limitations in the EnergyPlus Model Beyond the aforementioned differences, EnergyPlus did not allow the modeling of variable airflow operation and air leakage in parallel units, both of which were implemented in the EES FPTU models.

9.3. EnergyPlus Calculation Results

The annual energy consumption of the five zone VAV system with fixed airflow series and parallel FPTUs for five U.S. cities were estimated using EnergyPlus and summarized in Table 9.8. Three ECM scenarios were evaluated for both series and parallel FPTUs. These included capacity factors of 0%, 25%, and 50%. The 0% capacity factor would correspond to a FPTU with a maximum airflow capacity that would just match the design airflow requirement of the zone. The 25% and 50% capacity factors corresponded to FPTUs with maximum airflow capacities that were 25% and 50% larger, respectively, than the design airflows in a zone. In the cases with capacity factors of 25% and 50%, the airflow of the FPTU would be reduced to match the design airflow requirements of the zone to take advantage of the reduced power of the FPTU operating at the lower airflow rate compared to at its maximum rating. It was our understanding that ECM FPTUs would often have higher capacity factors to help reduce noise from the FPTU.

With PSC/SCR unit as the baseline, the differences in energy use between the PSC/SCR and 0% capacity factor ECM unit were generally less than about 0.2% for all cities. The table showed the benefit of installing series ECM FPTUs with maximum capacities larger than the design airflows. Increasing the capacity factor of the ECM series FPTUs from 0% to 50% reduced the system energy use in all cities. For example, in a cooling dominated climate like Houston, the energy use dropped from 82,736 kWh to 78,133 kWh, a reduction of 5.6%. In Chicago, the reduction was 3.8%.

Table 9.8 also showed the savings for parallel FPTUs over the fixed airflow series FPTUs. The savings for the PSC/SCR parallel over the PSC/SCR series FPTUs ranged from a low of

5.4% in Chicago to 10.7% in Phoenix. Because the fan doesn't run in cooling mode for a parallel FPTU, the largest savings for parallel units can be expected to be in cooling dominated climates. Thus, it was not surprising that the largest savings for the parallel over the series FPTU was in Phoenix. In contrast to the series ECM FPTUs, increasing the capacity factor for parallel ECM FPTUs provided little energy benefit over the 0% capacity factor ECM parallel FPTU. For example, going from 0% to 50% capacity factor parallel FPTU only reduced the estimated energy use by 1.5% in Houston and 1.1% in Chicago and San Francisco. Because leakage could not be directly modeled in EnergyPlus, it was not included in Table 9.8. Without leakage, the parallel units always used less energy than the series units in every city. For this small office building, the differences in energy use between using a fixed airflow ECM series FPTUs with a 50% capacity factor compared to a 50% capacity factor fixed airflow ECM parallel FPTU varied from less than 3% (Chicago and New York) to as high as 6.1% (Phoenix). These differences indicated while a strategically sized ECM series could help "close the gap" between the series and parallel units, there were still some performance advantages for parallel units with no leakage.

Table 9.8 - Annual Energy Consumption Estimated by EnergyPlus

OPTION	Annual Energy Use (kWh)				
	Houston	Phoenix	New York	Chicago	San Francisco
PSC/SCR Series	82516	87872	79618	84002	59670
0% Capacity Factor Series ECM	82736	87953	78820	84152	59778
25% Capacity Factor Series ECM	79637	84034	76955	82038	58206
50% Capacity Factor Series ECM	78133	82100	76048	81012	57588
PSC/SCR Parallel no leakage	75703	78414	74991	79502	56108
0% Capacity Factor Parallel ECM no leakage	75767	78481	74716	79548	56269
25% Capacity Factor Parallel ECM no leakage	74920	77550	74181	78927	55834
50% Capacity Factor Parallel ECM no leakage	74523	77114	73931	78643	55648

9.3.1 Annual Energy Savings of Fixed Airflow FPTU Options using EnergyPlus and EES

As noted earlier in this chapter, the two modeling methodologies (EnergyPlus and EES) employed different assumptions when modeling the simple five zone office building. Because of these differences, the absolute value of the energy use for the building in each of the cities might be expected to differ significantly. Another approach to comparing the models was to compare the percentage energy savings. This was the approach used below.

By using the zone peak design loads and the hourly zone load profiles generated by EnergyPlus, multiple runs were conducted by using the EES models with different FPTU options, including terminal units with PSC/SCR motors and ECMs with capacity factors of 0, 25%, and 50% in both series and parallel configurations. The comparisons were done by assuming the PSC/SCR FPTU would serve as the baseline in both the EES and EnergyPlus models. The estimated annual system energy use of the other FPTU configurations was compared to the baseline and presented as the percentage change in annual energy use (either increase or decrease) relative to the baseline scenario.

Table 9.9 showed the comparison of percentage changes in annual energy use relative to the baseline for fixed airflow series FPTUs for the five cities of Houston, Phoenix, New York, Chicago, and San Francisco. Although the percentage changes estimated by EnergyPlus and EES models differed, the trend in percentage energy changes with respect to ECM FPTU sizing were generally consistent in that larger capacity factors resulted in larger savings. Compared with the baseline scenario, both EnergyPlus and EES models showed that using fixed airflow ECM series FPTUs with large capacity factors (50%) could reduce the overall system energy consumption.

In contrast, the 0% capacity factor ECM units little advantage over the PSC/SCR units. In the city of Houston, for example, the EES model estimated that a series ECM FPTU with 0% capacity factor would increase overall energy use by 1.1% compared to the baseline. An increase of 0.3% was also observed in the EnergyPlus results. The EES models showed that the switch from PSC motors to 0% capacity factor ECM series FPTUs would increase the annual energy consumption in a range from 1.1 to 1.5%. The EnergyPlus models estimated a smaller percentage increase in the range of 0.1 to 0.3% compared with the baseline.

Table 9.9 - Change in Annual Energy Use of the Fixed Airflow Series FPTUs in Five Cities

Option	Change in Annual Energy Use (%)									
	Houston		Phoenix		New York		Chicago		San Francisco	
	EES	E+	EES	E+	EES	E+	EES	E+	EES	E+
PSC/SCR Series	Baseline									
0% Capacity Factor Series ECM	1.1	0.3	1.4	0.1	1.3	-1.0	1.1	0.2	1.5	0.2
25% Capacity Factor Series ECM	-2.2	-3.5	-2.6	-4.4	-1.9	-3.3	-1.8	-2.3	-2.7	-2.5
50% Capacity Factor Series ECM	-3.9	-5.3	-8.1	-6.6	-3.5	-4.5	-3.2	-3.6	-4.9	-3.5

Increasing the capacity factor of ECM FPTUs increased the percentage energy savings predicted by both the EES and EnergyPlus models. The percentage energy savings relative to the baseline scenario in Houston increased from 2.2% at a capacity factor of 25% to 3.9% at a capacity factor or 50% with the EES model. The EnergyPlus model estimated a higher percentage savings of 3.5% and 5.3% at capacity factors of 25% and 50%, respectively, in Houston. In San Francisco, the EES model estimated savings of 2.7% and 4.9% for capacity factors of 25% and 50%, respectively. For this city, the EnergyPlus model estimated slightly lower percentage savings of 2.5% and 3.5%, respectively, than the EES model did for the same capacity factors. In Phoenix, the EES model estimated lower energy savings (2.6% versus 4.4%) at the 25% capacity factor than the EnergyPlus model, but higher energy savings (8.1% versus 6.6%) than the EnergyPlus model at the 50% capacity factor. Both models provided similar trends with respect to increased capacity factors. The results showed that in some cases, one model estimated higher savings and in other cases, it estimated lower savings. Given the differences in modeling assumptions, the results indicated that either model could be used for estimating percentage energy savings of fixed airflow FPTU options.

9.3.2 Parallel Comparison with Five Cities Following the same approach used above for the fixed airflow series FPTU, the two models were used to estimate options for fixed airflow parallel FPTUs. Table 9.10 shows the comparison of percentage energy changes in systems with fixed airflow parallel FPTUs. Similar to the series FPTU comparisons, the annual energy consumption of the FPTUs with PSC/SCR motors was used as the baseline. Results of fixed airflow ECM units with different capacity factors were compared with the baseline and presented as the percentage changes.

For both the EES and EnergyPlus models, the estimated changes in annual energy use for the ECMs in the fixed airflow FPTUs was small. For the 0% capacity factor ECM units, the energy use increased slightly in most locations. In the parallel FPTU, the FPTU fan only ran in the deadband and heating modes. Thus, the fan did not run in cooling mode. For heating mode, the savings in fan motor energy for the ECMs with larger capacity factors tended to be offset by the additional heating energy needed to make up for the smaller amount of energy given off in the airstream by the ECMs. There should be some savings when the system was operating in the deadband mode, but as Table 9.10 showed, these savings were small.

Table 9.10 - Comparison of Parallel FPTUs with Five Cities

Fixed Airflow Option	Change in Annual Energy Use (%)									
	Houston		Phoenix		New York		Chicago		San Francisco	
	EES	E+	EES	E+	EES	E+	EES	E+	EES	E+
PSC/SCR Parallel no leakage	Baseline									
0% Capacity Factor Parallel ECM no leakage	0.1	0.1	0.2	0.1	0.3	-0.4	0.1	0.1	0.1	0.3
25% Capacity Factor Parallel ECM no leakage	-0.9	-1.0	-0.8	-1.1	-0.9	-1.1	-1.0	-0.7	-1.6	-0.5
50% Capacity Factor Parallel ECM no leakage	-1.4	-1.6	-1.2	-1.7	-1.5	-1.4	-1.6	-1.1	-2.5	-0.8

As with the fixed airflow series FPTUs, there were some cities where EES estimated higher energy savings (Houston and Phoenix), two other cities (Chicago and San Francisco) where EES estimated slightly smaller savings, and one city (New York) where EES savings were mixed

compared to the EnergyPlus estimated savings. Both models showed similar trends of increased energy savings with increased capacity factor for the ECM fixed airflow FPTU. However, compared to the application of higher capacity factor ECMs in fixed airflow series FPTUs, the energy changes were much smaller for the fixed airflow parallel ECMs.

9.3.3 Comparison Between EES and EnergyPlus Models with Different Outdoor Air Calculation Methods Tables 9.9 and 9.10 showed that both the EES and EnergyPlus models were capable of capturing the trends in the percentage energy changes in response to increasing the capacity factors of fixed airflow ECM FPTUs. While the estimated percentage energy savings varied between the EES and EnergyPlus models, there did not seem to be a discernable bias in the results that would preclude use of one model over the other for estimating impact of different options for fixed airflow FPTU cases. Given the differences in modeling approaches in and assumptions between the two models in Table 9.6, we were pleased by the consistent trends in estimating energy savings.

One of the major differences between the two modeling approaches was the way outdoor air fraction was calculated and implemented. The outdoor air calculation method in the EES model was modified to follow the method used in the EnergyPlus model. The annual system energy consumption in the system with series PSC FPTUs was then re-calculated and compared with the results with EnergyPlus in Table 9.11. The "as-is" referred to the base outdoor air calculation method that was shown in Table 9.6 was used in each model. For the "alternative" outdoor air calculation, the EES model was modified to mimic the outdoor air method used in EnergyPlus.

Table 9.11 - Comparison of EES and EnergyPlus Models with Different Outdoor Air Calculation Method

Outdoor air calculation method	Models	Houston	Phoenix	New York	Chicago	San Francisco
		Annual Energy Use (kWh)				
As-is	EnergyPlus	82516	87872	79618	84002	59670
	EES	81722	87837	68948	73059	45325
	Diff, %	-1.0	0.0	-13.4	-13.0	-24.0
Alternative	EnergyPlus	82516	87872	79618	84002	59670
	EES	78387	91628	74642	76034	59960
	Diff, %	-5.0	4.3	-6.3	-9.5	0.5

Results in Table 9.11 showed that the different outdoor air calculation approach significantly affected the total system energy use. For example, the modification in the outdoor air calculation decreased the energy difference between the two models in San Francisco from 24% to 0.5%. San Francisco had the largest difference in energy use between the two models in the "as-is" case. The modification reduced the differences in annual energy use in New York and Chicago, but increased the differences in Houston and Phoenix.

The different approaches to the outdoor air calculation would also lead to different mixing temperatures of return and outdoor air at the cooling coil inlet and, consequently, results in different cooling coil energy consumption. The preheat coil energy consumption was affected by the different outdoor air calculation methods. In the EES model, the preheat coil was located downstream of the mixing of the return and outdoor air. If the amount of outdoor air in the EES model was calculated the same was in EnergyPlus, then the amount of outdoor air would be based on the percentage of the primary airflow through the cooling coil. In this case, the preheat coil in EES would never be activated because the large percentage of the warm return air mixing with the outdoor temperature would make the mixed air temperature well above the primary temperature of 55°F. However, if the outdoor air was calculated as the percentage of zone supply air in the baseline EES model, the amount of return air may be smaller than the exhaust air in some instances. In this case, the EES model was programmed to exhaust 100% return air and replace it with outdoor air. When the outdoor dry-bulb temperature was below 55°F, the air was heated to 55°F by the preheat coil and delivered to different zones. Unlike the EES model, the EnergyPlus model placed the preheat coil in the outdoor air stream before mixing with the return air as was shown in Figure 9.1. Therefore, the preheat coil was activated whenever the outdoor dry-bulb temperature dropped below 55°F.

9.3.4 Comparison of Series FPTUs with Fixed and Variable Airflow Operations The comparison between EES and EnergyPlus models showed that the EES model was capable of charactering the energy savings with respect to motor types, terminal unit configurations, and capacity factors. However, the energy benefit of variable airflow operations relative to the fixed airflow operation was of more interest because of the large application of variable airflow ECM FPTUs. EnergyPlus did not allow the modeling of variable airflow operation in FPTUs. Therefore, the EES model was used to quantify the energy savings of variable airflow operations relative to the fixed airflow operation in both series and parallel FPTUs.

For systems with series FPTUs, the annual energy consumption of FPTU fans, heating coils, primary fan, primary cooling coil, and preheat coil at various combinations of motor types (PSC and ECM), capacity factor (0, 25, and 50%), and operation modes (fixed and variable airflow) were estimated by using EES for the same five cities used above: Houston, Phoenix, New York, Chicago, and San Francisco. It is our understanding that FPTUs with capacity factors as large as 50% may often be applied to reduce noise from the FPTU. For comparison purposes, the results of systems using PSC/SCR motors were used as the baseline scenarios. The results of other cases were compared with the baseline and presented as the percentage changes relative to the baseline.

Figure 9.5 shows the percentage energy changes relative to the baseline for several series FPTU configurations. The FA stood for fixed airflow operation while the VA stood for variable airflow operation. The percentage value after the FA and VA showed the capacity factor (C.F.) used in each energy calculation. The results were also summarized in Table 9.12. Both Figure 9.5 and Table 9.12 showed that increasing the capacity factor of ECMs had the benefit of reducing system energy use. For instance, in the fixed airflow operation, the use of ECMs with 0% capacity factor increased the system energy use by 1.1 to 1.5% compared with the use of traditional PSC motors for all the five cities. However, when ECMs were sized with non-zero capacity factors, the system energy consumption consistently decreased for all the five cities. At a capacity factor of 25%, the savings ranged from 1.8% in Chicago to 2.7% in San Francisco. When the capacity factor was increased to 50%, the savings increased and ranged from a low of 3.2% in Chicago to a high of 8.1% in Phoenix.

Variable airflow series ECM units provided larger savings. For example, the energy savings relative to the baseline scenario in the city of Houston increased from 7.1% at 0% capacity factory to 9.2% at a 50% capacity factory. In all cities, the largest energy savings was with the variable airflow ECM FPTU with a 50% capacity factor. The largest savings was in Phoenix with a 10.9% reduction while the smallest was in Chicago with a 6.4% reduction. These results provided solid evidence that significant energy savings could be achieved with variable airflow operations in series ECM FPTUs. Given a particular capacity factor, the variable airflow FPTU always provided greater energy savings relative to its fixed airflow counterpart.

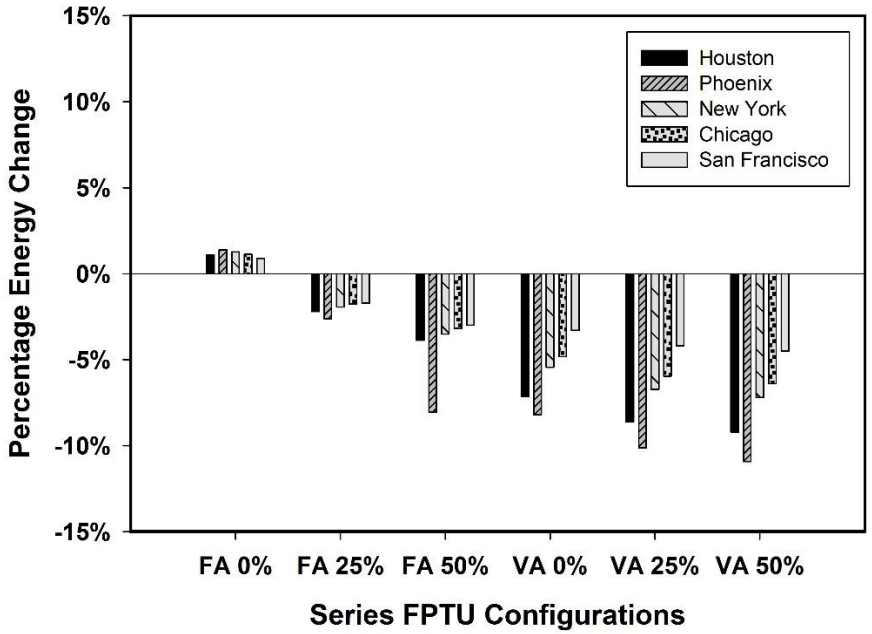

Figure 9.5: Percentage Energy Changes for Fixed and Variable Series FPTUs

Table 9.12 - Summary of Percentage Energy Changes for Series FPTUs

Series FPTU Option*	Change in Annual Energy Use (%)				
	Houston	Phoenix	New York	Chicago	San Francisco
FA PSC/SCR	Baseline Scenario				
FA 0% C.F.	1.1%	1.4%	1.3%	1.1%	1.5%
FA 25% C.F.	-2.2%	-2.6%	-1.9%	-1.8%	-2.7%
FA 50% C.F.	-3.9%	-8.1%	-3.5%	-3.2%	-4.9%
VA 0% C.F.	-7.1%	-8.2%	-5.4%	-4.8%	-5.3%
VA 25% C.F.	-8.6%	-10.1%	-6.7%	-6.0%	-6.7%
VA 50% C.F.	-9.2%	-10.9%	-7.2%	-6.4%	-7.2%

*C.F. indicates capacity factor

The savings with either fixed or variable airflow ECM FPTUs were generally largest in the cooling dominate climates such as Houston and Phoenix. Because the series FPTU fan was directly in the airstream, the lower power usage of the ECM fan motors operating at part load conditions not only saved the power input to the fan, but also introduced less heat energy into the airstream from the fan motor, which reduced the amount of cooling that had to be provided. Thus, it was not unexpected that the largest savings were in the cooling dominated climates.

9.3.5 Comparison of Parallel FPTUs with Air Leakage Figure 9.6 and Table 9.13 showed the comparison of fixed and variable airflow parallel FPTUs for different leakage levels. All of the fixed and variable airflow FPTUs were set at 25% capacity factor. The baseline was assumed to be the fixed airflow PSC/SCR parallel FPTU. Three levels of leakage (0, 5%, and 10%) were used, which were only applied to cooling operations. In Table 9.13 the percentage energy changes were relative to the baseline. FA and VA indicated fixed and variable airflow.

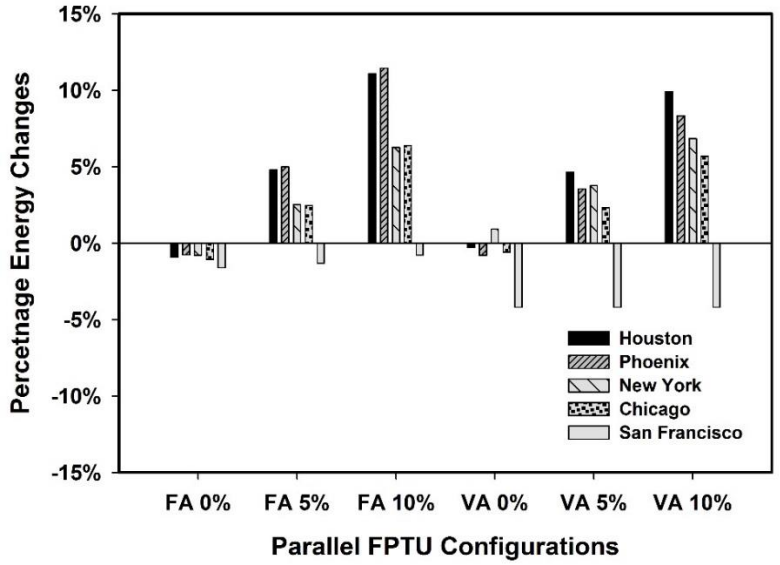

Figure 9.6: Percentage Energy Changes for Parallel FPTUs

Table 9.13 - Summary of Percentage Energy Changes for Parallel FPTUs

Parallel FPTU Option*	Change in Annual Energy Use (%)				
	Houston	Phoenix	New York	Chicago	San Francisco
FA PSC/SCR	Baseline Scenario				
FA 0% leakage, 25% C.F.	-0.9%	-0.8%	-0.8%	-1.0%	-1.6%
FA 5% leakage, 25% C.F.	4.8%	5.0%	2.5%	2.5%	-1.3%
FA 10% leakage, 25% C.F.	11.1%	11.5%	6.3%	6.4%	-0.8%
VA 0% leakage, 25% C.F.	-4.9%	-6.8%	-3.1%	-4.0%	-4.2%
VA 5% leakage, 25% C.F.	-1.3%	-3.1%	-1.5%	-2.6%	-4.3%
VA 10% leakage, 25% C.F.	2.7%	1.1%	0.0%	4.3%	-4.2%

*C.F. indicates capacity factor

The fixed airflow (VA) parallel ECM units with 0% leakage showed marginal differences in energy use when compared to the fixed airflow PSC/SCR baseline in all cities in Table 9.13.

For the variable airflow case with 0% leakage, employing variable airflow parallel units provided some savings over the baseline fixed airflow PSC/SCR. The largest savings was in Phoenix while the smallest was in only San Francisco showed any appreciable reduction in energy use from the baseline and in New York. Overall, the savings were modest and may be due to the much smaller energy use of the FPTU variable airflow ECM fan. The small energy benefits of using fixed airflow ECMs and advanced variable airflow control in parallel FPTUs was due to the fact that the parallel FPTU fans were only used in heating and deadband operations. While heating energy use increased with the variable airflow ECM fan, it did not completely offset the savings with the variable airflow fan. Thus, overall, there was energy savings with the variable airflow ECMs.

The results in Figure 9.6 and Table 9.13 also showed that the system energy use was affected by leakage levels in both fixed and variable airflow operations. In four of the five cities, as leakage increased, there was a corresponding increase in system energy consumption for both the fixed and variable airflow ECM units. San Francisco was the only exception where the energy savings showed only small changes in energy use with leakage. An example of the more typical trend was Houston. As the leakage level was increased from 0 to 10% for the fixed airflow ECM, the percentage energy change in Houston increased from -0.9% to 11.1%. For the variable airflow case, the savings dropped from -4.9% to 2.7%. The energy impact was not surprising considering that additional primary air was required in the presence of leakage to maintain the zone set point temperature. The energy change differed as the leakage level was increased. The different responses to increasing leakage levels were caused by the fact that the leakage was only limited to the cooling operation and the cooling energy use in each city varied due to different local climate conditions. Cities in the cooling dominated climates, such as Houston and Phoenix, showed a much greater energy impact of leakage than the cities in the heating dominated climates.

9.3.6 Comparison of Series and Parallel FPTUs with Different Performance Characteristics

In the above comparisons, the percentage energy changes of FPTUs with different performance characteristics, such as motor types, capacity factors for ECMs, airflow operations, and leakage levels for parallel units, were quantified relative to the baseline scenario in each category of series and parallel FPTUs. In this section, all of the different configurations were compared to a single baseline (PSC/SCR series FPTU). Using one baseline allowed for a comparison of

parallel, series, ECM, leakage/no leakage, etc. in one table – Table 9.14. This table presents the percentage energy savings of each FPTU configuration relative to the one baseline.

Traditionally, parallel FPTUs have been considered to be more energy efficient than series FPTUs because the terminal unit fans in parallel units would only operate intermittently. Results presented earlier in Table 9.8 from EnergyPlus supported the case for the savings of fixed airflow parallel units when no leakage was present. In looking at the entry for the zero leakage parallel PSC/SCR, "Parallel FA PSC/SCR", the zero leakage parallel fixed airflow ECM, "Parallel FA 0% leakage", and zero leakage parallel variable airflow ECM, "Parallel VA 0% leakage", in Table 9.14, all showed estimated savings as low as 8.2% and as high as 16.3%. Thus, if leakage can be eliminated in parallel units, there would be the potential for significant savings when compared to the baseline PSC/SCR series unit. As shown in the table, the application of ECM (either fixed or variable airflow) series units with a 50% capacity factor can also provide considerable savings over the PSC/SCR series units. For fixed airflow ECM series units, the biggest percentage savings were in Phoenix (8.1%) and San Francisco (4.9%) whereas for variable airflow ECM series, the biggest savings were in Phoenix (10.9%) and Houston (9.2%). The savings in variable airflow ECMs with 50% capacity factor were comparable to the savings of a zero leakage parallel PSC/SCR unit in Phoenix and Houston. The savings for variable airflow ECMs were smaller in New York, Chicago, and San Francisco than the PSC/SCR parallel units with zero leakage.

With as little as 5% leakage, the parallel units began to lose some of their advantage over fixed and variable airflow ECM series units, especially in the cooling dominated climates such as Houston and Phoenix. For example, the use of a fixed airflow ECM parallel unit with 5% leakage yielded an energy savings of 4.7% in Houston relative to the baseline, which was similar to the energy savings of 3.9% for the fixed airflow ECM series and not as good as the 9.2% savings of the variable airflow ECM series. Both ECM units were assumed to have capacity factors of 50%. In Phoenix, the energy savings of an ECM variable airflow series units with a capacity factor of 50% was 10.9% compared to 5.6% for the fixed airflow ECM parallel unit with 5% leakage and 12.9% for the variable airflow ECM parallel unit with 5% leakage. Leakage appeared to have the smallest impact on the performance on the parallel FPTUs in San Francisco. In that city, the fixed airflow ECM parallel unit with 5% leakage still provided a 13% savings compared to a 4.9% savings of the fixed airflow ECM with a 50% capacity factor. In

New York and Chicago, the fixed airflow ECM parallel unit with 5% leakage outperformed the fixed airflow ECM series with 50% capacity factor and was comparable in performance to the variable airflow ECM series with 50% capacity factor. The variable airflow ECM parallel unit with 5% leakage outperformed the variable airflow ECM series unit in those two cities.

At a leakage rate of 10%, the fixed airflow ECM parallel units performed worse than the fixed airflow ECM series units with 50% capacity factor in three cities (Houston, Phoenix, and Chicago) and worse than variable airflow ECM series units with 50% capacity factor in four (Houston, Phoenix, New York, and Chicago) of the five cities. Even with 10% leakage, in San Francisco, the fixed and variable airflow ECM parallel units outperformed the fixed and variable airflow ECM series units. Thus, while leakage negatively impacted the energy use of parallel FPTUs, the impact varied by city and type of application (fixed or variable airflow) in the small office building evaluated in this study.

Table 9.14 - Percentage Energy Changes of Series and Parallel FPTUs Relative to the Series FPTUs with Fixed Airflow and PSC Motors

Option	Change in Annual Energy Use (%)				
	Houston	Phoenix	New York	Chicago	San Francisco
Series FA PSC/SCR	Baseline Scenario				
Series FA 0% C.F.	1.1%	1.4%	1.3%	1.1%	1.5%
Series FA 25% C.F.	-2.2%	-2.6%	-1.9%	-1.8%	-2.7%
Series FA 50% C.F.	-3.9%	-8.1%	-3.5%	-3.2%	-4.9%
Series VA 0% C.F.	-7.1%	-8.2%	-5.4%	-4.8%	-5.3%
Series VA 25% C.F.	-8.6%	-10.1%	-6.7%	-6.0%	-6.7%
Series VA 50% C.F.	-9.2%	-10.9%	-7.2%	-6.4%	-7.2%
Parallel FA PSC/SCR	-9.0%	-10.1%	-10.0%	-8.2%	-11.8%
Parallel FA 0% leakage	-9.9%	-10.8%	-10.8%	-9.2%	-13.2%
Parallel FA 5% leakage	-4.7%	-5.6%	-7.8%	-6.0%	-13.0%
Parallel FA 10% leakage	1.0%	0.2%	-4.4%	-2.4%	-12.5%
Parallel VA 0% leakage	-13.5%	-16.3%	-12.8%	-11.9%	-15.5%
Parallel VA 5% leakage	-10.2%	-12.9%	-11.4%	-10.6%	-15.6%
Parallel VA 10% leakage	-6.6%	-9.1%	-10.1%	-4.3%	-15.5%

9.3.7 The Impact of Heating Coil Location in Parallel FPTUs on the System Energy Consumption As mentioned earlier, there were two configurations for parallel FPTUs that

differed in the heating coil location. While the heating coil was located at the terminal unit outlet in the traditional configuration, the alternative configuration placed the heating coil at the inlet of secondary airstream. The system energy use of parallel FPTUs with both traditional and alternative configurations were estimated to investigate the energy impact of heating coil location. Because removing the heating coil from the terminal unit outlet should theoretically decrease the flow resistance that the primary fan is working against, an additional run was performed with reducing the primary fan pressure rise by 0.1 in. w.g. (24.9 Pa). The results of the alternative configuration were compared with the result of traditional configuration and summarized in Table 9.15. The energy impact of heating coil location was minimal, showing less than 0.1% difference between the traditional and alternative configurations. Even with reducing the primary fan pressure rise, the percentage energy changes were less than 0.5% different from the baseline scenario.

Table 9.15 - Comparison of System Energy Consumption between Traditional and Alternative Parallel FPTUs

Option	Change in Annual Energy Use (%)				
	Houston	Phoenix	New York	Chicago	San Francisco
Parallel Traditional, PSC	Baseline Scenario				
Parallel Alternative, PSC	0.04%	0.10%	0.00%	-0.02%	-0.02%
Parallel Alternative, PSC, reduced primary fan pressure rise	-0.20%	-0.21%	-0.27%	-0.27%	-0.37%

9.4. Summary

A simple single story, five zone office building was developed to illustrate the use of the fixed and variable airflow FPTU models developed in Chapters 6 and 7. The magnitude of the energy results with the different FPTU configurations in this office building models may be different than those calculated in a model of a larger building where internal loads may be more dominate or in different types of buildings. It will be important for the FPTU models in Chapters 6 and 7 to be integrated into a larger building simulation model so building modelers can better estimate the impact of different FPTU configurations in different building applications.

The annual energy consumption of the office building was estimated using EnergyPlus. The zone peak loads and hourly load throughout a year that were generated from EnergyPlus were

used as input in EES models to estimate the annual energy consumption of preheat coil, primary cooling coil, primary supply fan, terminal unit fan, and supplemental heating coil. The fixed airflow FPTU results from the EES models were compared with the results from EnergyPlus to validate the EES models of series and parallel FPTUs. The results showed that both models were capable of capturing comparable estimates of percentage energy changes relative to the baseline scenario. The differences between the two models were caused by different component modeling approaches, system layout, and assumptions. The consistent trend in the system energy consumption predicted by the EES models in response to ECM oversizing demonstrated that the performance models of series and parallel FPTUs can be used to quantify the relative energy savings of different terminal unit configurations in terms of motor types, terminal unit types, and ECM oversizing effects.

EES was used to evaluate the energy impact of different FPTU performance characteristics that could not be investigated in the EnergyPlus model, such as the air leakage in parallel units and variable airflow operation. A summary of findings from these comparisons included:

- Fixed airflow ECM series units with capacity factors of 25% and 50% saved energy compared to PSC/SCR series units in all five cities. The percentage savings were largest in Phoenix and smallest in Chicago.
- Variable airflow ECM series units for all capacity factors (0 to 50%) saved energy compared to PSC/SCR series units in all five cities.
- Variable airflow ECM series units always saved energy when compared to a fixed airflow ECM series units operating at the same capacity factor.
- Increasing the capacity factor in ECM series units always provided reduced energy use for the range of capacity factors (0 to 50%) evaluated in this study. In a field application, items such as costs and physical size may limit how large a capacity factor can be used.
- The energy savings for variable airflow ECM series units was largest in the cooling dominated climates (Houston and Phoenix) and smallest in Chicago.
- With no leakage, the fixed airflow PSC/SCR parallel units provided significant energy savings when compared to the baseline PSC/SCR series units. This difference would point to the benefit of sealing seams and ensuring the backdraft damper on a parallel unit did not leak.

- The energy savings for variable airflow ECM series units compared to PSC/SCR parallel units varied by city. It was comparable in two cities (Houston and Chicago) and smaller in three cities (New York, Chicago, and San Francisco).
- Application of either fixed or variable airflow ECM technology to parallel units provided savings over the fixed airflow PSC/SCR parallel unit. The savings were larger for the variable airflow ECM units.
- The energy saving potential of parallel units was reduced significantly by leakage in four of the five cities evaluated in this study. Only San Francisco showed little impact of leakage on the performance of the HVAC system.
- The negative impact of leakage on the performance of parallel FPTUs was generally larger in the cooling dominated climates (Houston and Phoenix). Because leakage was only considered in cooling operations of parallel FPTUs, this finding was not unexpected.
- The impact of 10% leakage on the annual energy use of either the fixed or variable airflow parallel ECM units was significant and varied by city. For example, for the fixed airflow parallel ECM units with 10% leakage, their energy use was comparable to the energy use of the PSC/SCR series units in Houston and Phoenix. They still provided savings in New York, Chicago, and San Francisco compared to the PSC/SCR series units.
- When comparing variable airflow ECM series units with 50% capacity factors to the variable airflow ECM parallel units with 10% leakage, the series units provided larger energy savings in three cities (Houston, Phoenix, and Chicago) and smaller savings in New York and San Francisco.
- The impact of heating coil location in parallel FPTUs on the system energy consumption was negligible.

CHAPTER 10
CONCLUSIONS AND RECOMMENDATIONS

The conclusions and recommendations were divided into the major areas of this study. These included: fan/motor performance models, in-situ fan pressure differential for FPTUs, leakage in parallel FPTUs, fixed airflow FPTU models, variable FPTU models, comparison to prior work by Davis (2010), evaluation of annual performance of FPTUs, and integrating modeling changes into EnergyPlus.

10.1. Fan/Motor Performance Models

One purpose of this study was to develop models of fan/motor combinations that could readily be used in a mass and energy balance approach similar to that used in EnergyPlus. This study sought to fill a gap in performance data and models for both PSC motors controlled by SCRs and ECMs used in the fan/motor combinations in FPTUs.

For the PSC/SCR fan/motor combinations, three manufacturers provided detailed experimental data on fan/motor combinations employed in commercially available fan powered terminal units. The models developed from the data were simple linear relationships between either fan/motor efficiency and fan total pressure or between fan motor power and fan airflow. The fan total pressure and fan/motor efficiency relationships can be used directly in the current version of EnergyPlus with their fan power formulation. The relationship between power and airflow was a simple linear relationship with a slope of 0.372 W/(ft^3/min) or 788 W/(m^3/s). Being able to directly relate the power to the airflow eliminated the need to go through an intermediate step of specifying fan total pressure and fan/motor efficiency as currently required in EnergyPlus. Thus, a recommendation from this study would be that changes be made in EnergyPlus to accommodate a simple relationship between fan power and airflow for PSC motors controlled by SCRs. The simple relationships developed here should provide a user of building energy simulation programs with a more straightforward approach to reliably estimate the hourly and annual performance of SCR controlled PSC fan motors used in FPTUs. Should there be significant improvements in the efficiency of PSC motors in the future, the metholodgy used in this study could be used with new fan/motor data to provide the performance relationship needed to model the fan/motor combinations.

Electronically commutated motors are now widely applied in fan powered terminal units. This study included an analysis of a wide range of ECM fan/motor combinations provided by

four FPTU manufacturers. A third degree polynomial was fit to the part load data in the general format used by prior building energy simulation models. Unlike models in prior building energy simulation programs that focused solely on the part load performance of the fan, the part load model developed here included the fan/motor assembly. The analysis also provided a linear estimate of the power/airflow relationship for ECM fan/motors operating at their maximum ECM setting. An energy modeler should be able to directly use this relationship along with the third degree polynomial regression to estimate the hourly energy use of ECM fan/motors in FPTUs.

An issue was identified with the data for the fan/motor units whose power ratios were less than 80%. The issue showed up primarily in some of the 0.33 hp (249 W) units where the part load power fraction did not drop as much with lower airflow fractions as did the ECM fan/motor units that had higher power ratios. While the data on the lower power ratio units was not used in this analysis, it could be worthwhile to examine additional information on these units that could help provide more insights into the differences in their performance.

The analysis demonstrated that there was a significant energy benefit to using an ECM FPTU whose maximum airflow capacity was larger than the design airflow requirements for the zone but whose speed was reduced so the ECM FPTU operated at the design airflow. The models developed here allowed the user to easily estimate the savings from this type of ECM FPTU application, whether it was fixed or variable airflow. The analysis also suggested that it might be possible to determine an optimal FPTU size for a particular application if the part load model were coupled with a building simulation program and fuel and installation costs factored into an evaluation. Both ASHRE 90.1 (2010) and manufacturer's recommendations for noise reduction were pushing ECM FPTUs to be larger than the design airflows. As a consequence, building simulation models needed to include ECM FPTU models that captured the energy and power savings of operating these larger FPTUs at either the design airflow (fixed airflow applications) or below design airflow where the FPTU tracked the load.

The models developed here relied on data that could be readily obtained from manufacturers of ECM FPTUs in contrast to existing models that required the user to input fan and motor efficiency and fan pressure differential (EnergyPlus 2013). These data were typically not provided by manufacturers and must either be guessed or not known by the modeler in current building simulations. In addition, none of the current building energy simulation models

explicitly allowed the user to specify a larger FPTU than required by the zone load, then "dial" it back to the design airflow incorporate oversizing into the modeling of ECM FPTUs.

The models developed for fixed airflow applications needed only the design airflow of the zone and the maximum capacity (or capacity factor) of the FPTU to estimate the power used by the ECM unit. The model was used to analyze how capacity factor affects power usage for fixed airflow applications. Based on the analysis, applying a unit whose maximum airflow (or capacity factor) was 25% larger than the design airflow but operated at the design airflow would produce over a 30% power reduction in the FPTU fan compared to a unit that was just sized to match the design airflow. There appeared to be little benefit in power reduction for a unit whose maximum airflow capacity was more than 100% larger than the design airflow. While the analysis produced a continuous curve for the power savings for oversized units operating at the design airflow, actual applications of ECM FPTUs would be constrained by the maximum capacity of units offered by the manufacturers and other factors such as noise, cost, or physical size that could limit the airflow capacity of the unit.

For a variable airflow application, the ECM model only required the hourly airflow to meet the loads in a space, the maximum airflow (or capacity factor) of the FPTU, and the design airflow for the space. This model should be straightforward to incorporate into a building simulation program.

10.2. In-Situ Laboratory and Field FPTU Measurements

The data on laboratory in-situ static fan differential pressure rise showed that the pressure rise was as much as an order of magnitude lower than some sources have recommended. The data brought into question any past modeling efforts that might have been commissioned with such values for series or parallel FPTUs. The range for static differential pressure rise was measured to be in the range of 0.10 to 0.35 in. w.g. (25.0 to 87.2 Pa) for the range of 500 to 1300 ft^3/min (0.236 to 0.613 m^3/s) for an 8 inch (200 mm) inlet series FPTU supplied with a PSC motor and SCR controller.

The models developed from the data indicated that simple linear relationships existed between total airflow and fan differential static pressure. These relationships should provide a user of building energy simulation programs with the input and models needed to provide reliable estimates of the hourly and annual performance of SCR controlled fan motors used in

FPTUs. For the modeler desiring to model a generic VAV FPTU, the data presented here would be a significant improvement over anecdotal information available from internet sources.

Data from one manufacturer's 8 and 12 inch (20.3 and 30.5 cm) series FPTUs were also used for comparison to the in-situ data. These units used an ECM fan/motor combination as opposed to the PSC/SCR used in the first in-situ laboratory test. Results were comparable and the linear relationship for flow versus differential pressure rise also held. The 8 inch (20.3 cm) ECM unit had a differential pressure increase in the range of 0.24 to 0.28 in. w.g. (60 to 70 Pa). While the 12 inch (30.5 cm) had a pressure rise range of 0.24 to 0.37 in. w.g. (60 to 92 Pa). These data also showed that fan differential pressure rise was much less than commonly assumed.

The energy impact of common fan differential pressure and efficiency were explored using EnergyPlus. These data were typically not provided by manufacturers for the small fan/motor combinations found in FPTUs. As shown in Chapter 2, for SCR controlled FPTUs, the fan/motor efficiency ranged from 5 to 15% for fan pressure rises of 0.2 to 0.4 in. w.g. (60 – 100 Pa). These values demonstrated the "ideal" input for an EnergyPlus simulation would be a fan pressure rise less than 0.4 in. w.g. (100 Pa) and an efficiency less than 15%. These inputs were considerably lower than commonly assumed, or default values found in training materials and in on-line forums. An EnergyPlus model using a range of fan pressure rise inputs and fan/motor efficiencies confirmed that use of a "generic" pressure rise of less than 0.5 in. w.g. (124 Pa) and almost any efficiency would result in an overall HVAC system energy difference of less than 5%. However, FPTU fan energy could be up to 80% less and energy for supplemental heat was also substantially different.

Additional data were gathered in a limited field study on the main campus of Texas A&M University. Several series and two parallel FPTUs were instrumented for short-term temperature and pressure data. The results showed a consistent fan pressure rise of between 0.20 and 0.30 in. w.g. (60 – 75 Pa) for the series FPTU. These FPTUs had PSC motors with SCR controls. These results added more support that lower fan pressure rises should be used in energy simulation programs. In addition to the pressure rise, temperatures were recorded in the plenum near the FPTU and at the induction port to evaluate whether leakage was occurring in the parallel FPTUs. Of the two parallel FPTUs monitored in this way, only one showed evidence of leakage through the backdraft damper. The first parallel FPTU served an auditorium and primary flow was at minimum except for short intervals when the unit was in heating mode. Because the unit was at

minimum primary flow, no temperature difference (evidence of leakage) was recorded at the induction port. The second unit served a lobby/entrance area of an office building and was primarily in the cooling mode during the monitoring period. The consistent 60° (15.5°F) temperature at the induction port showed that the parallel FPTU was leaking primary air past the backflow damper and out of the induction port into the plenum. Leakage for this FPTU was also qualitatively determined through infrared thermography. The images clearly showed that cold air was leaking at the seams and backdraft damper of the unit.. This limited field study showed that leakage from a parallel FPTU can be detected in the field. We recommend further field study of FPTUs to better characterize their operation in buildings.

10.3. Leakage in Parallel FPTUs

Parallel FPTU leakage data and models that had been published previously by Edmondson et al (2011) were evaluated. Their data showed that downstream static pressure was the major variable driving leakage in parallel FPTUs. Analysis of the Edmondson et al (2011) data showed that constant percentage leakage with respect to the primary airflow could be used to estimate leakage in parallel FPTUs. The leakage data were grouped into three categories: low, medium, and high. These leakages ranged from approximately 2% of the primary airflow to as high as 15%. A constant percentage leakage model should be readily adaptable to a mass and energy balance model found in building energy simulation models. The percentage model should be used as a way to capture the effect of leakage in parallel FPTUs.

The leakage measurements analyzed for this study were with the FPTU fan off. Edmondson et al (2011) had identified three possible sources of air leakage in FPTUs: seams, penetrations, and the backdraft damper. The percentage leakage estimates should be applicable for a FPTU that operates a large majority of its time in cooling mode when the FPTU fan is off. However, if the FPTU operated a significant amount of time in heating or dead band modes, then the air leakage estimates from this study may overstate the actual leakage because there would be no leakage through the backdraft damper. Thus, the leakage model should be used with caution for those modes of FPTU operation. It is recommended that new leakage data be collected on FPTUs that might allow for quantification of the leakage from the three sources identified by Edmondson et al (2011).

10.4. Fixed Airflow FPTU Models

The basic equations needed to characterize the performance of fixed airflow series and parallel FPTUs using a mass and energy balance approach were developed in Chapter 6. The approach followed closely to that used in EnergyPlus for series and parallel FPTUs. A step-by-step process of how the basic equations should be used for each FPTU mode of operation was provided.

The series and parallel FPTU models in EnergyPlus included only fixed airflow fans and bases fan power calculations on fan pressure and efficiency inputs typically not provided by the manufacturers of these units. A simplified approach was used in this study to allow estimation of combined fan/motor power based on models developed in Chapter 2 for the PSC/SCR motors and in Chapter 3 for ECMs. The ECM model allowed the user to include FPTUs whose maximum rated airflows were larger than the design airflow of the zone. The airflow of the ECM FPTU could then be reduced to the design airflow to take advantage of the reduced power of the ECM at the lower speed to save fan energy compared to the PSC/SCR applications. The modelling methodology also included an option to allow blending of secondary and primary air for colder primary air applications.

The fixed airflow parallel FPTU model developed in this study included the traditional location of the heating coil at the exit of the FPTU as well as the alternative location in the secondary airstream. The parallel model also allowed the user to specify leakage. Models of parallel FPTUs in building simulation programs did not have an option for quantifying the impact of leakage from a parallel FPTU. As a result, modelers who simulated parallel FPTUs can be provided with an optimistic estimate of the energy use of systems with parallel FPTUs in them. Future versions of building simulations models should include leakage in parallel FPTUs to allow energy professionals an opportunity to accurately characterize the energy use of FPTU technologies installed in buildings.

10.5. Variable Airflow FPTU Models

The basic equations and logic needed to characterize variable airflow series and parallel FPTUs were provided in Chapter 7. These models used a mass and energy balance approach similar to that used in EnergyPlus (2013). For the series FPTU, two approaches were outlined for handling the variable airflow cooling operations. One approach varied the airflow linearly from full cooling to the beginning of the deadband region. The second approach varied the discharge temperature linearly from full cooling to the beginning of the deadband region. Both

should provide similar simulation results and allow the user to eliminate iterating each time step to obtain a solution. Both methods allow a user to simulate a FPTU with either a chilled water cooling coil or a direct expansion cooling coil and blend secondary air to produce conditions that eliminate condensation on the registers at full cooling or cold drafts in the deadband region. A step-by-step process of how the basic equations should be used for each FPTU mode of operation was provided.

The equations and steps needed to simulate variable airflow series FPTUs were outlined. The simplified approach to estimating the ECM fan power developed in Chapter 3 was incorporated into the model. The ECM fan/motor model also allowed the user to include FPTUs with maximum airflow capacities larger than that required at the design load in the zone.

The methodology for both the series and parallel FPTUs can be implemented into building simulation models that use an energy and mass balance approach. A step-by-step process of how the basic equations should be used for each FPTU mode of operation was provided. Both the traditional configuration where the heating coil was located at the discharge of the FPTU and the alternate configuration where the heating coil was located at the inlet to the secondary air were included in the modeling. Given the widespread use of ECMs in series FPTUs, future versions of building simulations models should include variable airflow series FPTUs to allow energy professionals an opportunity to accurately characterize the energy use of FPTU technologies.

10.6. Comparison to Davis (2010) Model

The results of both the fixed airflow series and parallel models were compared in Chapter 8 to a "black box" FPTU model developed by Davis (2010). The annual energy use from both approaches compared favorably. Comparisons were made for a small, five zone office building in five cities: Houston, Phoenix, Chicago, New York, and San Francisco. Davis (2010) reported results from these locations in his original analysis. Simulations were run for both PSC/SCR and ECM FPTUs. The heating and cooling loads in the building were generated by Davis (2007 and 2010) using the original DOE-2 building simulation program and were used as input into the EES model developed here. Davis (2010) normalized the loads in his simulations so all zones had the same design load which allowed Davis to apply the same size FPTU in each zone. These normalized loads were used for the comparisons to be consistent with Davis, but would unrealistic in a real building. The two modeling approaches agreed to within 4% in annual energy use for all FPTUs (parallel and series) except for one case in San Francisco for the

PSC/SCR series FPTU where the differences were 6%. For that case, the main contributor to the differences in energy use was the chiller energy use, not the FPTU fan or coil. While the two approaches used different ways to characterize the FPTU, the small differences in total energy use pointed to the fact that both MEB and black box approaches can be used to simulate FPTUs. The agreement between the two approaches provided us with confidence that the MEB models described in chapters 6 and 7 and implemented in EES could be reliably used to estimate annual energy use and savings of different FPTUs options.

10.7. Evaluation of Annual Performance of FPTUs

The annual energy consumption of a single story five zone office building was estimated by using EnergyPlus. The zone peak loads and hourly loads throughout a year generated from EnergyPlus were used as input to the EES models to estimate the annual energy use of the preheat coil, primary cooling coil, primary supply fan, terminal unit fan, and supplemental heating coil. The results from the EES modeling were compared with the results from EnergyPlus model to assess differences between the models for fixed airflow series and parallel FPTUs. The results showed that both models produced similar trends in estimating percentage energy changes relative to the baseline. Even though the estimated percentage changes varied with EES and EnergyPlus, there did not appear to be a consistent bias in the results for either model. The differences between results were caused by different component modeling approaches, system layout, and assumptions. An assessment of one assumption (outdoor air fraction) showed dramatic changes in the estimated annual energy use with the EES model and provided better agreement between the two models for some cities.

The fixed airflow results showed the benefits of utilizing ECM technology in series FPTUs with capacity factors up to 50%. For these ECM FPTUs, their maximum rated airflow would be larger than the design airflow in the zone, but the speed of the ECM would be reduced so the ECM FPTU just matched the design airflow in the zone. With the baseline being a series PSC/SCR FPTU, the annual energy savings varied from a low of 3.5% in New York and a high of 8.1% in Phoenix for a series ECM FPTU. The simulations showed smaller benefits to employing ECMs in parallel FPTUs.

Because EnergyPlus could not handle variable airflow ECM FPTUs, EES was used to evaluate options with this technology. Options included variation in capacity factors and leakage in parallel FPTUs. The major findings from the comparisons included:

1. Sizing both series and parallel ECM FPTUs with larger capacity factors can reduce HVAC system energy use. However, the benefit of larger capacity factor ECM FPTUs was larger in series units.
2. Greater energy savings can be achieved through the application of variable airflow operation in series ECM FPTUs in both cooling and heating dominated climates than with fixed airflow series ECM FPTUs.
3. The energy benefit of using variable airflow parallel ECM FPTUs was offset because additional heating energy was required to compensate for the reduced terminal unit fan heat gain caused by the more efficient motor operations.
4. At the ideal condition of no leakage, parallel units yielded energy savings relative to series units. However, the energy saving potential of parallel units was significantly reduced in all cities except San Francisco where the system ran much of the time in low heating/cooling loads.
5. Fixed airflow ECM parallel units with 5% leakage had smaller energy savings than the variable airflow series ECM units in cooling dominated climates (Houston and Phoenix), similar savings in heating dominated climates (New York and Chicago), and smaller savings in San Francisco. At higher leakage levels, variable airflow series FPTUs outperformed fixed airflow ECM parallel units in all cities except San Francisco.
6. The impact of heating coil location in parallel FPTUs on the system energy consumption was negligible.

10.8. Integrating Modeling Changes into EnergyPlus

From the analysis conducted in this study, seven specific improvements or changes needed in EnergyPlus were identified. These changes were identified in Chapter 7 and included: 1. PSC fan motors with SCR control, 2. ECM fan motors for fixed and variable airflow applications, 3.Realistic fan pressure differentials and fan/motor efficiencies, 4. Leakage in parallel FPTUs, 5. Alternative heating coil location in parallel FPTUs, and 6. Mixing of secondary air to ensure no condensation on registers or cold drafts. The Department of Energy (DOE) has a process for suggesting changes that include smaller issues that would be considered bug fixes to major issues which would be larger new features for EnergyPlus. In our estimate, Items 1 and 3 should fall under the smaller issues/bug fixes while Items 2, 5, and 6 would be larger new features. Item 4 (leakage in parallel FPTUs) might fall somewhere between being a minor or major

implementation in EnergyPlus. Smaller issues/bug fixes can be submitted to a website (identified in Chapter 7). The larger changes into EnergyPlus would require either submission to the DOE website and getting enough user support for DOE to include it in their update plan or separately contracting with an entity that has the expertise to program the changes into the appropriate EnergyPlus modules and submitting the final product to DOE. We recommend that AHRI pursue both avenues. Without substantial changes in the FPTUs models in EnergyPlus, users will not be capable of estimating the energy savings of the latest FPTU technologies (i.e., ECM and variable airflow) in their building models. As a consequence, users may draw erroneous conclusions about the effectiveness of FPTUs in buildings.

REFERENCES

AHRI. 2011. *ANSI/AHRI standard 880 (I-P) with addendum 1. Performance rating of air terminals*. Arlington, VA: Air-Conditioning, Heating, and Refrigeration Institute.

AMCA. 1999. *ANSI/AMCA standard 210-99. Laboratory methods of testing fans for aerodynamic performance rating.* Arlington Heights, IL: Air Movement and Control Association.

ASHRAE. 2001. ASHRAE Standard 62-2001, *Ventilation for Acceptable Indoor Air Quality*. Atlanta: ASHRAE.

ASHRAE. 2006. *ANSI/ASHRAE standard 130-1996 (RA 2006), Methods of Testing for Rating DuctedAair Terminal Units.* Atlanta: American Society of Heating, Refrigerating and Air-Conditioning Engineers, Inc.

ASHRAE. 2010. *ANSI/ASHRAE/IES standard 90.1-2010, Energy Standards for Buildings Except Low-Rise Residential Buildings*. Atlanta: American Society of Heating, Refrigerating and Air-Conditioning Engineers, Inc.

ASHRAE. 2012. *ASHRAE Handbook—HVAC Systems and Equipment*, Chapter 20, "Room Air Distribution Equipment." Atlanta: ASHRAE.

ASHRAE. 2013. *ASHRAE Handbook – Fundamentals*, Chapter 14, "Climatic Design Data." Atlanta: ASHRAE.

ASHRAE. 2013. *ANSI/ASHRAE/IES Standard 90.1-2013, Energy Standard for Buildings Except Low-Rise Residential Buildings.* Atlanta: American Society of Heating, Refrigerating and Air-Conditioning Engineers, Inc.

ASHRAE. 2013. *ASHRAE Standard 62.1-2013, Ventilation for Acceptable Indoor Air Quality.* Atlanta: ASHRAE.

BigLadder Software, 2013, http://bigladdersoftware.com/epx/docs/8-0/engineering-reference/index.html, referenced September 17, 2014.

BLAST, 1986. *Building Load Analysis and Stem Thermodynamic Programs: User's Manual* Version 3.0, Army Construction Engineering Research Laboratory, Champaign, Illinois.

Brandemuehl, M.J., Gabel, S., and Andresen, I. 1993. *HVAC 2 Toolkit: Algorithms and Subroutines for Secondary HVAC System Energy Calculations.* Atlanta: ASHRAE.

Bryant, J. and Bryant. S., 2015, *In Situ Fan Differential Pressure Rise for a Series VAV Fan Power Terminal Unit with SCR Control. ASHRAE Transactions*, 121(1).

CBSC 2010. *California Energy Code, California Code of Regulations*, Title 24, Part 6,

California Building Standards Commission, Sacramento, California.

CEC 2013. *Building Energy Efficiency Standards for Residential and Non-residential Buildings*. California Energy Commission, CEC-400-2012-004-CMF-REV2.

Clark, D. R. 1985, *HVACSIM+ Building Systems Equipment Simulation Program Reference Manual*, NBSIR 84-2996, National Bureau of Standards, Gaithersburg, Maryland. January.

Cramlet, A. 2008. *Performance of ECM Controlled VAV Fan Power Terminal Units*. M. Sc. Thesis, Texas A&M University, College Station, TX.

Davis, M. A. 2010. *Development of a Laboratory Verified Single-Duct VAV System Model with Fan Powered Terminal Units Optimized Using Computational Fluid Dynamics.* PHD Dissertation, Texas A&M University, College Station, TX. August.

Davis, M. 2015. Private communications exchanged via e-mails containing data, June 12.

Davis, M.A., Bryant, J.A., and O'Neal, D. 2012a. "*Modeling the Performance of ECM and SCR Parallel Fan-Powered Terminal Units in Single-Duct VAV Systems*", CH-12-018, *ASHRAE Transactions*, 118(1):908-18.

Davis, M.A., Bryant, J.A., and O'Neal, D. 2012b. "*Modeling the Performance of ECM and SCR Series Fan-Powered Terminal Units in Single-Duct VAV Systems*", CH-12-017, *ASHRAE Transactions*, 118(1).

Davis, M.A., O'Neal, D.L., Bryant J.A., and Cramlet, A. 2009. *Modeling the Performance of Single-Duct VAV Systems that use Fan Powered Terminal Units. ASHRAE Transactions* 115(1)

Davis, M.A., Bryant, J.A., O'Neal, D.L., Hervey, A., and Cramlet, A. 2007. *Comparison of the Total Energy Consumption of Series versus Parallel Fan Powered VAV Terminal Units*, ASHRAE Project 1292-RP Final Report, Phase 2, Energy Systems Laboratory, Texas A&M University, March.

DesignBuilder, 2014, http://www.designbuilder.co.uk/helpv3.1/Content/Fan_-_Constant_Volume.htm.

Edmondson, J., O'Neal, D.L., Bryant, J.A., and Davis, M.A. 2011a. *Performance of Series Fan Powered Terminal Units with Electronically Commutated Motors, ASHRAE Transactions*, Vol. 117, Pt. 2, June 2011.

Edmondson, J., O'Neal, D.L., Bryant, J.A., and Davis, M.A., 2011b, *Performance of Parallel Fan Powered Terminal Units with Electronically Commutated Motors, ASHRAE Transactions*, 117 (2):885-93.

EnergyPlus. 2013. *Air System Distribution Terminals.* In EnergyPlus Engineering Referencce: The Reference to EnergyPlus Calculations. Bekeley: Lawrence Berkeley National Laboratory.

EnergyPlus. 2014. http://groups.yahoo.com/group/EnergyPlus_Support/

F-Chart Software. 2014. *Engineering Equation Solver*, Version 9.695. Madison, WI

Faris, G., Int-Hout, D., O'Neal, D., Reid, C. . Private email communications, April 16, 2014.

Furr, J. O'Neal, D. L., Davis, M., Bryant, J., and Cramlet, A. 2007, ASHRAE Project 1292-RP: *Comparison of the Total Energy Consumption of Series versus Parallel Fan Powered VAV Terminal Units, Phase I Final Report*, ASHRAE, Atlanta, GA.

Furr, J., O'Neal, D., Davis, M.A., Bryant, J.A., and Cramlet, A. 2008. "*Performance of VAV Fan Powered Terminal Units: Experimental Results and Models for Parallel Units*", *ASHRAE Transactions*, 114(1).

Furr, J., O'Neal, D., Davis, M.A., Bryant, J.A., and Cramlet, A. 2008. *Performance of VAV Parallel Fan Powered Terminal Units: Experimental Results and Models* (RP-1291), *ASHRAE Transactions*, 114(1).

Furr, J., O'Neal, D.L., Davis, M., Bryant, J., and Cramlet, A. 2008a. *Performance of VAV Fan Powered Terminal Units: Experimental Setup and Methodology*. *ASHRAE Transactions*, 114(1).

Furr, J., D.L. O'Neal, M. Davis, J. Bryant, and A. Cramlet. 2008a. *Performance of VAV Series Fan-Powered Terminal Units: Experimental Results and Models* (RP-1292). *ASHRAE Transactions* 114(1):91–97.

Hydeman, M. and Eubanks, B. 2014. "*Advanced Control Sequences for HVAC Systems – Phase I Air Distribution and Terminal Systems*," ASHRAE Research Project Report 1455-RP. Atlanta: ASHRAE American Society of Heating, Refrigerating, and Air-Conditioning Engineers.

Int-Hout, D. 2015. *ECM Motors in Fan Powered Terminal Units*. https://www.krueger-hvac.com/files/white%20papers/white_paper_ecm.pdf

Janisse, N. 1969. *How to Control Air Systems, Heating, Piping and Air Conditioning*, 41(4), pp. 129-136.

Kimla, J.W. 2009, Optimized Fan Control in Variable Air Volume HVAC Systems Using Static Pressure Resets: Strategy Selection and Savings Analysis. M.S. Thesis, Texas A&M University, College Station, Texas.

Knebel, D. E., 1983. *Simplified Energy Analysis Using the Modified Bin Method*, American

Society of Heating, Refrigerating, and Air-Conditioning Engineers. Atlanta: ASHRAE.

Kolderup, E., Hong T., Hyderman, M., Taylor, S., and Stein, J., 2003. *Integrated Design of Large Commercial HVAC systems. Integrated Energy Systems: Productivity and Building Systems and Building Science*, San Francisco: California Energy Commission.

Li, X. Li, Y., and Seem, J.E., 2010. Dynamic Modeling of Mechanical Draft Counter-Flow Wet Cooling Tower with Modelica, International Refrigeration and Air Conditioning Conference, Purdue University, West Lafayette, Indiana.

Nailor Industries, Inc., 2014. *Sizing Fan Powered Terminals in Engineering Guide and Index*, Houston, TX.

O'Neal, D.L. 2015. *Development of Models to Simulate the Part-Load Performance of Oversized ECM Fan-Powered Terminal Units. ASHRAE Transactions* 121(2).

O'Neal, D.L, and Edmondson, J.L. 2016, *Characterizing Air Leakage in Parallel Fan-Powered Terminal Units, ASHRAE Transactions*, 122 (1).

O'Neal, D. L., Edmondson, J.L., and Yin, P., 2014, *Comparison of Performance Characteristics of SCR and ECM Controlled Series Fan Powered Terminal Units*, HVAC&R Research, 20:2, pp. 194-202.

O'Neal, D. L., Ingram, D., and Reid, C., 2015a, *Modeling Fan Power Terminal Unit Fan/Motor Combinations Controlled by Silicon Controlled Rectifiers, ASHRAE Transactions*, 121(1).

O'Neal, D.L., D. Ingram, and C.L. Reid. 2015b. *Simplified Model of the Fan/Motor Performance of Fan Powered Terminal Units that Utilize Electronically Commutated Motors*. *ASHRAE Transactions* 121(2).

Roman, A. and Heiligenstein, A. 2002. *SCR Power Theory Training Manual*. Chromalox Inc. PK501-1. LaVergne, TN.

Spitler, J.D., D.C. Hittle, D.L. Johnson, C.O. Pedersen. *1986 Fan Electricity Consumption for Variable Air,* Volume, *ASHRAE Transactions*, 92(2), pp. 5-18, 1986.

Stein, J. and Hydeman M.M. 2004. Development and Testing of the Characteristic Curve Fan Model. AN-04-3-1, *ASHRAE Transactions*, Vol. 110, Pt. 1.

Trane Inc., 2014. *Selection Procedure in Fan-Powered Series*, VAV-PROC008-EN, LaCross, WI.

Wang, F., Yoshida, H., and Miyata, M. 2004. *Total Energy Consumption Model of Fan*

Subsystem Suitable for Continuous Commissioning. AN-04-3-2, *ASHRAE Transactions*, Vol. 110, Pt. 1.

Yin, P. and O'Neal, D. L. 2014a, *Characterizing Airflow and power of VAV Series Fan-Powered Terminal Units from Component Data – Part I, ASHRAE Transactions,* 120(1).

Yin, P. and O'Neal, D. L. 2014b, *Characterizing Airflow and power of VAV Series Fan-Powered Terminal Units from Component Data – Part II, ASHRAE Transactions,* 120(1).

Zhang, H., Hoyt, T. Kaam, S., Goins, J., Bauman, F., Zhai, Y., Webster, T., West, B., Paliaga, G., Stein, J., Seidl, R., Tullym B. Rimmer, J. and Torftum, J. 2014, "*Thermal and Air Quality Acceptability in Buildings that Reduce Energy by Reducing Minimum Airflow from Overhead Diffusers.*" ASHRAE Research Project Report 1515-RP.

APPENDIX A

EVALUATION OF FAN MODEL FOR APPLICATION TO ECM FAN/MOTOR COMBINATIONS

A.1. Introduction

Variable air volume (VAV) systems maintain the zone thermal comfort by varying the conditioned air supplied to the zone. A central air handler unit (AHU) delivers air through a duct system to VAV terminal units that control the airflow based on the zone load. A terminal unit with a fan is called a fan-powered terminal unit (FPTU). FPTUs mix primary air from the AHU with recirculated air from the plenum space. Supplemental heat can be provided when needed to the air by a heating coil.

In recent years, electronically commutated motors (ECMs) have begun to be used to drive the fans in FPTUs. A DC voltage controller is used to vary the speed of the motor and the amount of airflow from the fan. For a variable airflow application, the ECM can be tied into a building automation system to provide the desired airflow to meet the zone load.

The purpose of this appendix was to evaluate existing fan models that have been used to characterize larger commercial fans and determine if they can be applied to the ECM fan/motor combinations used in FPTUs. Models by both Clark (1985) and Stein and Hydeman (2004) were evaluated using ECM fan/motor performance data from FPTU manufacturers. A new model was developed based on the Stein and Hydeman (2004) model that included a "pseudo" pressure ratio term to correlate fan/motor efficiency data. The model should provide building simulation modelers with a simple non-dimensional model to characterize ECM fan/motor performance for applications in fan powered terminal units.

A.2. Prior Work

Clarke (1985) originally published his model as a part of the reference manual for the public domain simulation model called HVACSIM+. The model included a dimensionless flow coefficient, ϕ, and pressure coefficient, ψ. The fan efficiency was modeled as a fourth degree polynomial:

$$\eta_{fan} = a_1 + a_2\phi + a_3\phi^2 + a_4\phi^3 + a_5\phi^4 \quad \text{(A.1)}$$

Where:

a_1, a_2, a_3, a_4, and a_5 were regression coefficients.

The non-dimensional flow coefficient, ϕ, was:

$$\phi = c_1 \frac{Q_{flow}}{ND^3} \quad \text{(A.2)}$$

where:

c_1 = constant

Q_{flow} = fan airflow in ft^3/min (m^3/s)

N = fan speed (rpm)

D = fan diameter in ft (m)

The fan efficiency could be fit to the flow coefficient data and then used to estimate the power of the fan:

$$Pow_{fan} = \frac{Q_{flow}\Delta P}{\eta_{fan}} \quad \text{(A.3)}$$

The model was developed based on the ideal fan affinity laws. For example, the airflow should be proportional to $1/(ND^3)$, which is in the denominator of the flow coefficient in Equation A.2. No explanation was provided on the origin of this model by Clarke (1985). Given that the efficiency was used in a standard calculation of fan power, it would appear that either fan static efficiency or fan total efficiency could be used as long as the corresponding static or total pressure was used in Equation A.3. Because the fan diameter and speed were a part of the non-dimensional flow coefficient, it was hoped that this model could normalize the performance of different sizes operating at different speed.

The Clarke (1985) model was in a list of component models published in the ASHRAE HVAC 2 Toolkit (Brandemuehl et al 1993). Wang et al (2004) proposed using the model for estimating a fan's contribution to total energy use in commercial buildings. They also had separate models for the fan motor, driveshaft, and inverter. Their application was primarily to large central air handlers. Kimla (2009) and Li et al (2010) applied this model to air handlers and cooling tower fans. These uses of the Clarke model focused on the performance of larger fans and not to the smaller fan/motor combinations found in FPTUs.

Stein and Hydeman (2004) developed a fan model for a wide range of fan types and sizes. It could estimate fan system energy over a range of operating conditions and was simple to integrate into a building simulation model. Their focus was also on larger fans. In their model, a system curve coefficient (SCC) was first calculated:

$$SCC = \frac{\Delta P_{static}}{Q_{flow}^2} \quad \text{(A.4)}$$

The SCC was a curve that passes through the origin and is along a line of constant fan efficiency. The fan efficiency was determined from manufacturer's data:

$$\eta_{fan} = \frac{Q_{flow}\Delta P_{static}}{Pow_{fan}} \quad \text{(A.5)}$$

In his paper, the above equation was written in IP units. It has been generalized here so either IP or SI units can be used. Manufacturer's data can be used in Equations A.4 and A.5 to calculate both SCC and η_{fan}. Because the ΔP_{static} in Equation A.4 was small and the airflow was a large number in IP units, the resulting values of SCC in IP units was very small – on the order of 10^{-7} to 10^{-9}. To better visualize the results, Stein and Hydeman (2004) created another term, gamma, defined as:

$$\gamma = -\ln(SCC) \quad \text{(A.6)}$$

When plotted against either SCC or γ, the efficiency showed a distinct peak. The authors also provided a third-order regression to fit the fan efficiency to gamma. They found that this approach was applicable for six types of fans: plenum, backward inclined, airfoil, mixed flow, propeller, and vane-axial with fixed blades. Equation A.6 was an unusual formulation because the logarithm was performed on SCC which was not dimensionless but had units of (in w.g)/(ft^3/min)^2 in IP units or Pa/(m^3/s)^2 in SI units.

Because both the Clarke (1985) and the Stein and Hydeman (2004) models were generic models, we wanted to see if they could be applied to the smaller fan/motor combinations found in FPTUs. The fans were typically forward curved blade fans integrated into a fan/motor assembly. In larger air handlers, the fan was tested separately from the motors. In FPTUs, the two were tested together because the fan motor was inside the fan squirrel cage. Building simulation software, such as EnergyPlus (2013), treated the fan/motor combinations in FPTUs the same way that large air handlers were treated. The user was expected to input fan and motor characteristics separately. Because these data were not available separately for ECM fan/motors, building energy modelers can be tempted to use the default value for fan efficiency in EnergyPlus (2013) as well as static pressures, both of which are much larger than the typical values found in FPTU fans and motors. There was a need to provide a model and data that better matched the actual performance of ECM fan/motor combinations in FPTUs.

A.3. FPTU ECM Fan/Motors

ECM fan/motor performance data from 36 units were provided by four manufacturers that were identified as manufacturers A, B, C, and D in the tables and figures below. The fan/motor assemblies were from FPTUs at various combinations of cabinet sizes, cabinet styles (underfloor or overhead), and cabinet profiles ("low" and "standard"), with motor sizes ranging from 0.33 hp (249 W) to 1 hp (746 W). Each cabinet design potentially produced different flow conditions entering the FPTU fan, which could generate differing air system effects that impact the overall fan performance. Also, two dual fan/motor assemblies were provided with 0.33 hp (249 W) and 0.75 hp (560W) motors respectively. Considering the variety in terms of motor sizes and cabinet designs, the 36 assemblies should cover the typical fan/motor combinations in FPTUs in field applications.

Performance data were collected by manufacturers in their own laboratories and provided to the authors through a representative of the AHRI so that the identity of the manufacturer remained anonymous. Manufactures were asked to provide both descriptive (see Table A.1) and performance data (see Table A.2) on each fan/motor combination. In Table A.2, the settings on the controllers were specified in DC voltages (typically from 0 to 10 V) or in percentages from 0 to 100%. Each manufacturer performed measurements at the ECM controller settings that they normally test their equipment. Thus, the ECM controller settings varied from manufacturer to manufacturer.

Table A.1 Descriptive Data for FPTU and Fan/Motor Combinations

Item
Fan Model Number
Series or Parallel FPTU Application
Primary Inlet Diameter
Design range of airflow of FPTU
Recommended operating pressures
Maximum recommended airflow
Minimum recommended airflow
Fan manufacturer
Motor manufacturer
Motor Size
Fan discharge dimensions

Table A.2 Detailed Measured Performance Data on each FPTU Fan/Motor Combination

Item	Units
ECM Setting	voltage or value
discharge static pressure	in w.g. (Pa)
Airflow	ft^3/min (m^3/s)
Current	Amps
volt-amps	volt-amps
power factor	-
power	W
motor speed	rpm
power/airflow	W/(ft^3/min) W/(m^3/s)

An identification procedure was developed for reporting each fan/motor combination. Because all of the fan motors in this paper were ECMs, all designations start with “ECM”. The

rated fan motor size, in horsepower, was converted to its decimal equivalent and multiplied by 1000. For example, the identification of a 0.5 hp (373 W) unit would be 0.500 multiplied by 1000 to give a value of 500. A 0.5 hp (373 W) fan/motor from manufacturer A was identified as ECM-500A. If a manufacturer had more than one fan/motor combination of the same size, such as manufacturer B had for 0.5 hp (373 W), then the first fan/motor was identified as ECM-1000B1 and the second as ECM-1000B2. For cases where there were dual fan/motors in a FPTU, the unit was identified with a 2x before the unit size. For example, the first 0.75 hp (560 W) from manufacturer A would be designated as ECM-2x750A1.

Figure A.1 shows the power versus airflow data for the fan/motor ECM-750A2. For a given static pressure, the power decreased nonlinearly as the fan airflow dropped from about 2,000 ft^3/min (0.94 m^3/s) down to 500 ft^3/min (0.24 m^3/s). Along a given constant static pressure curve, the fan affinity laws would predict that the fan power would be a function of the cube of the airflow, which is consistent with the shape of the curves shown in Figure A.1. For a constant airflow, the power increased as the static pressure increased. It should be noted that not all fan/motors showed the same uniform trends seen in Figure A.1. In some cases, the lines of constant static pressure crossed. However, this figure illustrated the trend shown by many of the units.

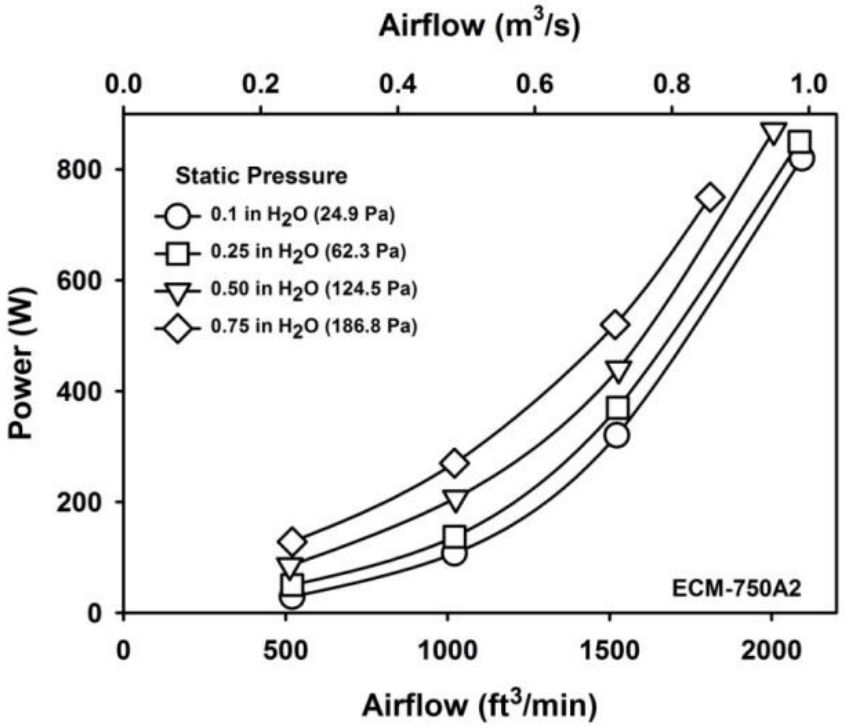

Figure A.1: Power Versus Airflow for ECM-750A2 ECM Fan/Motor Combination

Figure A.2 showed fan/motor static efficiency as a function of fan static pressure and airflow. The static efficiency increased as the static pressure increased for a given airflow. The static efficiency decreased as the airflow increased for a given static pressure. Figure A.2 also illustrated that the static efficiency varied significantly with both static pressure and airflow. At the least efficient operating condition, which was at the highest airflow and lowest static pressure, the static efficiency was as low as 5%. At the most efficient operating condition at lowest airflow and highest static pressure, the static efficiency could be over 30%. The highest operating static pressure for the fan/motor assemblies was 0.75 in w.g. (187 Pa). Laboratory measurements conducted in Chapter 4 found that static pressures across the fan in a series FPTU ranged from 0.128 to 0.246 in w.g. (31.9 to 61.3 Pa). Thus, FPTU fans may operate more often at the lower end of the static pressure range in Figure A.2 rather than the upper end.

While building simulation programs like EnergyPlus require the user to choose a single efficiency for operation of an ECM fan/motor, Figure A.2 demonstrated the difficulty of specifying a single efficiency over the entire expected operating range by showing that efficiency is dependent on both static pressure and airflow rate. Because static pressures and airflows change in a VAV system to meet the varying zone load, choosing a single "correct" efficiency may be difficult. Restricting the user to choosing one value applicable to the whole range of operating conditions of a FPTU may introduce significant errors in modeling an ECM FPTU.

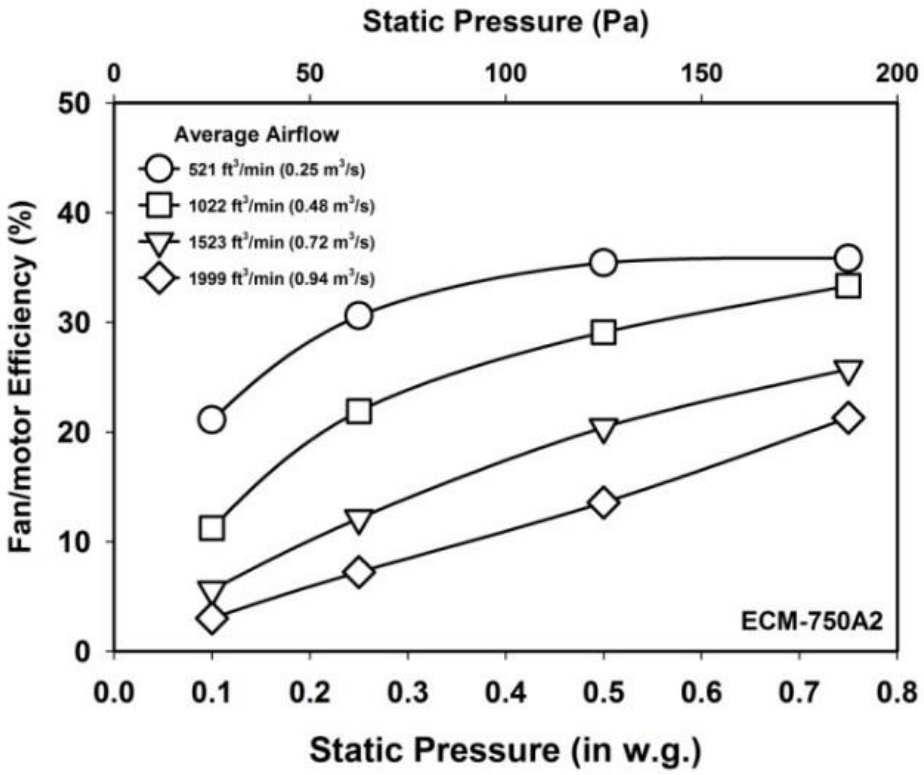

Figure A.2: Fan/Motor Efficiency Versus Fan Static Pressure for ECM-750A2

A.4. Clarke Model Evaluation

The ECM fan/motor data were processed using the Clarke (1985) model. Figure A.3 shows the fan/motor static efficiency versus the Clarke airflow coefficient for five fan motors in the range of 0.75 to 1.0 hp (560 to 746 W). The static efficiency decreased with airflow coefficient. For a particular fan/motor combination, the static efficiency could be modeled as a function of the airflow coefficient by fitting the data into the Clarke model. However, no generic model could be developed based on the Clarke model. For example, for a flow coefficient of 3.0 in Figure A.3, the static efficiencies varied from approximately 3 to 33%, depending on the specific fan/motor combination. Thus, it would appear the Clarke (1985) model, as originally formulated, provided only a limited tool for characterizing the fan/motor combinations in FPTUs.

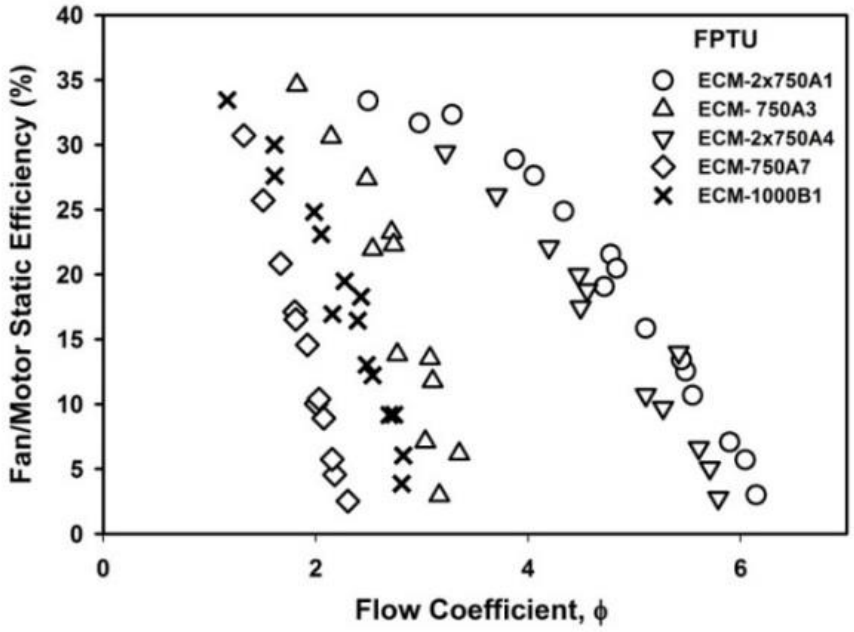

Figure A.3: Plots of the Fan/Motor Static Efficiency Versus the Flow Coefficient for Several of the Larger Fan/Motor Combinations

When plotting the data for the Clarke (1985) model, some of the units with smaller motor sizes showed a consistent trend to what is shown in Figure A.4 for unit ECM-333D3. At higher ECM settings (typically over 35% of the maximum setting on the controller), the data showed the same trends for the larger fan/motor units as was shown in Figure A.3. At the lower ECM settings, the data deviated significantly from that at the higher settings. Similar trends in the part load data were seen in Chapter 3 for some ECM fan/motor combinations. Because the power data provided by manufacturers were for fan/motor combinations and not just fans, it was possible that the power use of the controller could impact the static efficiency results. For units with smaller motors at lower speeds, the fan power consumption was relatively small (~15 to 25 W). One manufacturer who made measurements of one controller found that the power consumption of the controller was about 7 W for a 0.5 hp (373 W) motor. The trends shown in Figure A.4 were similar to the results of all of the 0.33 hp (246 W) and 0.5 hp (373 W) fan/motor combinations. If the results from the lower ECM settings were eliminated from the data sets, then the plots looked similar to those for the larger fan/motor combinations shown in Figure A.3.

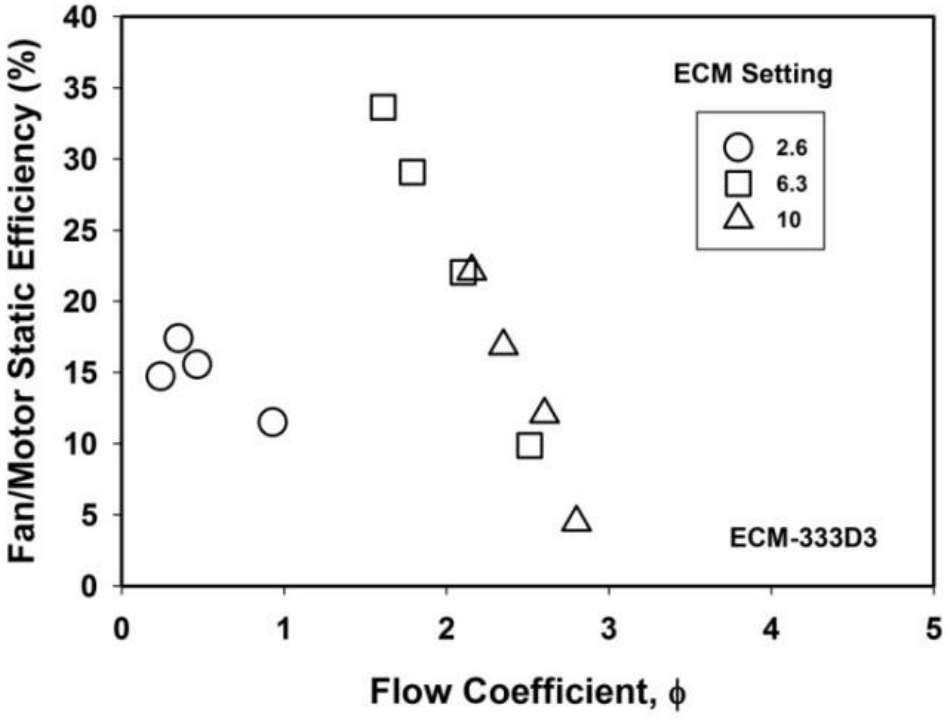

Figure A.4: Static Efficiency Versus Flow Coefficient for Fan/Motor Combination ECM-333C3.

A.5. Stein and Hydeman Model Evaluation

The fan/motor data were processed by using the Stein and Hydeman (2004) model. Figure A.5 showed a plot of fan/motor static efficiency versus gamma for seven of the 0.75 hp (560 W) fan/motor combinations from three manufacturers. We have plotted gamma as if it did not have units even though it contained a logarithm of variables that do have units. The static efficiencies increased with decreasing gamma for each fan/motor combination. As with the Clarke (1985) model, the data points for an individual ECM fan/motor could be fit with a non-linear curve. Unlike the fans in Stein and Hydeman (2004) paper that had a distinct peak, none of these units showed a peak in efficiency. All fans appeared to asymptotically approach a maximum static efficiency between 35 and 40%. Compared with the results shown in Figure A.3, Figure A.5 indicated that the Stein and Hydeman model provided a better job of compressing the data from different fan/motors. For example, at a gamma of 15, the fan/motor efficiency only varied from approximately 10 to 33%. By contrast, the spread in the data for the Clarke model varied from 3 to 33% for a flow coefficient of 3. Some of the compression may be due to the fact that gamma

was a logarithmic function. Although an improved representation was observed in Figure A.5, it would still be difficult to use the Stein and Hydeman (2004) model to capture the entire static efficiency performance over a wide range of ECM fan/motor combinations given the fact that Figure A.5 only included units with 0.75 hp (560 W) fan motors. Even for the results with one single size motor, considerable efficiency variations were observed for a given gamma value.

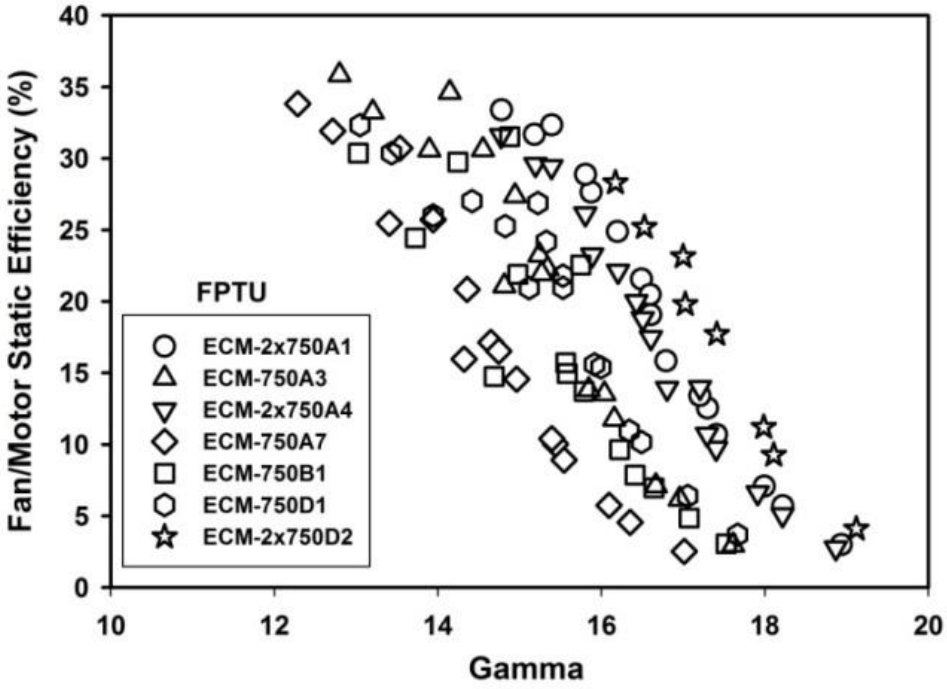

Figure A.5: Static Efficiency Versus Gamma for the 0.75 hp (560 W) Fan/Motor Combinations

As with the Clark model, all of the 0.33 hp (248 W) and 0.50 hp (373 W) fan/motor combinations showed significant deviations at the ECM settings below about 33% of the maximum setting for the controllers. Figure A.6 showed static efficiency results for three units with 0.33 hp (248 W) fan motors for the purpose of illustrating the issue at the lower settings.

Based on Figure A.5, it would be appear that for an individual fan/motor combination, the Stein and Hydeman (2004) model can be used to estimate the static efficiency. However, given the wide variations in static efficiency versus gamma for the fan/motor units, it would be difficult to use it as a general model.

A.6. Development of New Model

Even without the issue in the static efficiency data at the low ECM settings, both the Clarke (1985) and Stein and Hydeman (2004) models were not able to provide a generic model that allowed a modeler to estimate the static efficiency for a wide range of fan/motor combinations. A number of possible variations of these models were considered. One that appeared promising is discussed below.

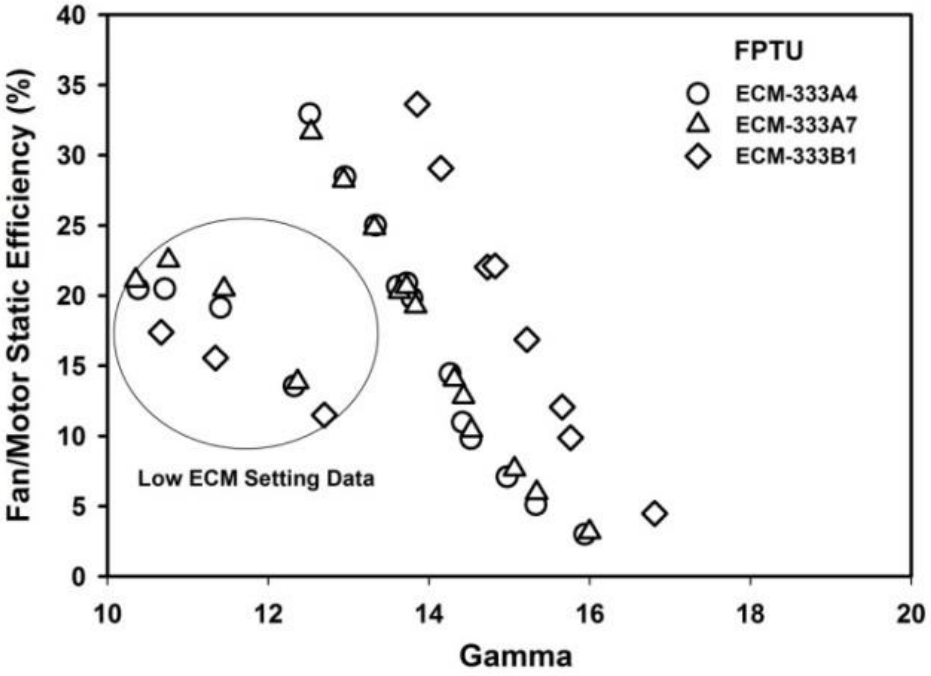

Figure A.6: Static Efficiency Versus Gamma for Three 0.33 hp Fan/Motor Combinations

When considering the system curve coefficient (SCC) in Equation A.4 that was a part of the Stein and Hydeman (2004) model, it seemed unusual that the developers did not non-dimensionalize SCC. Non-dimensionalization has the potential to bring possible geometric and other measured variables into a single non-dimensional variable that might better correlate the static efficiency. In SCC, the numerator was a pressure term while the denominator was a flow squared term. Flow squared is often associated with the velocity pressure in a duct system or fan. Thus, we looked at revising the denominator so that a velocity pressure of the air leaving the fan would be used instead of using the square of the airflow.

$$P_v = \frac{\rho\left(\frac{Q_{flow}}{A}\right)^2}{2g} \quad \text{(A.7)}$$

where:

ρ = density of air

A = cross sectional area = w*D

g = gravitational constant

w = width of the fan

D = diameter of the fan

The fan airflow, Q_{flow}, was the same airflow used in the Stein and Hydeman (2004) model. The data on the fan/motor combinations included both single and double fans. Table A.3 showed the range in the fan/motor data we analyzed. There was a wide range in airflows, motor sizes, and fan widths. The fan diameters only varied from 9 to 12.8 inches (22.9 to 32.5 cm). The fan static pressures ranged from 0.1 to 0.75 in w.g. (25 to 187 Pa).

Table A.3 Range of Fans Used in this Study

Value	Motor Size hp (W)	Airflow ft^3/min (m^3/s)	Fan Diameter in (cm)	Fan Width in (w)
Min	0.33(248)	250 (0.12)	9(22.9)	2(5.1)
Max	1.0 (746)	4000(1.89)	12.8(32.5)	12.6(32.0)

After experimenting with different areas for Equation A.7, it was decided to use an area that was formed by the product of the fan width (w) times the fan diameter (D) provided the best correlation for a wide range of the data. The SCC would then become a ratio of static pressure produced by the fan divided by a velocity pressure based on the airflow of the fan divided by area formed by the produce of w and D. Instead of using SCC, we defined this new term as the "pseudo" pressure ratio:

$$P_r = \frac{\Delta P_s}{P_v} = \frac{\Delta P_s}{\frac{\rho\left(\frac{Q_{flow}}{A}\right)^2}{2g}} = \frac{\Delta P_s}{\frac{\rho\left(\frac{Q_{flow}}{wD}\right)^2}{2g}} \quad \text{(A.8)}$$

This "pseudo" pressure ratio was then estimated for the fan/motor combinations over each unit's range of static pressures and airflows. As with the Clarke(1985) and the Stein and Hydeman(2004) models, the static efficiency data at low ECM settings for units with 0.33 hp (246 W) and 0.50 hp (373 W) fan motors were problematic. The static efficiency data at these

low ECM settings were eliminated from the data sets, and the fan/motor static efficiency was plotted against the pressure ratio. The result was shown in Figure A.7. This figure included data from eleven 0.33 hp (248 W), four 0.50 hp (373 W), seven 0.75 hp (560 W), and three 1.0 hp (746 W) fan/motor combinations. Not all of the 36 fan/motor combinations could be used. In some cases, only partial data sets were provided, which included two 0.33 hp (248 W), one 0.50 hp (373 W), and one 0.75 hp (560 W) fan/motor combination. Six other 0.33 hp (246 W) and one 0.50 hp (373 W) fan/motors combinations that had previously been identified as having problematic part load performance data in Chapter 3 were also not used here.

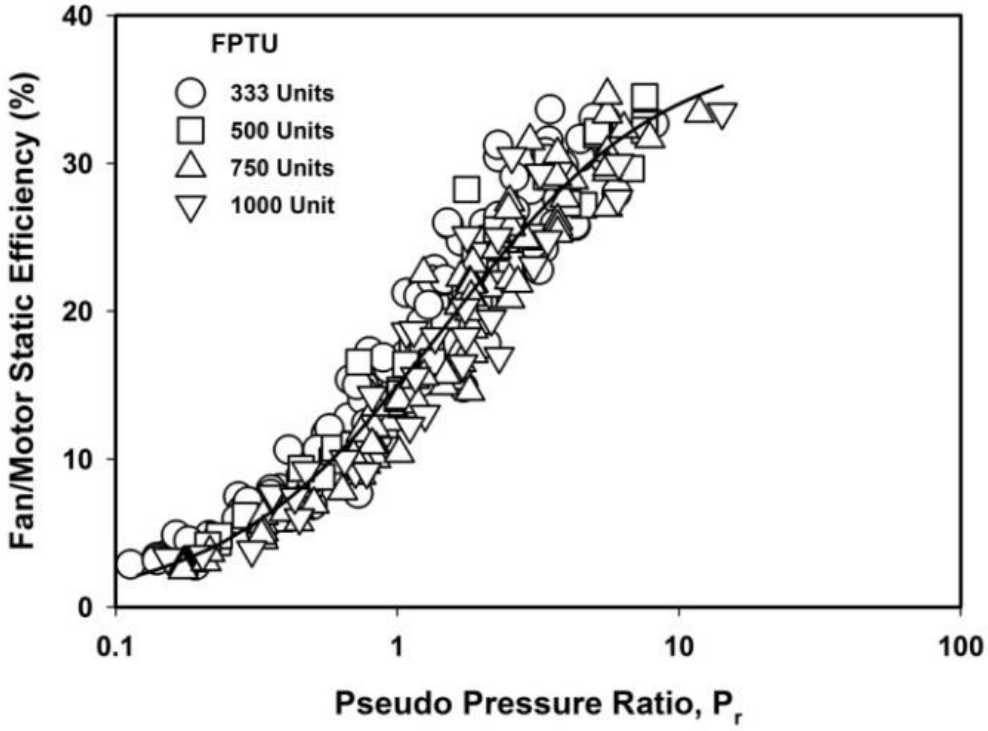

Figure A.7: Plot of Fan/Motor Static Efficiency Versus the Pseudo Pressure Ratio

The data for the fan/motor static efficiency, η_{fm}, versus pseudo pressure ratio in Figure A.7 were fit to the following logit expression:

$$\eta_{fm} = A_1 \left(\frac{1}{1 + e^{-(B_0 + B_1 log_{10} P_r)}} \right) \quad \text{(A.9)}$$

The constants in Equation A.9 were given by:

$A_1 = 37$

$B_0 = -0.436$

$B_1 = 2.579$

While there was scatter in the data, we were surprised at how well the data grouped along the best fit line for the wide range of fan sizes. For someone modeling smaller fan/motor assemblies used in fan powered terminal units, Equation A.9 could be used as a generic model for estimating the static efficiency. Considering that Equation A.9 was developed based on 25 fan/motor assemblies from various combinations of motor sizes and cabinet configurations, the output from Equation A.9 should be representative for many ECM FPTUs used in commercial buildings. It is important to note that the correlation in Equation A.9 should not be used to estimate static efficiencies at ECM settings below 35% for units with motor sizes smaller than 0.5 hp (373 W). For the logit expression, A_1 represents the asymptotic value of the static efficiency. Because these data did not extend beyond a pseudo pressure ratio above 15, it is not recommended to use this correlation above that value.

A.7. Application to Energy Models

The model developed here gives a researcher a generic model that allows them, with the right geometric and flow information on an ECM fan/motor combination to estimate the fan/motor static efficiency. In EnergyPlus (2013), both the fan and fan motor efficiency are expected to be input separately. The value coming out of Figure A.7 and Equation A.9 is the combined value of fan/motor efficiency. We would recommend using the value from Figure A.7 as the fan efficiency and assume the motor efficiency is 100%. This product would give the same effective fan/motor efficiency as in Figure A.7. EnergyPlus (2013) also requires the user to specify a pressure differential across the fan. In calculating the pseudo pressure ratio in Equation A.8, the researcher will have used the static pressure differential and airflow that goes with the estimated fan/motor efficiency. From our discussions with FPTU manufacturers, it is important that a researcher use realistic fan static pressure differentials in both Equation A.8 and in input to EnergyPlus. Fan static pressure differentials vary as the FPTU adjusts to the load in the zone. We have seen systems with fan static pressures operating near the low end (0.1 in w.g. (25 Pa)) of the data used in this study. Lacking any other data, a researcher should consider using 0.25 in w.g. (62 Pa). This value is used in the ANSI/AHRI (2011) test procedure for terminal units. All of the fan/motors used in this study operated at or less than a maximum static pressure of 0.75 in w.g. (187 Pa). Thus, the calculation procedure should never be used with static pressure higher than the maximum used here.

A.8. Summary

Two available fan models that were designed to estimate the performance of larger fans in commercial buildings were evaluated to determine whether they could be applied to the ECM fan/motor combinations used in commercially available fan powered terminal units. Results show that both the Clarke (1985) and Stein and Hydeman (2004) models were able to correlate the data well for an individual fan/motor combination. However, neither model could be used as a generic model to represent a large number of fan/motor combinations.

A variation of the Stein and Hydeman (2004) model was developed based on the data from 25 fan/motor combinations, which included a pseudo pressure ratio as the primary explanatory variable for predicting the static efficiency. The model should be applicable for most of the ECM fan/motor combinations found in fan powered terminal units. A user can estimate the fan static efficiency using the correlation, along with the knowledge of airflow, fan static pressure, and the width and diameter of the fan. It is important to note that the model should not be used to estimate static efficiencies for units with a motor size smaller than 0.5 hp (373 W) at the ECM settings below about 35% of the maximum setting. While these data used to develop the new model cover a wide range of fan/motor applications in FPTUs, the model should be used with caution if applied beyond the range of the data that was used to develop it.

APPENDIX B

PUBLICATIONS FROM AHRI 8012 PROJECT

As stated in the original proposal, ASHRAE was the preferred venue for publishing data and models from the effort on this project. A list of the papers that were published, in press, or under review at the time of the writing of the final report are listed below. Paper number 6 won a best paper award from ASHRAE.

Published or In Press:

1. J. A. Bryant and B. Kanaan, "Differential Pressure Rise Measurements and Impact in EnergyPlus Modeling for Series VAV Fan Powered Terminal Units", Accepted for Publication in *ASHRAE Transactions*, Vol. 123, Pt. 2, June 2017.

2. D. O'Neal, P. Yin, and D. Ingram, "Evaluation of Fan Models for Application to ECM Fan/Motor Combinations", *ASHRAE and IBPSA-USA SimBuild 2016*, Building Performance Modeling Conference, Salt Lake City, UT, August 2016.

3. P. Yin, C. Reid, and D. L. O'Neal, "Using a Mass and Energy Balance Approach to Model the Performance of Parallel Fan-Powered Terminal Units with Fixed Airflow Fans," *ASHRAE Transactions*, Vol. 122, Pt. 2, June 2016.

4. C. Reid, D.L. O'Neal, and P. Yin, "Characterizing the Performance of Fixed Airflow Series Fan-Powered Terminal Units Using a Mass and Energy Balance Approach," *ASHRAE Transactions*, Vol. 122, Pt. 2, June 2016.

5. D. O'Neal, and J. Edmondson, "Characterizing Air Leakage in Parallel Fan-Powered Terminal Units," *ASHRAE Transactions*, Vol. 122, Pt. 1, pp. 343-353, January 2016.

6. D. O'Neal, D. Ingram, and C.L. Reid, "Modeling Fan-Powered Terminal Unit Fan/Motor Combinations Controlled by Silicon Controlled Rectifiers", *ASHRAE Transactions*, Vol. 121, Pt. 2, pp. 342-350, July 2015.

    - Won the 2015 Best Technical Paper Award from ASHRAE.

7. Bryant, J. and Bryant. S., 2015, *In Situ Fan Differential Pressure Rise for a Series VAV Fan Power Terminal Unit with SCR Control. ASHRAE Transactions*, Vol. 121, Pt. 2, pp. 334-341.

8. D. O'Neal, D. Ingram, and C.L. Reid, "A Simplified Model of the Fan/Motor Performance of Fan-Powered Terminal Units That Use Electronically Commutated Motors," *ASHRAE Transactions*, Vol. 121, Pt. 2, pp. 306-320, July 2015.

9. D. O'Neal, "Development of Models to Simulate the Part-Load Performance of Oversized ECM Fan-Powered Terminal Units," *ASHRAE Transactions,* Vol. 121, Pt. 2, pp. 321-333, July 2015.

Under Review or In Preparation:

1. P. Yin and D. L. O'Neal, "Modeling Variable Airflow Series Fan-Powered Terminal Units with a Mass and Energy Balance Approach," Submitted to *ASHRAE Transactions,* Vol. 124, Pt. 1.

2. D. O'Neal, P.Yin, and D. Lu, "Evaluation of the Annual Energy Performance of Series and Parallel Fixed Airflow Fan Powered Terminal Units," Submitted to *ASHRAE Transactions,* Vol. 124, Pt. 1.

3. P. Yin, C. Reid, and D. L. O'Neal, "Modeling Variable Airflow Parallel Fan-Powered Terminal Units with a Mass and Energy Balance Approach," Submitted to ASHRAE *Transactions,* Vol. 124, Pt. 1.

4. B. Kanaan and J. Bryant, "In Situ Field Measurements for Series and Parallel Fan Powered Terminal Units," In preparation for submission to *ASHRAE Transactions,* Vol. 124, Pt. 2.

5. P. Yin, C. Reid, and D. L. O'Neal, "Evaluation of the Energy Savings of Variable Airflow Fan Powered Terminal Units," In preparation for submission to ASHRAE *Transactions,* Vol. 124, Pt. 2.